UNIVERSITÄTSKLINIKUM HAMBURG-EPPENDORF

Institut für Immunologie

Prof. Dr. Marcus Altfeld

Development of nanobody and antibody tools to investigate P2X purinergic signaling in inflammation

Dissertation

zur Erlangung des Doktorgrades Dr. rer. biol. hum. / PhD
an der Medizinischen Fakultät der Universität Hamburg.

vorgelegt von:

Tobias Stähler, geb. Schäfer
aus Kreuztal

Hamburg 2023

Angenommen von der
Medizinischen Fakultät der Universität Hamburg am: 14.04.2023

Veröffentlicht mit Genehmigung der
Medizinischen Fakultät der Universität Hamburg.

Prüfungsausschuss, der/die Vorsitzende: Prof. Dr. Friedrich Koch-Nolte

Prüfungsausschuss, zweite/r Gutachter/in: Prof. Dr. Jörg Heeren

Prüfungsausschuss, dritte/r Gutachter/in: Prof. Dr. med. Peter Bannas

Table of contents

Publication list:

Schäfer W*, **Stähler T***, Espinoza CP, Danquah W, Knop H, Rissiek B, Haag F, Koch-Nolte F. *Origin, distribution, and function of three frequent coding polymorphisms in the gene for the human P2X7 ion channel.* Front Pharmacol. 2022

Stähler T, Danquah W, Demeules M, Gondé H, Hardet R, Haag F, Adriouch S, Koch-Nolte F, Menzel S. *Development of Antibody and Nanobody Tools for P2X7*. Methods Mol Biol. 2022

Brock VJ, Wolf IMA, Er-Lukowiak M, Lory N, **Stähler T**, Woelk LM, Mittrücker HW, Müller CE, Koch-Nolte F, Rissiek B, Werner R, Guse AH, Diercks BP. *P2X4 and P2X7 are essential players in basal T cell activity and Ca2+ signaling milliseconds after T cell activation*. Sci Adv. 2022

Hambach J, Fumey W, **Stähler T**, Gebhardt AJ, Adam G, Weisel K, Koch-Nolte F, Bannas P. *Half-Life Extended Nanobody-Based CD38-Specific Bispecific Killercell Engagers Induce Killing of Multiple Myeloma Cells*. Front Immunol. 2022

Pape LJ, Hambach J, Gebhardt AJ, Rissiek B, **Stähler T**, Tode N, Khan C, Weisel K, Adam G, Koch-Nolte F, Bannas P. *CD38-specific nanobodies allow in vivo imaging of multiple myeloma under daratumumab therapy*. Front Immunol. 2022

Hambach J*, **Stähler T***, Eden T, Wendt D, Tode N, Haag F, Tolosa E, Altfeld M, Fathi A, Dahlke C, Addo MM, Menzel S, Koch-Nolte F. *A simple, sensitive, and low-cost FACS assay for detecting antibodies against the native SARS-CoV-2 spike protein*. Immun Inflamm Dis. 2021

Baum N, Eggers M, Koenigsdorf J, Menzel S, Hambach J, **Stähler T**, Fliegert R, Kulow F, Adam G, Haag F, Bannas P, Koch-Nolte F. *Mouse CD38-Specific Heavy Chain Antibodies Inhibit CD38 GDPR-Cyclase Activity and Mediate Cytotoxicity Against Tumor Cells*. Front Immunol. 2021

Tian T, Heine M, Evangelakos I, Jaeckstein MY, Schaltenberg N, **Stähler T**, Koch-Nolte F, Kumari M, Heeren J. *The P2X7 ion channel is dispensable for energy and metabolic homeostasis of white and brown adipose tissues*. Purinergic Signal. 2020

Unpublished manuscripts

Jäckstein MY*, Fischer AW*, **Stähler T**, Heine M, Behrens J, Mann O, Pfeifer A, Scheja L, Koch-Nolte F and Heeren J. *Purinergic adipocyte-macrophage crosstalk promotes degeneration of thermogenic brown adipose tissue*. (in preparation, 2022)

* shared first authorship

Congress and retreat poster presentations:

Stähler T, Seyfried F, Jäckstein MY, Heeren J, Koch-Nolte F. *P2X5-specifc antibodies*. EuroMAbNet meeting (2022)

Stähler T, Jäckstein MY, Heeren J, Koch-Nolte F. Tools to investigate the localization and function of P2X4, P2X5 and P2X7 in T cells, macrophages, and adipocytes. Retreat of the SFB1328 (2021)

Stähler T, Jäckstein MY, Heeren J and Koch-Nolte F. *P2X5 - a dominant marker of brown adipocytes*, SFB1328 poster presentation (2021), virtual.

Eden T, Menzel S, **Schäfer T**, Eichhoff A, Haag F, Koch-Nolte F. *Nanobodies from transgenic mice*. European Congress of Immunology (2018)

1 Introduction

In this thesis, antibodies and nanobodies were developed and characterized as tools to allow the in-depth research of purinergic signaling. The focus lies on purinergic signaling in immunology and inflammation. The antibody tools were designed primarily to investigate adipose tissue inflammation.

The following introduction starts with a general overview of the defense mechanisms of the innate and adaptive immune system with a focus on antibodies, the specifics of camelid-derived heavy chain antibodies (hcAbs) and nanobodies, and the methods for antibody generation and development. Secondly, the fundamentals of purinergic receptor signaling are outlined with a focus on the structure and function of the P2X ion channels P2X7 and P2X5. Finally, adipose tissue, particularly brown adipose tissue, and its function of lipid storage and heat generation are described.

1.1 The innate and adaptive immune system

Evolution has shaped the defense against pathogens into a race of adaptation between the pathogen and host. Mammals have developed a two-phased response against invading pathogens of different types, the innate and the adaptive immune systems. The first line of defense is generated by a variety of anatomical barriers like the skin, mucosal surfaces, or intestinal epithelia. Invading pathogens are further retained by defensins, the complement system, or anti-microbial peptides. When these defense systems fail or are bypassed, cellular components of the innate immune system come into play (Janeway 1989). Sensory cells such as macrophages or dendritic cells detect so-called danger- or pathogen-associated molecular patterns (DAMPs and PAMPs) like lipopolysaccharides from bacteria or extracellular adenosine 5′-triphosphate (ATP) (Zhang and Mosser 2008; Ghiringhelli et al. 2009).

ATP is well known as the intracellular energy currency. In the extracellular space, ATP is uncommon and is detected as a DAMP signal by P2 receptors, resulting in the excretion of proinflammatory cytokines (Di Virgilio et al. 2020). The activation of the innate immune system occurs within a few minutes and lasts for days. In contrast, the adaptive immune system takes several days to fully develop a pathogen-specific

response, but this lasts for weeks and can even persist up to several decades in the form of an immunological memory response (Janeway et al. 2001b).

T and B lymphocytes carry receptors on their cell surface which are specific for a single antigen. T cells are activated by their T-cell receptor (TCR), binding to processed peptides which are presented by MHC I and MHC II complexes on the surface of other cells (Hwang et al. 2020). The B-cell receptor does not rely on presented peptides and can even bind unprocessed native epitopes. However, B cell activation requires a second signal. The B cell itself presents peptides from internalized pathogens via MHC II to interact with T-follicular helper cells (TFH), which were previously activated by a professional antigen-presenting cell (APC). TFH help results in enhanced proliferation and production of antibodies by the antigen-specific B cell (De Silva and Klein 2015).

1.2 Antibodies

1.2.1 Conventional antibodies and llama hcAbs

Antibodies are secreted B-cell receptors. All conventional antibodies share the same basic structure composed of two polypeptide chains called the light and heavy chains (see **Figure 1.1 A**). The light chain (25 kDa) contains two domains, a variable and a constant domain (VL and CL, respectively). The structure of the heavy chain (50 kDa) differs between antibody classes. It also contains a variable domain (VH), combined with different numbers of constant (CH) domains. While IgG, IgD and IgA contain three CH domains, IgM and IgE contain four CH domains (Schroeder and Cavacini 2010). Light and heavy chains are connected by a disulfide bond. The “Y” shape of antibodies results from the pairing of two light/heavy chain units via a variable number of disulfide bonds. The two arms of the “Y” are formed by the variable and first constant domains of the light and heavy chains, while the single “leg” of the antibody is composed of the C-terminal ends of the two heavy chains.

The antigen-binding fragment (Fab) contains the variable (VH) and the first constant (CH1) domains of the heavy chain along with the VL and CL domains of the light chain, held together via hydrophobic interactions and disulfide bonds (Chothia et al. 1998). At the C-terminus of the CH1 a so called “hinge”-region connects the Fab with the

crystallizable fragment (Fc). The hinge region also connects the two heavy chains through multiple disulfide bonds while maintaining flexibility to allow binding to the antigen at different angles (Lakbub et al. 2018). The Fc fragment consists of the remaining constant domains of the heavy chain (CH2 and CH3 in IgG). This constant region mediates the effector functions of antibodies, such as antibody-dependent cellular cytotoxicity (ADCC) and complement-dependent cytotoxicity (CDC) (Mielke et al. 2019).

Antibodies can be presented in various formats with different effector functions. Thus, introducing mutations into the Fc domains can modulate effector functions by affecting their binding to Fc-receptors. Enzymatic digestion or genetic engineering can be used to eliminate the Fc domain (Derer et al. 2012). Following enzymatic digestion with papain, the antibody is cleaved above the disulfide bonds of the hinge region, resulting in two identical Fab fragments. Digestion with pepsin, on the other hand, results in a cleavage below the hinge, generating a single $F(ab')_2$ fragment containing two Fab fragments still connected by disulfide bridges. The two antigen binding domains (VH & VL) can be isolated and interconnected by genetic engineering, generating a single chain variable fragment (scFv) or scFab (**Figure 1.1 A**) (Crivianu-Gaita and Thompson 2016).

In addition to the conventional antibodies described above, camelids produce special heavy chain only antibodies (hcAb) that lack both the light chain and the CH1 domain (Hamers-Casterman et al. 1993). Therefore, a hcAb is approximately 2/3 of the size of conventional IgG antibodies (90 and 150 kD, respectively) (**Figure 1.1 B**). The antigen binding fragment is composed of only one domain called VHH (variable domain of the heavy chain of hcAb) or nanobody (Nb). These fragments are easily cloned genetically as a string of beads or as homo- and heterodimers (Chanier and Chames 2019). Due to their small size of 2-3 nm and the low molecular weight (~15 kDa), nanobody monomers are readily excreted from the serum via renal filtration. To enhance its serum half-life, the VHH can be fused to an albumin-specific nanobody or the Fc part of an IgG (Hoefman et al. 2015).

All immunoglobulin domains have the same basic structure, a beta-barrel interconnected by a disulfide bond (Bork et al. 1994). However, the variable immunoglobulin domains have a special feature in that they are genetically encoded

by two or three genetic elements. VL domains arise by recombination of V and J elements, VH domains by recombination of V, D, and J elements. This V(D)J recombination, in combination with additional somatic mutations, enhance the diversity of the complementarity-determining region (CDR) loops dramatically (Roth 2014). The V (variable) elements encode the framework of the variable domain including the CDR1 and CDR2. The D (diversity) elements are responsible for the high variety of the CDR3. The J (joining) elements link the variable domain to the CH1 domain of conventional antibodies or the hinge of heavy chain only antibodies. The variable domains of light chains of conventional antibodies do not contain D elements and are only rearranged from V- and J elements (Sun et al. 2012).

The structures of the antigen-binding domain of a conventional antibody and a nanobody are juxtaposed as a schematic ribbon model in **Figure 1.1 C**. The CDR3 loops (blue) of the Fab sit next to each other in the “core” of the planar binding paratope in the middle of the pairing variable domains. The variable domain of the nanobody is more flexible due to the lack of VL pairing. In conventional antibodies, the surface between the paired VL and VH contains conserved hydrophobic amino acid residues such as W47, L45, and V37 in the VH, which interact with the surface residues P44, F87 and F98 of VLs (Wang et al. 2009). These amino acids have mostly mutated to hydrophilic amino acids (e.g. QREL) during camelid evolution to confer better solubility without the VL element (Vu et al. 1997).

To give a comparison of the size of both antibody fragments, a surface model of the Fab CR3022 and the nanobody H11-D4 is shown, where both fragments bind to the receptor-binding domain (RBD) of SARS-CoV2 simultaneously (PDB: 6YZ7) (Huo et al. 2020) (see **Figure 1.1 C**).

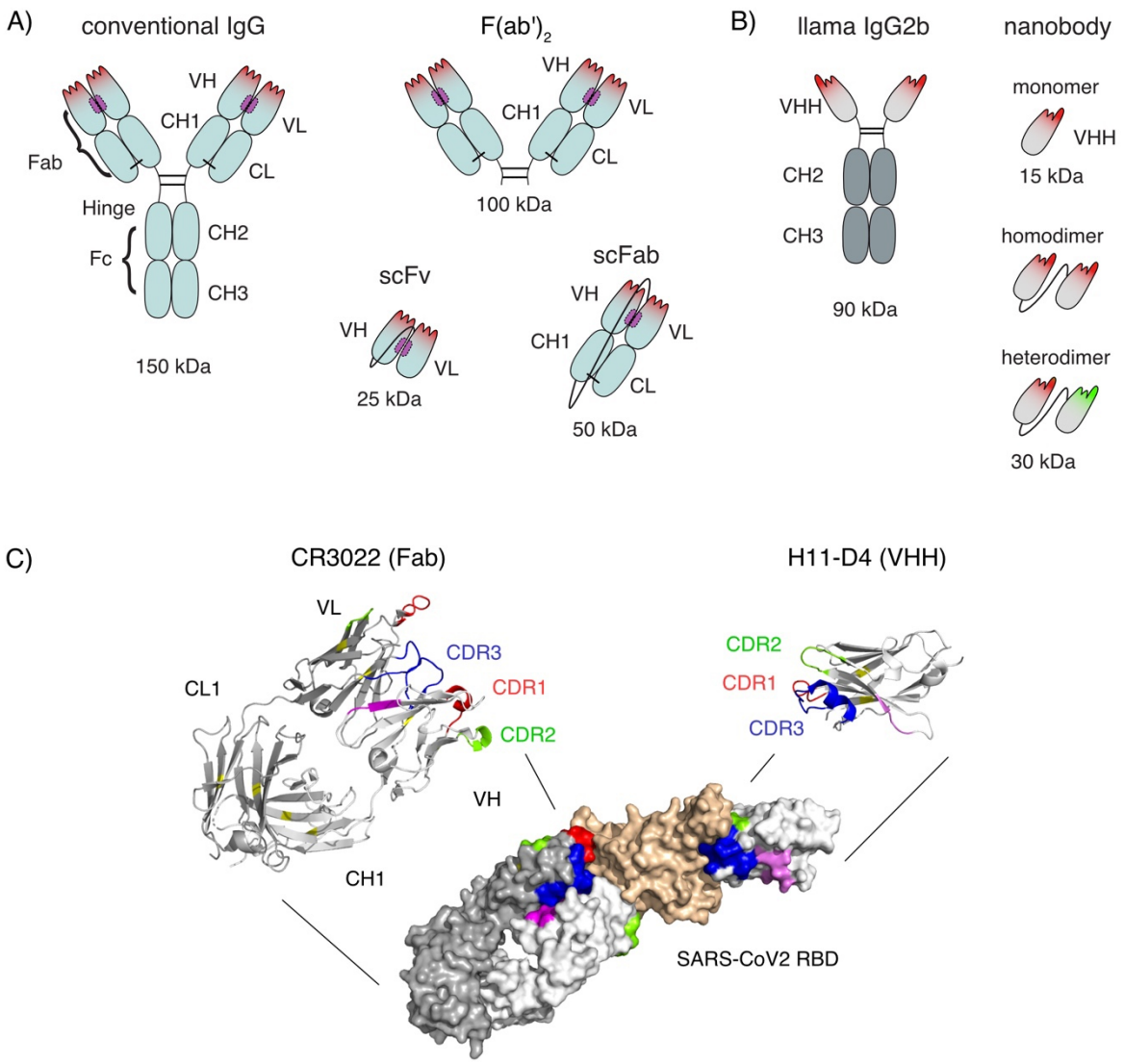

Figure 1.1 Conventional and camelid heavy chain antibodies. Schematic overview of conventional antibodies and llama hcAbs. A) Conventional antibodies are composed of two light chains, each paired with a heavy chain, respectively. By enzymatic digestion, the antigen-binding, and the constant (Fc) parts of a conventional antibody can be separated. Genetic engineering allows the production of scFvs and scFabs with peptide linkers. B) Llama heavy chain only antibodies are devoid of a light chain and lack the CH1 domain. Nanobodies, the antigen binding domain of hcAbs, can easily be cloned as homo- or heterodimers. C) Surface model showing simultaneous binding of Fab CR3022 and nanobody H11-D4 to the RBD of SARS-CoV2 (PDB: 6YZ7) (Huo et al. 2020). The schematic ribbon models of the SARS-CoV2 RBD-specific Fab CR3022 and Nb H11-D4 highlight the CDR1 (red), CDR2 (green) and CDR3 (blue) respectively. The surface amino acids involved in the VH-VL interaction of the Fab and the corresponding hydrophilic amino acids on the VHH are highlighted in magenta.

1.2.2 Polyclonal-, monoclonal antibodies and hybridoma technology

Antibodies are produced after repeated vaccinations or immunizations, by which the immune system is subjected repetitively to an injected immunogen (e.g. recombinant proteins, inactivated viruses). By ballistic cDNA immunization or injection of mRNA, the body´s own cells are stimulated to produce the immunogen themselves (Eden et al. 2017). The resulting proteins are processed and presented to naïve T cells via MHC I on the cell surface of all transduced cells and additionally via MHC II when detected and taken up by antigen-presenting cells (Kambayashi and Laufer 2014). Activated T cells in turn activate antigen-specific B cells, which mature, and undergo class switch and repetitive somatic hypermutation (Janeway et al. 2001a). The resulting plasma cells produce large amounts of specific antibodies with high affinities. These polyclonal antibodies can be harvested directly from the blood as immune serum. By comparing the pre-immune serum (PIS) and the immune serum (IS) after several boost immunizations, e.g. via ELISA, the specific antibody response of the animal to the antigen can be assessed.

Polyclonal antibodies can be purified directly from the serum via Protein A or immobilized antigen on agarose beads. Such antibodies are often used as secondary reagents, as the multitude of binding sites to the antigen results in an amplified detection signal (Magaki et al. 2019).

In contrast, monoclonal antibodies are derived from a single B cell clone and can be discovered via recombinant methods, e.g. sequencing of the B-cell receptor gene, or via the classical hybridoma technology developed by Milstein and Köhler in 1975 (Kohler and Milstein 1975). After several boost immunizations of a mouse, the entire cells of the spleen and lymph nodes are fused with immortalized myeloma Sp2/0 cells. Random fusion events between a murine immune cell and a myeloma cell are induced by polyethylene glycol (PEG). The subsequent addition of Hypoxanthine, Aminopterin and Thymidine (HAT) to the culture media allows only the growth of fused cells. Unfused spleen cells naturally die after a few days in culture, and unfused myeloma cells are depleted by Hypoxanthine. Ten days after seeding onto 96 well plates, the growth of single cell colonies can be observed. The antigen specificity of secreted antibodies in the culture supernatants can be analyzed by ELISA with immobilized antigen. Potentially multiple B cell clones are separated from each other by limiting

dilution subcloning to receive a single B cell clone that secretes a monoclonal antibody (Stähler et al. 2022). This clone can be sequenced, such that the antigen binding domains can readily be optimized, manipulated, and cloned in a manner of choice. As hybridoma technology is time consuming and sometimes inefficient, a shortcut can be taken by sequencing the antigen-specific BCRs of single sorted B cell clones directly after immunization (Viant et al. 2021).

1.2.3 Lama-IgH transgenic mice (LaMice)

Nanobodies, the small antigen-binding fragment of camelid hcAbs, have proven to be a promising tool. They contribute to scientific applications and have found their way into clinics as well. The common way to generate nanobodies is to immunize a llama or alpaca with a protein or via genetic immunization (Eden et al. 2017). However, the housing of camelids is expensive, and large quantities of protein are needed for immunization. In addition, llamas and alpacas respond not only with hcAbs but also with conventional antibodies (Muyldermans 2013).
The Koch-Nolte lab at the UKE in Hamburg has generated a llama IgH-transgenic mouse model called LaMice, which exclusively produces camelid hcAbs (Eden 2018). In these mice, the classical and well-implemented hybridoma technology can be applied after immunization to generate hybridoma clones that constantly produce hcAbs. This method is not feasible with B cells derived from the blood of immunized llamas.

The first step in generating transgenic mice that carry the llama immunoglobulin locus was to generate a bacterial artificial chromosome (BAC) genetic library from a llama liver. This BAC library contained all the necessary genetic elements to generate hcAbs (Wesolowski 2011). The first llama IgH-transgene, TE01, was produced by BAC recombineering and contained one V-element, all D and J elements as well as a CH1-deficient IgM locus. By further genetic recombination, a llama IgG2b locus and locus control regions were added. For TE02, five additional V elements were included. To generate TE03, the CH3-CH4-TM1-TM2 domains of llama IgM were exchanged against its mouse counterpart to improve signal transduction and expression of the

transgenic B-cell receptor (BCR) (Pinaud et al. 2001). The TE01-03 BACs were linearized and injected into fertilized oocytes by pronuclear injection and backcrossed to immunoglobulin deficient JHT mice (Chen et al. 1993).

So far, LaMice have demonstrated their ability to generate nanobodies against highly immunogenic viral target proteins (e.g. AAV) (Pantelic 2018). However, proof is still missing that these LaMice can also produce nanobodies targeting less immunogenic endogenous proteins, protected by self-tolerance. A potentially helpful approach would be to backcross the LaMice to *knock out* mice of the target antigen. This should allow the development of nanobodies specific for the knocked-out protein, as it will be recognized as foreign.

1.2.4 Phage display technology

Phage display technology is used to screen for interactions between diverse proteins and other molecules, like peptides, or DNA, using filamentous bacteriophages (e.g. M13). This technology makes use of the fact that phages provide a spatial linkage of protein and its coding genetic information (Smith 1985). The displayed protein is genetically fused to a surface protein of the phage. After its production in bacteria, the phage carries a few copies of the protein of interest on its surface, allowing the interaction with its target molecules. With this technology, large libraries can be screened for binders. This is especially useful for the screening of antibody libraries from immunized animals. The M13 bacteriophage has been widely used to develop antibodies derived by phage display (Huang et al. 2012). Since 1985, Greg Winter's group has made several modifications to improve the technology. For example, the minor coating protein (pIII) of the M13 helper phage is trypsin cleavable, rendering the cleaved helper phage non-infective (Kristensen and Winter 1998). In addition to the bacteriophage, a plasmid (phagemid) is needed that mediates the genetic fusion of antibody fragments with the pIII gene and enables the packaging of the plasmids into the produced phage. Further improvements have been made by adding affinity (e.g. His_6) and detection tags (e.g. c-myc) between antibody fragment and PIII. In contrast to the helper phage p3, the phagemid-encoded p3 is resistant to trypsin, and trypsin cleavage therefore only restricts reinfection of helper phages after display. In addition,

an amber stop codon allows either the production of antibody-P3 fusion proteins in amber suppressor *E. coli* strains (e.g. TG1), or of only the tagged antibody fragment in non-suppressor strains (e.g. HB2151) (Chinestra et al. 2012). To select binders, the antibody-displaying phages are subjected to protein immobilized on plastic, beads, or transfected cells. By thoroughly washing the material, non-binding phages are eliminated. Through bacterial reinfection, the residual phages are amplified and can be used for additional rounds of so-called 'bio-panning'. After multiple rounds, high-affinity antibodies can be retrieved.

1.3 Purinergic receptor signaling

ATP is a ubiquitously occurring molecule of energy metabolism and is active as a signal molecule in diverse biological processes (Khakh and North 2006). ATP and NAD^+ can be released into the extracellular space from cells under pathological and physiological conditions (Burnstock 2006). The conveying of signals between cells based on extracellular adenine nucleotides is often termed "purinergic signaling". **Figure 1.2** shows a schematic composition of proteins involved in purinergic signaling during inflammation.

In immune cells, P2X7 plays an important role in inflammasome activation. In a first step, P2X7-expressing immune cells are primed and activated, e.g. by LPS, via toll like receptors such as TLR4, thereby inducing transcription, among others, of the genes for IL-1b, IL-18, and Gasdermin D via nuclear factor 'kappa-light-chain-enhancer' of activated B-cells (NF-κb) signaling. These are synthesized as cytoplasmic pro-forms (pro-IL-1β, pro-IL18, and pro-GSDMD). As a second signal, extracellular ATP-mediated P2X7 activation results in the influx of calcium and the efflux of potassium. The prolonged exposure of P2X7-expressing cells to ATP results in a dye-permeable 'macropore' that allows the entrance of large hydrophilic substances like YO-PRO1 or DAPI, ultimately leading to cell death (Di Virgilio et al. 2018).

The reduction of intracellular potassium levels leads to NLRP3 inflammasome assembly (Yaron et al. 2015). The NLRP3 inflammasome complex cleaves pro-caspase-1 to active caspase-1, which in turn cleaves IL-1β and IL-18 precursors as

well as pro-GSDMD to their respective active forms (Broz and Dixit 2016). The mature N-terminal fragment of GSDMD reaches the plasma membrane and forms pores that allow the release of cleaved IL-1β and IL-18 into the extracellular space. Prolonged pore formation leads to pyroptosis of the signaling cell (Evavold et al. 2018; Liu et al. 2016).

The balance between pro-inflammatory ATP and anti-inflammatory adenosine signaling is important for tissue homeostasis (Colgan et al. 2006; Hasko and Cronstein 2004). Extracellular ATP amounts are regulated by NTPDases like CD39, which degrades ATP and ADP to AMP (Zimmermann 2000). ATP and ADP are sensed by P2 receptors and result in either pro- or anti-inflammatory signaling depending on the P2Y receptor involved (Klaver and Thurnher 2021). Further degradation by 5'NT (CD73) results in the generation of anti-inflammatory adenosine, a P1 receptor (e.g. A2A) ligand (Allard et al. 2017). Adenosine deaminase degrades AMP further to inosine (Cristalli et al. 2001).

The receptors of the P2 family become activated by extracellular ATP or ADP and can be divided into two subfamilies: The P2Y receptors are G-protein coupled receptors whereas the P2X receptors are non-selective, in majority homo-trimeric ion channels, whereas heterometic P2X receptors have been reported for P2X2/P2X3 and P2X4/P2X7 (Lewis et al. 1995; Schneider et al. 2017). P2X receptors allow the influx of Ca^{2+} and Na^{+} as well as the efflux of K^{+} (Di Virgilio et al. 2001). Seven homologues of the P2X receptors (1-7) were discovered in the last decades with different subcellular localizations and tissue distribution, e.g. P2X4 is predominantly found in lysosomes and P2X7 on plasma cell membranes (Qureshi et al. 2007). P2X5 is dominantly expressed in brown adipose tissue and P2X7 is ubiquitously expressed on cells of the immune system (Surprenant 1996; Ussar et al. 2014; Xu et al. 2014).

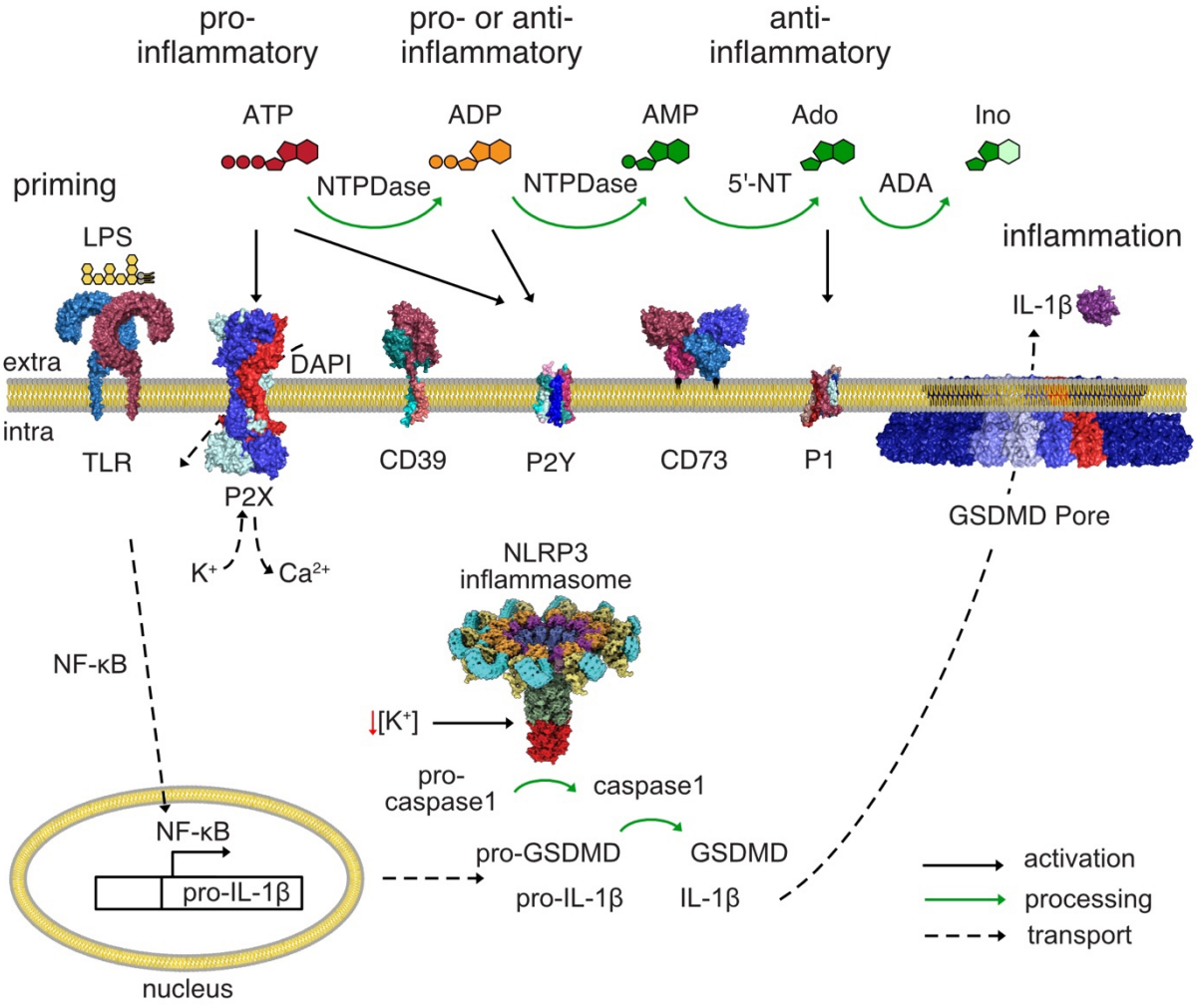

Figure 1.2 Schematic of inflammatory purinergic signaling. LPS primes immune cells via TLR4 and results in the transcription of precursors of the inflammasome and cytokines like pro-IL-1β. P2 receptors are activated by ATP, mediating the efflux of potassium and influx of calcium. Decreasing potassium concentrations result in the assembly of the NLRP3 inflammasome and activation of caspase-1, which cleaves pro-IL-β and pro-GSDMD to their respective active forms. GSDMD pores release IL-1β and eventually lead to pyroptosis. ATP and ADP degradation by NTPDases (CD39) and 5'NT (CD73) result in the generation of adenosine, an A2Aa agonist promoting anti-inflammatory signaling. ADA further degrades adenosine to inosine. activation = black arrow, processing = green arrow, transport = dashed arrow.

1.3.1 P2X receptor architecture

All P2X ion channels have two transmembrane domains, intracellular N- and C-termini, and a large extracellular domain that forms the ATP binding sites between two adjacent P2X monomers (**Figure 1.3 A**). P2X7, in contrast to the other P2X ion channels, has a much longer intracellular C-terminal domain that accounts for up to

40% of the mass of the ion channel. In 2009, Karasawa *et al*. described the appearance of a zebrafish P2X4 monomer as a dolphin-like structure (Kawate et al. 2009). The two transmembrane domains (green) are represented by the tail (**Figure 1.3 A**), the extracellular domain forms the lower body (cyan) with a dorsal fin (orange) and a right flipper (red). The ATP binding pocket (red pearls) is located between the left flipper (yellow), head (pink) and upper body (purple) domains, tucked between two P2X7 monomers of the P2X7 homotrimer (**Figure 1.3 B**). By including the crystalized cytoplasmic ballast domain (black) of rat P2X7 discovered by McCarthey at al. in 2019, the dolphin analogy can be extended with a beach ball as indicated in the schematic dolphin (**Figure 1.3 A**). This C-terminal cytoplasmic domain is palmitoylated and is postulated to be responsible for the prevention of channel desensitization (McCarthy et al. 2019). The common P451L loss-of-function SNP in the cytoplasmic tail of murine P2X7 is responsible for ATP-mediated cation flux, NAD-sensitivity, pore formation and cell death but not ion channel current (Young et al. 2006) (Adriouch et al. 2002).

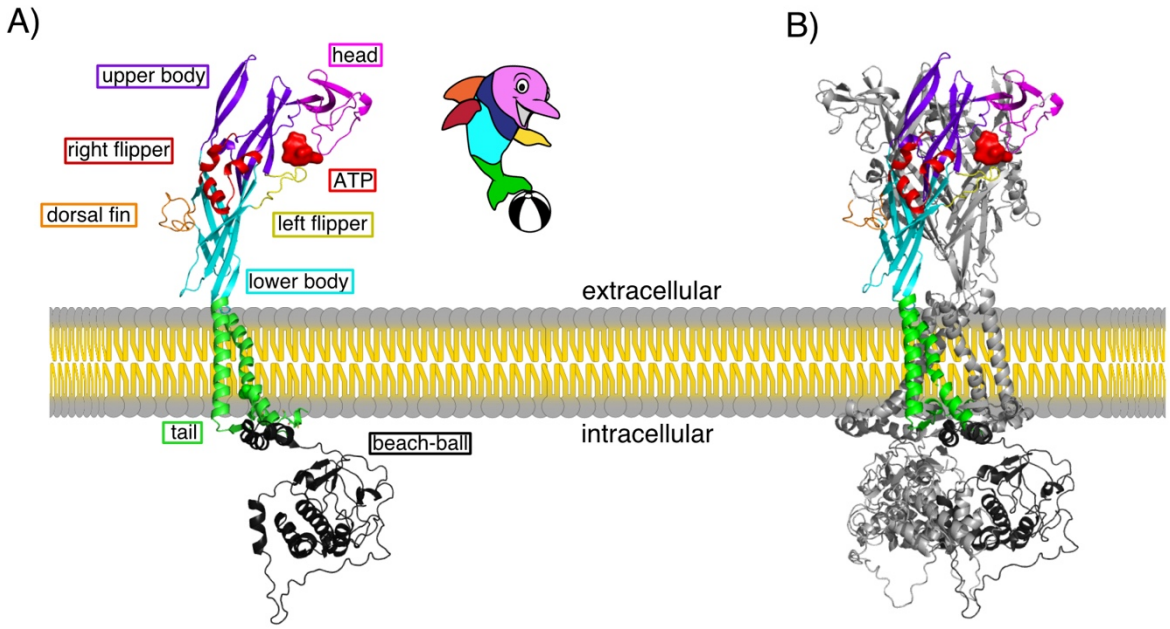

Figure 1.3 Structure model of the hP2X7 ion channel. A) hP2X7 monomer color coded to the dolphin analogy on the right with extracellular head (pink), upper body (purple), right flipper (red), left flipper (yellow), dorsal fin (orange) and lower body domain (turquoise). Bound ATP is shown as a red surface model. The two transmembrane "tail" domains are color coded green; the intracellular cytoplasmic domain is color coded black. B) Homotrimer structure of the hP2X7 receptor. The hP2X7 model was generated with Alpha Fold 2 (Varadi et al. 2022; Jumper et al. 2021).

The seven P2X ion channels show differences in the sensitivities to ATP. P2X1-6 are activated by ATP concentrations (EC50) at around 1-50 μM whereas P2X7 requires >100 μM to evoke a current (Illes et al. 2021; North and Surprenant 2000). In addition, P2X7 is the only ion channel that completely lacks desensitization over a longer period of time (North 2002).

1.3.2 P2X5

In recent decades, while a lot of effort has been devoted to investigating P2X ion channels in general, functional studies of the P2X5 family member have been quite sparse. This neglect is based on the fact that the human P2X5 ion channel was considered to be nonfunctional, in contrast to murine P2X5 (King 2022). A first study identified a P2X5 isoform lacking exon 10 that is highly transcribed in the central nervous system (CNS) as well as immune cells (Lê et al. 1997). The same study postulated two isotypes, P2X5A and P2X5B, whereby both cDNAs lacked exon 10, while the latter lacked exon 3 as well (North 2002). In 2001, Cox *et al*. suggested that a full length human P2X5 ion channel including exon 10 could exist due to the finding of a corresponding clone in Genbank (clone AF168787.1) (Cox et al. 2001). Bo *et al*. were the first to clone and express the full length human P2X5 ion channel by inserting exon 10 into the cDNA of a human lung small cell carcinoma clone (Genbank BE791872) (Bo et al. 2003). Robust receptor inward currents were measured by the electrophysiological analysis of whole-cell patch clamp of transiently transfected HEK293 cells. The ATP sensitivity of the full length human P2X5 ion channel was thereby determined to be approximately 4 μM, comparable to the rat P2X5 receptor (Bo et al. 2003), as was later confirmed by other studies (Sun et al. 2019; Kotnis et al. 2010). Duckwitz *et al*. showed by truncating exon 10 that eleven amino acids N-terminally to the second transmembrane domain were sufficient to allow the formation of a trimeric ion channel. However, all 22 amino acids of exon 10 were required to evoke currents (Duckwitz et al. 2006). Interestingly, exon 10 is skipped in most humans. This is caused by the single nucleotide polymorphism (SNP) rs891746 which affects expression with high dominance in human populations, with the exception of some African subpopulations (Kotnis et al. 2010). Splicing of exon 10 renders the

Δexon 10 variant non-responsive to ATP in contrast to the full length-variant (Bo et al. 2003).

In addition to its expression in the CNS and immune cells (Lê et al. 1997), the P2X5 ion channel is highly expressed on the cell surface of beige and brown adipocytes, but not in white adipocytes of mice and humans (Ussar et al. 2014). Therefore, P2X5 has been suggested as a new promising cell surface marker of thermogenic adipocytes.

Moreover, P2X5 receptor expression is elevated during cold exposure and in activated thermogenic brown adipose tissue (BAT) in mice (Razzoli et al. 2016; Ussar et al. 2014; Garcia et al. 2016).

1.4 Adipose tissue

Adipose tissue has several functions in mammals, from energy storage to energy expenditure and tissue homeostasis. Adipose tissue is mainly composed of adipocytes, nerve- and connective tissue as well as immune cells (Frayn et al. 2003). Classically, adipose tissue is divided into two groups that differ in origin and function. White adipose tissue (WAT) is mainly located under the skin (subcutaneous) or in the peritoneal cavity (visceral) and is critical for energy storage, endocrine communication, and insulin sensitivity (Trayhurn and Beattie 2001; Pelleymounter et al. 1995). BAT on the other hand is located in the supraclavicular area in adult men, is responsible for lipid storage and the facultative generation of heat by non-shivering thermogenesis, well known from postnatal infants (Cannon and Nedergaard 2004).

BAT thermogenesis is controlled by sympathetic nerve signaling. Under cold stress, the hypothalamus activates brown adipocytes via nerve fibers. Nerve endings thereby release norepinephrine, which activates β3-adrenergic receptors on brown adipocytes, resulting in lipolysis of stored lipids (Lowell and Flier 1997). The released lipids are transported into mitochondria by carnitine palmitoyl transferase I (CPT1) for beta-oxidation. Thermogenic adipocytes expressing uncoupling protein 1 (UCP1) can release stored protons from the inner mitochondrial membrane and generate heat (Cannon and Nedergaard 2004; Schulz 1991).

The thermogenic capacity of BAT is an important contributor to whole-body energy expenditure. Due to the unfavorable body surface to volume ratio in small rodents, for

example, cold activation results in a rise of total energy expenditure of up to 80% (Ouellet et al. 2012). As BAT has a high capacity to burn excess fuels such as glucose and lipids to produce heat, brown adipocytes have been suggested to be of special interest as targets to prevent obesity and related diseases (Moonen et al. 2019; Ussar et al. 2014; Garcia et al. 2016).

Humans living at thermoneutrality suffer from BAT involution (the loss of thermogenic BAT capacity) with decreased mitochondrial mass and decreased lipid consumption (de Jong et al. 2019). In addition, it has been shown that lower BAT amounts are associated with cardiovascular diseases and metabolic diseases such as type 2 diabetes (Saito et al. 2009). In obesity, tissue metabolic and endocrine functions are altered, and the condition is associated with a higher release of pro-inflammatory molecules (Roberts-Toler et al. 2015). The infiltration of immune cells into BAT is linked to lipolysis, the release of fatty acids from stored triglycerides (Kosteli et al. 2010). In obese WAT, macrophages are recruited and surround large dying adipocytes, also referred to as crown-like structures (Lumeng et al. 2008). This has also been observed for BAT during thermoneutrality (Fischer et al. 2020).

2 Aim of the thesis

The aim of this thesis was to develop new tools for investigating purinergic signaling. For this, four work packages were designed:

1. The aim of the first work package was to generate and characterize nanobodies against mouse immunoglobulin subclasses that can be used as secondary reagents.
2. The aim of the second work package was to select novel P2X7-specific nanobodies. To obtain nanobodies binding to a different epitope than previously selected nanobodies, selection were to be performed under conditions where the dominant epitope of P2X7 is masked.
3. The aim of the third work package was to generate and characterize novel monoclonal antibodies targeting P2X5, an ATP-gated ion channel implicated to play a role in brown adipose tissue.
4. The aim of the fourth work package was to elucidate the role of P2X4 and P2X7 receptors in a mouse inflammation of brown adipose tissue inflammation. As *P2rx4*$^{-/-}$, *P2rx7*$^{-/-}$ double knockout mice cannot be generated by crossbreeding, *P2rx4*$^{-/-}$ mice were to be injected with P2X7 inhibiting nanobodies to create transiently double deficient Balb/c mice.

3 Material and methods

The following chapter summarizes the material used during the studies, e.g. laboratory equipment, consumables, chemicals, antibodies, and mice. In the subsequent Methods section, the diverse methodologies (e.g. molecular cloning, immunizations, and screening procedures) are outlined and explained in detail.

3.1 Material

3.1.1 Laboratory equipment

Equipment	Model	Company
Analytical scale	Type 1412	Sartorius
Autoclave	Varioclave	H+P Labortechnik
Centrifuges	Rotanta 460 R	Hettich
	5417R	Eppendorf
	5430	Eppendorf
	Biofuge pico	Heraeus
Electroporator	MicroPulser	Bio-Rad Laboratories, Inc.
ELISA plate reader	Voctor 3	Perkin-Elmer
Flow cytometers	FACS Canto II	BD Biosciences
	FACS Celesta	BD Biosciences
	FACS Aria A1	BD Biosciences
Gelelectrophoresis chamber	40-0708	Peqlab biotechnology
Gelelectrophoresis power supply	P25 Bio1015 LVD	Biometra
Gene Gun system	Helios®	Bio-Rad
SDS-Page chamber	Xcell SureLock miniCell	Thermo Fisher Scientific
SDS-Page power supply	Voltmeter PowerPac 200	Bio-Rad
Heat block	Thermomixer compact	Eppendorf
Incubator (Bacteria)	Multitron Pro	Infors HT
Incubator (mammalian cells)	MCO-20AIC	Sanyo Electric Co.
Micropipettes	Research	Eppendorf
Microwave	M 637 EC	Miele
Neubauer cell chamber	Improved	Carl Roth
Photometers	Nanodrop 2000c	Peqlab Biotechnology
	Ultraspec 2000	Pharmacia Biotech
Roller	Mixer SRT6	Stuart
Sterile flow hood	BSB4	Gelair
	HeraSafe	Heraeus
Tubing Prep station	1652420	Bio-Rad
Table scale	Scout Pro	Ohaus
Thermocycler	T3	Biometra
Thermocycler	T Gradient	Biometra
UV transilluminator	Type TI 1	Biometra
Ultrasonic bath	Super RK	Bandelin
Water bath	1007	Labortechnik

3.1.2 Consumables

Consumable	Type	Supplier
Cell culture flasks	T25, T75, T225	Greiner bio-one
Cell culture plates	24- & 96-well	Thermo Fisher Scientific
Centrifugational filters	Amicon-ultra	Merck
Electroporation cuvette	0.1 cm, Gene pulser	Bio-Rad Laboratories, Inc.
ELISA plates	Nunc MaxiSorp	Thermo Fisher Scientific
Erlenmeyer flask	50 ml – 500 ml	STEMCELL technologies
Falcon tubes	15 ml, 50 ml volume	Greiner bio-one
Gloves	Nitrile, Dermagrip	WRP
μDish	35 mm high	Ibidi
Pipette Tips	Variations	Sarstedt
PD-10 desalting columns	-	Cytiva
SDS-PAGE gels	Precast-mini, 10% Bis-Tris	Thermo Fisher Scientific
Cell strainer	70 μm	Thermo Fisher Scientific
Zeba™Spin desalting columns	0.5 ml	Thermo Fisher Scientific

3.1.3 Kits

Kit	Type	Supplier
NucleoSpin	RNA mini	Macherey-Nagel
NucleoSpin	PCR Clean up	Macherey-Nagel
NucleoSpin	Plasmid	Macherey-Nagel
BCA Protein Assay Kit	-	Thermo Fisher Scientific
EZ-Link Sulfo-NHS-Biotin	-	Thermo Fisher Scientific

3.1.4 Chemicals and Reagents

Equipment	Supplier
2xYT	Thermo Fisher Scientific
AEBSF	Merck
Anti-Anti (100x)	Gibco
Agar (gelelectrophoresis)	Merck
Agar (bacterial plates)	Carl Roth
Alexa Fluor™ 647 NHS-Ester	Thermo Fisher Scientific
ATP	Sigma
Aqua ad iniectabilia	Braun
Bacto-Trypton	Thermo Fisher Scientific
BSA	Merck
Carbenicillin	Merck
$CaCl_2$	Carl Roth
ClonaCell™-HY PEG	Stemcell technologies
Depilatory cream	Pharmacy
DMEM Medium	Thermo Fisher Scientific
DMSO	Thermo Fisher Scientific
DNA gel loading die (6x)	New England Biolabs
dNTPs	Thermo Fisher Scientific
Dithiothreitol (DTT)	Thermo Fisher Scientific
Ethanol, 99.9%	Merck
EZ-Link™ Sulfo-NHS-LC-Biotin	Thermo Fisher Scientific

Fetal calf serum (FCS)	Thermo Fisher Scientific
Geneticin	Thermo Fisher Scientific
Glucose	Carl Roth
Glycerol	Merck
FreeStyle 293 Expression Medium	Thermo Fisher Scientific
Hepes	Thermo Fisher Scientific
HIS-Select® Nickel Affinity Gel	Merck
IgG Elution buffer (pH2.8)	Thermo Fisher Scientific
Imidazole	Thermo Fisher Scientific
Freund's Complete Adjuvant	Sigma
Freund's Incomplete Adjuvant	Sigma
Instant blue™ coomassie staining	VWR
JetPEI	Polyplus
Kanamycin	Merck
L-Glutamine	Thermo Fisher Scientific
LB Agar	Carl Roth
LB Medium	Carl Roth
Lysis Buffer A2	Macherey-Nagel
Magnesium sulfate	Carl Roth
MES Running Buffer	Thermo Fisher Scientific
Neutralization Buffer A3	Macherey-Nagel
Non-essential amino acids	Thermo Fisher Scientific
NuPAGE LDS Sample Buffer (4x)	Thermo Fisher Scientific
NuPAGE Sample Reducing Agent (10x)	Thermo Fisher Scientific
Paraformaldehyde (PFA)	Merck
PBS wo $mg^{2+,}$ ca^{2+} (1x, 10x)	Thermo Fisher Scientific
PBS with $mg^{2+,}$ ca^{2+} (1x, 10x)	Thermo Fisher Scientific
Pluronic™ F-68	Thermo Fisher Scientific
KCl	Carl Roth
Polyethylenglycol (PEG) 8000 MW	Carl Roth
Polyvinylpyrrolidone (PVP, MW 360.000)	Merck
Protein A-Sepharose CL-4B	Merck
Protein G Sepharose 4 Fast flow	GE Healthcare
Resuspension Buffer A1	Macherey-Nagel
Roti-Safe	Carl Roth
Silica dry packs	Carl Roth
Sodium Pyruvate	Thermo Fisher Scientific
Sodium chloride	Carl Roth
Sulfuric acid (1M)	Carl Roth
TAE-Buffer (50x)	Thermo Fisher Scientific
TE-Buffer	Macherey-Nagel
Tefzel tubing	Bio-Rad
TMB-Substrate	Bethyl
Tris-EDTA (10 mM)	Biomol
Triton X-100	Carl Roth
Tryptone	Carl Roth
Tubing Cutter	Bio-Rad
Tween20	Carl Roth
Yeast extract	Carl Roth

3.1.5 Media

Bacterial media:

Medium	Ingredients
2xYT	31 g/l in ddH_2O
2xYT/carb/glu	2x YT, 1/1000 carbenicillin, 2% Glucose
2xYT/carb/kana	2x YT, 1/1000 carbenicillin, 1/1000 kanamycin
LB-medium	25 g/l in ddH_2O
LB-agar	40 g/l in ddH_2O
LB/carb/glu-agar	LB-agar, 1/1000 carbenicillin, 2% Glucose
SOC-medium	2 % Tryptone, 0,5 % yeast extract, 8,6 mM NaCl, 2,5 mM KCl, 20 mM mgSO4, 20 mM Glucose in ddH_2O

Cell culture media:

Medium	Ingredients
DMEM (complete)	DMEM medium, 2 mM L-Glutamine, 1 mM Sodium pyruvate, 10 mM HEPES, 1x NEA (non-essential amino acids), 5 % FCS
RPMI (complete)	RPMI 1640 medium, 5% FCS, 1xHFCS,1 mM Na-pyruvate, 5 mM L-glutamine, 50 g/l gentamycin
RPMI freezing medium	RPMI complete, 45% FCS, 10% DMSO
HAT-Medium	RPMI (complete), 1xHAT, 24 μM β-mercaptoethanol
HT-Medium	RPMI 1640, 2 mM L-Glutamine, 1 mM Sodium pyruvate, 10 % FCS
F17 complete medium	F17, 4 mM L-Glutamine, 0.1 % Pluronic, 1% FCS, 25 μg/ml Geneticin
F17 feeding medium	F17, 4 mM L-Glutamine, 0.1 % Pluronic, 25 μg/ml Geneticin, 20% Tryptone
F17 transfection medium	F17, 4 mM L-Glutamine, 0.1 % Pluronic
Adipocyte differentiation medium	DMEM, 4.5 g/l glucose, 10% NCS, 1% P/S, 1% Anti-Anti, 2,4 nM insulin, 1µM rosiglitazone

3.1.6 Buffers

Medium	Ingredient
PEG/NaCl	PEG6000 (20%) + NaCl (2,5M) in ddH2O
Spermidine solution	0.05 M in ddH_2O
ELISA blocking buffer	0.5% BSA, 0.05% Tween in PBS-/-
ELISA washing buffer	0.05% Tween in PBS-/-
Erythrocyte lysis buffer	155 mM NH4Cl, 10 mM KHCO3, 0.1 mM EDTA, in ddH_2O, pH 7.2
FACS buffer	0.5% BSA, 1 mM EDTA in PBS-/-
Kinetics buffer	0.01 % BSA, 0.002% Tween-20 in PBS-/-
RIPA buffer (10x)	50 mM Tris-HCl, 5 mM EDTA, 150 mM NaCl, 1 mM Na-pyrophosphate, 1 mM NaF, 1 mM Na-vanadate, 1% NP-40, in ddH_2O pH 7.4
TBS-T	20 mM Tris, 150 mM NaCl, 0.1% (v/v) Tween 20 in ddH2O

3.1.7 Antibodies and cell dyes

Anti (species reactivity)	Clone/Ref/Isotype	Host	Type	Supplier
APC-Cy7 LIVE/DEAD™	/	/	/	Thermo Fisher Scientific
c-myc tag	9E10	rabbit	monoclonal	AG Nolte, Hamburg
CD11b-A647 (mouse)	M1/70	rat	monoclonal	BioLegend
CD16/CD32 (mouse)	2.4G2	rat	monoclonal	BioXCell
CD45-PE-Cy7 (mouse)	30-F11	mouse	monoclonal	BioLegend
Ig(H+L)-A647 (rabbit)	711-606-152	goat	polyclonal	Jackson Immuno Research
Ig(H+L)-HRP (rabbit)	111-035-144	goat	polyclonal	Jackson Immuno Research
Ig(H+L)-HRP (lama)	Lab0001	rabbit	polyclonal	Covalab
IgG1-Bv421 (mouse)	RMG1-1	rat	monoclonal	BioLegend
MAC2 (mouse)	M3/38	rat	monoclonal	Santa Cruz
P2X7 (m/h/r)	APR-004	rabbit	polyclonal	alomone
VHH (lama)	mAbH0077	mouse	monoclonal	Ablynx
Unknown	6.3 (IgG2c,κ)	mouse	monoclonal	SouthernBiotech
CD235a (human)	HIR2 (IgG2b,κ)	mouse	monoclonal	eBio
CD19 (human)	HIB19 (IgG1,κ)	mouse	monoclonal	eBio
CD8a (rat)	G28 (IgG2a, κ)	mouse	monoclonal	Biolegend
CD15 (human)	HI98 (IgM, κ)	mouse	monoclonal	eBio
γ-Tubulin (mouse)	EPR16793	rabbit	monoclonal	abcam

3.1.8 Plasmids

Plasmid	Supplier
pAX50	Ablynx (Sanofi)
pCSE2.5	Dr. Thomas Schirrmann, Braunschweig
pcDNA3.1	Thermo Fisher Scientific

3.1.9 Enzymes

Enzyme	Supplier
Q5 Polymerase	New England Biolabs
T4 Ligase	New England Biolabs
Antarctic Phosphatase	New England Biolabs
BamHi /-HF	New England Biolabs
NcoI /-HF	New England Biolabs
NotI /-HF	New England Biolabs
PciI	New England Biolabs
SfiI	New England Biolabs
XbaI	New England Biolabs
Antarctic Phosphatase	New England Biolabs
Trypsin-EDTA	Thermo Fisher Scientific

3.1.10 Gel electrophoresis standards

Plasmid	Supplier
GeneRuler 1Kb DNA ladder	Thermo Fisher Scientific
Supermarker	75 µg/ml IgG, 100 µg/ml BSA; 10 µg/ml Lysozyme
Precision Plus Protein	Bio-Rad

3.1.11 Oligonucleotides

Primer	Sequence 5'-3'
CMV	CGC AAA TGG GCG GTA GGC GTG
BGH	TAG AAG GCA CAG TCG AGG
LMB3	CAG GAA ACA GCT ATG AC
TE#150 (rev llama IgM, cDNA)	GGA AGA CAC GTT CTT CTC GAT GAC C
TE#154 (rev llama IgG2b, cDNA)	GGC CTT GGA GAT GGT CTT CTC GATG G
TE#161 (fwd llama, PCR1)	GGC TCA GGT GCA GCT GGT GGA GTC TG
TE#149 (rev llama IgM, PCR1)	CAC GAA ACC AGG ACA CGG AGA TCT CC
TE#153 (rev llama IgG2b, PCR1)	CGC ACC TCA GCG CCA TCA ATG TAC C
TE#155 (fwd llama, PciI, PCR2)	GGT GAC ATG TCT CAG GTG CAG CTG GTG GAG TCT G
TE#157 (rev llama IgM, NotI. PCR2)	CAC GCT GGG GGG CAG ATC GGC GGC CGC TGA GGA GAC GGT GAC C
TE#156 (rev llama IgG2b, NotI, PCR2)	TGG TTG TGG TTT TGG TGT CGC GGC CGC TGA GGA GAC GGT GAC C
TE#158 (fwd llama, linker)	ACA CTC TTT CCC TAC ACG ACG CTC TTC CGA TCT CTC AGG TGC AGC TGG TGG AGT CTG
TE#159 (rev llama IgM, linker)	TGA CTG GAG TTC AGA CGT GTG CTC TTC CGA TCT GAA GTG CCA GAG AAG CCG TCT CG
TE#160 (rev llama IgG2b, linker)	TGA CTG GAG TTC AGA CGT GTG CTC TTC CGA TCT GGA CAC TTG GAT TCT GTT GTA GGA TTG G
Barcode sequences (rev)	CAA GCA GAA GAC GGC ATA CGA GAT NNN NNG TGA CTG GAG TTC AGA CGT GTG
P2X5 genotyping fwd	GGC TGG GGA CTG ACC TAA AC
P2X5 genotyping rev	ATC ATC AAC GTG GGC TCT GG
P2X5 sequencing	CCT CTT TTC CCA CGC CTA TTC TGA TCT TGC

3.1.12 Cell lines

Cell line	Supplier
HEK293-6E, human embryonal kidney cells	Dr Yves Durocher (National Research Council Canada, Ottawa, Canada)
HEK293-T	AG Nolte
CHO.it	AG Di Girolamo, Corda, Italy
Sp2/0-Ag14	ATC
NK92-FcR transfected	AG Nolte
LP1-Luc	AG Nolte

3.1.13 Bacteria and phages

Cell line	Genotype	Supplier
Electrocompetent TG1	[F´ traD36 proA+B+ lacIqZ ΔM15] supE thi-1 Δ(lac-proAB) Δ(mcrB-hsdSM)5(rK- mK-)	Lucigen
Chemocompetent XL1-Blue	recA1 endA1 gyrA96 thi-1 hsdR17 supE44 relA1 lac [F proAB lacIqZΔM15 Tn10 (Tetr)]	Agilent
KM13	Trypsin-Sensitive Helper Phage	Biocat

3.1.14 Animals

Animal	Supplier
LgIgHtg_JHT_TE01 (TE01 LaMouse)	UKE
LgIgHtg_JHT_TE02 (TE02 LaMouse)	UKE
LgIgHtg_JHT_TE01 (TE03 LaMouse)	UKE
Balb/c.P2rx4^{tm1Rass}	UKE
F1 (Brown Norway rat x Wister rat)	UKE

3.2 Methods

3.2.1 Animal experiments

Animal experiments were approved by the Animal Welfare Officers of the University Medical Center Hamburg-Eppendorf and Behörde für Gesundheit und Verbraucherschutz Hamburg. Mice were housed in individually ventilated cages (IVC). The mice used in these experiments were Balb/c.P2rx4^{tm1Rass}, llama IgH-transgenic mice (TE01, TE02, TE03 LaMice, Nolte Lab, UKE). Rats (F1 of Brown Norway x Wistar with a heterozygous MHC, Nolte Lab, UKE) were housed in regular cages. Animals received food and water ad libitum.

3.2.2 Protein Immunization

Two TE01, two TE02 and two TE03 LaMice were prime- and boost immunized with a mix of hcAbs. Immunogens MU1067-mIgG2c and l+10-mIgA were produced by transient transfection of HEK293-6E. Immunogens were purified by Protein A affinity chromatography and buffer exchange against PBS$^{+/+}$. 30 μg of MU1067-mIgG2c hcAb and 30 μg of l+10-mA hcAb were mixed with either Freund's Complete Adjuvant (CFA, 85% paraffin oil, 15% mannide monooleate containing 0.1 mg/ml heat killed and dried

Mycobacterium tuberculosis) for the prime immunization or Freund's Incomplete Adjuvant (IFA, 85% paraffin oil, 15% mannide monooleate) for boosts 1-3. 20 weeks old LaMice, housed in individually ventilated cages (IVC) were anaesthetized using Isoflurane. Each mouse received two subcutaneous injections in the neck and lower back respectively. Boost immunizations were carried out three weeks apart. For the final boost (4^{th}), antigen was mixed with 0.9% NaCl and mice were injected subcutaneously, intraperitoneally, and intravascularly via the tail vein. Three days after the final boost, mice were euthanized by CO_2. Final blood was collected by heart puncture.

3.2.3 Gene gun immunization of rats

Rats were genetically immunized using the Helios® Gene Gun system. Gene Gun ammunition was prepared as follows: 50 μg cDNA expression vectors were diluted in 50 μl Tris-EDTA. 100 μl spermidine was added and the mix was used to resuspend 25 mg gold particles, vortexed and incubated in an ultrasonic bath for 1 min. To precipitate DNA, 100 μl of $CaCl_2$ was added dropwise while vortexing, and the mixture was incubated for 10 min. Solution was centrifuged at 16.000 rpm at 4°C. Supernatant was discarded. Gold particle pellet was washed with 1 ml absolute ethanol and subsequently with 1 ml PVP-ethanol. Pellet was resuspended in 3 ml PVP-ethanol. Tefzel tubing was washed with absolute ethanol and dried using N_2-gas and applied to the tubing preparation apparatus. Vortexed DNA-conjugated gold particles were sucked into the tubing using a syringe, and DNA was sedimented for 3 min without gas supply. Tubing was rotated while being dried with N_2-gas, then cut into 20 mm cartridges using the tubing cutter apparatus. Cartridges were stored under dry conditions at 4°C in the presence of a silica pack. Prior to the first (pre-immune serum) and after the third immunization (immune-serum), blood was drawn to estimate the immunization success by immunofluorescence microscopy or flow cytometry of target transfected CHO cells.

Rats were anesthetized using isoflurane and fixed on a heating pad on their backs. Belly skin hair was shaved with clippers and a depilatory cream to remove residual hair which otherwise blocks gold particle penetration into the skin. Rats received 6

gene gun shots on the abdominal skin at 250-300 psi gas pressure. The quality of gold particle delivery was estimated by brownish, non-removable coloring at the site of application. The final boost immunization was carried out with 10^7 transiently transfected HEK cells 3 days before sacrifice.

3.2.4 Hybridoma fusion of splenocytes of immunized rats

Monoclonal antibodies were isolated from an immunized rat using hybridoma technology. Immunized rats were euthanized with CO_2 and final bleed was taken by heart puncture. Spleen was dissected with sterile instruments and placed on a 70 µm-cell strainer, minced with sterile scissors, and passed through the filter with a syringe plunger. Filter was rinsed with RPMI Medium. Cells were centrifuged and resuspended in RPMI Medium. HAT-sensitive SP2/0 myeloma cell line was cultivated in RPMI complete with β-mercaptoethanol and gentamycin. SP2/0 cells were harvested by centrifugation and resuspended in RPMI medium. 10^7 spleen cells were mixed with $3*10^7$ SP2/0 cells and pelleted again. Supernatant was discarded and pellet was loosened by tapping. PEG was added dropwise for 1 min while swirling gently. PEG replaced the water between the cells to allow for random fusion events between myeloma cell and lymphocyte. Mixture was supplied dropwise with 10 ml RPMI complete and centrifuged for 10 min at 1600 rpm. Pellet was resuspended in 5 ml RPMI+ gentamycin and 1 ml was used for plating; the other 4 ml were frozen in N_2. 0.5 ml were mixed with 80 ml HAT-Medium and plated on four 96-well plates, the other 0.5 ml were mixed with 160 ml HAT-Medium and plated on 8 96-well plates to generate two different cell densities. Hybridomas were grown for 10 days at 37°C. Growing colonies were inspected visually and were resuspended with a pipette. 80 µl cell suspension were transferred to new 96-well plate containing 200 µl HT-medium. 40 µl were again transferred with a multichannel pipette to obtain a copy of the test plate named ‘culture plate’ into 200 µl HT-medium. After four days of culture, medium of the ‘test plate’ was analyzed for specific antibodies by immunofluorescence microscopy of transiently transfected HEK or CHO cells. Wells which contained positive clones were further cultured in 24-well and 6-well dishes. Hybridomas confirmed to be positive were subcloned by limiting dilution to obtain a single clone.

3.2.5 Preparation of cell lysates for RNA preparation

Mouse spleen as well as axial, inguinal and cervical lymph nodes were prepared with sterile dissection instruments and stored on ice cold PBS -/-. Tissue was minced with scissors on a 70 μm nylon cell strainer and mashed with a plunger to obtain a single cell suspension. Cells were washed with 10 ml PBS -/- and aliquoted á 10^7 cells in 1.5 ml tubes. The cells were pelleted by centrifugation at 1600 rpm for 5 min. Pellet was loosened by tapping and carefully resuspended in 350 μl RA1 lysis buffer (NucleoSpin® RNA Kit) + 3.5 μl β-mercaptoethanol. Cell lysates were snap frozen in liquid nitrogen and stored at -80°C until RNA preparation.

3.2.6 Preparation of RNA from cell lysates

RNA from cell lysates were prepared according to manufacturer's instructions using the NucleoSpin® RNA mini kit. Eluted RNA concentration was quantified by nanodrop and stored at -80°C.

3.2.7 Specific reverse transcription-PCR of LaMice VHH fragments

Reverse transcription of total RNA into cDNA was carried out using the following reagents.

Amplificate	**Primer**
Lama IgM	TE#150
Lama IgG2b	TE#154

Component	**Volume [μl]**
RNA (1.5 μg)	x
Reverse primer (10 μM)	1
dNTPs (100 mM)	0.1 μl each
ddH_2O	to 38
Total	40

The reverse primers used were specific for llama IgM and llama IgG. All components were mixed and incubated for 10 min at 65 °C and then cooled to 4°C for 5 min. 10 µl RNA-mix were size fractionated by agarose gel electrophoresis to determine RNA quality.

The residual RNA-Mix was further mixed with the following reagents and incubated for 10 min at 55°C followed by 10 min at 80°C to generate cDNA. cDNA was purified using the Gel and PCR clean up kit and stored at -20°C.

Component	**Volume [µl]**
RNA-mix	30
RNAseOut	1
First strand buffer (5x)	8
DTT (0,1 M)	1.5
Superscript IV RT (200 U/µl)	1
Total	25

3.2.8 Polymerase chain reaction

The general polymerase chain reaction (PCR) was mixed by combining the following reagents. The amount of DNA was adjusted for each experiment.

Component	**Volume [µl]**
ddH_2O	9.75 - X
Q5 Puffer (5x)	5
Q5 High GC Enhancer (5x)	5
dNTPs (2 mM each)	2.5
Primer fwd (10 µM)	1.25
Primer rev (10 µM)	1.25
DNA	X
Q5 Polymerase	0.25
Total	25 µl

PCR products were separated via gel electrophoresis to analyze amplification success and bands of the appropriate size were cut out with a scalpel and purified using the PCR and DNA clean up kit (MN)

3.2.9 PCR1 to amplificate nanobody coding regions from llama IgG and llama IgM of LaMice

To specifically amplify nanobody coding regions from 5 µl o llama IgM and llama IgG cDNA, the following PCR reaction was carried out:

Primer	Llama IgM	Llama IgG
forward	TE#161	TE#161
reverse	TE#149	TE#153

Temp (°C)	Duration	cycles
98	30	
98	10	
63	30	30x
72	60	
72	300	
4	∞	

3.2.10 PCR2 to add restriction sites to nanobody coding regions

PciI and NotI restriction sites were introduced to nanobody coding regions via PCR using the following reagents and 50 ng purified PCR1 product.

Primer	Llama IgM	Llama IgG
forward	TE#161	TE#161
reverse	TE#149	TE#153

Temp (°C)	Duration	cycles
98	30	
98	10	
65	20	30x
72	60	
72	300	
4	∞	

3.2.11 PCR3 to add linker and barcode sequences to nanobody libraries for NGS analysis

Universal linkers were introduced 5' and 3' to nanobody libraries by PCR using the following reagents and 50 ng purified PCR2 product:

Primer	ID
forward	TE#158
reverse	TE#159

Temp (°C)	Duration (s)	cycles
98	30	
98	10	
55	30	4x
72	60	
98	10	
67	30	30x
72	60	
72	600	
4	∞	

With the following Barcode PCR, Nucleotide barcodes were added to VHH libraries for NGS. 50 ng of purified Linker PCR product were used:

Primer	ID
forward	TE#158
reverse	Barcode primer

Temp (°C)	Duration	cycles
98	30	
98	10	
67	30	30x
72	60	
72	600	
4	∞	

3.2.12 NGS Sequencing of nanobody libraries

Nanobody libraries from immunized LaMice were PCR-amplified as described in the preceding sections. Nanobody libraries, supplied with linker, adapter and specific barcode sequences were pooled equimolarly, quality checked with a Bioanalyzer instrument and sequenced by the UKE core facility team 'immune repertoire sequencing'; in person, Nuray Akyüz and colleagues, using the Illumina Miseq System. Further data processing was performed by Stephan Menzel, UKE. MiSeq

data output was analyzed with MiXCR (Bolotin et al. 2015). The UKE bioinformatics facility (Malik Alawi) supplied data manipulation workflows.

3.2.13 P2RX5 genotyping

To genotype the SNP rs891746 in the human P2RX5 gene 100 µl of blood were drawn by dermal capillary puncture. Genomic DNA was purified using the DNEasy Blood and Tissue Kit following the manufacturer's instructions. 100 ng genomic DNA were PCR-amplified using the following primers and cycle temperatures:

Primer	ID
forward	P2X5 genotyping fwd
reverse	P2X5 genotyping rev

Temp (°C)	Duration	cycles
98	30	
98	10	
55	30	30x
72	45	
72	120	
4	∞	

The PCR amplificate was purified by gel electrophoresis followed by a PCR and DNA clean up step according to the manufacturer's instructions. DNA was subjected to Sanger sequencing using the P2X5 sequence primer (compare **3.2.19**).

3.2.14 Agarose gel electrophoresis

Digested or PCR amplified DNA was separated by agarose gel electrophoresis. For a 1% agarose Gel, 1 g of agarose was heated in 100 ml TAE-Buffer until fully dissolved. Liquid agarose was mixed with 5 µl RotiSafe and poured into a mold with an appropriate comb. DNA was supplied with 6x Loading Dye and pipetted into every second well of the gel to reduce spillover and contamination. DNA was size fractionated at 100 Volt. Gene Ruler 1 kb was used to estimate the size of separated DNA.

3.2.15 Extraction of DNA from agarose gels and PCR reactions

Electrophoreticaly separated DNA from agarose gels or PCR reactions was purified with the NucleoSpin PCR and DNA Clean-up. In short, agarose gel size-fractionated DNA was placed on a UV transilluminator, and bands were cut with sterile scalpels. Gel pieces were dissolved in NTI buffer and purified via the supplied column following the manufacturer's protocol. Eluted DNA concentration was determined and stored at 4°C until use.

3.2.16 Enzymatic restriction digestion

Purified DNA was digested enzymatically with restriction enzymes that cut specific palindromic sequences. Digestion reactions were mixed in 20 µl total volume with 1 U of the respective restriction enzymes. A double digestion with two restriction enzymes can be applied, when both enzymes have the same activity in the appropriate buffer. For example, NEB's '-HF' Enzymes are 100% active in the CutSmart buffer system.

3.2.17 Ligation of DNA

Ligation of restriction enzyme-digested nanobody libraries or DNA inserts were carried out as follows in a vector-to-insert ratio of 1:3. Total DNA concentration was kept below 10 ng/µl.

Component	**Volume [µl]**
DNA insert	X
Open Vector	100 ng
T4-Ligase®	1
T4-Ligase® Buffer	3
ddH_2O	Ad 30

Temp (°C)	**Duration**
16	14 h
65	10 min
4	∞

Ligation product was directly used for heat shock transformation or purified with the PCR and DNA clean up kit (MN) and eluted in ddH_2O when electroporation followed.

3.2.18 Phage Display technology

In this work nanobody immune libraries from a P2X7 immunized *Lama glama* (405) were already present in the pAX50 phagemid as TG1 *E. coli* stocks prepared by Welbeck Danquah (Danquah 2012). In short, phage display was performed as follows: TG1 *E. coli* were grown in medium until log phase and infected with KM13 helper phage. Produced phages were subjected to negative selection on untransfected and subsequently for positive selection on transiently transfected HEK cells. After substantial washing, phages were eluted from the cells by trypsination and re-amplified in native TG1. The resulting phage library was subjected to a second round of panning.

3.2.18.1 Production of helper phage

Native TG1 *E. coli* were grown in 70 ml 2xYT medium w/o antibiotics to OD_{600} = 0.4 and infected with 5 µl KM13 phage stock at 37°C without shaking for 60 min. Kanamycin was added 1/1,000, and phages were produced over night at 37°C at 220 rpm shaking. Bacterial suspension was centrifuged at 4600 rpm for 15 min. Phages were precipitated from the supernatant by mixing 35 ml supernatant with 8.75 ml PEG/NaCl. Phages were precipitated for four hours rolling at 4°C and centrifuged at 4,600 rpm for 10 min. Pellet was resuspended in 1 ml $PBS^{-/-}$, transferred to a microtube, and centrifuged at 14,000 rpm at 4°C several times to remove insoluble pelleted material. Precipitation was repeated using 250 µl PEG/NaCl per ml of phages. After 30 min on ice, phage pellet was resuspended in 1 ml $PBS^{-/-}$ and repetitively centrifuged until no more precipitated pellet was observed.

3.2.18.2 Determination of infectious phage titer

The infectious titer was determined by infection of exponentially growing native TG1 *E. coli* with titrated phages. In a 96-well plate, 95 µl of TG1 *E. coli* were infected with 5 µl serially diluted phages (1:10 in $PBS^{-/-}$-BSA) and incubated for 30 min at 37°C. 5 µl infected *E. coli* were transferred to LB agar plates containing kanamycin (for helper

phage titer) or carbenicillin (for immune-library phages). After overnight incubation, grown colonies were counted.

3.2.18.3 Production of Nb-displaying phages

Production of phages containing nanobodies on the surface was similar to the production of helper phages. TG1 *E. coli* libraries incorporating the phagemid were grown in 10 ml 2xYT/carb/glu to an OD_{600} from 0.1 to 0.4. TG1 were infected with a multiplicity of infection (MOI) of ten and incubated for 30 min at 37°C without shaking. Additional 30 min at 37°C shaking allowed expression of the kanamycin resistance of infected *E. coli*. Suspension was centrifuged at 4000 rpm for 10 min, washed once with 2xYT medium and centrifuged again to remove glucose. Pellet was resuspended in 50 ml 2xYT with carbenicillin and kanamycin and incubated over night at 28°C shaking at 180 rpm to produce nanobody phages. Phages were purified as described in the 'Production of helper phage' section. Infectivity of phages carrying a nanobody was estimated by infection of native TG1 *E. coli* and plating on LB agar plates containing carbenicillin. The carbenicillin resistance is encoded on the pAX50 phagemid vector.

3.2.18.4 Cell panning of phage libraries

Selection of nanobodies for mouse and human P2X7 binders was carried out on transiently transfected HEK293-T cells. First, $1x10^{10}$ phages were incubated in complete DMEM for 1 h while the cells were prepared. HEK293-T cells were harvested by trypsination and blocking in complete DMEM. Cells were washed twice with complete DMEM to get rid of residual trypsin. $1x10^{10}$ blocked phages were mixed with $1x10^{6}$ untransfected HEK cells for negative selection and incubated for 1 h at 4°C rolling. HEK cells were pelleted by centrifugation at 1,600 rpm for 5 min. Supernatant was carefully aspirated and centrifuged again. Supernatant was then subjected to untransfected HEK cells and mouse or human P2X7 transiently transfected HEK cells. Cells were rolled for 1 hour at 4°C and pelleted by centrifugation at 1,600 rpm for 5 min. HEK cells were resuspended in 10 ml DMEM and centrifuged again. This

procedure was repeated 15 times in total. Pelleted cells were washed twice with $PBS^{-/-}$ and resuspended in 500 µl 1x trypsin. After incubating for 15 min at RT, cells were pelleted at 13,000 rpm. 500 µl supernatant containing eluted phages was mixed with 50 µl AEBSF + 0.1% BSA. 5 ml exponentially grown native TG1 *E. coli* were then infected with 400 µl eluted phages for 30 min at 37°C without shaking and an additional 30 min while shaking at 180 rpm. 5 µl (1/5,000) and 1 µl (1/20,000) of infected *E. coli* was plated on LB/carb/glu agar to determine library size. Residual *E. coli* were plated on multiple 2xYT/carb/glu agar plates and harvested the next day by scraping and pooling of grown colonies. TG1 libraries were stored as glycerol stocks or infected with helper phage to produce nanobody phages for the next round of panning.

3.2.19 Sanger sequencing of plasmids or PCR amplificants

DNA Sequencing was performed using the commercial Eurofins Genomics Sanger sequencing service. The following mix was prepared and sent in barcoded tubes:

Component	Volume [µl]
DNA (0.5 - 1.5 µg)	X
Sequencing primer (100 µM)	2
ddH_2O	Ad 17

Sequences were provided as files, including the sequencing quality to be downloaded from the eurofins genomics website. Sequences were analyzed using SnapGene (Dotmatics) and 4Peaks (nucleobytes).

3.2.20 Chemo-competent XL1 Blue *E. coli*

To generate chemo-competent bacteria, 5 ml 2xYT-Medium were inoculated with a colony of a fresh stock of XL1 Blue *E. coli* grown overnight on LB-agar without antibiotics. Cells were pelleted after overnight culture by centrifugation at 4,600 rpm and resuspended in 5 ml 2xYT Medium. 1 ml of the suspension was used to inoculate 50 ml 2xYT Medium in a shaker flask and grown until exponential phase (OD_{600} of 0.3-0.4). Cells were pelleted by centrifugation at 4,600 rpm, resuspended in 100 mM $CaCl_2$ and pelleted again. *E. coli* were resuspended in 1 ml 100 mM $CaCl_2$ + 15% glycerol in

$PBS^{-/-}$ and incubated for 1h on ice. Cells were aliquoted à 100 µl and stored at -80°C until use.

3.2.21 Transformation by heat shock

Heat shock transformation of bacteria was performed as follows: 25 µl chemo-competent *E. coli* was mixed with 100 ng plasmid DNA and incubated for 15 min on ice. Cells were subjected to a hot water bath (42°C) for 30 sec and cooled down to 4°C again for 2 min. Mix was supplied with 500 µl SOC medium and incubated at 37°C for 1 h shaking. 50 µl solution were streaked on LB agar plates containing appropriate antibiotics. Residual *E. coli* were centrifuged, pellet was taken up in 50 µl SOC and streaked on an additional LB agar plate + antibiotics as well to obtain 10 times more colonies.

3.2.22 Transformation by electroporation

Electroporation of nanobody-libraries into electrocompetent TG1 *E. coli* was performed as follows: TG1 cells were thawed on ice. 25 µl aliquots of TG1 were supplied with 2 µl of desalted ligation product, mixed by flicking and then placed on ice. Mix was transferred to ice cold electroporation cuvettes and electroporated using the 'EC1' setting on a MicroPulser Electroporator.
Mix was immediately resuspended in 975 µl SOC recovery medium and incubated for 60 min at 37°C shaking. 50 µl were streaked on an LB agar plates containing appropriate antibiotics. Residual *TG1* were centrifuged and streaked on additional agar plates to be scraped the next day.

3.2.23 DNA preparation of bacterial cultures

Plasmid-DNA from *E. coli* overnight cultures was prepared using the commercially available kits and solutions from Macherey-Nagel. In short, 2xYT-Medium was inoculated with one colony of plated *E. coli* and grown overnight. *E. coli* was harvested by centrifugation. Medium was discarded and *E. coli* was taken up in resuspension

buffer, lysed for 5 min and neutralized. Insoluble precipitate was discarded, and solution was purified using the supplied columns or precipitated with isopropanol for 96-well DNA preparation. Pelleted DNA was washed with 70% Ethanol, centrifuged, dried, and resuspended in TE-Buffer. DNA was stored at 4°C for short term or -20°C for long term storage.

3.2.24 Mammalian cell culture

Maintenance of CHO, non-/adherent HEK293-6E and HEK293-T, and SP2/0 mammalian cells was executed under sterile conditions on a laminar flow bench. Cell culture media additives were sterile filtered before being added to the respective Media (DMEM, RPMI, F17 293). Adherent mammalian CHO and HEK293-T cells were cultured in FCS-containing complete DMEM. For subculturing, cells were washed with $PBS^{-/-}$ before subjection to 1/10 of culture volume of Trypsin-EDTA and incubation for 5 min at 37°C. Trypsin was inactivated with 5 times the volume DMEM complete and centrifuged at 1600 rpm. Supernatant was discarded, cells were resuspended in DMEM complete, diluted 1/5-1/10 and cultivated for 2 to 3 days until the next passage. Non-adherent myeloma cell line Sp2/0 was cultivated in RPMI complete medium by splitting 1/15 every 2 to 3 days in fresh medium until the next passage.
Non-adherent HEK293-6E cells were maintained in FreeStyle 293 Expression Medium. Adherent HEK293-6E cells were maintained in F17 complete medium.
Cell concentrations were determined with a Neubauer cell chamber. 10 µl cell suspension was mixed with 90 µl Trypan blue and 10 µl were pipetted into one cleft of the chamber. Cells were counted, excluding the dead cells which took on the blue dye. The cell concentration in cells/ml is the counted number of cells times 10,000 divided by the number of squares * dilution factor.

3.2.25 Transient transfection for surface expression of proteins

CHO or HEK293-T cells were transfected at 50-70% confluency one day after passaging. Here an exemplary transfection of 5 ml is outlined. The protocol can be adjusted to higher culture volumes with a 1:1 ratio. 5 µg plasmid DNA was mixed with

150 mM NaCl to a final volume of 250 µl and vortexed shortly. In parallel, 20 µl PEI reagent (0.32 mg/ml stock) was mixed with 150 mM NaCl to a final volume of 250 µl and vortexed shortly. PEI Mix was added dropwise to the diluted DNA, vortexed for 30 seconds, and incubated for a further 20 mins. 500 µl PEI-DNA mix was added dropwise directly onto the cells. Transfection efficiency was monitored by co-transfection with an expression vector for nuclear-localized GFP (GFP-NLS) in a ratio of 1:10. Transfection success was analyzed by observing GFP expression via fluorescence microscopy.

3.2.26 Transient transfection for protein production

Production of nanobodies and nanobody-hcAbs was carried out using transient transfection of non-adherent and adherent HEK293-6E cells and the pCSE2.5 eucaryotic expression vector. The transfection mix composition was identical to that for the transfection for surface-expressed proteins, except for omitting the GFP-NLS transfection control (see **Section 3.2.25**). His-tagged nanobody constructs were produced in non-adherent HEK293-6E cells in FreeStyle 293 expression medium without feeding medium supplementation.

Fc-fusion proteins were produced in adherent HEK293-6E. Cells were passaged and transfected the next day at around 40-60% confluency in the appropriate medium. Culture medium was exchanged against FCS-free F17 transfection medium shortly before transfection. One day post transfection, adherent HEK293-6E were supplemented with F17 feeding medium.

3.2.27 Confocal microscopy

CHO cells were seeded on an Ibidi µ-Dish one day before transfection. Cells were transfected according to **Section 3.2.25**. 24-48 h after transfection, cells were washed once with 10 ml $PBS^{+/+}$ and fixed with 100 µl 2% PFA for 10 min at room temperature. Fixed cells were washed twice with $PBS^{+/+}$, and images of expressed GFP fusion proteins were acquired using a spinning-disk confocal microscope (Visitron), a 100x

magnification objective (Zeiss) and a sCMOS camera (Orca-Flash 4.0, C13440-20CU Hamamatsu). Images were analyzed using ImageJ.

3.2.28 Immunofluorescence microscopy

For immunofluorescence microscopic analysis of pre- and immune sera of immunized rats and other antibodies, CHO cells were transiently transfected with the target antigen and nuclear GFP as a transfection control in T25 flasks according to **Section 3.2.25**. Cells were harvested one day later and seeded on 96-well plates. 2 days post transfection, CHO cells were fixed using 2% PFA for 10 min at room temperature. Cells were washed twice with $PBS^{+/+}$. Rat pre- and immune sera were diluted in DMEM complete and incubated for 30 min. Cells were carefully washed twice using 250 µl $PBS^{+/+}$ and incubated with 100 µl PE-conjugated polyclonal rat IgG-specific secondary antibody (1/500) in DMEM complete for 30 min. For the last 5 min, 5 µl DAPI (1 mg/ml) was added to stain all nuclei. Cells were washed twice with 200 µl $PBS^{+/+}$ Images were analyzed using ImageJ.

3.2.29 SDS-Page & Coomassie staining

HEK293-6E supernatants were analyzed after transient production via sodium dodecyl sulfate polyacrylamide gel electrophoresis (SDS-PAGE). 10 µl supernatant were mixed with 5 µl LDS Sample buffer (4x), 2 µl reducing agent (10x) and 3 µl ddH2O, then heated for 10 min at 70°C. Samples were applied to NuPAGE 10% Bis-tris mini precast gels and separated for 30-40 mins at 200 Volt. Gels were lifted from the casting mold and submerged in Instant blue Coomassie staining for 1 h and subsequently in ddH2O for de-staining overnight. Application of the in-house Super Marker (75 µg/ml IgG, 100 µg/ml BSA; 10 µg/ml Lysozyme) allowed the estimation of protein amounts and molecular weight in HEK293-6E supernatants.

3.2.30 Purification by affinity chromatography (Protein A/G, Ni-NTA)

Antibodies from HEK293-6E supernatants were purified using affinity chromatography. After estimating the amount of protein present in the supernatant after SDS PAGE analysis, appropriate amounts of affinity matrix were used not to exceed its capacity. His-tagged proteins were purified using immobilized metal affinity chromatography (IMAC) with nickel NTA (Ni-NTA) Sepharose (capacity 15 mg/ml for a 30 kDa protein). Fusion proteins carrying an Immunoglobulin Fc were purified using Protein A or protein G Sepharose (20 mg/ml for human IgG). Gravity flow columns were filled with affinity gel and washed three times with 10x column volume (cv) $PBS^{-/-}$. HEK293-6E supernatants were applied and run through the matrix by gravity flow. The matrix was washed again with 10x cv $PBS^{-/-}$. Elution buffer was applied, and three separate fractions were taken. Elution buffer for His-tagged proteins contained 250 mM Imidazole in $PBS^{-/-}$. Fc-fusion proteins were eluted by a low-pH elution buffer (pH 2.8), which was immediately neutralized by pre-loading the collection tubes with 1M Tris (pH 9). Fractions of every flow-through were taken to estimate purification efficiency by SDS-PAGE. Resin-packed columns were regenerated for later reuse by elution of all remaining bound proteins with eight cv of elution buffer and subsequently with 10 cv $PBS^{-/-}$.

3.2.31 Buffer exchange and concentration of purified proteins

To exchange the buffer components of Protein A- or Ni-NTA-eluted proteins, Sephadex G-25 PD-10 desalting columns were used. Storage buffer was released by gravity flow. Column was washed with 4 cv $PBS^{+/+}$ and purified fractions were applied. After entering the packed bed, proteins were eluted with 3.5 ml $PBS^{+/+}$. Eluted proteins were concentrated with Amicon ultra centrifugal filters with an appropriate molecular weight cut off (MWCO).

3.2.32 Enzyme-linked immune sorbent assay

To evaluate the specificity of pre- and immune sera as well as antibodies, an enzyme-linked immune sorbent assay (ELISA) was applied. 100 ng of target protein and control

antigens in 100 µl PBS were coated on a 96-well MaxiSorp plate overnight. Plates were blocked with 250 µl blocking buffer for 1 h. HEK293-6E supernatants were diluted 1/20, and pre- and immune sera were titrated in blocking buffer. 100 µl of sample was added to the wells and incubated at RT on a shaker. Plates were washed three times with 250 µl washing buffer by addition of buffer and beat out over the sink. 100 µl HRP-conjugated secondary antibody diluted 1/1,000 was applied and incubated for 30 min on a plate shaker at RT. Plates were washed four times and subjected to 100 µl of TMB substrate per well. After 15-30 min of incubation at RT, reaction was stopped with 50 µl sulfuric acid. OD_{450} was measured on a Victor plate reader (Perkin Elmer).

3.2.33 Conjugation of antibodies to biotin and fluorescent dyes

Proteins were functionalized by conjugation to EZ-Link™ Sulfo-NHS-LC-Biotin for immobilization on the surface of biolayer interferometry sensors. Purified proteins were labeled with a 20-fold molar excess of biotin following manufacturer`s protocol. To remove unconjugated biotin, proteins were desalted using Zeba™ Spin desalting columns following the manufacturer`s protocol. The functionality of biotinylated proteins was evaluated by binding to streptavidin-conjugated BLI sensors.
Fluorescent dye conjugation (e.g. Alexa Fluor 647, A647) was carried out following the manufacturer`s protocol. In short, 1 mg of monoclonal antibody was mixed with 1/10th1 M sodium bicarbonate and applied to the vial containing the fluorochrome. Conjugated antibodies were purified by desalting columns to remove free dye. Degree of fluorochrome labeling was estimated by nanodrop. Fluorochrome-conjugated antibodies were evaluated by titration on cells with transiently transfected target protein.

3.2.34 Biolayer interferometry

Protein-protein interactions were analyzed using Biolayer Interferometry (BLI). The BLItz system (Sartorius) uses functionalized biosensor tips which are sequentially dipped in various solutions, followed by measurement of the reflection of light on the sensor tip. The signal intensity is proportional to the number of molecules that are

bound to the sensor. With this dip-and-read technology, real-time measurements of protein-protein interactions can be observed. **Figure 3.1** shows a general BLI assay to determine nanobody affinity. Functionalized biosensors (e.g. streptavidin-conjugated) were submerged in kinetics-buffer to release the protective sensor coating. After a short buffer step, the sensors were dipped in a protein-solution (e.g. biotinylated mouse IgG), which bound to the sensor until saturation. Sensors were dipped in buffer to release non-bound protein and subsequently incubated with the protein of interest (e.g. VHH-anti mouse IgG) to analyze association (k_{on}). During a following dissociation step in kinetics-buffer, the dissociation rate (k_{off}) was determined. By dividing k_{off}/k_{on} the affinity (K_D) of the protein-protein interaction was calculated. Affinities were calculated by curve fitting the association and dissociation phases using GraphPad Prism 9. By loading different biotinylated antibody isotypes, the specificity of the associated VHH was determined.

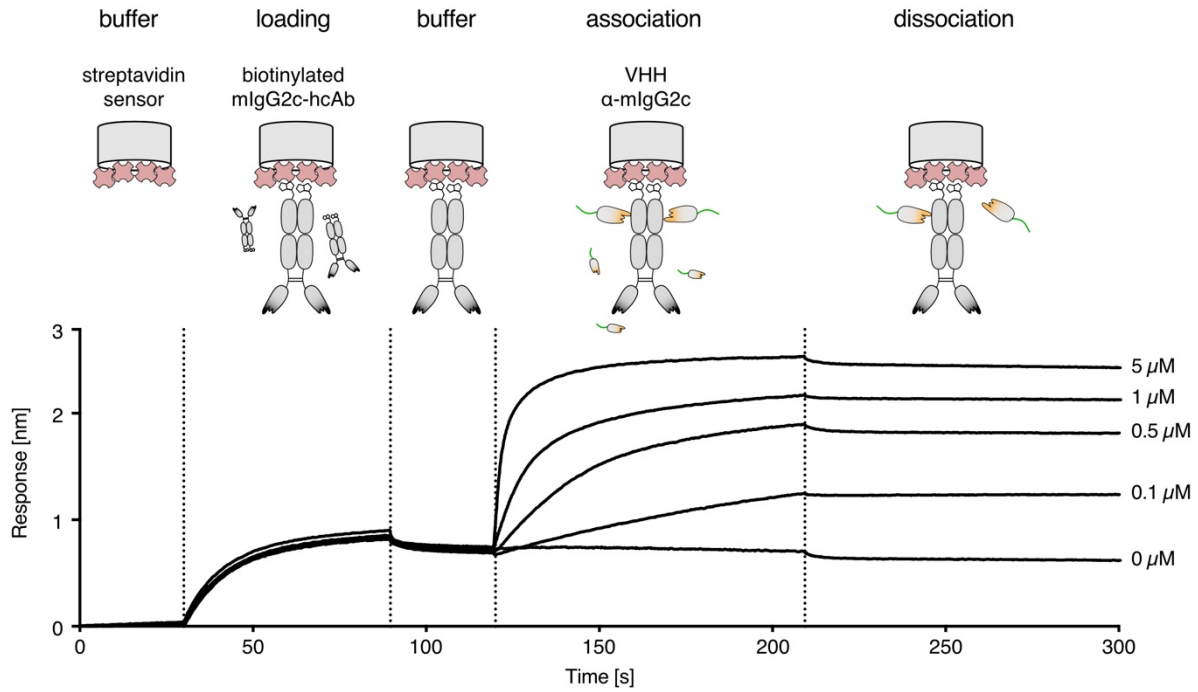

Figure 3.1 Schematic of a biolayer interferometry assay to determine nanobody affinity. Streptavidin sensors are dipped into buffer and subsequently loaded with biotinylated mIgG2c hcAbs. After a second buffer step to observe the loading stability, anti mIgG2c nanobody monomers are associated in a range of concentrations. During the last step, the dissociation of the nanobodies can be observed.

3.2.35 Flow cytometry

Single cells in a diverse mixture of cell populations can be analyzed using flow cytometry. In general, cell suspensions were labeled directly with fluorochrome-conjugated antibodies or with antibodies and corresponding fluorochrome-labeled secondary antibodies. Cells of a mixture were analyzed individually by using a thin microfluidic system. Cells are hit with a laser with defined wavelength which excites the fluorophores of bound antibodies. Photons emitted from the fluorophores were detected and enhanced via photomultipliers. The detection of light scatter allows estimation of the size and granularity of cells. By using several lasers and defined wavelength filters, multiparametric analysis can be performed. However, it is important to pair low abundant cell surface molecules correctly with bright fluorochromes, and to compensate fluorophore emissions correctly.
In this work diverse analyses were carried out using this method, e.g. the analysis of VHH-rbIgG hcAbs binding HEK293-T cells transiently transfected with mP2X7 or hP2X7.

3.2.36 Epitope binning

To evaluate if two different antibodies detect the same epitope, an epitope binning experiment was applied using flow cytometry.
In general, cell stainings were prepared in 96-well format or FACS-tubes. 100 µl cell suspensions were supplied with 20 µl antibody- (VHH-mFc hcAb-) containing HEK6E cell culture supernatants, control antibodies, or plain medium to block cell surface binding sites, and incubated for 20 min. 5 µl detection antibody (VHH-rbFc hcAb) containing HEK6E cell culture supernatant was added and incubated for 10 min. HEK-cells were washed three times with FACS-buffer and supplied with an A647-conjugated polyclonal rbIgG-specific secondary antibody. After washing twice with 2 ml FACS-buffer, HEK cells were analyzed using a flow cytometer.

3.2.37 Antibody dependent cellular cytotoxicity assay

To investigate the blocking efficiency of the MU1067-specific binder, a bispecific killer cell engager- (BiKE-) dependent cellular cytotoxicity assay was performed.
The BiKE used in this assay is trimeric nanobody constructs, consisting of a nanobody binding to CD16a on the surface of NK92 natural killer (NK) cells and a nanobody binding to CD38 (MU1067) on the target myeloma cell line. The third nanobody targeting albumin enables a longer serum half-life of the BiKE. In this assay luciferase expressing LP-1 Luc cells were used as a target, to allow a readout of killing efficiency. Simultaneous binding of CD16 and CD38 links killer cell and target cell and permits release of perforins, ultimately resulting in the killing of the target cell.
CD16-expressing $CD38^{-/-}$ NK92 cells were loaded with either α-CD38 BiKE or an isotype control BiKE (s-14) for 15 min at RT. Bike-Loaded NK92 cells were washed with PBS-/- and further incubated with MU1067-specific nanobody-rbIgG hcAbs for another 15 min to block the αCD38 nanobody MU1067. 30,000 LP-1 Luc target cells were loaded with luciferin solution in a 96-well plate and incubated for 20 min at 37°C. 50 μl loaded and blocked NK92 cells were added in an effector to target ratio of 3 to 1 in triplicates. The bioluminescence signal was determined every 15 min at 37°C.

3.2.38 Pharmacological BAT remodeling

Mice were injected on three consecutive days with 10 mg/kg etomoxir and 1 mg/kg CL316,243 (Eto&CL). For investigation of P2X7 involvement, 13A7-dim-αAlb was injected (70 μg/mouse) i.p. 4 h before Eto&CL treatment. Mice were sacrificed 24 h after the third Eto&CL injection. For immunohistochemistry analysis, BAT tissues were prepared and fixed with 3.7% formaldehyde and paraffin embedded. H&E staining was performed as described above (Fischer et al. 2019). Macrophages were stained using rat anti-MAC2 and secondary antibody HRP-anti-rat-Ig. Nuclei were counterstained using hematoxylin. Pharmacological treatments and histology stainings were performed by Michelle Yvonne Jäckstein, AG Heeren (UKE)

3.2.39 Flow cytometric analysis of macrophage infiltration

To distinguish BAT-resident from circulating cells, mice were anaesthetized and injected with 70 μg of anti-CD45-Per-CP antibody prior to sacrifice and preparation of BAT. The anti-CD45 antibody stains all immune cells present in blood vessels, but does not penetrate into tissues in the short time between injection and sacrifice. Mice were perfused with PBS-/-. BAT was harvested, minced and digested with collagenase D and dispase II for 45 min at 37°C. Tissue homogenate was filtered, and stromal vascular fraction (SVF) was harvested by centrifugation. Cell pellets were taken up in erythrocyte lysis buffer and incubated for 3 min at RT. After washing and blocking Fc-receptors using anti-CD16/CD32, cells were incubated with mAb77 detecting the injected 13A7-dim-αAlb. Subsequently cells were stained with fluorochrome-conjugated antibodies for mIgG1 (BV421), CD45 (PE-Cy7), CD11b (A647) and a Live/DEAD™(APC-Cy7) staining to exclude dead cells. After washing, cells were analyzed by flow cytometry. Pharmacological treatment of mice and preparation of tissues were performed by Michelle Yvonne Jäckstein, AG Heeren (UKE)

3.2.40 Western blot analysis of BAT

Tissue homogenates were generated from BAT in 10x RIPA buffer using a tissue lyser (QIAGEN). After 10 min of centrifugation at 13,000 rpm, lysate without fat was isolated and protein amounts were quantified using a BCA kit. 20 μg protein were separated by SDS-PAGE and blotted on nitrocellulose membranes. Membranes were blocked with 5% milk in TBS-T. Primary rabbit anti-γ-Tubulin and rat anti-MAC2 antibodies were incubated over-night in TBS-T. After washing, bound primary antibodies were detected using the respective HRP-conjugated secondary antibody. Membranes were imaged using ECL on an Amersham Imager 600 (GE). Western blot analysis was performed by Michelle Yvonne Jäckstein, AG Heeren (UKE)

3.2.41 Immunofluorescence of differentiated brown adipocytes

Primary brown adipocytes were differentiated and cultured *in vitro*. Interscapular BAT of WT Balb/c mice was dissected and minced. After digestion and sedimentation on ice for 30 min, cells of the middle layer were passed through a 40 μm strainer and pelleted. Pre-adipocytes were resuspended in differentiation media and seeded in 12-well plates. Medium was changed daily for 6-8 consecutive days. Cells were rinsed with PBS -/-, fixed with PFA, and stained with 1/200 diluted pre- and immune sera (after third boost) of rats which had been genetically immunized with human and mouse P2X5 expression plasmids. After washing, PE-conjugated anti-rat-Ig secondary antibodies were incubated, and nuclei were counterstained with DAPI. Differentiation of adipocytes and immunofluorescent imaging was performed by Michelle Yvonne Jäckstein, AG Heeren (UKE).

3.2.42 Quantitative PCR of P2X4, P2X5 and P2X7 expression

Quantitative PCR (QPCR) analysis of P2X4, P2X5 and P2X7 was performed as follows: Adipose tissue was homogenized using a TissueLyser (QIAGEN). After addition of chloroform, cell debris was pelleted by centrifugation for 15 min at 13.000 rpm. RNA was isolated from the upper phase by Ethanol precipitation and purification using the NucleoSpin RNA II kit, following manufacturer's instructions. RNA was reverse transcribed into cDNA as described previously (Fischer et al. 2021). cDNA levels were determined by TaqMan® quantitative PCR using appropriate probes and normalized to tbp (TATA-box binding protein as a housekeeper gene). qPCR analysis was performed by Michelle Yvonne Jäckstein, AG Heeren (UKE).

4 Results

The Results chapter is divided into four separate sections. **Section 4.1** describes the generation of nanobodies specific for a nanobody-based mouse IgG2c hcAb from protein-immunized LaMice. **Section 4.2** covers the selection of nanobodies specific for mouse and human P2X7 (m/hP2X7) from phage display libraries of DNA-immunized *Lama glama*. **Section 4.3** describes the generation of polyclonal sera and a monoclonal antibody against human P2X5 (hP2X5) from DNA-immunized rats. The final **Section 4.4** covers the implementation of a transient functional double knockout of P2X4 and P2X7 via the nanobody-based inhibition of P2X7 in *P2rx4*$^{-/-}$ mice and its use to investigate the role of P2X4 and P2X7 in an inflammatory model of brown adipose tissue.

4.1 Discovery of nanobodies specific for VHH-mIgG2c hcAbs from LaMice by direct cloning

This chapter describes the generation of nanobodies against the Fc portion of mouse IgG2c and mouse IgA by immunization of llama-Ig-transgenic LaMice. The aim of these experiments was to use IgG2c and IgA as a model antigens to investigate the capability of LaMice to generate nanobodies against mammalian antigens in response to protein immunizations, and to compare the three generations of LaMice with regard to their capacity to respond to immunization. All LaMice generations (TE01, TE02, TE03) responded with a positive immune serum against the antigens. However, only NGS libraries and nanobodies from TE03 were analyzed in detail.

4.1.1 Protein immunization

Capacity of LaMice to generate nanobodies against mouse immunoglobulins was evaluated. To generate secondary reagents against the Fc-portion of mouse immunoglobulins, two hcAbs, MU1067-mIgG2c and I+10-mIgA hcAbs were used for immunization. MU1067-mIgG2c is a CD38-specific nanobody fused to the Fc portion of mouse IgG2c, and I+10-mIgA is a *Clostridioides difficile* toxin A (CDTA)-specific nanobody fused to the Fc portion of mouse IgA.

Two TE01, two TE02 and two TE03 LaMice were immunized with a mix of MU1067-mIgG2c and I+10-mIgA hcAbs in complete Freund's adjuvant (CFA) for the initial and incomplete Freunds adjuvant (IFA) for subsequent boost immunizations. Three days after the final boost, mice were euthanized, and blood, spleen and lymph nodes were harvested (**Figure 4.1.1 A**). Serum was analyzed for the presence of specific hcAbs using ELISA. The results indicate a range of antibody responses by LaMice to the two antigens. Serum from mice TE01-24 and TE03-32 did not show any detectable antibody response. The other four mice showed detectable antibodies specific for MU1067-mIgG2c. Two mice (TE02-28 and -29) also showed detectable antibodies specific for I+10-mIgA. None of the mice had any detectable serum antibodies that reacted with hen egg lysozyme (HEL), which was used as a negative control (**Figure 4.1.1 B**).

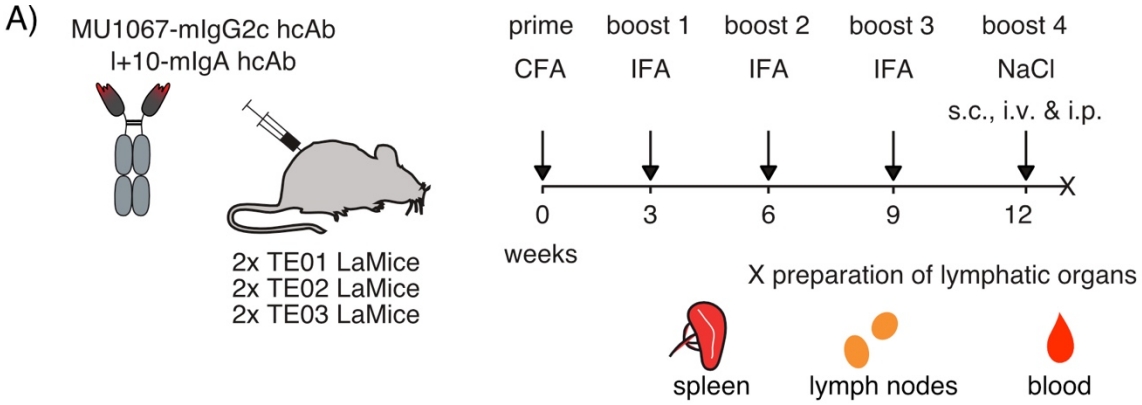
A)
MU1067-mIgG2c hcAb
I+10-mIgA hcAb
2x TE01 LaMice
2x TE02 LaMice
2x TE03 LaMice
prime
boost 1
boost 2
boost 3
boost 4
CFA
IFA
IFA
IFA
NaCl
s.c., i.v. & i.p.
0
3
6
9
12
X
weeks
X preparation of lymphatic organs
spleen
lymph nodes
blood

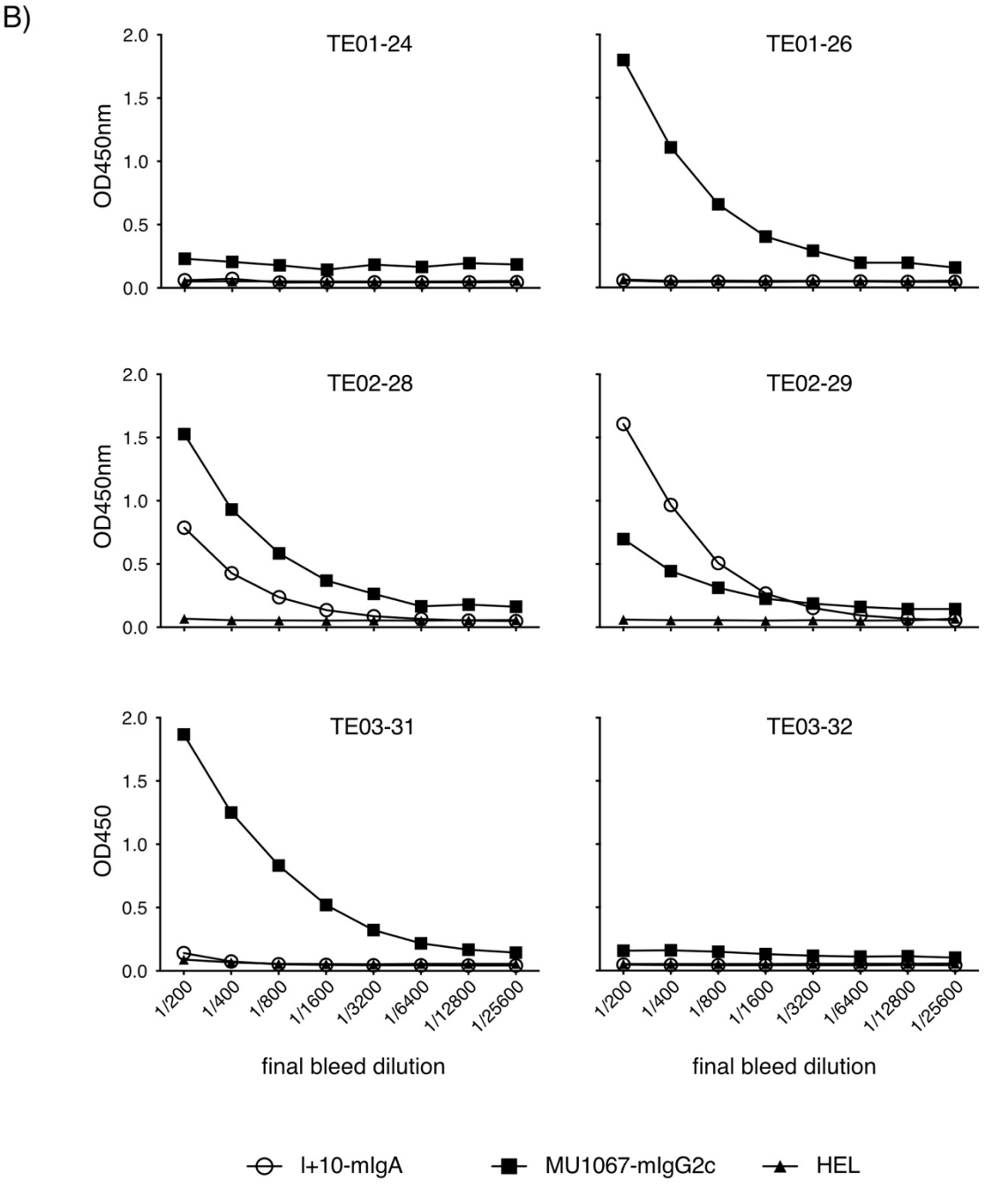
B)
TE01-24
TE01-26
TE02-28
TE02-29
TE03-31
TE03-32
OD450nm
OD450
2.0
1.5
1.0
0.5
0.0
1/200
1/400
1/800
1/1600
1/3200
1/6400
1/12800
1/25600
final bleed dilution
I+10-mIgA
MU1067-mIgG2c
HEL

Figure 4.1.1 LaMice elicit an antigen-specific serum antibody response after prime and boost immunization with VHH-hcAbs. A) Two LaMice of each generation (TE01, TE02 & TE03) were immunized five times in intervals of three weeks with MU1067-mIgG2c and I+10-mIgA hcAbs. The initial immunization was carried out by subcutaneous (s.c.) injection of the hcAbs together with CFA in a water-in-oil emulsion. IFA was used in the three following booster immunizations. For the final boost, the hcAbs were diluted in PBS and injected s.c., intraperitoneally (i.p.), and intravenously (i.v.) into the tail vein. Each immunization contained 30 μg MU1067-mIgG2c and 30 μg I+10-mIgA. Three days after the final boost, mice were sacrificed, and blood was drawn by heart puncture for serum preparation. Spleen and lymph nodes were dissected, minced, and single cell suspensions were lysed for RNA preparation. B) ELISA plates were coated with 100 ng of either MU1067-mIgG2c, I+10-mIgA or HEL. Wells were incubated with serially diluted LaMice serum in PBS. Bound llama hcAbs were detected with HRP-conjugated anti-llama IgG (H+L) polyclonal antibody.

4.1.2 Nanobody library generation for cloning and next generation sequencing

For nanobody library generation, the nanobody coding regions were PCR-amplified from spleen and lymph node RNA and cloned into a mammalian expression vector. Spleen and lymph nodes were minced, aliquoted and lysed separately. Total RNA was extracted, and RNA quality was evaluated by agarose gel electrophoresis (**Figure 4.1.2 A, left).** Two dominant bands at the expected sizes of 28S and 18S ribosomal RNA with an intensity ratio of 2:1 indicate high-quality RNA.

Specific reverse primers for llama IgM and llama IgG2b were used to reverse-transcribe the RNA into cDNA (**Figure 4.1.2 A, right**). By nested PCR, nanobody-encoding regions were amplified. In the first PCR step (PCR1), the VHH repertoires of llama IgM and llama IgG2b were amplified separately using a specific forward primer binding at the respective 5' end of the VHH-encoding region and reverse primers binding within the respective CH2-encoding regions. Amplification products were analyzed by agarose gel electrophoresis (**Figure 4.1.2 B**). Bands of expected size were detected in both, spleen and lymph nodes, and for both, llama IgM- and llama IgG2b-specific PCR products. However, band intensities were lower for IgG2b than for IgM in both, spleen and lymph nodes.

This PCR amplicon was then used as a template for a subsequent PCR (PCR2). Agarose gel electrophoresis analyses of PCR2 are shown in **Figure 4.1.2 C**. PCR2 introduced a 5' PciI and a 3' NotI restriction site that enabled cloning into the

mammalian expression vector pCSE2.5/s+16-dimer-rbIgG, which contained the coding sequences for a nanobody-rabbit IgG heavy chain antibody (rbIgG hcAb) (**Figure 4.1.2 D**).

To prepare the vector, the fragment coding for s+16 dimer was removed from the vector backbone by digestion with NcoI and NotI, leaving the coding regions for the N-Terminal IgH leader peptide and the C-Terminal hinge and Fc-domains of rbIgG within the vector backbone. The pCSE2.5 backbone was purified by agarose gel electrophoresis. The PciI/NotI-digested PCR2 reaction product containing the VHH repertoire of the immunized mice was then ligated into the vector backbone between the coding regions for the IgH leader sequence and for the hinge, CH2 and CH3 domains of rabbit IgG. The restriction enzymes PciI and NcoI generate compatible cohesive ends and can thus be used as partners in cloning strategies. Since immunoglobulin V gene regions often contain NcoI sites, PciI was chosen to avoid NcoI digestion during insert preparation.

In parallel, the PCR1 amplicon was further amplified with primers containing 5' and 3' linkers (**Figure 4.1.2 E**) and subsequently with specific adapters and a barcode (**Figure 4.1.2 F**) for analysis by next generation sequencing (NGS). To reduce amplification bias, each reaction was performed in triplicate or quadruplicate.

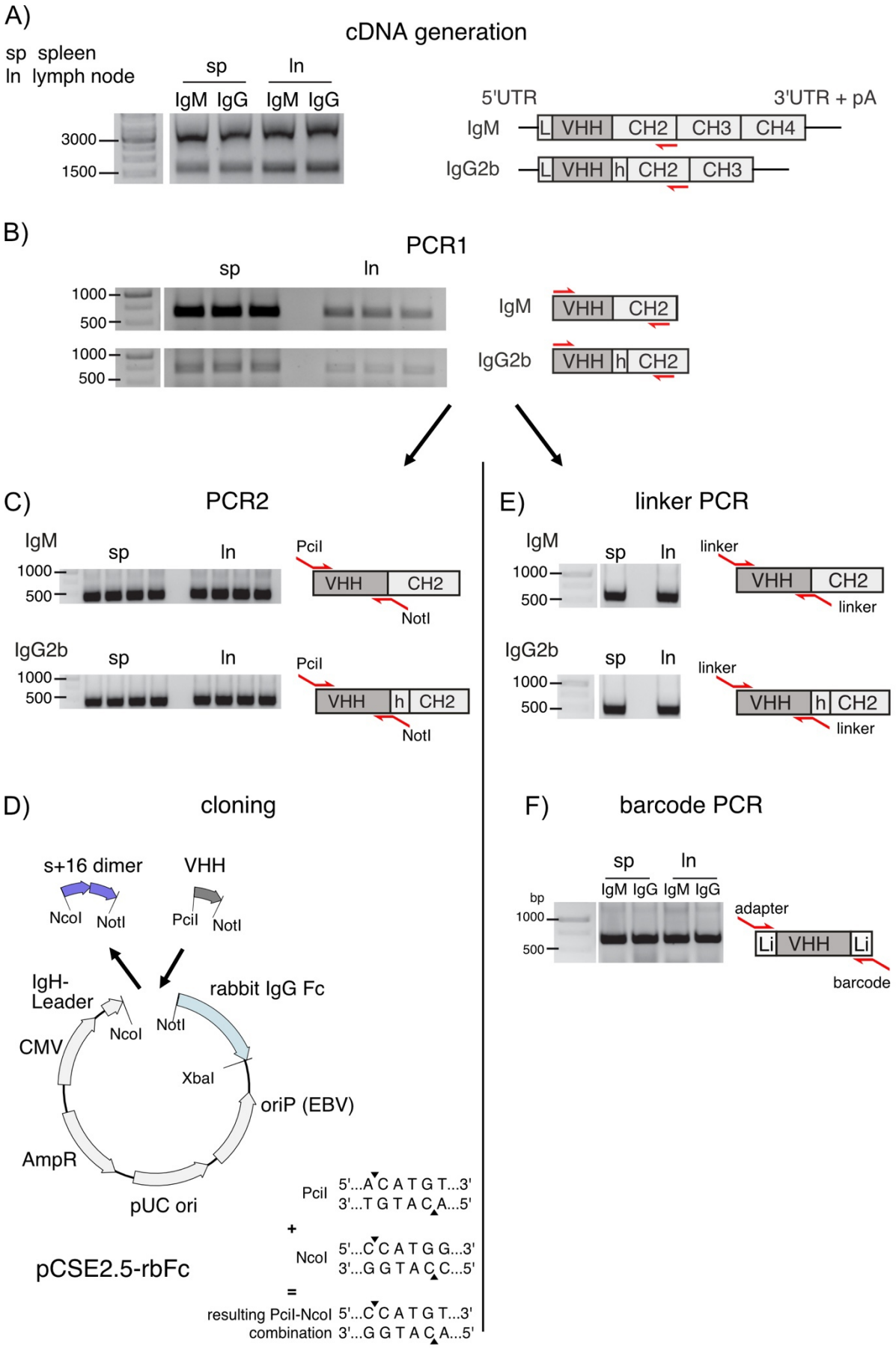
A)
cDNA generation
sp spleen
ln lymph node
sp
ln
IgM IgG IgM IgG
3000
1500
5'UTR
3'UTR + pA
IgM
L VHH CH2 CH3 CH4
IgG2b
L VHH h CH2 CH3
B)
PCR1
sp
ln
1000
500
1000
500
IgM
VHH CH2
IgG2b
VHH h CH2
C)
PCR2
IgM
sp
ln
1000
500
PciI
VHH CH2
NotI
IgG2b
sp
ln
1000
500
PciI
VHH h CH2
NotI
E)
linker PCR
IgM
sp
ln
1000
500
linker
VHH CH2
linker
IgG2b
sp
ln
1000
500
linker
VHH h CH2
linker
D)
cloning
s+16 dimer
NcoI
NotI
VHH
PciI
NotI
IgH-
Leader
NcoI
NotI
rabbit IgG Fc
CMV
XbaI
oriP (EBV)
AmpR
pUC ori
pCSE2.5-rbFc
PciI 5'...A C A T G T...3'
3'...T G T A C A...5'
+
NcoI 5'...C C A T G G...3'
3'...G G T A C C...5'
=
resulting PciI-NcoI 5'...C C A T G T...3'
combination 3'...G G T A C A...5'
F)
barcode PCR
sp
ln
IgM IgG IgM IgG
bp
1000
500
adapter
Li VHH Li
barcode

Figure 4.1.2 The VHH-encoding region of the IgM and IgG2b repertoire of hcAb-immunized LaMice is PCR-amplified from spleen and lymph node RNA for cloning into pCSE2.5 expression vector and next-generation sequencing. A) RNA of spleen and lymph nodes of LaMouse TE03-31 was prepared, and RNA integrity was evaluated by agarose gel electrophoresis. RNA was reverse-transcribed into cDNA using specific reverse primers, binding 3' of the CH2 region of either llama IgM or llama IgG2b. B) cDNA of llama IgM and llama IgG2b was PCR-amplified separately with a forward primer binding at the 5' end of the VHH-encoding region and reverse primers binding within the CH2-encoding region of IgG2b or IgM, respectively. Amplification products were analyzed by agarose gel electrophoresis. The pooled amplicons of quadruplicate reactions were used for subsequent PCR steps. C) PciI and NotI restriction sites at the 5'- and 3'-ends were introduced by forward and reverse primers respectively. D) The coding region for the s+16-dimer was excised from the mammalian expression vector pCSE2.5 with NcoI and NotI restriction enzymes. The amplified nanobody repertoire was digested with PciI and NotI and ligated into the digested pCSE2.5 vector downstream of the region coding for the IgH leader peptide and an intron, as well as upstream of the coding region of the hinge, CH2 and CH3 domains of rbIgG (Fc). The fused compatible PciI and NcoI site cannot be re-digested by either enzyme. E, F) The PCR1 amplicon was separately PCR-amplified for NGS analysis. Linker pairs were added during the first PCR (linker PCR) to the 5'- and 3'-ends of the VHH-encoding region. F) Specific barcodes were introduced in a subsequent PCR (barcode PCR) to deconvolute the readings after NGS into their respective libraries. Primers, binding to their respective complementary sequences within the constructs, are indicated as red arrows.

4.1.3 Evaluation of the immune repertoire by next generation sequencing

In addition to the cloning into a mammalian expression vector for production and screening, the nanobody immune libraries were also directly investigated by next generation sequencing (NGS). Libraries, supplied with linker, adapter, and specific barcode sequences were pooled equimolarly, quality checked with a Bioanalyzer instrument, and sequenced by the core facility of the UKE using the Illumina Miseq System. Further data processing was performed by Stephan Menzel, UKE. MiSeq data output was analyzed with MiXCR (Bolotin et al. 2015).

The obtained nanobody sequences were mapped to the germline V elements from the three LaMice BACs TE01-TE03. Nanobodies with the same nucleotide sequence from framework 1 to framework 4 were counted and sorted for abundancy. The clone with the highest abundancy in NGS likely corresponds to the most B cell clone with the

highest levels of llama hcAb encoding mRNA in the respective organ three days after the final boost.

Table 4.1.1 shows the analysis of spleen and lymph node of LaMouse TE03-31. Between 1,000 and 3,000 clones passed the quality check from the MiXCR software and were analyzed further. The top 50 most abundant clones made up 16% - 36% of each library. The diversity of the libraries is shown in subsequent columns. Library 31 LN IgG2b had 10 distinct families. 7 of the 10 families had more than 2 members. Three families were represented with only one member. These 10 clone families appeared in the top 50 with an abundancy of 0.2 % to 5.2 %, resulting in a theoretical chance to obtain the highest abundant clone in 5 out of 100 randomly picked colonies after plating transformed *E.coli*. The number of distinct families was higher in the IgM compartment compared to IgG2b. In addition, the number of families with more than 2 variants was lower in IgM compared to IgG2b, corresponding to the higher numbers of single clones in the IgM compartment caused by a higher diversity.

Table 4.1.1 The 50 most abundant VHH sequences obtained by NGS from immunized LaMouse 31 are derived from 6-21 distinct nanobody families. Sequences were determined by NGS. The total number of sequences is indicated (analyzed sequences). A clone is defined as a set of identical nucleotide sequences. Clones were ranked according to the number of identical sequences. Families are defined as clones derived from the same V-D-J recombination, variants within a family differ by one or more amino acids. Single clones contain only a single sequence.

library	analyzed sequences	sum of clone fraction in Top 50	abundancy range of Top 50 clones (%)	distinct families	families with 2 or more variants	single clones
31 Sp IgM	1304	281 (22%)	0.1 - 5.0	8	2	6
31 Sp IgG2b	2881	1027 (36%)	0.2 - 1.6	6	4	2
31 LN IgM	1170	191 (16%)	0.1 - 3.5	21	3	18
31 LN IgG2b	3250	922 (28%)	0.2 - 5.2	10	7	3

Sequences which were found in the immune library after the direct cloning approach (compare **Supplementary Figure 9.2**) were identified in the NGS sequences as well. The number of members in each family (with more than 2 variants) are shown in **Table 4.1.2**. Nanobody family A had the highest abundancy in the libraries derived from spleen IgM and IgG2b as well as lymph node IgM. The family composition in 31 LN IgG2b was different. In the top 50 clones of 31 LN IgG2b family A had a reduced number compared to the abundancy of A in the other libraries. Only families A and D

were present in both spleen and lymph node. Families D and E have shown to be mIgG2c hcAb-specific, families F and G were MU1067-specific as demonstrated in **Sections 4.1.6** and **4.1.8** respectively.

Table 4.1.2 Two abundant families of VHH sequences are found within the IgG and IgM compartments of immunized LaMouse 31. Families are defined as clones derived from the same V-D-J recombination. Families were arbitrarily designed with the names A-G. Numbers indicate the number of sequences from the respective family within the sequences obtained by NGS indicated in **Table 4.1.1.**

library	**clone family**							
	A	B	C	D	E	F	G	Other
31 Sp IgM	42	-	-	-	-	-	-	8
31 Sp IgG2b	27	-	-	10	-	-	-	13
31 LN IgM	28	-	-	-	-	-	-	22
31 LN IgG2b	6	5	19	5	2	4	3	6

Table 4.1.3 lists the characteristics of individual members of the clone families D, E, F, and G (compare **Supplementary Figure 9.1**). All members of these families are derived from the same V element with the germline amino acid motif “QREL”. Deviations from the most highly abundant clone of each family within the CDR3 sequence are marked with a cyan background to show hypermutations in the CDR3. None of the individual clones had a higher abundance than 1.1% of the whole sequence space. Although this number is low, family members were found via the direct cloning and screening approach (compare **Section 4.1.5**). Between 2 and 17 hypermutations were found in the framework regions 1-3 of families D-G. Clone TSM-D1 was found via the direct cloning approach and is identical to the most abundant clone found in family D by NGS. TSM-D2 is closely related, showing only two amino acids difference to TSM-D1. TSM-D3 differs only in one amino acid in FR1 to a clone found with an abundancy of 0.3 % by NGS. Clone TSM-E1 is identical to the second most abundant clone of family E found in NGS. Clone TSM-F1 has the highest similarity to the second most abundant clone of family F, but differs in seven amino acids. Clone TSM-G1 is closely related to the most abundant member of family G found in NGS with 2 amino acid difference.

Table 4.1.3 Characteristics of clone families D-G and their family members derived from LaMouse 31 lymph node IgG2b repertoire. V element usage (V), third complementary determining region (CDR3), abundancy of clones in the respective nanobody repertoire (range) and the sum of abundancies for each family (sum), number of somatic hypermutations (SMH), identified target antigen (antigen), related clones isolated by direct cloning with number of divergent amino acids (Isolate).

family	V	CDR3	range	sum	SMH	antigen	isolate
D	QREL	CNAGLVPYGY	1.1%	2.5 %	6	mIgG2c hcAb	TSM-D1 (0), TSM-D2 (2)
	QREL	CNAGLVPYGY	0.5%		9		
	QRVL	CNAGLLPYGY	0.4%		17		
	EREL	CNAGLVPYGY	0.3%		10		TSM-D3 (1)
	QREL	CNAGLVPYGY	0.2%		4		
E	QREL	CTLGYSGGYYYTGDY	0.6%	0.9 %	4		
	QHDL	CTLGYNGGYYYTGDY	0.3%		9		TSM-E1 (0)
F	QREL	CNADPGWGRGEYDY	0.9%	1.9 %	2	MU1067	
	QREL	CNADPGWGRGEYDY	0.4%		3		TSM-F1 (7)
	QREM	CNADPGWGRGEYDY	0.4%		9		
	QREL	CNADPGWGRGEYDY	0.2%		5		
G	QREW	CHADSPRHLMDY	0.7%	1.6 %	7		TSM-G1 (2)
	QRKW	CHADPPRHLMDY	0.5%		6		
	QREW	CHADPPRHLMDY	0.4%		7		

4.1.4 Evaluation of cloned nanobody library quality by sequencing and production as VHH-rbIgG hcAbs

To evaluate the quality of the cloned libraries, TG1 *E. coli* were electroporated with the spleen- and lymph node-derived VHH-repertoire of IgM and IgG2b in the pCSE2.5 vector and plated onto LB-agar containing ampicillin. The next day, 48 clones were picked from each IgM- and IgG-derived repertoire respectively, and plasmid DNAs were prepared in a 96-well format. Plasmids in the first two rows were Sanger-sequenced to estimate library quality and diversity (**Figure 4.1.3 A**). Plasmids carrying an intact VHH insert were identified by readable sequences of a complete VHH open reading frame (ORF). Legible sequences were aligned to the respective germline VHH-encoding region, sorted by the length of the CDR3 and grouped into families (**Supplementary Figure 9.2**). Plasmids containing the same or a highly similar sequence in the framework regions and CDR3 were identified as progeny of a common B cell clone. Wells were labeled with a letter according to the identified family by NGS (**Figure 4.1.3 A**). Plasmids with illegible sequences were scored as negative (labeled "x" in **Figure 4.1.3 A**). Clones containing the ORF of s+16-dimer were scored

as religation products (e.g. "s" in **Figure 4.1.3 A**) The results show that the libraries from the spleen of mouse 31 contained 50% and 42% intact nanobody-encoding sequences from IgM- and IgG2b-specific amplifications respectively. The libraries derived from lymph nodes contained 83% and 75% legible nanobody-encoding sequences from IgM- and IgG2b-specific amplifications respectively. Similar analyses were performed for the other five mice (compare **Supplementary Figure 9.2**).

In parallel, an aliquot of the purified plasmid DNA was used to transfect HEK293-6E cells in a 96-well format to produce secreted VHH-rbIgG hcAbs in 100 μl serum-free medium. Cell culture supernatants were harvested five days post transfection, and the proteins in the supernatants from 24 wells (i.e. of the first two rows of a 96-well plate) per lymphatic organ were analyzed by SDS-PAGE and Coomassie staining (**Figure 4.1.3 B**). The results show a visible band at the expected size of a VHH-rbIgG heavy chain (~45 kDa) in most lanes. Lanes corresponding to the s+16-dimer religated clones show a band of the expected size of the s+16-dimer-rbIgG heavy chain (~60 kDa). The results indicate effective transfection with and efficient production of VHH-rbIgG hcAbs from most plasmids. The fraction of clones yielding detectable rbIgG hcAbs from the spleen-derived libraries was 75% (IgM) and 50% (IgG2b), and that of the lymph node-derived libraries was 92% (IgM and IgG2b).

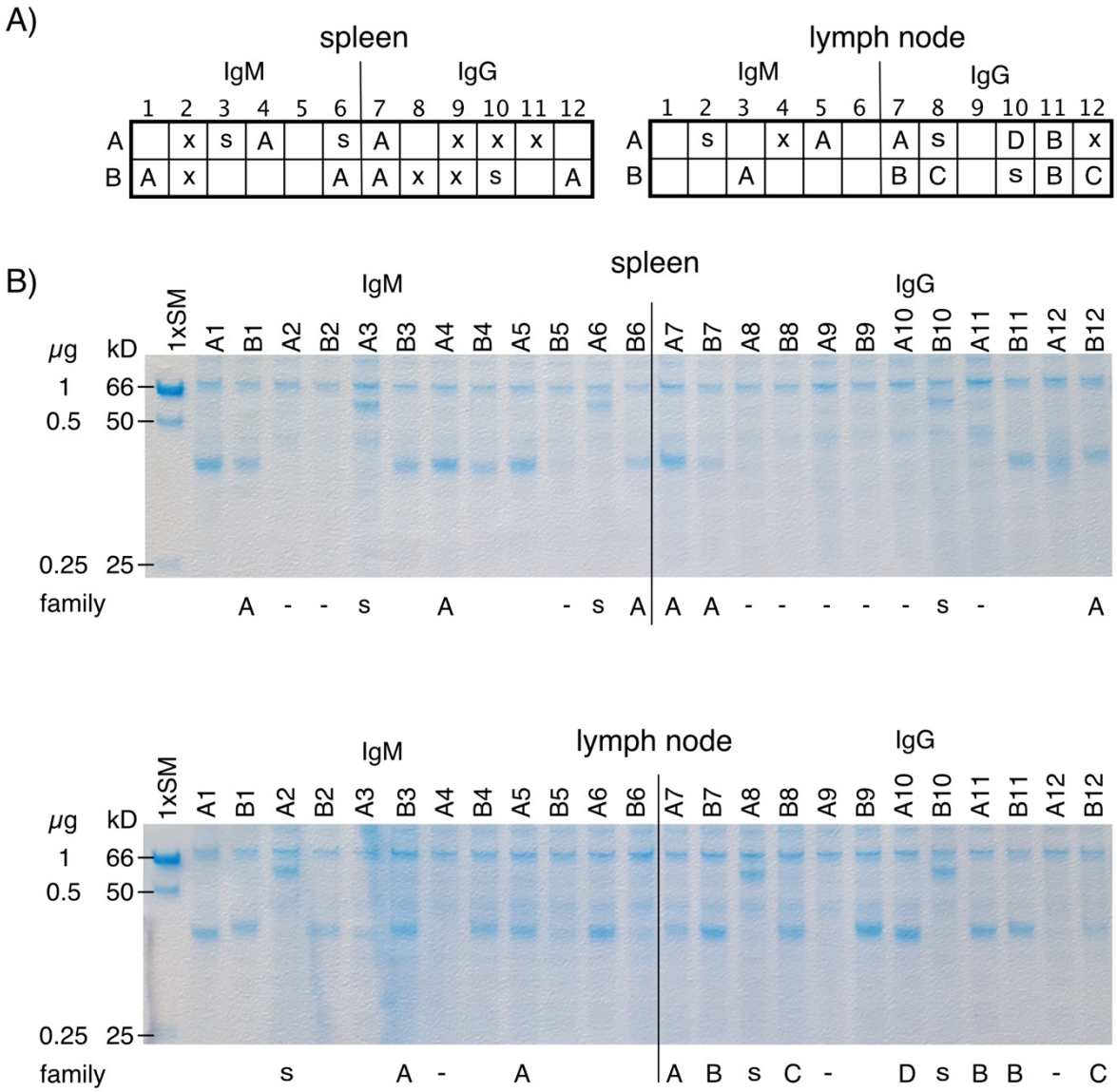

Figure 4.1.3 Cloned nanobodies are well expressed as rbIgG hcAbs. Schematic of the first two rows of a 96-well plate with samples from mouse 31. A) Individual *E. coli* colonies from the VHH-rbIgG hcAb libraries were picked and plasmid DNA was prepared in a 96-well format. Plasmid DNA of the first two rows were Sanger-sequenced. s+16-dimer religations are marked as “s”. Non-readable sequences are marked “x“. Plasmids derived from the same B cell clone, i.e., identical, or highly similar sequences of framework region and CDR3 are labeled with capital letters “A”, “B”, “C” and “D” according to the families identified by NGS, unique sequenced clones are left blank. B) Plasmids were used to transiently transfect HEK cells in 96-well plates. Proteins in HEK cell culture supernatants (5 µl/lane) were analyzed 6 days after transfection by SDS-PAGE and Coomassie staining. Members of distinct clonal families are designated with the same capital letters as in A). Non-producers are marked with “-“.

4.1.5 Screening for MU1067-mIgG2c- or l+10-mIgA-specific clones

VHH-rbIgG hcAbs containing HEK cell supernatants were screened for binding to MU1067-mIgG2c or l+10-mIgA hcAbs by ELISA. ELISA plates were coated with hcAbs MU1067-mIgG2c, l+10-mIgA, or hen egg lysozyme (HEL) as a negative control. ELISA results of LaMouse TE03-31 in **Figure 4.1.4 A** are shown as a color-coded combination of the respective OD_{450} values for MU1067-mIgG2c or HEL antigens. None of the supernatants contained antibodies binding l+10-mIgA hcAbs. This is in line with the l+10-mIgA negative serum results of LaMouse TE03-31 (compare **Figure 4.1.1 B**). MU1067-mIgG2c-specific binders (green) were mainly found in the IgG2b lymph node library. Wells containing hcAbs binding to HEL are marked by yellow squares. The most abundant clonal family, A as well as clonal families B and C, did not show any detectable binding to a hcAb. However, three wells with family A members showed a strong binding to HEL (spleen IgM B1, lymph node IgM B3 and lymph node IgG A7). The HRP-conjugated mouse IgG-specific secondary rabbit antibody ("cc") detected mouse immunoglobulins, whereas the secondary HPR conjugated polyclonal anti-rabbit antibody did not bind to the coated mouse immunoglobulins (nc). A polyreactive VHH-rbIgG, identified in an earlier discovery campaign, reacted with all coated antigens. All clones showing a positive MU1067-mIgG2c result were retransformed in *E. coli* and sequenced. Positive clones were assigned to the families identified by NGS (labeled green in **Figure. 4.1.4 A**, also compare **Table 4.1.2** and **Section 4.1.3**). Cell culture supernatants obtained from HEK cells transfected with plasmid DNA from re-transformed clones were analyzed for the presence of rbIgG hcAbs that bind MU1067-mIgG2c. Initially positive results, which could not be confirmed after re-transformation and re-production, are marked with an "x" in the respective well. Supernatants of confirmed positive clones were further analyzed for binding to nanobody dimer JK36-MU1067-his-myc by ELISA. **Figure 4.1.4 B** shows ELISA OD_{450} results as bar graphs. Clones from wells F11, C10, A10, H09 and D10 bound MU1067-mIgG2c, but not the nanobody dimer JK36-MU1067-his-myc, suggesting that these clones recognize mIgG2c. Clones from wells G11 and H10 bound JK36-MU1067-his-myc as well as MU1067-mIgG2c and are therefore expected to recognize the MU1067 nanobody. None of the binders bound l+10-mIgA or HEL.

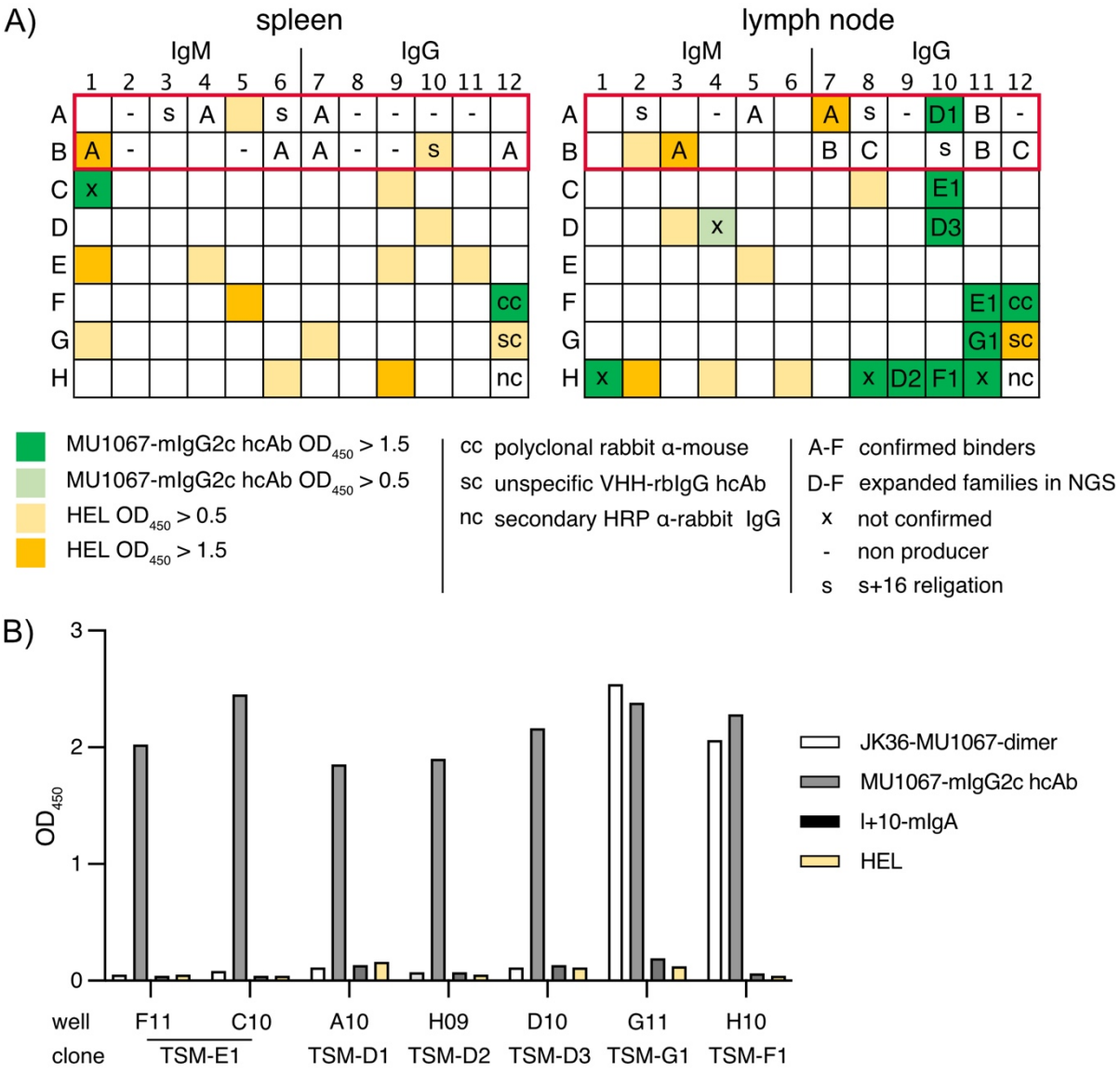

Figure 4.1.4 Cloned IgM- and IgG2b- repertoires, expressed as VHH-rbIgG hcAbs contain MU1067- and mIgG2c-specific nanobodies. A) Schematic representation of ELISA results from the LaMouse TE03-31 spleen and lymph node nanobody repertoire. HEK cell culture supernatants prepared as described in **Figure 4.1.3** were screened for specific hcAbs by ELISA. Plates were coated with 100 ng of either MU1067-mIgG2c, l+10-mIgA or HEL. Wells were incubated with 1/20 diluted HEK cell culture supernatants in PBS. Bound rbIgG hcAbs antibodies were detected with horse radish peroxidase (HRP)-conjugated anti-rabbit IgG (H+L) polyclonal antibody. HcAb binding to MU1067-mIgG2c are color coded green (OD450 > 1.5 dark green, OD450 > 0.5 light green). Unspecific binding to hen egg lysozyme (HEL) is shown in yellow (OD_{450} > 1.5 dark yellow, OD450 > 0.5 light yellow). MU1067-mIgG2c-binders were sequenced and clones were assigned to the families found in NGS (letter designations as in **Table 4.1.2**). B) Clones yielding a positive signal were retransformed, sequenced and re-transfected into HEK-6E cells. Supernatants were harvested and re-analyzed by ELISA as in A). Supernatants were additionally analyzed for binding to the biparatopic nanobody dimer JK36-MU1067-his-myc. HEL was used as negative control.

Four antigen-specific families were identified, two binding mIgG2c and two binding MU1067. An alignment of the corresponding VHH sequences is shown in **Supplementary Figure 9.1**. The nanobody sequences from well C10 and F11 were identical. The clones from the IgG2b lymph node library of LaMouse 31 show substantial somatic hypermutations (cyan background), identified as deviations from their corresponding VHH germline sequence, characterized by the "QREL" motif within FR2 (magenta).

To verify the specificity and to determine the affinity of the selected VHHs, nanobodies were cloned and expressed in a monomeric format (**Figure 4.1.5 A**).

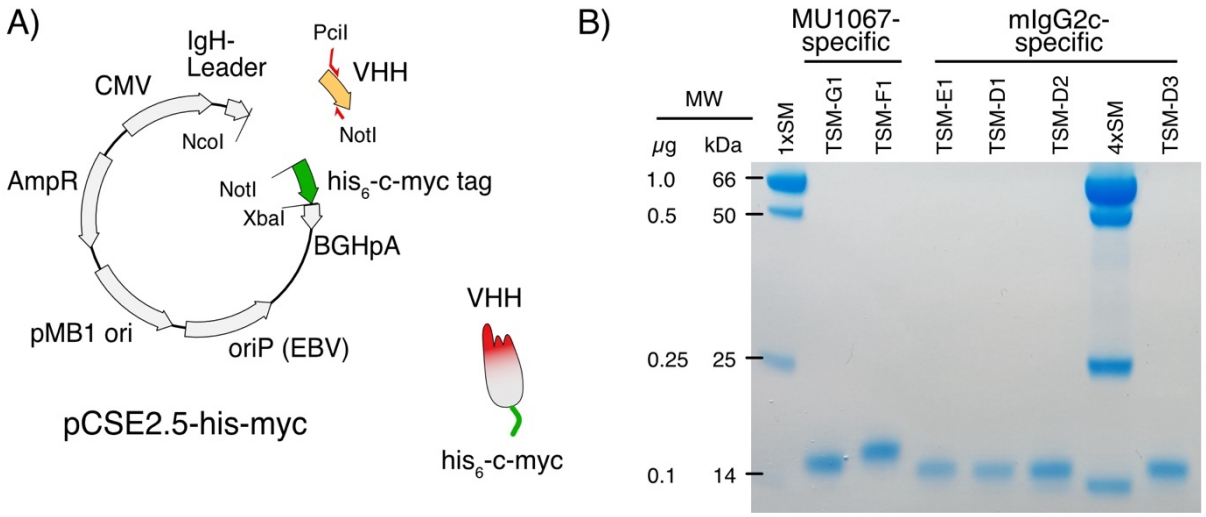

Figure 4.1.5 Nanobody reformatting to monomers and purification. A) Nanobody monomer cloning schematic. VHHs were amplified by PCR, introducing a 5' PciI site and a 3' NotI site (red arrows) and cloned into a pCSE2.5 vector to be in frame with a C-terminal hexa-histidine-tag and c-myc-tag. The resulting nanobody monomer (VHH-his$_6$-c-myc) is shown schematically. B) Monomers were produced by transient transfection of HEK cells. 6 days after transfection, monomers were purified from cell culture supernatants by Ni-NTA affinity chromatography and competitive elution with imidazole. Buffer was exchanged by size exclusion chromatography on PD-10 columns and proteins were concentrated by centrifugation through filters with a molecular weight cut-off of 5 kDa. Proteins were size fractionated by SDS-PAGE and visualized by Coomassie staining.

As indicated in **Figure 4.1.2 D**, the fusion site of PciI-digested insert and NcoI-digested vector is recognized by neither of the two restriction enzymes. The VHH-encoding region of the VHH-rbIgG was therefore PCR-amplified with a primer pair introducing a PciI site (5') and a NotI site (3'). The amplicon was cloned into a NcoI & NotI-digested

pCSE2.5-his-myc vector backbone upstream of a C-terminal hexa-histidine-tag for purification and a c-myc-tag for detection in flow cytometry. A schematic of the resulting VHH-his-c-myc protein is depicted next to the vector (**Figure 4.1.5 A**). Nanobody monomers were produced in HEK cells and purified by Ni-NTA affinity chromatography. Purified nanobodies migrated with the correct size of ~16 kDa in SDS-PAGE (**Figure 4.1.5 B**).

4.1.6 Cross-reactivity and affinity of mIgG2c-specific clones

Specificity and affinity of the clones that specifically bound the Fc part of mIgG2c was then analyzed by biolayer interferometry (BLI). Different biotinylated mouse immunoglobulins – namely MU1067-mIgG2c hcAb, and conventional antibodies with the isotypes mIgG2c, mIgM, mIgG1, mIgG2a and mIgG2b – were immobilized on streptavidin sensors to probe binding of nanobody monomers from families D and E. The members of both families only bound to MU1067-mIgG2c hcAb and a mIgG2c monoclonal antibody containing a kappa light chain. They showed no binding to any other mouse immunoglobulins (**Figure 4.1.6 A**). As the MU1067-mIgG2c hcAb (~90 kDa) is approximately half the size of the conventional mIgG2c monoclonal antibody (~150 kDa), more MU1067-mIgG2c hcAbs were immobilized on the sensor surface and the signal was higher in comparison to the conventional mIgG2c antibody. Affinity of nanobodies was determined by immobilization of biotinylated MU1067-mIgG2c hcAbs on streptavidin sensors and association of titrated VHH-his_6-c-myc monomers. Family E has the highest affinity with a dissociation constant (K_D) of 4 nM. TSM-D1, TSM-D2 and TSM-D3 cover a range of affinities with 66 nM, 157 nM and 176 nM respectively (**Figure 4.1.6 B**).

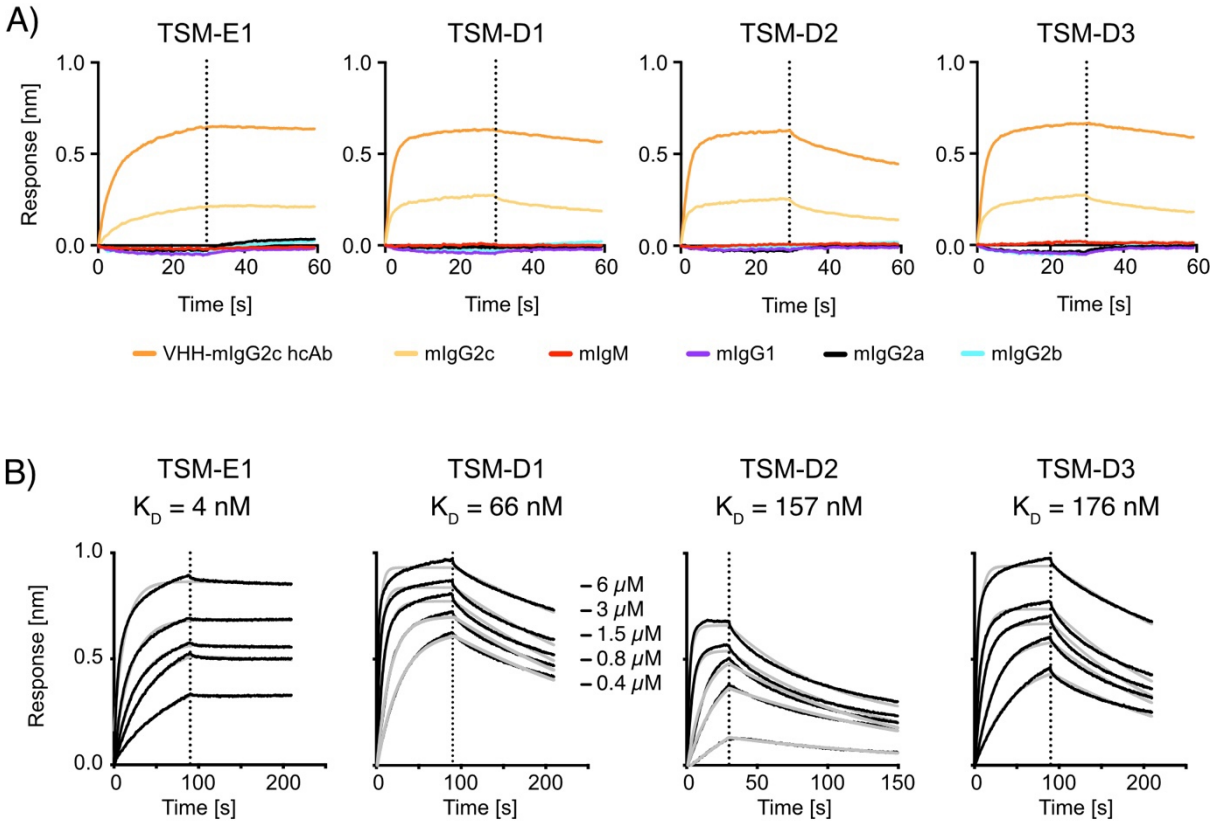

Figure 4.1.6 Nanobodies TSM-D1-D3 and TSM-E1 specifically bind mIgG2c with affinities in the range of 4-180 nM. Binding specificity and affinity was determined using BLI. A) Biotinylated mouse monoclonal antibodies mIgG2c (yellow, clone 6.3), mIgM (red, clone HI98), mIgG1 (purple, clone HIB19), mIgG2a (black, clone G28) or mIgG2b (cyan, clone HIR2), or biotinylated MU1067-mIgG2c hcAb (orange), were immobilized on streptavidin sensors until complete saturation (not shown) and subsequently incubated with mIgG2c-specific VHH-his-c-myc monomers from families D and E. Sensor is dipped into kinetics buffer containing VHH-his-c-myc (6 μg/ml) for 30 seconds (association phase). Then the sensor was dipped into kinetics buffer to observe dissociation for 30 seconds. The dotted line indicates the transition from association to dissociation step. B) Streptavidin sensors were saturated with biotinylated MU1067-mIgG2c hcAb (not shown) and subsequently dipped in serially diluted nanobody monomers (6 μM - 0.4 μM) for 30-90 seconds to observe association. Subsequently sensors were dipped in kinetics buffer for 120 seconds to analyze dissociation. Dissociation constants (K_D) were calculated using a non-liner fit (gray curves) using GraphPad Prism 9.

4.1.7 Application of mIgG2c-specific nanobodies in flow cytometry

Next, the utility of the mIgG2c-specific nanobodies as secondary reagents for flow cytometry was tested, thereby further confirming their specificity. In **Figure 4.1.7 A,** transiently transfected HEK cells expressing hP2X7 were first incubated with hP2X7-

specific 3c23-mIgG2c hcAb or an isotype control and subsequently with mIgG2c-specific nanobody-his-c-myc monomers. Bound monomers were detected with an AF647-conjugated monoclonal antibody specific for the c-myc tag (clone 9E10). TSM-E1 had the highest signal intensity. The members of family D had a lower signal intensity, which is in line with their lower affinity (compare **Figure 4.1.6 B**). In **Figure 4.1.7 B,** the same experiment was repeated with mIgG2c-specific clones in a VHH-rbIgG hcAb format, detected by polyclonal AF647-conjugated anti-rbIgG $F(ab')_2$-fragment. As a result of the bivalent binding and the polyclonal detection, the signal intensities increased in comparison to the respective monomers.

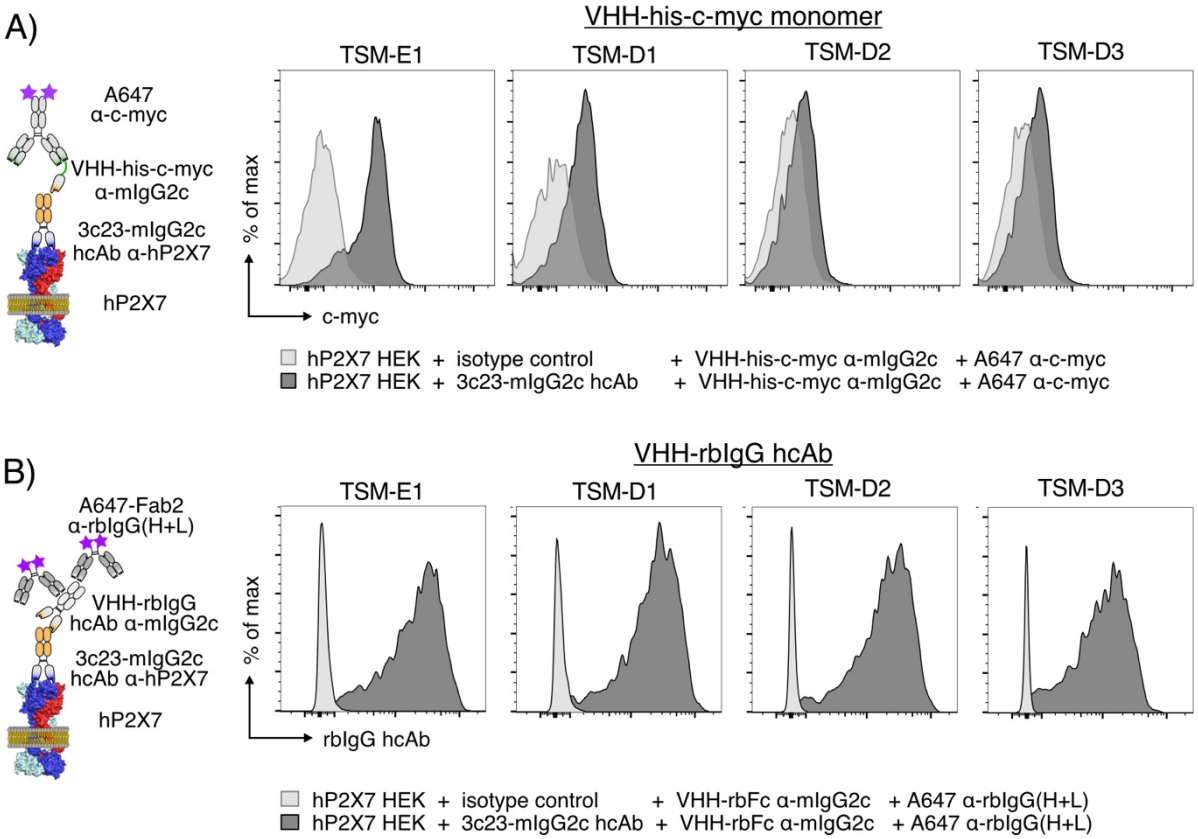

Figure 4.1.7 Nanobodies TSM-D1-D3 and TSM-E1 are useful tools as secondary antibodies in flow cytometry. Capacity of mIgG2c-specific nanobodies to detect cell surface bound mIgG2c was analyzed by flow cytometry. Experiment schematic is indicated on the left. For A) and B) hP2X7 transiently transfected HEK cells were incubated with hP2X7-specific 3c23-mIgG2c hcAb or an isotype control. A) HEK cells were further incubated with mIgG2c-specific VHH-his-c-myc monomers. Bound monomer was detected by AF647-conjugated c-myc-specific monoclonal antibody (clone 9E10). B) Alternatively, binding of surface immobilized mIgG2c was analyzed using mIgG2c-specific VHH-rbIgG hcAbs and AF647-conjugated rbIgG-specific polyclonal $F(ab')_2$-fragments.

4.1.8 Cross-reactivity and affinity of MU1067-specific clones

The cross-reactivity to other VHHs and the affinity of the MU1067-specific clones were analyzed further. Purified nanobody monomers (VHH-his_6-c-myc) were captured by penta-his-specific mIgG1-coated BLI sensors via the C-terminal his_6-tag until saturation and subsequently dipped into kinetics buffer containing either MU1067-rbIgG hcAb, 7E2-rbIgG hcAb, AE1-rbIgG hcAb or l-10E-rbIgG hcAb (**Figure 4.1.8 A**). Of the tested hcAbs, only MU1067-rbIgG was bound by the immobilized his-tagged TSM-G1 and TSM-F1 nanobody monomers. Thus, amino acids within MU1067 that differ from those of the other tested nanobodies 7E2 (mP2X7-specific), AE1 (AAV-specific) and L-10 (ToxA-specific) are potential binding sites for the nanobodies TSM-G1 and TSM-F1 (**Figure 4.1.8 B**).

The affinity of the MU1067-specific binders TSM-G1 and TSM-F1 was determined by BLI. Biotinylated MU1067-hIgG1 hcAbs were immobilized on streptavidin sensors until saturation and subjected to titrated TSM-G1 or TSM-F1 nanobody monomers. The graphs shown in **Figure 4.1.8 C** indicate a high affinity (6 nM) with a slow off-rate for nanobody TSM-G1 and a low affinity (232 nM) for TSM-F1.

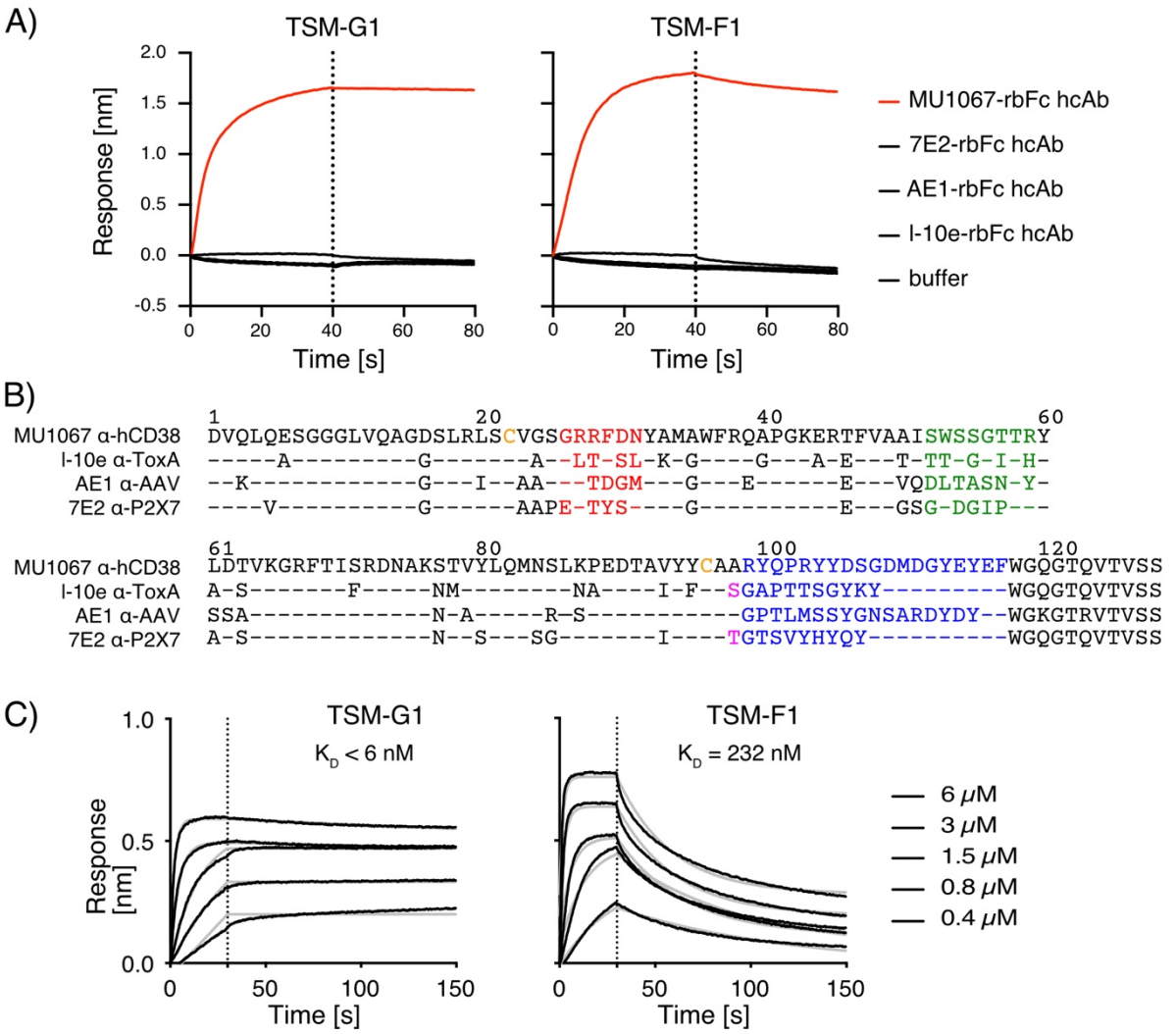

Figure 4.1.8 Nanobodies TSM-G1 and TSM-F1 specifically recognize the MU1067 nanobody. A) MU1067-specific hexa-histidine-tagged nanobody monomers TSM-G1 and TSM-F1 were immobilized on biosensors coated with a penta-his-specific mAb (mIgG1) until complete saturation (not shown). Biosensors were then dipped into kinetics buffer containing either MU1067-rbIgG hcAb, 7E2-rbIgG hcAb, AE1-rbIgG hcAb or I-10E-rbIgG hcAb for 40 sec association phase. For the next 40 sec, the sensor was dipped in kinetics buffer to monitor dissociation. Buffer change is indicated with a dotted line. B) Amino acid sequence alignment of the analyzed VHHs in comparison with MU1067. Divergent amino acids are indicated with the respective amino acid, identical amino acids are indicated with a hyphen. CDR1 (red), CDR2 (green) and CDR3 (blue), framework regions FR1, FR2, FR3 and FR4 (black) and numbering is according to the Kabat scheme (Kabat *et al.* 1991). C) Affinity of nanobody monomers (VHH-his-c-myc) to MU1067 was determined by biolayer interferometry as described above. Streptavidin sensors were saturated with biotinylated MU1067-hIgG1 hcAbs and dipped into kinetic buffer containing serially diluted nanobody monomers (6 μM - 0.4 μM) for 30 s (association phase) and subsequently in kinetics buffer for 120 s to monitor dissociation. Dissociation constants (K_D) were calculated using a non-liner fit (gray curves) and analyzed using GraphPad Prism 9.

4.1.9 Blocking of MU1067 – hCD38 interaction with nanobodies TSM-G1 and TSM-F1

Since nanobodies TSM-G1 and TSM-F1 bound specifically to MU1067, it was investigated whether they might be anti-idiotypic antibodies directed against the paratope, with which MU1067 binds its antigen CD38. In BLI experiments, immobilized biotinylated MU1067-hIgG1 did not bind hCD38 when MU1067 was pre-blocked with TSM-G1-rbIgG or TSM-F1-rbIgG hcAbs, but did associate to hCD38 without blocking (**Figure 4.1.9 A**). To evaluate if both nanobodies TSM-G1 and TSM-F1 bind the same epitope on MU1067, both were incubated sequentially on immobilized biotinylated MU1067-hIgG1. When TSM-G1 was associated first, no additional binding was observed by the subsequent incubation with an equimolar mix of TSM-G1 and TSM-F1 (black dashed curve). When TSM-F1 was associated first, the signal intensity was reduced by the subsequent incubation of TSM-G1 and TSM-F1, indicating a displacement of TSM-F1 due to the higher affinity of TSM-G1 (**Figure 4.1.9 B**).

MU1067 is a component of a bispecific natural killer cell engager (BiKE) that is capable of mediating NK-dependent cell lysis of CD38-expressing myeloma cells (Hambach et al. 2022). The BiKE consists of three VHHs binding human albumin, human CD16 and human CD38, respectively. Upon linkage of natural killer (NK) cells expressing CD16 (FcγRIIIa) (effector cells) and multiple myeloma cells expressing human CD38 (target cells) via the BiKE, NK cells release perforins, which leads to the lysis of the myeloma cells (Hambach et al. 2022). To evaluate whether the MU1067-binding antibodies have a functional effect *in vitro*, their capacity to block this BiKE was tested in an antibody-dependent cellular cytotoxicity (ADCC) killing assay. The NK cell line NK-92 was first incubated with either MU1067-BiKE or an isotype control (s-14-BiKE) and subsequently with TSM-G1- or TSM-F1-rbIgG hcAbs. CD38-expressing LP1-luc cells that also express luciferase were added as target cells, and killing was assessed as loss of luminescence due to the decreasing number of viable cells. While the s-14-BiKE had no effect, the MU1067-BiKE efficiently mediated the killing of the LP1-luc target cells by the NK-92 cells (**Figure 4.1.9 C**). This killing was not blocked by the isotype control hcAb (L-10E-rbIgG hcAb) or the TSM-F1-rbIgG hcAb. However, the TSM-G1-rbIgG hcAb (red curve) effectively blocked the interaction between MU1067 and hCD38 and reduced the killing of LP-1-luc cells to background levels.

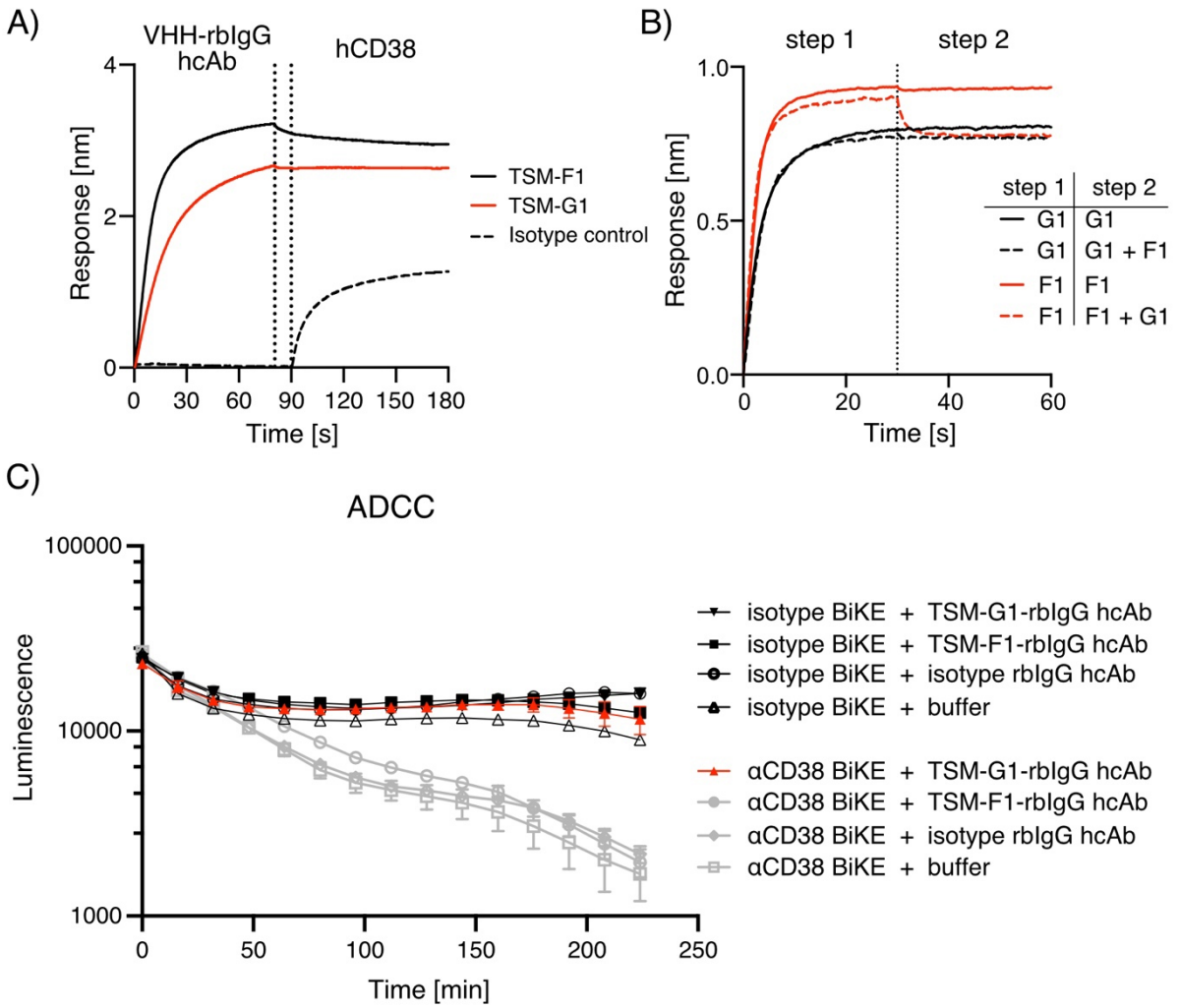

Figure 4.1.9 Nanobody TSM-G1 but not TSM-F1 blocks the binding of the MU1067 nanobody to hCD38. A) Biotinylated MU1067-hIgG1 hcAb was immobilized on streptavidin sensors until complete saturation (not shown). Biosensors were subsequently dipped into kinetics buffer containing TSM-G1-rbIgG, TSM-F1-rbIgG hcAb or an isotype control (L-10E-rbIgG hcAb). After a 10 sec buffer step, sensors were dipped into kinetics buffer containing the recombinant extracellular domain of hCD38. B) Streptavidin sensors saturated with biotinylated MU1067-hIgG1 hcAb were dipped in HEK cell culture supernatants containing TSM-F1-rbIgG (red) or TSM-G1-rbIgG hcAbs (black). Subsequently sensors were dipped into the same supernatant (solid line) or a mix of both supernatants (dashed line). Buffer changes are indicated with dotted lines. C) CD16-expressing NK-92 cells were incubated with a bispecific nanobody dimer (BiKE = **bi**specific **k**iller-cell **e**ngager) composed of the CD16-specific nanobody C21(Behar et al. 2008) linked to either the CD38-specific MU1067 nanobody or an isotype control nanobody s-14. The NK-92 cells were washed and then further incubated with HEK cell culture supernatants containing the MU1067-specific TSM-G1-rbIgG or TSM-F1-rbIgG hcAbs or an isotype control (L-10E-rbIgG hcAb). BiKE-loaded NK-92 cells were then co-incubated with CD38-expressing LP-1-luc target cells in the presence of luciferin in an effector-to-target ratio of 3 to 1 for 4h at 37°C (in triplicate samples). Luminescence intensity was measured every 15 min on a Victor plate reader.

In summary, nanobodies specific for the MU1067-mIgG2c heavy-chain antibody could be obtained by protein immunization of LaMice. Four families of binders were identified both by NGS sequencing and by cloning of the nanobody immune repertoire into a eucaryotic expression vector with subsequent screening of HEK supernatants. While two families targeted the N-terminal MU1067 domain, two families recognized the C-terminal mIgG2c region of the immunogen. Isolated candidates of these families have proven to be highly specific to mIgG2c with nanomolar affinities. The MU1067-specific nanobodies demonstrated high affinities as well as the potential to block the interaction with its target antigen CD38.

4.2 Generation of P2X7-specific nanobodies from *Lama glama* 405 by phage display

This chapter presents the selection of P2X7-specific nanobodies from a VHH library previously generated from a llama (llama 405) immunized against mouse and human P2X7 (mP2X7 and hP2X7), with the aim of discovering nanobodies directed against novel epitopes of P2X7. To this end, a fresh phage library was produced in *E. coli* using a library previously generated in the Koch-Nolte lab by Welbeck Danquah (Danquah 2012). Two rounds of panning of the fresh phage library were performed on mP2X7 and hP2X7, respectively. The second panning round involved blocking the epitope of the dominant clone isolated from panning round one, using the respective VHH clone in the format of a rbIgG hcAb.

4.2.1 Llama 405 libraries are enriched for P2X7-binders after panning on HEK cells transiently transfected with mouse or human P2X7

Immune libraries of llama 405 were generated previously by Welbeck Danquah from the Koch-Nolte lab in cooperation with Ablynx (Sanofi). A llama (*Lama glama*) was genetically immunized with one prime and three boost immunizations of cDNA encoding mP2X7 and hP2X7 in two-week intervals. A fourth boost contained HEK cells stably transfected with mP2X7 and hP2X7. The llama was finally boosted with immune-precipitated mouse and hP2X7 on agarose beads (**Figure 4.2.1 A**). Peripheral blood lymphocytes were isolated four and ten days after the final boost. cDNA was generated from each library, pooled and VHH-coding regions were PCR amplified and cloned into phagemid vector pAX50. The immune library was electroporated into TG1 *E. coli* (Danquah 2012; Stähler et al. 2022).

Counting the colony-forming units (cfu) of the plated TG1 *E. coli* revealed that library PBL5+6 contained between 9×10^7 - 2.5×10^8 cfu with legible insert percentages of 82% - 91% (Danquah 2012).

Figure 4.2.1 B illustrates the panning of a freshly prepared phages generated from the TG1 *E. coli* library. Immune TG1 *E. coli* libraries were infected with KM-13 helper phage to produce fresh phages that carry nanobody-his-myc-P3 fusion proteins on the surface and the respective packaged VHH gene, resulting in a phage library size of

1.2 x 10^{12} phages/ml. The phage library from llama 405 was first subjected to panning on untransfected HEK cells to reduce poly-specific phages (negative selection). Subsequently, the library was separately panned on HEK cells transiently transfected with mP2X7 or hP2X7 to positively select P2X7-specific phages. Extensive washing of cells removed unspecific or low affinity binders. Phages were harvested by trypsination and used to infect native TG1 *E. coli,* resulting in a bacterial library of either mouse or human P2X7-enriched phages. Sequencing of phagemids from both bacterial libraries revealed the previously selected m/hP2X7 cross-reactive 1c81 as the dominant clone in the library panned on hP2X7. This nanobody was cloned into pCSE2.5-rbIgG and reformatted as a heavy-chain antibody with the Fc region of rbIgG (1c81-rbIgG hcAb).

In the second round of panning, the two libraries were again negatively selected on untransfected cells. Before and during the subsequent positive selection, HEK cells transiently transfected with mP2X7 or hP2X7 were incubated with hcAb 1c81-rbIgG in order to obtain phage libraries depleted of VHHs that bind the same epitope as 1c81 (**Figure 4.2.1 B**)

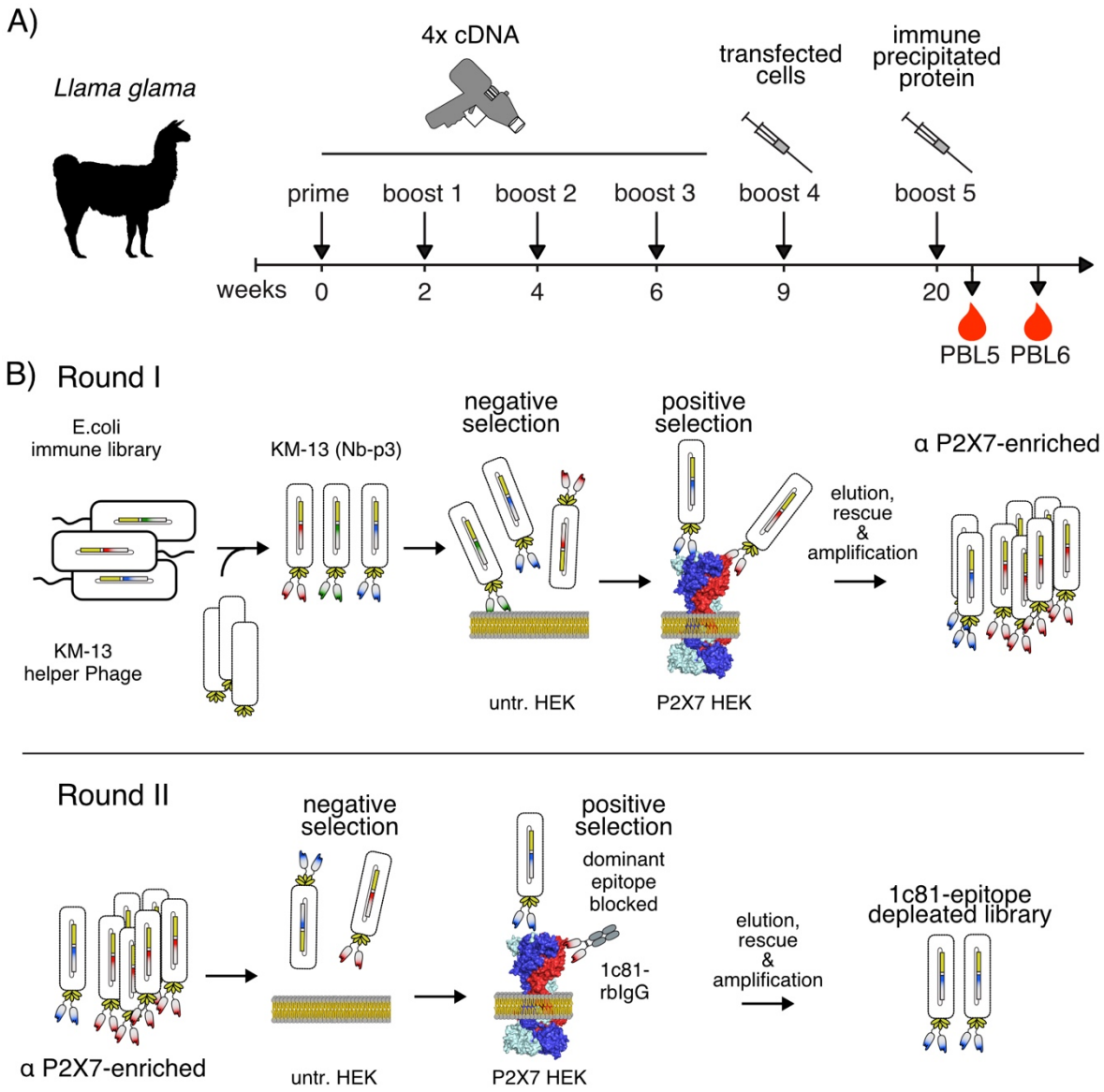

Figure 4.2.1 Schematic illustration of the immunization of llama 405 and selection of P2X7-specific nanobodies from the llama 405 VHH-phage-display library by panning on P2X7-transfected cells. A) *Lama glama* 405 was genetically immunized four times with P2X7-encoding cDNA, followed by immunization with HEK cells transiently transfected with human or mouse P2X7, and immunization with immune precipitated protein. The VHH repertoire was PCR amplified from peripheral blood lymphocytes (PBL) isolated four days (PBL5) and ten days (PBL6) after the final boost, and phage-display libraries were cloned as described previously (Danquah 2012; Stähler et al. 2022). B) Phages were produced by infecting TG1 *E. coli* immune libraries with KM-13 helper phages at a multiplicity of infection (MOI) of ten. 10^{11} phages of the immune library were incubated with untransfected HEK cells (negative selection) and subsequently with HEK cells transiently transfected with either mouse or human P2X7 (positive selection). Phages were rescued by trypsination and reamplification in TG1 *E. coli*. Sequencing revealed a previously identified nanobody 1c81 (Danquah 2012; Stähler et al. 2022) as the dominant isolated clone. The second round of panning was performed on P2X7-transfected HEK cells in the presence of a large excess of 1c81-rbIgG hcAb.

After each panning round, the output - i.e., the number of remaining infective phages - was determined by plating TG1 *E. coli* infected with trypsin-eluted phages (compare **Table 4.2.2**). The llama 405 library showed a 2000-fold increase in phages binding to mP2X7 and a 20-fold enrichment in phages binding hP2X7 over phages panned on untransfected HEK cells after the first panning round. After the second panning round, where the dominant epitope was blocked by 1c81 rbIgG hcAb, the enrichment was much smaller (2.6- and 1.3-fold).

Table 4.2.2 Input and output of first and second panning rounds of llama 405 libraries. Enriched indicates the product of output of transfected cells over output of untransfected cells.

Round 1				**Round 2**			
panned on	**input**	**output**	**enriched**	**panned on**	**input**	**output**	**enriched**
mP2X7	$1*10^{11}$	$2.5*10^{7}$	2000	mP2X7 (1c81 blocked)	$1*10^{11}$	$1.5*10^{6}$	2.6
				untransfected		$5.8*10^{5}$	
hP2X7		$2.8*10^{5}$	21	hP2X7 (1c81 blocked)		$3.5*10^{7}$	1.3
				untransfected		$2.7*10^{7}$	
untransfected		$1.3*10^{4}$					

Enriched = Output transfected / output untransfected

4.2.2 Enrichment of panned llama 405 libraries for P2X7-binding nanobodies is confirmed on the sequence level

Thirty two clones were sequenced from each library after two panning rounds. Nanobody sequences were grouped into families and analyzed for abundancy, V-usage, CDR3 amino acid sequence and CDR3 length (**Table 4.2.3**). The families were sorted for abundancy of isolated clones with a similar CDR3 sequence and matching somatic hypermutations (**Supplementary Figure 9.3**). As an example, nanobodies of family A were isolated 16 times with 11 different variants. The maximum difference in amino acid residues within the family is 15. Variations of amino acids in the CDR3 sequence are highlighted with bold letters. The length of the CDR3 is given in number of amino acid residues. All but two families (C and H) from pannings on mouse P2X7 have a CDR3 of 15 amino acids. VHHs from the same family as previously isolated nanobodies are indicated in the last column (Danquah 2012).

Families A, B, D and F were isolated from both panning rounds on mouse P2X7. In the second round, fewer isolates from family A but more isolates from family B and D

were found. The single member of family F was found once in both panning rounds. Families C and H were only enriched in round 2.

Table 4.2.3 Nanobodies selected by panning from llama 405 immune libraries on HEK cells transfected with mouse P2X7. Panning of phage display libraries was performed as illustrated in **Figure 4.2.1**. VHHs selected in rounds one and two are depicted above and below the double line. Families are defined as clones derived from the same V-D-J recombination, isolates indicates the number of clones within the family, variants the number of variants within a family differ by one or more amino acids, max diff the maximal number of amino acids differences between two members of the family.

pan	fam	framework	isolated	variants	max diff	CDR3	length	previous isolates
1	A	EREF	16	10	15	TGTVLDVTSEVVYVD	15	1c20
	B	EREF	5	5	9	DSDTYLPIQVDAFRY	15	3c6
	D	EREF	5	3	3	APRVWLGIIPSLYDY	15	-
	E	EREF	1	1	0	STQYYIARASYEYDL	15	-
	F	EREF	1	1	0	SPVLSIVLDPRGLEY	15	8c7
	G	ERRF	1	1	0	SNTVQDVTSEVVYTY	15	-
2	A	EREF	4	4	5	TGTVLDVTSEVVYVD	15	-
	B	EREF	8	4	15	DSDTYLPVREDAYYY	15	3c6
	C	GLEW	3	2	6	GNT	3	-
	D	EREF	3	3	4	APRVWLGIIPSLYDY	15	-
	F	EREF	1	1	0	SPVLSIVLDPRGLDY	15	-
	H	GLEW	1	1	0	SPTVVAPRYDY	11	-

The nanobody families derived from panning rounds on hP2X7-transfected cells are listed in **Table 4.2.4**. Eight families were identified as hP2X7-binders. The previously isolated nanobody 1c81 belongs to the dominant family I. Seven other new families (H, J, K, L, M, N, O, P, C) had not been isolated thus far. None of the families isolated on mouse P2X7 were found in the first panning round on hP2X7. By blocking the 1c81-epitope, all but family M disappeared in the second panning round. However, three new families (C, P and Q) were isolated, of which only family Q had been previously isolated from llama 405 (clone 3c23) (Danquah 2012). Interestingly, family C with its short CDR3 of three amino acids accounted for the majority of sequences picked and was also isolated from the second round on mP2X7-transfected HEK cells. Subsequent analyses revealed that these nanobodies also bound to untransfected HEK cells (see below, **Figure 4.2.3**).

Table 4.2.4 Nanobodies selected by panning of llama 405 immune libraries on HEK cells transfected with human P2X7. Panning of phage display libraries was performed as illustrated in **Figure 4.2.1**. VHHs selected in rounds one and two are depicted above and below the double line. Families are defined as clones derived from the same V-D-J recombination, isolates indicates the number of clones within the family, variants the number of variants within a family differ by one or more amino acids, max diff the maximal number of amino acids differences between two members of the family.

pan	fam	framework	isolated	variants	max diff	CDR3	length	previous isolates
1	H	GLEW	4	1	0	SPTVVAPRYDY	11	-
	I	ELEF	19	5	4	HSETR**D**GTR**T**FDRPSLYNY	19	1c81
	J	EREF	3	3	5	NS**A**TQSSSWGFDRPS**L**YNY	19	-
	K	EREG	1	1	0	GTLVFEDMNMDSDFDVCGVMDY	22	-
	L	EREF	1	1	0	GPNWSTSFRRPDTYDY	16	-
	M	GPEW	1	1	0	SGTVVPGPIGYDY	13	-
	N	EREL	1	1	0	EIRDGEYIRTEIG	13	-
	O	EREF	1	1	0	DDYLALVAGRIGS	13	-
2	C	GLEW	15	7	5	GNT	3	-
	M	GPEW	1	1	0	SGTVVPGPIGYDY	13	-
	P	EREG	3	2	9	GRGIYDWRRFEEWEYDY	17	-
	Q	EREF	2	1	0	ADETLGAVPNFRLHEKYEYEY	21	3c23

4.2.3 Cloning candidates in pCSE2.5 rbIgG

Selected human and/or mouse P2X7-specific nanobodies were cloned from the prokaryotic phagemid vector pAX50 into the pCSE2.5 vector resulting in an expression vector for a bivalent nanobody rbIgG hcAb as shown schematically in **Figure 4.2.2 A**. Transient transfection of these vectors HEK-6E cells and analysis of proteins in cell supernatants six days post infection by SDS-PAGE and Coomassie staining revealed detectable bands (**Figure 4.2.2 B**). With the exception of families N and O, the supernatants of each family show a band at ~45 kDa corresponding to the expected size of a nanobody rbIgG hcAb. The band of the D2 rbIgG hcAb shows a slightly higher apparent molecular weight, probably as a result of glycosylation since a somatic hypermutation in the CDR2 resulted in a potential N-glycosylation site (N-Y-T).

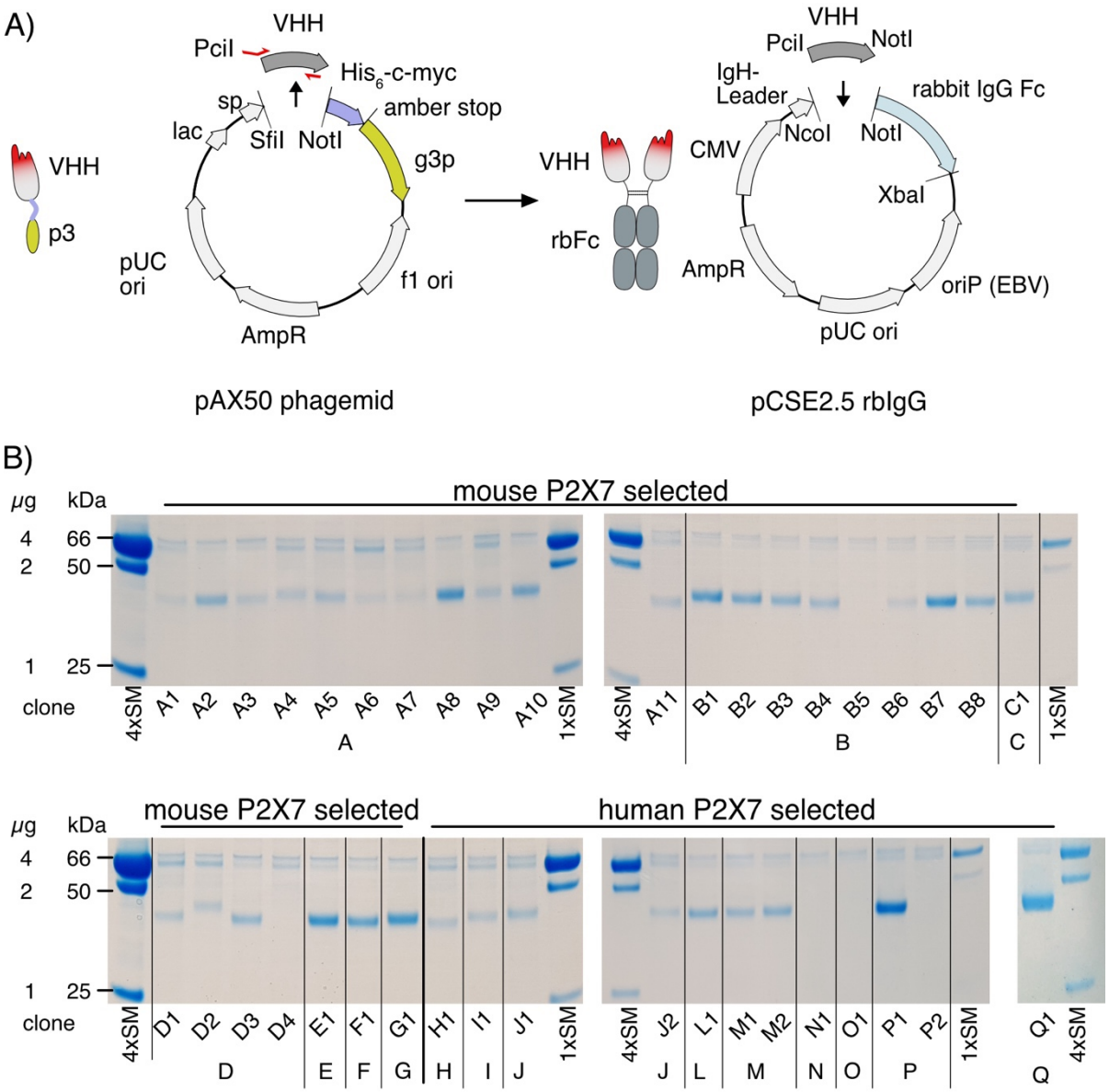

Figure 4.2.2 Nanobodies selected from llama 405 express well as rbIgG hcAbs. A) Schematic of a nanobody expressed from the pAX50 vector including a C-terminal hexa-histidine, a trypsin cleavable c-myc tag and the P3 protein of KM-13 in the open reading frame. Introduction of a 5'-PciI and a 3'-NotI restriction site by PCR allows the cloning of the VHH into pCSE2.5 upstream of hinge, CH2 and CH3 of rbIgG. B) HEK cells were transiently transfected with the cloned nanobody expression vectors and cell culture supernatants were analyzed 6 days later by SDS-PAGE for the presence of hcAbs. Clone families are indicated by letters A-G. Families A-H were isolated from libraries panned on mP2X7 and families H-P on hP2X7. Family H was isolated from mP2X7 and hP2X7 pannings.

4.2.4 FACS analyses show binding of hcAbs to mP2X7, hP2X7, or both

The reactivity of the hcAb-containing supernatants with P2X7 was evaluated by flow cytometry. HEK cells were transiently transfected with mP2X7 or hP2X7 and co-transfected with nuclear GFP. Co- and untransfected HEK cells were incubated with HEK-6E cell supernatants containing nanobody-rbIgG hcAbs selected from the two panning rounds of llama 405. After washing the cells, bound rbIgG hcAbs were detected with AF647-conjugated rabbit-specific polyclonal $F(ab')_2$ secondary antibody. Most GFP-positive cells were expected to also express P2X7 due to co-transfection (molar ratio 1:10). GFP positive cells were therefore gated and analyzed for AF647 fluorescence intensity (**Figure 4.2.3 A**). The results of the FACS screening are shown in **Figure 4.2.3 B**. Binding to untransfected HEK cells is shown by white histograms, to hP2X7 (light grey) and to mP2X7 (dark gray). Families A, B, D, E, F and G are mP2X7-specific. Family members TSL-B5 and TSL-D4 did not show a visible band in the SDS-PAGE analysis of the supernatants showing poor or absent production (compare **Figure 4.2.2**). However, TSL-B5 still resulted in a slightly positive signal whereas family member TSL-D4 did not. Families L, P and Q are hP2X7-specific. Families H, I and J are cross-reactive to mouse and human P2X7. Family C evidently contains a nanobody that binds also to untransfected HEK cells, as indicated by a similar shift of all three MFI curves to the right. Family M did not react to any target. Families N and O did not produce and did not show binding.

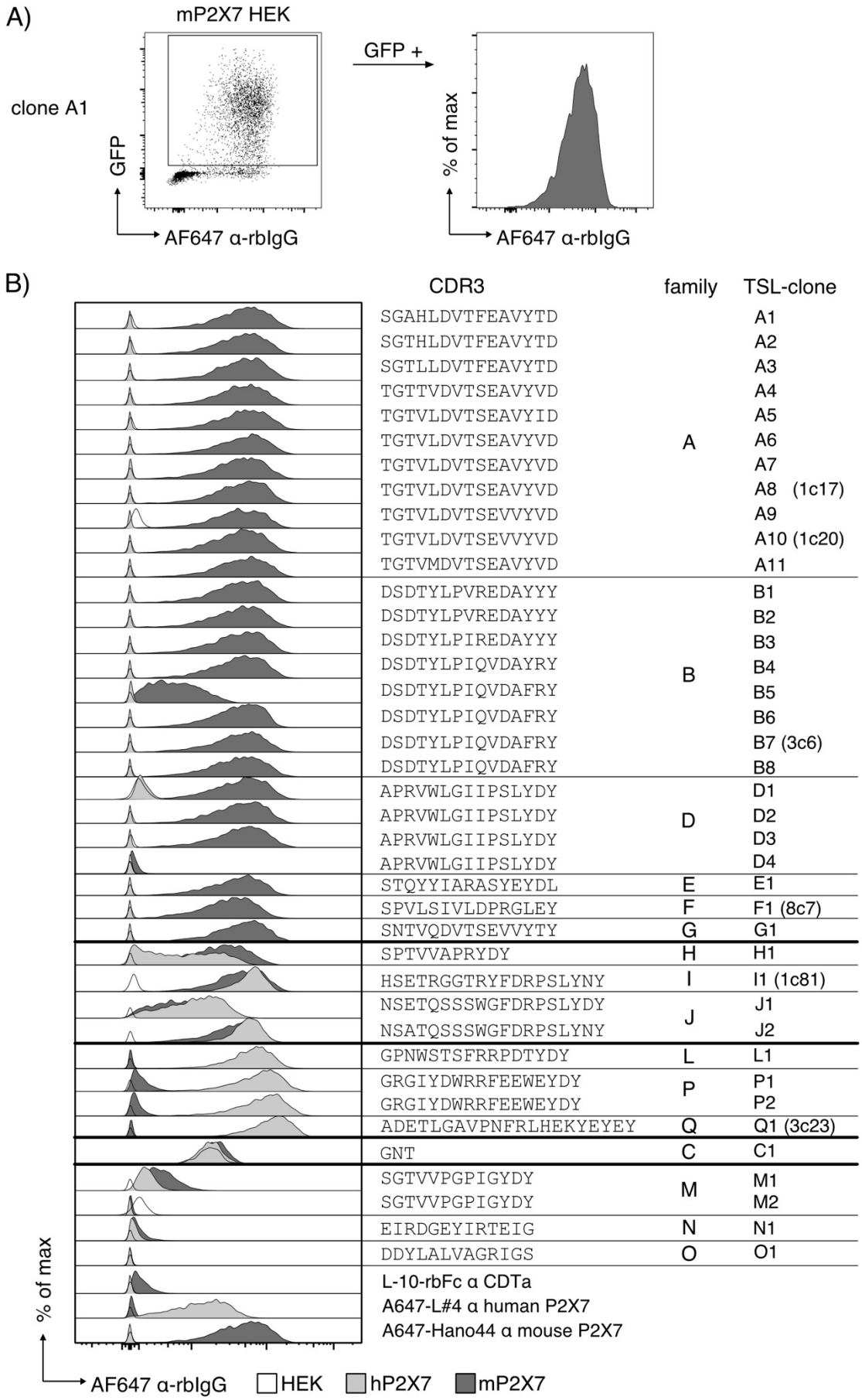
A)
mP2X7 HEK
clone A1
GFP
AF647 α-rbIgG
GFP +
% of max
AF647 α-rbIgG
B)
CDR3
family
TSL-clone
SGAHLDVTFEAVYTD A1
SGTHLDVTFEAVYTD A2
SGTLLDVTFEAVYTD A3
TGTTVDVTSEAVYVD A4
TGTVLDVTSEAVYID A5
TGTVLDVTSEAVYVD A6
TGTVLDVTSEAVYVD A7
TGTVLDVTSEAVYVD A8 (1c17)
TGTVLDVTSEVVYVD A9
TGTVLDVTSEVVYVD A10 (1c20)
TGTVMDVTSEAVYVD A11
A
DSDTYLPVREDAYYY B1
DSDTYLPVREDAYYY B2
DSDTYLPIREDAYYY B3
DSDTYLPIQVDAYRY B4
DSDTYLPIQVDAFRY B5
DSDTYLPIQVDAFRY B6
DSDTYLPIQVDAFRY B7 (3c6)
DSDTYLPIQVDAFRY B8
B
APRVWLGIIPSLYDY D1
APRVWLGIIPSLYDY D2
APRVWLGIIPSLYDY D3
APRVWLGIIPSLYDY D4
D
STQYYIARASYEYDL E1
E
SPVLSIVLDPRGLEY F1 (8c7)
F
SNTVQDVTSEVVYTY G1
G
SPTVVAPRYDY H1
H
HSETRGGTRYFDRPSLYNY I1 (1c81)
I
NSETQSSSWGFDRPSLYDY J1
NSATQSSSWGFDRPSLYNY J2
J
GPNWSTSFRRPDTYDY L1
L
GRGIYDWRRFEEWEYDY P1
GRGIYDWRRFEEWEYDY P2
P
ADETLGAVPNFRLHEKYEYEY Q1 (3c23)
Q
GNT C1
C
SGTVVPGPIGYDY M1
SGTVVPGPIGYDY M2
M
EIRDGEYIRTEIG N1
N
DDYLALVAGRIGS O1
O
L-10-rbFc α CDTa
A647-L#4 α human P2X7
A647-Hano44 α mouse P2X7
% of max
AF647 α-rbIgG
HEK
hP2X7
mP2X7

Figure 4.2.3 Cloned nanobodies contain mP2X7, hP2X7-specific or cross-reactive families. Of 16 nanobody families selected from llama 405, six specifically bind mouse P2X7 (A, B, D, E, F, G), three human and mouse P2X7 (H, I, J), and three human P2X7 (L, P, Q). Family C is unspecific. HEK cells transiently co-transfected with expression constructs for GFP and either mouse or human P2X7 were incubated with HEK cell culture supernatants containing rbIgG hcAbs. Bound rbIgG hcAbs were detected with A647-conjugated rabbit-IgG specific $F(ab')_2$. A) Gating was performed on GFP+ cells. B) Histograms of A647-fluoresence intensity were sorted according to reactivity with mouse P2X7 (dark gray), human P2X7 (light gray), both, unspecific or neither. Reactivity with untransfected HEK cells is shown in empty histograms. Family and clone is indicated on the righty including the name in brackets if it was previously isolated.

4.2.5 Epitope binning of mouse and human P2X7 binders

To determine how the epitopes of the selected nanobodies relate to those of previously selected P2X7-specific nanobodies, cross-blocking experiments using recombinant hcAbs containing the Fc part of different species were performed. **Figure 4.2.4 A** depicts the experimental set-up. The epitope binning was performed by flow cytometric analysis of HEK cells transiently co-transfected with mouse or human P2X7 and nuclear GFP. The cells were preincubated with a hcAb containing the Fc part of mouse IgG2c as blocker (1c81-mIgG). In the presence of the blocker, hcAbs with the Fc of a rbIgG were added as detector. After washing the cells, bound rabbit hcAbs were detected via polyclonal A647-conjugated rabbit-specific $F(ab')_2$ antibodies. In **Figure 4.2.4 B** exemplary plots of unblocked, 1c81-mIgG-blocked or 3c23-mIgG-blocked human P2X7 demonstrate that 1c81 and 3c23 bind to different epitopes. For each blocking antibody, the MFI of the detecting antibody within the GFP-positive gate was set in relation to the corresponding MFI of unblocked cells, and is given as the percentage of residual binding at the bottom right of each plot. Self-blockade of 1c81-rbIgG with 1c81-mIgG2c (top middle plot) or 3c23 self-blockade (bottom right plot) results in 4% and 1% residual detection signal respectively. The 1c81-rbIgG detection signal is slightly reduced to 86% when P2X7-transfected cells are previously incubated with 3c23-mIgG2c. Blockade with 1c81 reduces 3c23 signal to 31%, indicating that the epitopes probably overlap slightly.

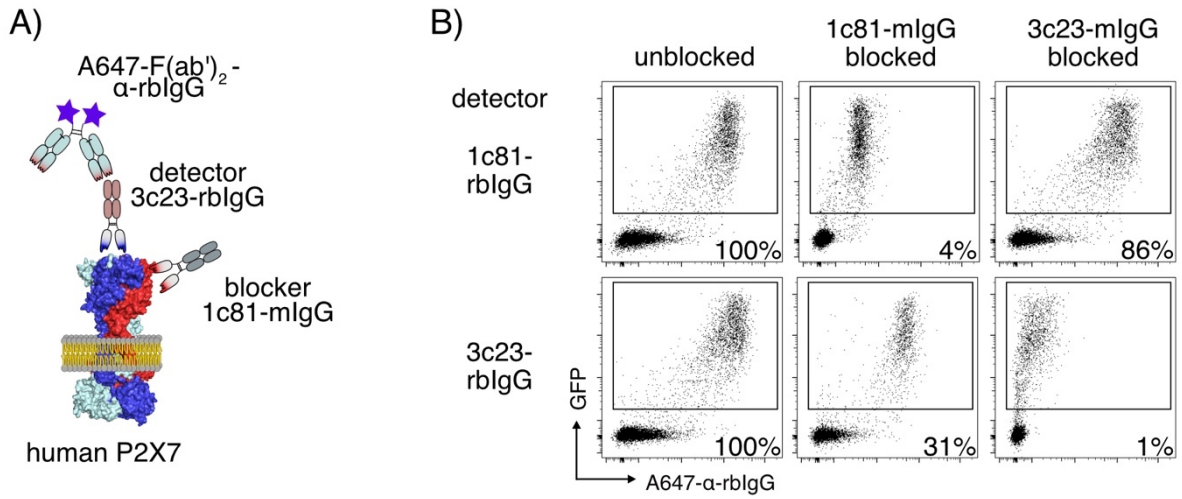

Figure 4.2.4 Cross-blockade of nanobodies on HEK cells transiently transfected with human P2X7. A) Schematic of the experimental set-up showing human P2X7 occupied with 1c81-mIgG as blocking hcAb and simultaneous binding of 3c23-rbIgG as detecting hcAb via a AF647-conjugated rabbit-specific F(ab')2 antibody. B) HEK cells were transiently transfected with human P2X7 and co-transfected with GFP in a ratio of 10 to 1. The cells were incubated with supernatants containing nanobodies as mIgG2c hcAbs or 10 μg/ml (mAb L4) for 20 min to occupy, i.e. block P2X7. Subsequently, supernatants containing VHH-rbIgG hcAbs were added to the cells. Bound rbIgG hcAbs were detected with polyclonal A647-conjugated rabbit-specific F(ab')2 antibodies. To quantify the residual rbIgG hcAb binding after blocking with mIgG2c hcAbs, the mean A647 fluorescence intensity (MFI) was compared to the MFI of unblocked GFP+ cells (square) and is indicated as a percentage at the bottom right of each plot.

Three previously isolated nanobodies specific for human P2X7 (1c81, 1c113 and 3c23) and five for mouse P2X7 (1c81, 13A7, 14D5, 8G11 and 7E2) (Danquah 2012; Danquah et al. 2016) as well as the hP2X7-specific monoclonal antibody L4 (Buell et al. 1998) were used to characterize the epitopes of representative nanobodies from each family isolated in this work. The epitope binning results are summarized in **Table 4.2.6**. for hP2X7 and in **Table 4.2.7** for mP2X7-specific nanobodies.

For hP2X7, three new families (L, P and J) were identified by the panning of llama 405 immune libraries. 1c81 and 3c23 only slightly affect each other's binding to P2X7. Family P binds to the same epitope as 3c23 as suggested by almost absent residual binding of TSL-P1 and TSL-P2 (1% and 3%). Families J and L evidently bind to the same epitope as 1c81 and 1c113. Strikingly, TSL-J2 and TSL-L1 even show enhanced binding (189% and 113%) in the presence of the 3c23 hcAb. The mAb L4 (Buell et al. 1998) blocks binding of all nanobodies except 3c23 and family P.

Table 4.2.6: Cross-blockade results of hP2X7-specific nanobodies. Numbers are percentages of residual signal intensity in comparison to the unblocked signal intensity. Self-blockade is indicated within thick borderlines. Enhanced binding in the presence of the blocking nanobody is indicated in green.

human P2X7		blocking nanobody – mIgG2c hcAb (Llama / mouse origin)			
		1c81 (llama 405)	1c113 (llama 418)	Mab L4 (mouse)	3c23 (llama 405)
detection nanobody - rbIgG hcAb	1c81	4	1	1	86
	1c113	2	2	2	83
	TSL-J1	4	0	1	92
	TSL-J2	10	4	3	189
	TSL-L1	1	8	15	113
	3c23	31	53	86	1
	TSL-P1	38	72	105	1
	TSL-P2	45	72	109	3

Three mouse P2X7-specific nanobody families (D, E and G) identified in this work had not previously been isolated from llama 405. All isolated mouse P2X7-specific nanobodies, as well as nanobodies 13A7 and 14D5 isolated from different llamas (416 & 418) by Welbeck Danquah, seem to bind an epitope overlapping with that of 1c81. Blocking with 1c81 results in complete blockade of all detection antibodies. However, other nanobodies used for epitope blockade of P2X7 do not completely block binding. Nanobodies TSL-F1 and TSL-E1 show a smaller decrease in signal intensity (37-71%) when P2X7 epitopes are blocked with 13A7-, 14D5-, 8G11- and 7E2-mIgG2c hcAbs. Detection by E1 is even slightly enhanced in the presence of 8G11- and 7E2-mIgG2c hcAbs, which indicates a distinct binding epitope. An incomplete block was observed for some nanobodies when the same nanobody was used for blocking and detection (self-blockade), e.g. as in the case of 7E2 (67%), potentially indicating low affinity of the nanobody.

Table 4.2.7: Cross-blockade results of mP2X7-specific nanobodies. Numbers represent % of residual signal intensity in comparison to the unblocked signal. Self-blockade is indicated within bold borderlines.

mouse P2X7		blocking nanobody - migG2c hcAb (isolated from llama)				
		1c81 (405)	13A7 (416)	14D5 (418)	8G11 (411)	7E2 (413)
detection nanobody - rbIgG hcAb	8G11	1	2	3	26	35
	TSL-J1	1	4	2	29	39
	1c81	2	2	1	24	57
	TSL-B1	1	1	1	20	20
	TSL-H1	1	190	3	22	28
	TSL-J2	4	3	15	20	35
	14D5	1	1	19	12	20
	7E2	1	11	25	42	67
	13A7	1	11	39	31	66
	TSL-D2	1	10	46	43	70
	TSL-A1	2	10	42	35	72
	TSL-G1	3	18	46	51	70
	TSL-F1	5	40	53	71	71
	TSL-E1	4	37	57	115	105

In summary, tow new nanobody families (L, P) that specifically bind hP2X7, three new families (D, E, G) that bind mP2X7 and two new nanobody families (H, J) that, like 1c81, bind both mP2X7 and hP2X7, were selected from the phage-display library of llama 405. The binders were characterized in terms of specificity for the mouse or human ortholog of the P2X7 ion channel. In addition, the relative positions of their epitopes compared to those of the previously isolated nanobodies were determined by flow cytometry, resulting in the identification of one family (P) that binds the same epitope as 3c23. The binning experiments for mouse P2X7 revealed that all newly and previously identified nanobodies recognize an epitope that overlaps with that of 1c81 hcAb. However, the binding of the mP2X7/hP2X7 cross-reactive nanobody (TSL-H1) to mP2X7 is strongly enhanced in the presence of the 13A7 hcAb.

4.3 Generation and characterization of P2X5-specific antibodies from rats

This chapter describes the generation of polyclonal mP2X5-specific antisera and a monoclonal antibody that specifically recognizes the human P2X5 receptor. Firstly, the ORFs coding for mouse and human P2X5 were analyzed and ordered as gene blocks. Secondly, the ion channel was expressed in CHO cells as a C-terminal GFP fusion protein. Thirdly, mP2X5 and hP2X5 eucaryotic expression vectors were used to genetically immunize three rats. Polyclonal sera were found to bind overexpressed mouse and human P2X5 on transiently transfected cells, as well as endogenous mP2X5 on *in vitro* differentiated mouse brown adipocytes. Finally, hybridoma cloning was used to isolate a hP2X5-specific antibody.

4.3.1 Most Europeans and East Asians, carry two defective alleles of the *P2RX5* gene while most Sub-Saharan Africans carry one or two functional alleles

The distribution of the previously identified gene-inactivating SNP (rs891746) in the *P2RX5* gene (Kotnis et al. 2010) was analyzed using data from the 1.000 genome project and the Ensemble database (Phase 3) (Clarke et al. 2012). 81% of the sequenced individuals have a C at position 3685513 on chromosome 17 (GRCh38.p13 referenced). In European, East Asian, and North American populations the defective SNP is found at a frequency of 100%, 100% and 95% respectively. In contrast, the functional allele of the *P2RX5* gene is found in most African subpopulations (69%).

To set up a screening assay for this SNP, a 300 bp fragment which included the SNP was amplified from genomic DNA by PCR with primers flanking this region. The SNP was sequenced by using a downstream reverse primer. **Figure 4.3.1 B** shows representative sequencing chromatograms. The corresponding base calls are indicated below each peak as well as the position of exon 10 and the following intron containing the SNP on the coding strand. The left chromatogram represents the homozygous SNP in a European male with a “G” resulting in a splicing defect of exon

10. The right sequence is derived from genomic DNA of a male with a European mother and a Sub-Saharan African father, indicating heterozygosity with one allele coding for the functional and one allele coding for a non-functional P2X5 receptor. As the distribution of this SNP is highly polarized with populations between populations from Europe and Africa, ancient genomes were analyzed.

The “ancient genome browser” of the Max Planck Institute for Evolutionary Anthropology (MPG EVA) provides an access tool to analyze ancient genomes (https://bioinf.eva.mpg.de/jbrowse). The Vindija and Altai Neanderthal genome have been sequenced with high coverage (Meyer et al. 2012; Prufer et al. 2014). In **Figure 4.3.1 C** a schematic is shown representing the archaic phylogenetic tree of Neanderthals and Denisovans that developed in parallel to the modern human (homo sapiens). Both carry the functional allele of the *P2RX5* gene. The ancestral P2X5 trimer was folded using Deepminds Alphafold2 (Varadi et al. 2022; Jumper et al. 2021) to illustrate the position of exon 10 and the second transmembrane domain (**Figure 4.3.1 D**). As the C-terminal end was folded with a low confidence score, the model shows the ion channel in a truncated version (without amino acids 367-444).

The alignment of the amino acid sequence of the defective human P2X5 lacking exon 10 with intact P2X5 of Neanderthal, chimpanzee, rat and mouse indicate that the ancestral human P2X5 ion channel carries the segment encoded by exon 10 and is functional (**Figure 4.3.1 E**).

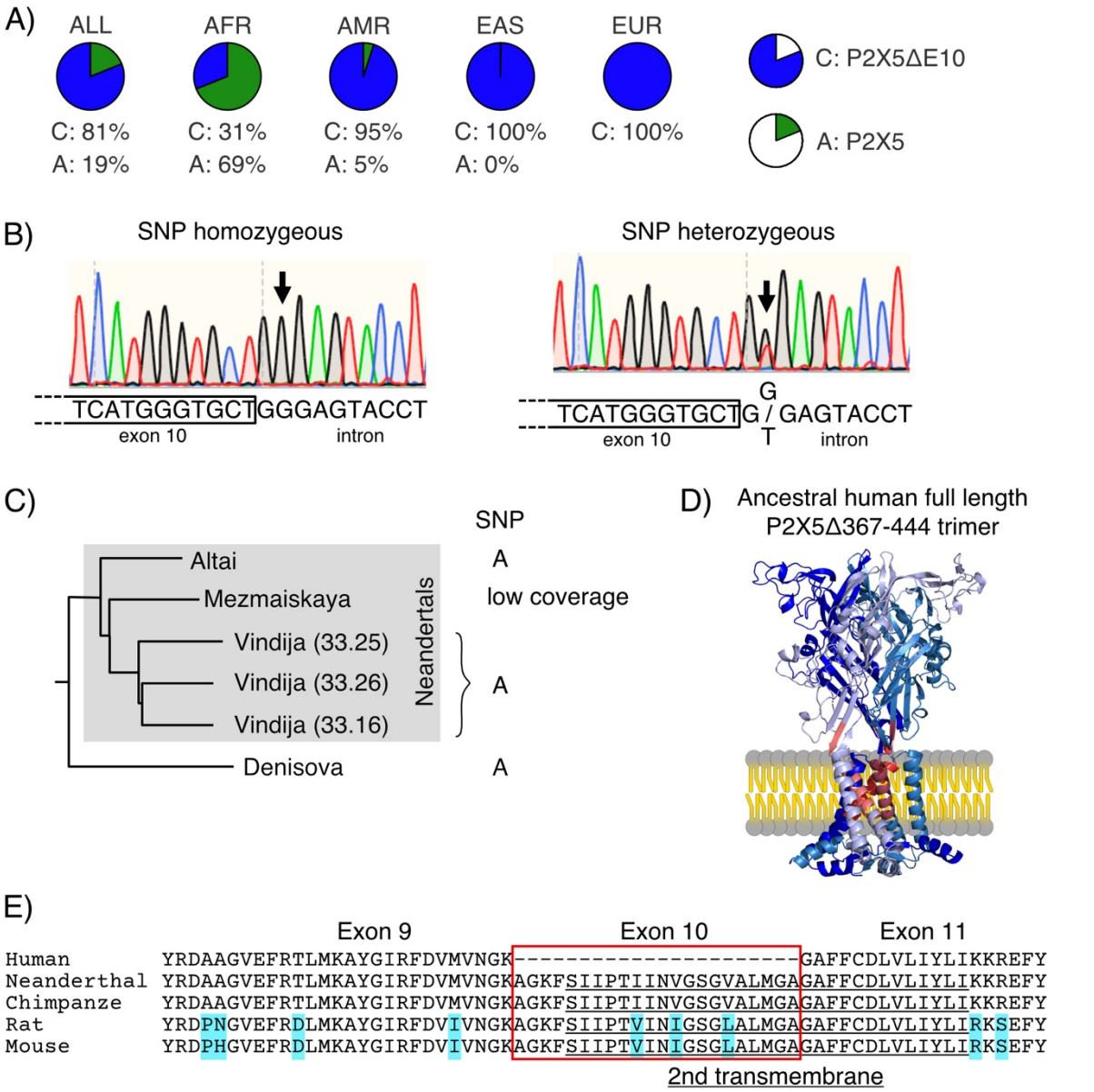

Figure 4.3.1 100% of analyzed European and East Asians are homozygous for the defective P2X5 allele. A) Frequency of the rs891746 SNP in human populations as pie charts, Africa (AFR), America (AMR), East-Asia (EAS) and Europe (EUR). B) Genotyping of the rs891746 SNP in a homozygous European (top) and a heterozygous male with African-American ancestry (bottom). C) Phylogenetic tree of Neanderthal and Denisovan genome with high coverage including the SNP coding for the functional P2X5. D) hP2X5 trimer as a ribbon model predicted by Alphafold2 (C-terminally truncated (Δ367-444). Each hP2X5 monomer is indicated in a different shade of blue. The exon 10, incorporating half of the 2nd transmembrane domain, is colored red. E) Amino acid alignment of the defective human P2X5 lacking the region encoded by exon 10, neanderthal, chimpanzee, rat, and mouse P2X5 from position 300-375 covering the C-terminal end of the extracellular domain, the region encoded by exon 10 (red box) and the second transmembrane domain (underlined). Divergent amino acid residues are colored cyan. A) modified from Phase 3 human genome project. C) modified from MPI EVA (Press release, Max Planck Institute for Evolutionary Anthropology, Leipzig, 19th March 2013).

4.3.2 Recombinant mouse and human P2X5 express well and are located on the cell surface

The full-length open reading frames of mouse P2X5 (Uniprot ID: Q3UYI1) and hP2X5 (Uniprot ID: Q93086 + neanderthal exon 10) were ordered as gene blocks from Twist Biosciences. The genes were codon-optimized for homo sapiens to streamline eucaryotic expression in HEK cells. In **Figure 4.3.2,** an amino acid alignment of human, chimpanzee, mouse and rat P2X5 shows the sequence conservation between the species. Amino acids which differ between mouse and rat are indicated by a red background. Eight of the 24 amino acids which differ between mouse and rat are located in the extracellular domain of P2X5. 131 amino acids differ between the hP2X5 and the rat P2X5 (rP2X5), of which 57 amino acids are extracellular. These species-specific amino acid differences indicate potential binding sites of antibodies raised in immunized rats.

The full length ORFs were cloned into a eucaryotic expression vector (pcDNA3.1) including a C-terminal eGFP. Following transient transfection of CHO-cells, expression of the GFP fusion proteins at the plasma membrane was visualized by fluorescence microscopy. The mouse variant showed lower expression levels but was expressed exclusively at the plasma membrane. The human variant was expressed more strongly, but also showed a high degree of ectopic expression at additional subcellular sites.

A)

```
                                  intra cellular                transmembrane 1
Homo_sapiens          MGQAGCKGLCLSLFDYKTEKYVIAKNKKVGLLYRLLQASILAYLVVWVFLIKKGYQDVDT   60
Pan_troglodytes       MGQAGCKGLCLSLFDYKTEKYVIAKNKKVGLLYRLLQASILAYLVVWVFLIKKGYQDVDT   60
Mus_musculus          MGQAAWKGFVLSLFDYKTAKFVVAKSKKVGLLYRVLQLTILLYLLIWVFLIKKSYQDIDT   60
Rattus_norvegicus     MGQAAWKGFVLSLFDYKTAKFVVAKSKKVGLLYRVLQLIILLYLLIWVFLIKKSYQDIDT   60
                      ****. **: ******** *:*:**.********:**  ** **::*******.***:**

Homo_sapiens          SLQSAVITKVKGVAFTNTSDLGQRIWDVADYVIPAQGENVFFVVTNLIVTPNQRQNVCAE   120
Pan_troglodytes       SLQSAVITKVKGVAFTNTSDLGQRIWDVADYVIPAQGENVFFVVTNLIVTPNQRQNVCAE   120
Mus_musculus          SLQSAVVTKVKGVAYTNTTMLGERLWDVADFVIPSQGENVFFVVTNLIVTPNQRQGICAE   120
Rattus_norvegicus     SLQSAVVTKVKGVAYTNTTMLGERLWDVADFVIPSQGENVFFVVTNLIVTPNQRQGICAE   120
                      ******:*******:***: **:*:*****:***:********************.:***

Homo_sapiens          NEGIPDGACSKDSDCHAGEAVTAGNGVKTGRCLRRENLARGTCEIFAWCPLETSSRPEEP   180
Pan_troglodytes       NEGIPDGACSKDSDCHPGEAVTAGNGVKTGRCLRRENLARGTCEIFAWCPLETSSRPEEP   180
Mus_musculus          REGIPDGECSEDTDCHAGESVVAGHGLKTGRCLRVGNSTRGTCEIFAWCPVETKSMPTDP   180
Rattus_norvegicus     REGIPDGECSEDDDCHAGESVVAGHGLKTGRCLRVGNSTRGTCEIFAWCPVETKSMPTDP   180
                      .****** **:* *** **:*.**:*:*******  * :***********:**.* * :*
                                                 extra cellular
Homo_sapiens          FLKEAEDFTIFIKNHIRFPKFNFSKSNVMDVKDRSFLKSCHFGPKNHYCPIFRLGSVIRW   240
Pan_troglodytes       FLKEAEDFTIFIKNHIRFPKFNFSKSNVMDVKDRSFLKSCHFGPKNHYCPIFRLGSVIRW   240
Mus_musculus          LLKDAEGFTIFIKNFIRFPKFNFSKANVLETGNKHFLKTCHFSSTNLYCPIFRLGSIVRW   240
Rattus_norvegicus     LLKDAESFTISIKNFIRFPKFNFSKANVLETDNKHFLKTCHFSSTNLYCPIFRLGSIVRW   240
                      :**:**.*** ***.**********:**::. :: ***:***. .* *********::**

Homo_sapiens          AGSDFQDIALEGGVIGINIEWNCDLDKAASECHPHYSFSRLDNKLSKSVSSGYNFRFARY   300
Pan_troglodytes       AGSDFQDIALEGGVIGINIEWNCDLDKAASECHPHYSFSRLDNKLSKSVSSGYNFRFARY   300
Mus_musculus          AGADFQDIALKGGVIGIHIEWDCDLDKAASHCNPHYYFNRLDNKHTQSISSGYNFRFARY   300
Rattus_norvegicus     AGADFQDIALKGGVIGIYIEWDCDLDKAASKCNPHYYFNRLDNKHTHSISSGYNFRFARY   300
                      **:*******:****** ***:********.*:*** *.***** ::*:***********
                                                        exon 10   transmembrane 2
Homo_sapiens          YRDAAGVEFRTLMKAYGIRFDVMVNGKAGKFSIIPTIINVGSGVALMGAGAFFCDLVLIY   338
Pan_troglodytes       YRDAAGVEFRTLMKAYGIRFDVMVNGKAGKFSIIPTIINVGSGVALMGAGAFFCDLVLIY   360
Mus_musculus          YRDPHGVEFRDLMKAYGIRFDVIVNGKAGKFSIIPTVINIGSGLALMGAGAFFCDLVLIY   360
Rattus_norvegicus     YRDPNGVEFRDLMKAYGIRFDVIVNGKAGKFSIIPTVINIGSGLALMGAGAFFCDLVLIY   360
                      ***  ***** **********:*************:**:***:****************
                                  intra cellular
Homo_sapiens          LIKKREFYRDKKYEEVRGLEDSSQEAEDEASGLGLSEQLTSGPGLLGMPEQQELQEPPEA   398
Pan_troglodytes       LIKKREFYRDKKYEEVRGLEDSSQEAEDEASGLGLSEQLTSGPGLLGMPEQQELQEPPEA   420
Mus_musculus          LIRKSEFYRDKKFEKVRGQKEEDNVEVE-AN--EMEQELPEDKPLERV------HQDEQA   411
Rattus_norvegicus     LIRKSEFYRDKKFEKVRGQKEDANVEVE-AN--EMEQERPEDEPLERV------RQDEQS   411
                      **:* *******:*:*** ::. :   : *.   :.::  ..  *  :      ::  ::

Homo_sapiens          KRGSSSQKGNGSVCPQLLEPHRST--------------------422
Pan_troglodytes       KRGSSCQKGNGSVCPQLLEPHRSGHLQNAQVNLEQLQTVEM---461
Mus_musculus          LELAQSGRKQNSNCQVLFEPARSGLQENAFVNMKPSQILQTVKT 455
Rattus_norvegicus     QELAQSGRKQNSNCQVLLEPARFGLRENAIVNVKQSQILHPVKT 455
                       . :.. : :.* *  *:** *
```

B)

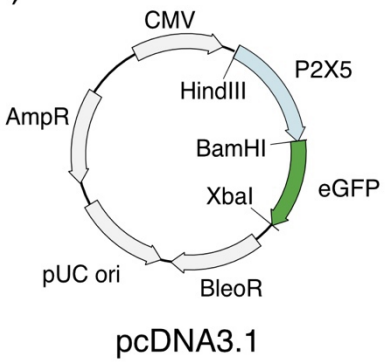

pcDNA3.1

C)

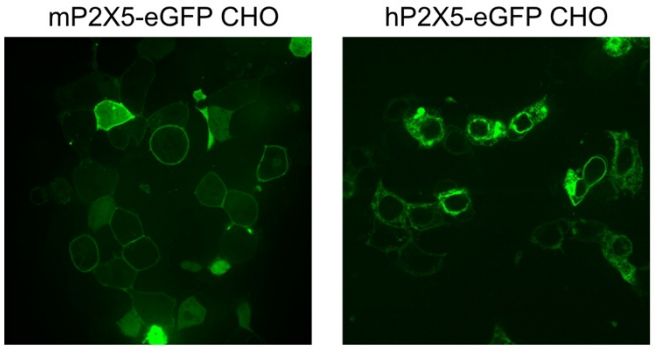

4.3.2 The highly conserved P2X5 ion channel is well expressed with a C-terminal GFP fusion protein in CHO cells. A) Amino acid alignment of the human, chimpanzee, mouse, and rat P2X5 ion channel. Non-conserved amino acids between chimp & human or rat & mouse are colored cyan or red respectively. Important domains are framed with a red box (exon 10), underlined (second transmembrane domain) or have an orange font (N-linked glycosylation sites). Grey background indicates the intracellular n- and c-terminus. Asterisks below the alignment indicate residues conserved in all 4 sequences. B) Cloning schematic of the P2X5 receptor in frame with a C-terminal eGFP. C) Plasma membrane localization of GFP by CHO cells transiently transfected with mouse or human P2X5-eGFP.

4.3.3 Gene gun immunization of rats

Three rats (R21.18, R21.21 and R21.22) were gene-gun immunized four times with the mP2X5-eGFP and hP2X5-eGFP expression vectors coupled to gold nanoparticles in three-week intervals. Successful delivery of gold nano particles into the skin was indicated by brownish coloring at the particle penetration sites (**Figure 4.3.3**).

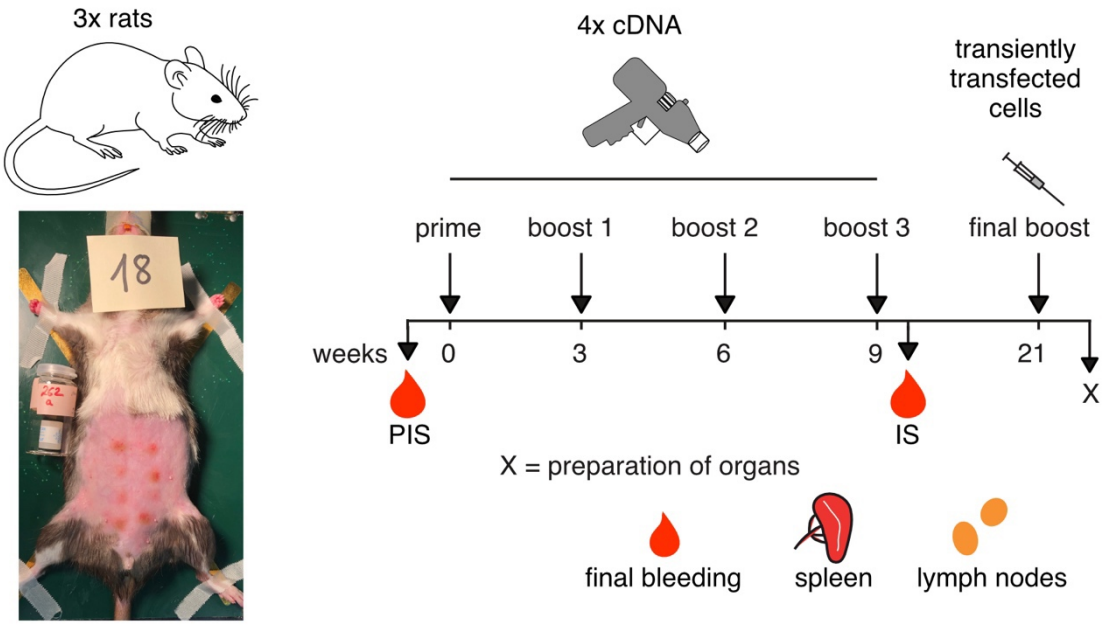

Figure 4.3.3 Gene gun immunization schedule. Three rats were genetically immunized four times with eucaryotic expression vector containing the ORF of human P2X5 or mouse P2X5 with a C-terminal GFP. For each immunization rats were anaesthetized and immobilized on a heating pad back side down and abdominal skin was depilated. Rat abdominal skin after a gene gun immunization and container for ammunition is depicted. The rats' final boost was with human and mouse P2X5 transiently transfected HEK cells. They were bled three days later. Lymphatic organs, spleen and lymph nodes were extracted to isolate B cells for hybridoma fusion.

The final boost was carried out using transiently transfected HEK cells. Prior to the first immunization and after the 3rd boost, serum was drawn to evaluate the antibody response. Three days after the final boost, a final bleed was obtained by heart puncture. Spleen, and lymph nodes cells were prepared from the sacrificed animals for fusion with Sp2/0 myeloma cells to generate antibody secreting hybridomas (Koch-Nolte et al. 1999).

4.3.4 Immune sera of rats react specifically to human P2X5-eGFP on transiently transfected CHO and HEK cells

The presence of P2X5-specific antibodies in the immune sera was assessed by incubating CHO cells transiently transfected with hP2X5-eGFP with the titrated final bleed sera. Bound antibodies were detected with fluorochrome-conjugated rat IgG-specific secondary antibodies. Cell nuclei were counterstained with DAPI (**Figure 4.3.4 A**). Additional experiments to assess immune sera for the presence of P2X5-specific antibodies were performed on transiently transfected HEK cells and analysis by flow cytometry (**Figure 4.3.4 B**). The results show that the sera contain antibodies that bind HEK cells transiently transfected with the ancestral hP2X5-eGFP, but do not bind cells transfected with hP2X7-eGFP, which was used as a negative control.
To isolate a monoclonal antibody, hybridoma technology was applied. Cells from spleen and lymph nodes were prepared and fused to SP2/0 myeloma cells to generate hybridoma cells (**Figure 4.3.4 C**). Fused cells of R21.18 were plated on twelve 96 well plates. Two weeks later, the supernatants of 150 growing single clones were screened for the presence of rat antibodies that bind to cells expressing mP2X5-eGFP or hP2X5-eGFP. The supernatants of 25 clones showed reactivity. To exclude potential GFP-specific clones, a secondary screening was carried out with cells expressing mP2X5 and hP2X5 without a C-terminal GFP (**Figure 4.3.4 D**). One clone (R21.18-A34) that produced antibodies that specifically bind ancestral hP2X5 was confirmed by immunofluorescence microscopy (IFM) (**Figure 4.3.4 E**). The hybridoma was subcloned to obtain homogeneous clones secreting the monoclonal antibody. Flow cytometry showed that subclone mAb R21.18-A34#19 bound to hP2X5 independently of the presence of the C-terminal eGFP domain (**Figure 4.3.3 F**).

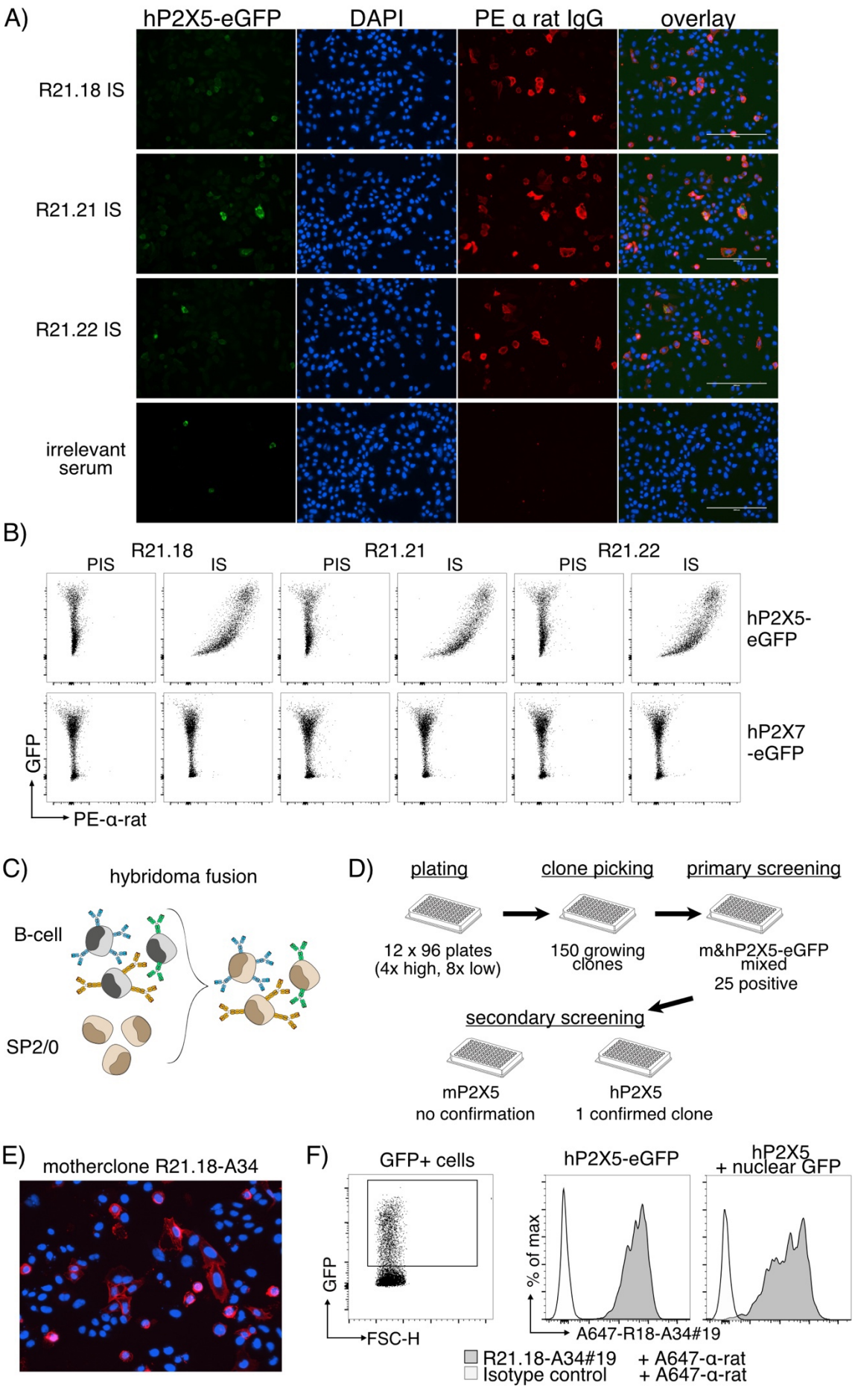
A)
hP2X5-eGFP
DAPI
PE α rat IgG
overlay
R21.18 IS
R21.21 IS
R21.22 IS
irrelevant serum
B)
R21.18
R21.21
R21.22
PIS
IS
hP2X5-eGFP
hP2X7-eGFP
GFP
PE-α-rat
C)
hybridoma fusion
B-cell
SP2/0
D)
plating
clone picking
primary screening
12 x 96 plates (4x high, 8x low)
150 growing clones
m&hP2X5-eGFP mixed
25 positive
secondary screening
mP2X5
no confirmation
hP2X5
1 confirmed clone
E)
motherclone R21.18-A34
F)
GFP+ cells
hP2X5-eGFP
hP2X5 + nuclear GFP
GFP
FSC-H
% of max
A647-R18-A34#19
R21.18-A34#19 + A647-α-rat
Isotype control + A647-α-rat

Figure 4.3.4 The sera of three immunized rats and the cell culture supernatant of hybridoma R21-18-A34 contain antibodies that specifically bind cells expressing hP2X5 . A) CHO cells were transiently transfected with ancestral hP2X5-eGFP. 48h after transfection, cells were fixed with 2% PFA for 10 min and incubated with 1/400 diluted immune sera of rats 21.18, 21.21 and 21.22 or a control serum. Bound antibodies were detected using a PE-conjugated rat IgG-specific polyclonal secondary antibody. Nuclei were counterstained with DAPI. Microscopy images of hP2X5-eGFP, DAPI and PE α-rat are combined in an overlay. B) HEK-T cells were transiently transfected with either hP2X5-eGFP or control antigen hP2X7-eGFP. After 24h cells were incubated with 1/400 diluted rat pre-immune serum or immune serum. Bound rat antibodies were detected using a PE-conjugated polyclonal antibody. Cells were analyzed by flow cytometry. C) Schematic of hybridoma fusion of B cells and SP2/0 mouse myeloma cells. D) Schematic of hybridoma plating and screening. E) CHO cells transiently transfected with hP2X5 stained with hybridoma mother clone R21.18-A34. F) HEK-T cells were transiently transfected with a hP2X5-eGFP fusion protein or hP2X5 co-transfected with nuclear GFP. hP2X5 was detected with A647-conjugated mAb R21.18-A34#19.

4.3.5 Antibodies in the sera of the immunized rats recognize endogenous mP2X5

The presence of mouse P2X5-specific antibodies in the immune sera of rats R21.18, R21.21 and R21.22 was confirmed by IFM stainings of CHO-cells transiently transfected with mP2X5-eGFP (**Figure 4.3.5 A**). Pre- and immune sera of R21.18 were additionally evaluated for the presence of mP2X5-specific antibodies by comparing the staining of CHO cells transiently transfected with mP2X5 (without the GFP domain) with *in vitro* differentiated brown adipocytes (**Figure 4.3.5 B**).

The expression of mP2X5 in adipocytes was quantified using qPCR (**Figure 4.3.5. C**). Brown adipocytes were differentiated for 9 days, and P2X4, P2X5, and P2X7 mRNA levels were evaluated. In contrast to P2X4 and P2X7, the expression P2X5 rose substantially over the course of differentiation. qPCR and brown adipocyte differentiation was conducted by Michelle Yvonne Jäckstein, AG Heeren (UKE).

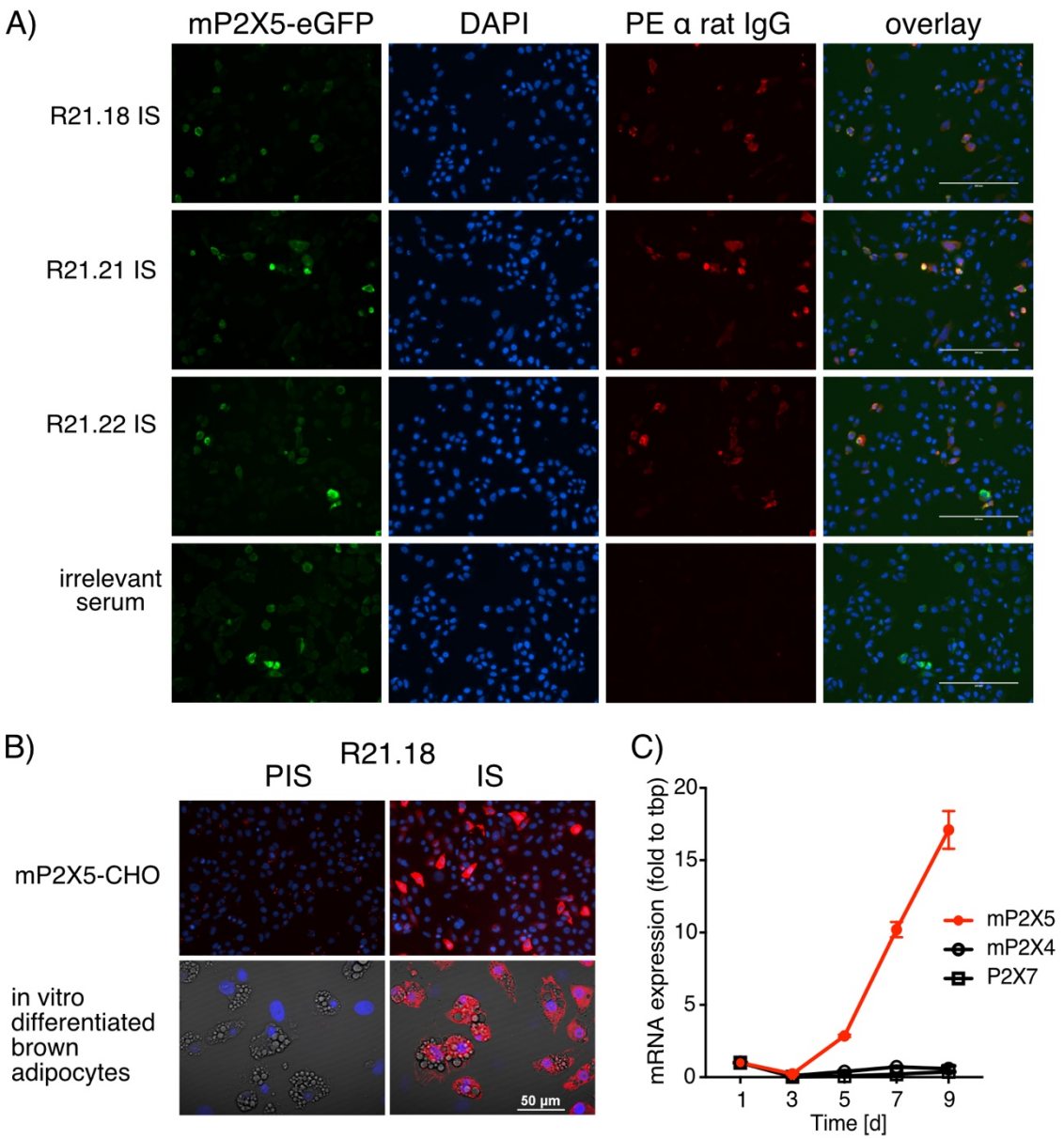

Figure 4.3.5 Antibodies from rat immune sera specifically detect mP2X5 on the cell surface of transiently transfected CHO cells and endogenous expressing *in vitro* differentiated brown adipocytes. A) CHO cells were transiently transfected with mP2X5-eGFP. 48h after transfection, cells were fixed with 2% PFA for 10 min and incubated with serially diluted immune sera of rats 21.18, 21.21 and 21.22. Nuclei were counterstained with DAPI. Pictures of mP2X5-eGFP, DAPI and PE α-rat are combined in overlay. B) CHO cells overexpressing transiently transfected mP2X5 (w/o GFP), or brown adipocytes differentiated *in vitro* for 9 days were stained with pre- and immune serum of R21.18. Bound antibodies were detected with PE-conjugated anti rat IgG (H+L). C) Quantification of P2X4, -5, and -7 mRNA in brown adipocytes during differentiation normalized to tbp (TATA binding protein housekeeping gene).

In summary, the ORFs of the mouse and human P2X5 ion channels were cloned into a eucaryotic expression vector and used to generate polyclonal antibodies by genetic immunization of three rats. Additionally, a monoclonal antibody specific for the human P2X5 ion channel was isolated. The polyclonal antibodies were shown to recognize endogenously expressed P2X5 on the surface of differentiated mouse brown adipocytes.

4.4 Generation and analysis of a functional P2X4/P2X7 double knockout mouse model

This chapter outlines the establishment of a P2X4/P2X7 double deficient mouse model, and its application to a model of pharmacologically induced BAT inflammation. The first two sections characterize and describe the P2X7 inhibiting half-life extended nanobody construct 13A7-dim-αAlb and the mouse model of futile thermogenic activation. In the last section, a functional double knock-out of P2X4 and P2X7 is established by injecting the P2X7 antagonistic nanobody 13A7-dim-αAlb into *P2rx4*$^{-/-}$ Balb/c mice. It is then shown that simultaneous blockade of P2X4 and P2X7 signaling rescues the BAT from pharmacologically induced inflammation.

4.4.1 13A7 specifically and effectively blocks ATP-induced activation of mouse P2X7

13A7-dim-αAlb is a homo-dimeric mP2X7-specific nanobody fused to an anti-albumin nanobody to extend its half-life *in vivo* (**Figure 4.4.1 A**) (Danquah et al. 2016). The construct was efficiently produced in HEK 6E cells and purified from 6-day supernatants by Ni-NTA affinity chromatography via its C-terminal hexa-histidine tag. The purified 13A7-dim-αAlb was essentially free of contaminants as assessed by SDS-PAGE analysis (**Figure 4.4.1 B**).

The specificity and function of 13A7-dim-αAlb, for example its capacity to block the release of IL-1β by LPS-primed and ATP-activated blood leucocytes, have been previously described by (Danquah et al. 2016) and are illustrated in **Figure 4.4.1 C**.

To evaluate the inhibitory potency of 13A7-dim-αAlb *in vivo*, the sensitivity of primary peritoneal macrophages to ATP was analyzed 2h and 96h after injection of the 13A7-dim-αAlb into mice. The results show that ATP-induced DAPI uptake was strongly reduced in 13A7-dim-αAlb-treated mice in comparison to PBS-treated mice at 2h and at 96h after injection (**Figure 4.4.1 D,** from Danquah et al., 2016).

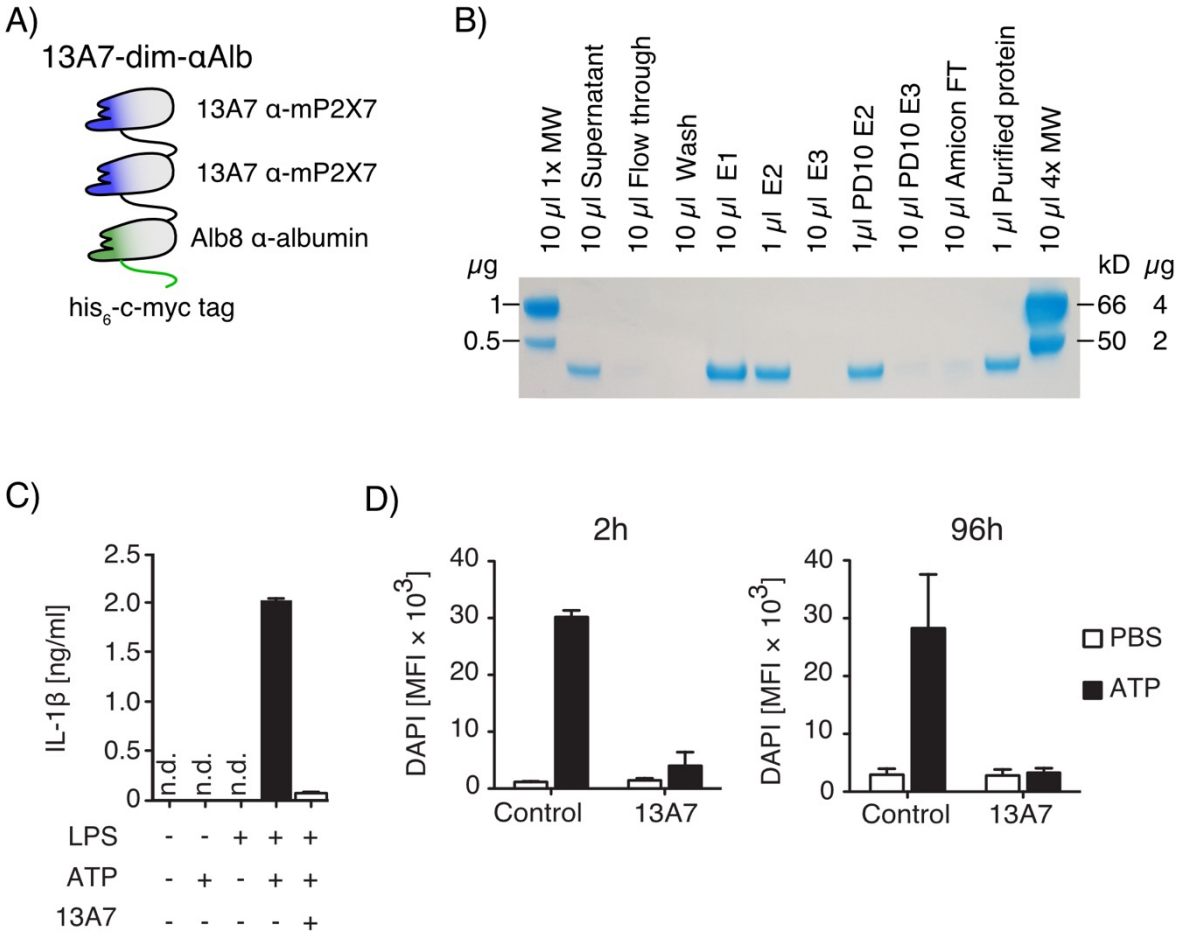

Figure 4.4.1 The nanobody trimer 13A7-dim-αAlb blocks ATP-mediated P2X7-activation of mouse peritoneal macrophages. A) Schematic representation of 13A7-dim-αAlb-his-c-myc with a mP2X7-specific nanobody homodimer (13A7, blue CDR loops) and the albumin-specific nanobody (Alb8, green CDR loops) in frame with a C-terminal hexa-histidine and a c-myc tag (green line). B) 6 d after transient transfection of HEK-6E cells, 13A7-dim-αAlb was purified from the cell culture supernatant via Ni-NTA affinity chromatography. Proteins in the indicated aliquots of the indicated fractions during purification were analyzed by SDS-PAGE and Coomassie staining (HEK cell supernatant; Ni-NTA-column flow through, wash, eluates E1-E3; E2 and E3 after desalting on a PD-10 column and centrifugation through an Amicon filter (cut-off 5 kD). C) IL-1β released by cells in heparinized fresh mouse blood was determined by ELISA after incubation of cells for 4h in the presence or absence of LPS and a 13A7 nanobody dimer, and a 20 min treatment with ATP (n=3). n.d. = not detectable. D) Peritoneal macrophages were prepared from mice 2 and 96 hours after injection of 13A7-dim-αAlb or control-dim-αAlb. DAPI uptake was analyzed by flow cytometry after treatment of cells with PBS or ATP for 20 min. Data is mean ± SD. C) is from Figure S3, D) is from Figure 4 of Danquah *et al.* (2016).

4.4.2 Treatment of mice with etomoxir & CL316243 causes inflammation and remodeling of brown adipose tissue

WT C57BL/6 (B6) mice were injected with a combination of the β3-adrenergic agonist CL316,243 (CL), which activates brown adipose tissue by mimicking sympathetic stimulation, and Etomoxir (Eto), a blocker of the mitochondrial fatty acid transport protein carnitine palmitoyl transferase 1 (CPT1) which results in mitochondrial dysfunction and loss of the uncoupling protein UCP1. Mice were treated with CL/Eto on three consecutive days and BAT was harvested after 72h (**Figure 4.4.2 A**). Histology of tissue sections showed a strong increase of staining for MAC2/Galectin-3, an established biomarker of macrophage activation, inflammation and tissue fibrosis (Henderson and Sethi 2009) as well as typical crown-like structures reflecting tissue remodeling (**Figure 4.4.2 B**).

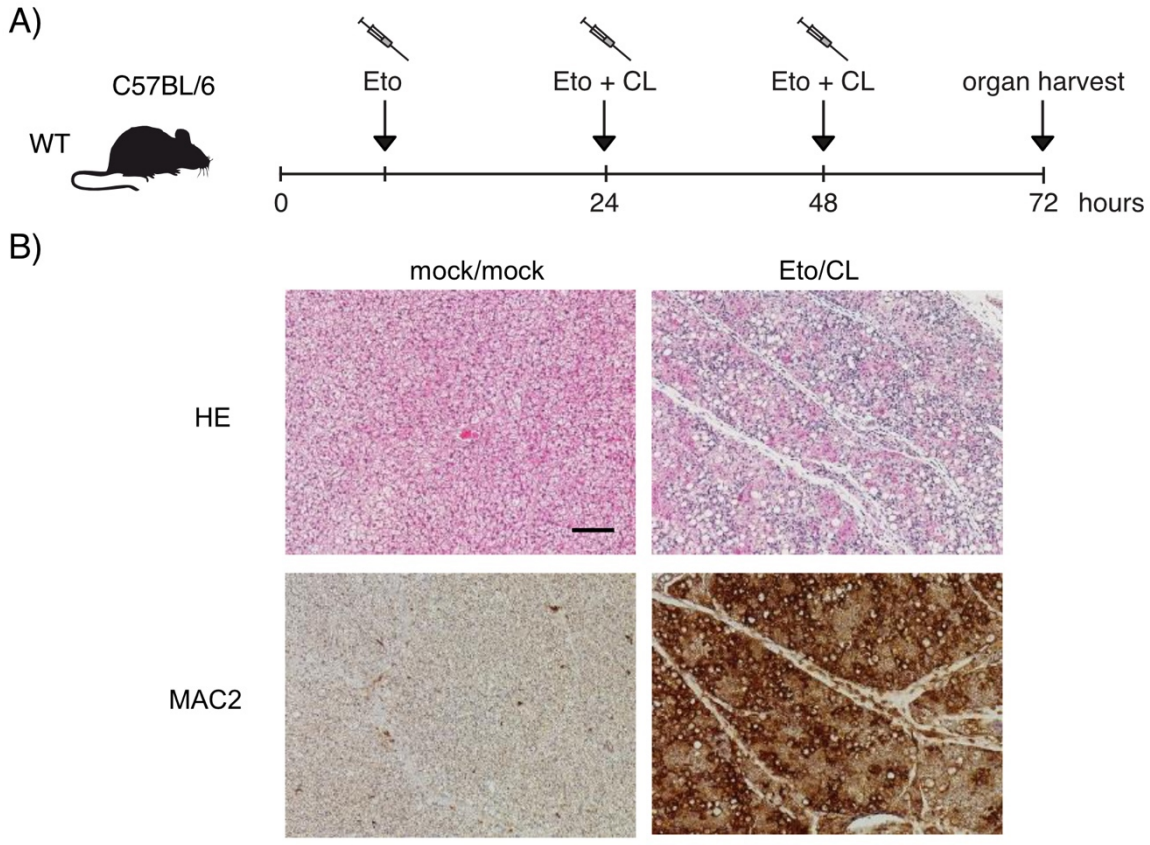

Figure 4.4.2 Combined treatment of B6 mice with Eto & Cl results in strong inflammation of brown adipose tissue. A) B6 were treated with the β-oxidation inhibitor Eto and the β3-adrenergic agonist CL as indicated in the scheme. BAT was prepared on d3. B) Representative images showing H&E staining and MAC2 immunostaining of BAT from Eto/CL- and control-treated mice. Histology images were adapted from Jäckstein, Dissertation (Jäckstein 2022)

4.4.3 The transient double knockout of P2X4 and P2X7 prevents monocyte infiltration into inflamed BAT

Since it has been shown that P2X4 and P2X7 can have mutually compensatory effects (Weinhold et al. 2010), the effect of simultaneously blocking of P2X4 and P2X7 was evaluated in this model. As *P2rx4* and *P2rx7* are tandem genes on chromosome 5, it is practically impossible to generate a *P2rx4*/*P2rx7* double knockout by backcrossing mice (**Figure 4.4.3 A**). To circumvent this problem, *P2rx4*$^{-/-}$ mice were injected with the 13A7-dim-αAlb to block ATP-mediated gating of the P2X7 ion channel. Subsequently, the effects of the double knockout on BAT inflammation were studied in the BAT-inflammation model described above. In contrast to **Section 4.4.2** the double knockout experiments were performed with mice on the Balb/c background. To discriminate tissue-resident monocytes from those present in the vasculature, a PerCP-conjugated anti-CD45 antibody was injected i.v. shortly before sacrifice of the mice (**Figure 4.4.3 B**).

The results show that inactivation of the *P2rx4* gene or nanobody-mediated blockade of P2X7 alone was not sufficient to prevent BAT inflammation. BAT of both, WT mice injected with 13A7-dim-αAlb, and of *P2rx4*$^{-/-}$ mice responded to CL/Eto treatment with elevated MAC2 staining and crown formation, at similar levels as WT mice. Only the combination of 13A7-dim-αAlb treatment and genetic inactivation of *P2rx4* and 13A7 treatment prevented CL/Eto-induced MAC2 immune staining and tissue remodeling of BAT (**Figure 4.4.3 C**). The results of Western blot analyses of BAT tissue from individual mice show that the combination of P2rx4 gene inactivation and treatment with 13A7-dim-αAlb prevented the CL/Eto-induced loss of UCP1 as well as the increase of MAC2 (**Figure 4.4.3 D**).

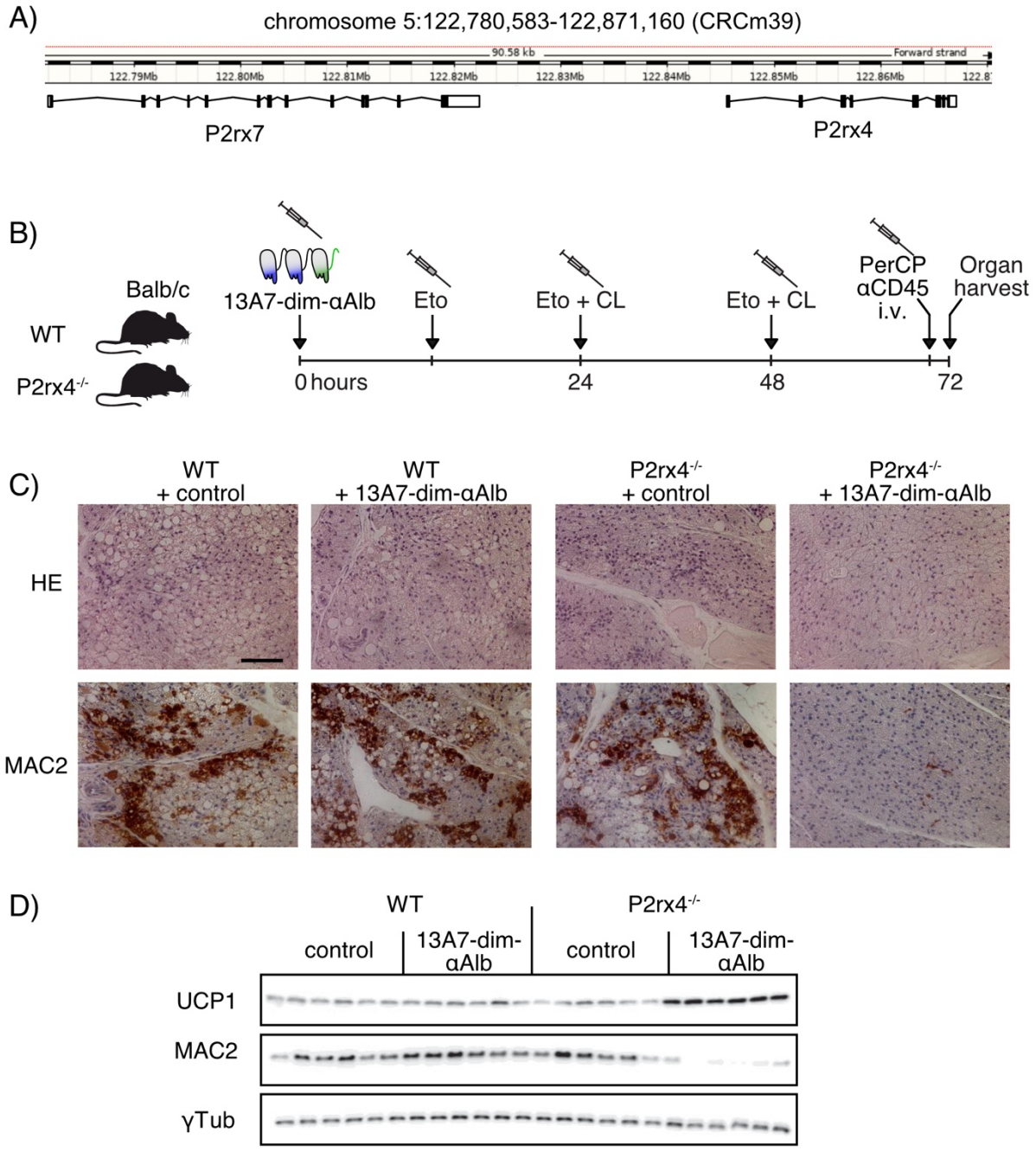

Figure 4.4.3 Simultaneous blockade of P2X4 and P2X7 prevents CL/Eto induced BAT inflammation and remodeling. A) Tandem location of the *P2rx7* and *P2rx4* genes on mouse Chromosome 5, separated by a distance of only ~20 kilobases. B) Schematic of a transient P2X4/P2X7 double knockout. WT or *P2rx4*-/- Balb/c mice were injected with 3.5 mg/kg 13A7-dim-αAlb 4h prior to Eto/CL treatment. 1 min prior to BAT preparation, PerCP-conjugated anti-CD45 antibody was injected i.v. to stain immune cells localized in the vasculature. C) Representative H&E and MAC2 immunostaining images of BAT from WT or *P2rx4*-/- Balb/c mice treated with 13A7-dim-αAlb or a control construct. D) Western blot analysis of UCP1 and MAC2 protein levels in BAT from CL/Eto-treated mice. γ-Tubulin was used as loading control. Histology and western Blot images were prepared by Michele Jäckstein, 2022 (Jäckstein 2022)

Monocyte infiltration into BAT was quantified by flow cytometry. BAT from two mice was pooled, resulting in 3 pools per group of *P2rx4*$^{-/-}$ Balb/c mice, receiving 13A7-dim-αAlb or a control construct prior to CL/Eto treatment. One min before sacrifice, mice received an injection of αCD45/PerCP to stain vascular leukocytes (**Figure 4.4.3 A**). BAT was harvested and enzymatically digested to obtain the stromal and vascular fraction of cells containing endothelial cells, adipocytic precursors, pericytes, pre-adipocytes and leukocytes. After depletion of erythrocytes and blocking of Fc-receptors to reduce unspecific binding of fluorochrome-conjugated antibodies, cells were stained with LIVE/DEAD™-APC-Cy7, αCD45-PE-Cy7 and αCD11b-AF647. The staining of CD45 with a second fluorophore was used to discriminate vascular cells from stromal cells. Thus, within the CD45-PE-Cy7+ population, tissue-resident monocytes were CD45-PerCP^{low}, while vascular monocytes were CD45-PerCP^{hi}. The gating strategy is outlined in **Figure 4.4.4 A**, and representative FACS plots of BAT monocytes from mice from each treatment group are shown in **Figure 4.4.4 B**. Quantification of live cells, vascular, and tissue-resident monocytes is shown in **Figure 4.4.4 C**. The results show that P2rx4-/- mice treated with 13A7-dim-Alb show a significantly higher proportion of live cells and a significantly lower proportion of stromal monocytes that the other groups.

By using the well-characterized P2X7-inhibitory 13A7-dim-αAlb nanobody construct, a combined functional deficiency of P2X4 and P2X7 ion channel activity was achieved in *P2rx4*$^{-/-}$ Balb/c mice. In contrast to *P2rx4*$^{-/-}$ knockout or P2X7 antagonism alone, this double targeting strategy prevents the CL/Eto-induced, inflammation, monocyte infiltration and remodeling of BAT.

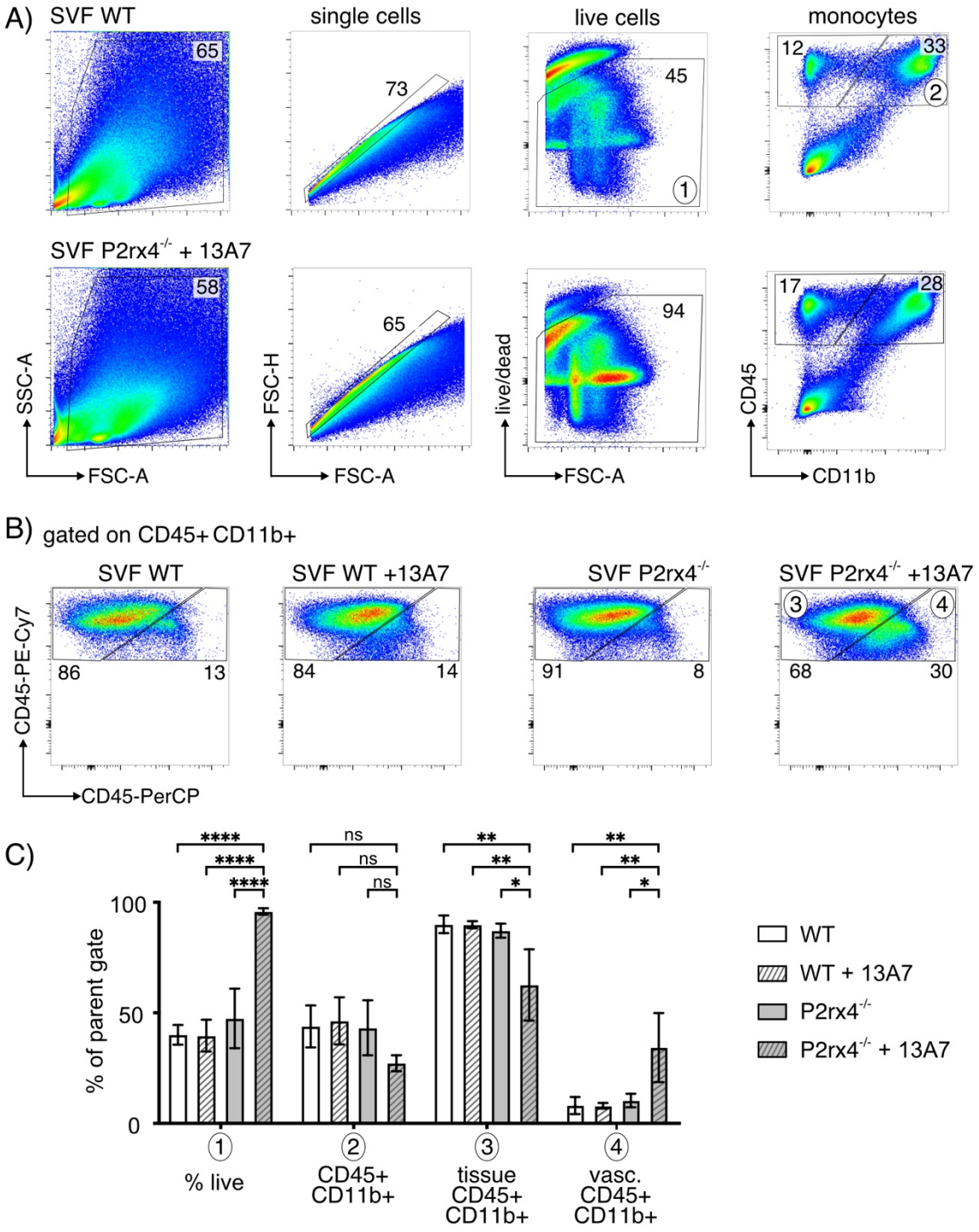

Figure 4.4.4 Combined inactivation of P2X4 and blockade of P2X7 reduces CL/Eto-induced loss of cell viability and monocyte infiltration into BAT. A) Gating strategy to evaluate CL/Eto-induced loss of cell viability and infiltration of monocytes (CD45+/CD11b+ cells) into BAT. B) FACS plots illustrating the staining of monocytes (gated on CD45+/CD11b+ cells) with CD45-PerCP (injected i.v. 1 min before sacrifice) and CD45-PE-Cy7 (*ex vivo* staining). Vascular monocytes are PerCP^{hi}/PECy7^{hi}, activated stromal monocytes are PerCP^{lo}/PE-Cy7^{hi}. C) Quantification of cell viability total monocytes, and the proportion of stromal and vascular monocytes in BAT. Data are mean ± S.E.M. with n=6, (two BATs pooled per group). Student's t test was used for statistical analysis.

5 Discussion

In this study new nanobody and antibody tools have been developed and applied to investigate purinergic signaling during inflammation. Firstly, it was shown that newly developed llama-Ig-transgenic LaMice respond to protein immunization to generate nanobodies specific for mouse IgG2c, thereby generating a useful secondary reagent for further studies on purinergic signaling. Secondly, new nanobodies recognizing novel epitopes of mouse and human P2X7 were isolated by phage display from an existing library derived from a genetically immunized llama. Thirdly, new poly- and monoclonal antibodies against an interesting player of purinergic signaling, the P2X5 ion channel, were raised by genetic immunization and hybridoma technology. Finally, by creating a combined deficiency of P2X4 and P2X7 ion channel activity, a new mouse model to study the involvement of P2X4 and P2X7 purinergic signaling during inflammation of brown adipose tissue was established. In contrast to single inactivation of either of the two genes, simultaneous functional “knockout” of both ion channels prevented the massive invasion of immune cells seen in a pharmacological model of BAT inflammation.

In the following chapter, these findings are discussed and put into context.

5.1 Generation of high-quality secondary reagents in LaMice

Since the discovery of the heavy chain only antibodies camelids in 1989 (Hamers-Casterman et al. 1993), nanobodies have proven to be tools of extensive flexibility, useful both in diagnostics as well as therapeutics. This led to the creation of a spin-off company (Ablynx) from the Vlaams Interuniversitair Instituut voor Biotechnologie (VIB). In 2018 Ablynx’s first drug ‘Caplacizumab’, a bivalent nanobody targeting von - Willebrand factor (vWF), was approved by the FDA for the treatment of acquired thrombotic thrombocytopenic purpura. Just recently (2022), a second therapeutic agent was approved, which contains a nanobody-based chimeric antigen receptor (CAR) which targets the B cell maturation antigen (BCMA) for treatment of patients with multiple myeloma.

To date, nanobodies have been mostly generated from immunized camelids or synthetic libraries. Several transgenic mouse strains have been developed that can

produce heavy chain antibodies (Janssens et al. 2006), e.g. by using genes for human variable domain (in most cases VH3). However, the human VH domain is prone to aggregation, as the hydrophobic amino acids in the framework region 3 are still present. Camelid VHH elements have undergone a million years of evolution to form soluble, non-aggregating V elements. The LaMice used in this study can select between 6 different VHH elements and one VH3 element from llama to generate hcAbs to target immunogens.

In this study, LaMice developed in the Koch-Nolte lab at the UKE were immunized with I+10-mIgA and MU1067-mIgG2c hcAb to produce nanobodies specific for either for the N-terminal nanobody or the mIgG2c Fc-region. Several mIgG2c-specific binders were identified by direct cloning of the nanobody immune repertoire into an eucaryotic expression vector and subsequent expression as heavy chain-only antibodies. The isolated nanobodies were thoroughly characterized for specificity and affinity, and assigned to families on the basis of common motifs in their CDR3 regions. Nanobody families D and E proved to be highly specific for mIgG2c with medium to high affinity in the low nanomolar range and did not bind to other mouse immunoglobulins (IgM, IgG1, IgG2a or IgG2b) (compare **Figure 4.1.6**).

Common laboratory mouse strains carry different allelic variants of the *Igh* locus encoding the immunoglobulin heavy chain. Notably, the IgG2a and IgG2c isotypes have been identified as allelic variants at the same locus. Thus, C57BL/6 (B6) mice have the *IgG2c* genotype (Zhang et al. 2012), whereas Balb/c mice carry the *IgG2a* genotype (Morgado et al. 1989).

Figure 5.1 A shows an amino acid alignment of the hinge, CH2, and CH3 domains of mouse IgG2a and IgG2c. The CH2 domain contains 7, the CH3 domain 32 divergent amino acids, which represent potential binding sites of the nanobody families D and E.

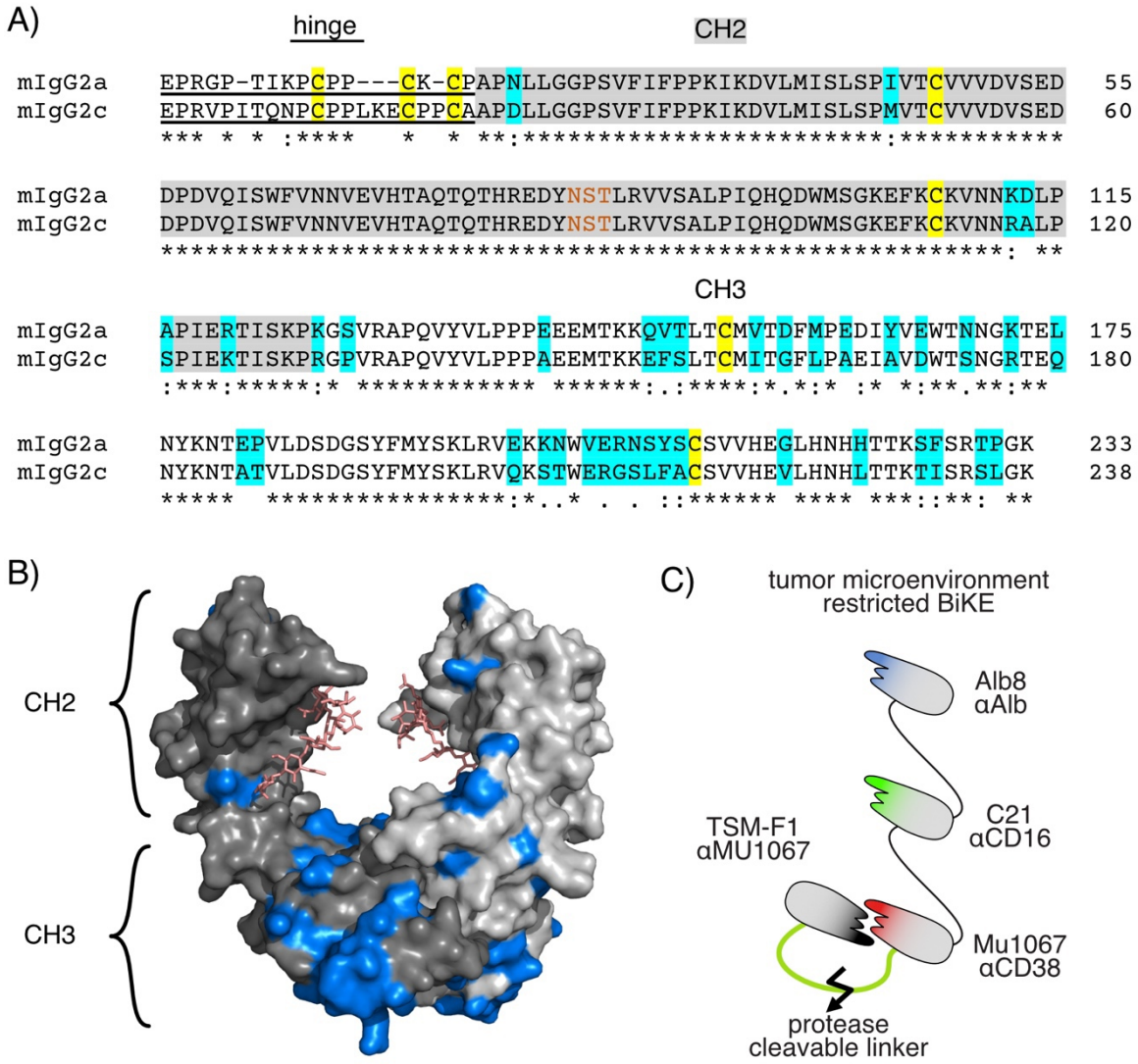

Figure 5.1 Potential binding sites of mIgG2c-specific nanobody family D and application of MU1067-specific idiotypic nanobodies. A) Alignment of mouse IgG2a and mouse IgG2c. The hinge region is underlined, the CH2 domain is highlighted in grey. Cysteines are highlighted in yellow. The glycosylation site in the CH2 is marked in orange font. Amino acid differences between mouse IgG2a and mouse IgG2c are highlighted in cyan. B) Cartoon of the crystal structure of mouse IgG2c (PDB 6BHQ, (Falconer and Barb 2018)). Amino acids color coded as in A). C) Schematic of a potential tumor microenvironment-activated BiKE with a half-life-extending Albumin-specific VHH (blue), a CD16-specific VHH to target NK cells (green), and the CD38-specific MU1067 (red). TSM-F1 (black) is linked to MU1067 by a protease cleavable linker (green line) and masks the paratope of MU1067.

In contrast to the IgG2c-specific nanobodies, families G and F were identified as specific binders of the N-terminal nanobody MU1067. These nanobodies do no cross react with other nanobodies derived from the same V-element (defined by the “EREF” motif in framework region 2 (compare **Figure 4.1.9**). Since the CDR loops contain the

most divergent amino acids, it is not unlikely that these form (part of) the binding site of nanobody families G and F. Biolayer interferometry analyses indicated that MU1067-specific nanobody families G and F block the interaction of MU1067 with its target CD38 (**Figure 4.1.9 A**). In a functional ADCC killing assay, nanobody TSM-G1 exhibited a substantial blocking effect, whereas TSM-F1 blocked only poorly, if at all (**Figure 4.1.9 C**). The difference in affinity between the two nanobodies, as determined by BLI (compare **Figure 4.1.8 C**), implies that a high affinity of the nanobody is necessary to effectively block the MU1067 – CD38 interaction. As can be seen in the BLI plot (**Figure 4.1.8 C**), 50% of nanobody monomer TSM-F1 was already dissociated from its target after 2 min.

In parallel to the direct cloning approach, additional binders were identified by direct next generation sequencing of the immune repertoire **Table 4.1.3**. Thus, this strategy represents an additional source of valuable binders. These clones can easily be ordered as gene-blocks from a commercial supplier and cloned into an appropriate vector for production and evaluation.

The clones identified in this study likely represent only a fraction of the mIgG2c- or MU1067-specific antibody repertoire of the analyzed LaMice. The direct cloning approach identified the B cell clones producing the most abundant mRNA in the lymph nodes and spleen of the immunized animals at the time of sacrifice. This approach has the potential to find low affinity nanobodies, as no selection pressure is applied in comparison to phage display. However, high affinity clones with low abundance might be hidden in the libraries and might not have been identified due to the low number of picked clones. Therefore, for later studies, it seems advisable that both, direct cloning and phage display strategies be applied to ensure a more effective extraction of specific binders from the immunized animals. Both of these strategies rely on PCR amplification of the VHH repertoire. Considering the high degree of sequence identity in the framework regions, it is possible that incomplete amplificates hybridize with templates from a different clone. The ensuing completion of chimeric VHH in the next PCR cycle could result in PCR artefacts, e.g. the "contamination" of a low abundant VHH sequence by portions from a high abundant clone. This problem could be circumvented using nanobody discovery strategies that do not rely on PCR

amplification from mixtures of RNAs, e.g. classic hybridoma or chip-based single B cell screening technologies, such as the Berkeley Beacon platform (Winters et al. 2019).

In conclusion, LaMice are a promising tool to generate nanobodies specific for protein immunogens. As LaMice are genetically naïve to mouse antibodies and only produce llama IgM and llama IgG2b, they are inherently a good source to generate nanobodies specific for mouse immunoglobulins or VH domains.

In addition, anti-idiotype nanobodies were identified which are specific for MU1067. This is potentially interesting because MU1067 is a potential candidate for the development of a potential CD38-specific CAR-T or bispecific T cell engager (BiTE) strategy. It has been shown that anti idiotypic antibodies can be used for better on-target and less off-target toxicity in such settings (Geiger et al. 2020). Geiger *et al*. demonstrated that by masking the anti-CD3 antibody with a protease cleavable linked anti-idiotype scFv, a CD3-FOLR1 BiTe was only active in the tumor microenvironment (TME) where the protease was present. In a similar fashion, TSM-F1 (or TSM-G1 with a reduced affinity to MU1067) could be used to mask the CD38-targeting MU1067 nanobody (**Figure 5.1 C**). This would allow CD38-expressing cells to be targeted only in the tumor microenvironment without effecting CD38-expressing cells in the periphery. In addition, anti-idiotypic antibodies have been used to analyze the pharmacodynamics (PD) and pharmacokinetics (PK) of therapeutic antibodies in humans (Lim et al. 2015; Chin et al. 2015). LaMice are therefore a valuable source for developing anti-idiotypic nanobodies as shown in **Section 4.1.9.**

In addition, the possibilities of using Crispr Cas9/technology to specifically delete a target gene of interest in the genome of LaMice (Zuo et al. 2017) or of crossing a target-knockout mouse strain with LaMice offers opportunities to target new epitopes of the knocked-out target protein by immunization. Further studies are needed to evaluate if other targets like ion channels or GPCRs can also be used for immunization. Ballistic genetic immunization of ion channels has already been successfully applied by the generation of P2X4- and P2X7-specific nanobodies from llamas as well as antibodies from rats and rabbits (Bergmann et al. 2019; Stähler et al. 2022). Whether or not this methodology is applicable to LaMice still needs to be evaluated.

5.2 Generation of nanobodies from llama 405

The Koch-Nolte Lab in Hamburg has previously developed nanobodies and antibodies from genetically immunized llamas that target players of purinergic signaling, including the P2X ion channels (Bergmann et al. 2019; Danquah et al. 2016). Danquah *et al.* isolated P2X7-potentiating (14D5) and -antagonizing (13A7) nanobodies from two llamas (418 and 416 respectively) immunized with cDNA-encoding mP2X7. The bivalent, half-life extended 13A7-dim-αAlb ameliorated inflammation in a mouse model of allergic contact dermatitis and in an experimental glomerulonephritis model. Two human P2X7-specific nanobodies (3c23, 1c113) and a mouse/human cross-reactive nanobody (1c81) were isolated from llama 405. Nanobodies 3c23 and 1c81 block the ATP-mediated Ca^{2+} influx and IL-1β-release from endotoxin-exposed human monocytes (Danquah et al. 2016). Winzer *et al.* used hcAbs composed of nanobodies 1c113 and 3c23 to investigate T-cell subsets for P2X7 expression and sensitivity to ATP. The γδ-T cell subset was identified as one of the main hP2X7-expressing cell populations that demonstrated reduced DAPI uptake and CD62L shedding when P2X7 antagonizing 3c23 hcAb was applied (Winzer et al. 2022). Pinto-Espinoza *et al.* demonstrated binding of the nanobody 1c81-dim-αAlb to mouse microglia after intracerebral injection. In addition, they showed that intramuscular injection of 1c81-dim-αAlb-encoding AAV1 resulted in sufficient nanobody production within the animal to attain the full occupancy of microglial P2X7 in vivo, even 120 days after AAV-injection (Pinto-Espinoza et al. 2022).

Studies by Eichhoff *et al.* and Mann *et al.* harnessed the P2X7-specificity of 1c81 to mediate the transduction of P2X7-expressing cells with adeno-associated viral vectors (AAV) that display nanobody 1c81 on the viral capsid. HEK cells transfected with P2X7 or cells endogenously expressing P2X7 were transduced much more effectively with the nanobody-displaying AAV than P2X7-deficient cells (Mann et al. 2022; Eichhoff et al. 2019).

Because P2X7-specific nanobodies constitute valuable research tools, in this thesis the immune library of llama 405 was re-analyzed by phage display to isolate additional, P2X7-binders. Emphasis was placed on the recovery of nanobodies that bind epitopes distinct from that of the m/hP2X7 cross-reactive nanobody 1c81. To achieve this aim,

the epitope of 1c81 was masked during the second round of panning (compare **Figure 4.2.1**). Enrichment of mP2X7-specific and of hP2X7-specific phages, including 1c81 (family I) in the first panning rounds on mouse or human P2X7-expressing HEK cells was verified by sequence analyses (**Table 4.2.2, Supplementary Figure 9.3**). The second panning round on hP2X7-transfected cells in the presence of 1c81 resulted in the enrichment of phages that bound also to untransfected cells, i.e. family C, as revealed by sequencing (compare **Table 4.2.4** and **Figure 4.2.3**). In addition, a new nanobody family (P) with two members (P1, P2) was recovered that binds hP2X7 independently of 1c81, as demonstrated by epitope binning experiments (**Table 4.2.6**). The lack of isolates from family I, to which 1c81 belongs, after the second panning round demonstrates that the epitope blocking strategy was successful. The epitope binning experiments also revealed that the epitopes of 1c81 and 3c23 on hP2X7 overlap slightly (compare **Figure 4.2.4**). Therefore, it may be worthwhile to try to enhance the blocking capacity of 1c81 and 3c23 alone by combining both nanobodies into one heteromeric dimer.

The low output number of panning round two on mP2X7-transfected cells indicated that most mP2X7 binders were blocked by nanobody 1c81. This was confirmed by the epitope binning analysis, in which blocking mP2X7 with 1c81-mIgG2c hcAb resulted in a complete reduction of binding by all other isolated families. Interestingly, nanobodies 13A7 and 14D5 block one another, indicating that they bind to overlapping epitopes, but each has an opposing effect on ion channel function. The determination of their exact binding sites on mouse P2X7, e.g. by cryo electron microscopy, will allow further insights into ion channel functioning. Potential binding sites could also be achieved by alanine-scanning mutagenesis of mP2X7 and hP2X7, e.g. as has been demonstrated for the human nerve growth factor (Hongo et al. 2000).

As of central and peripheral tolerance mechanisms in mammals avoid antibodies which bind to self-antigens, antibodies against species orthologues of a protein typically bind residues or regions of the ortholog that differ from self (Nemazee 2017). An alignment of the amino acid sequences of host and target P2X7 identifies the residues in the extracellular domain in which the host differs from target (**Figure 5.2**). As the *Lama glama P2rx7* sequence is not available, the close relative *vicugna pacos P2rx7* was used for alignment (Richardson et al. 2019).

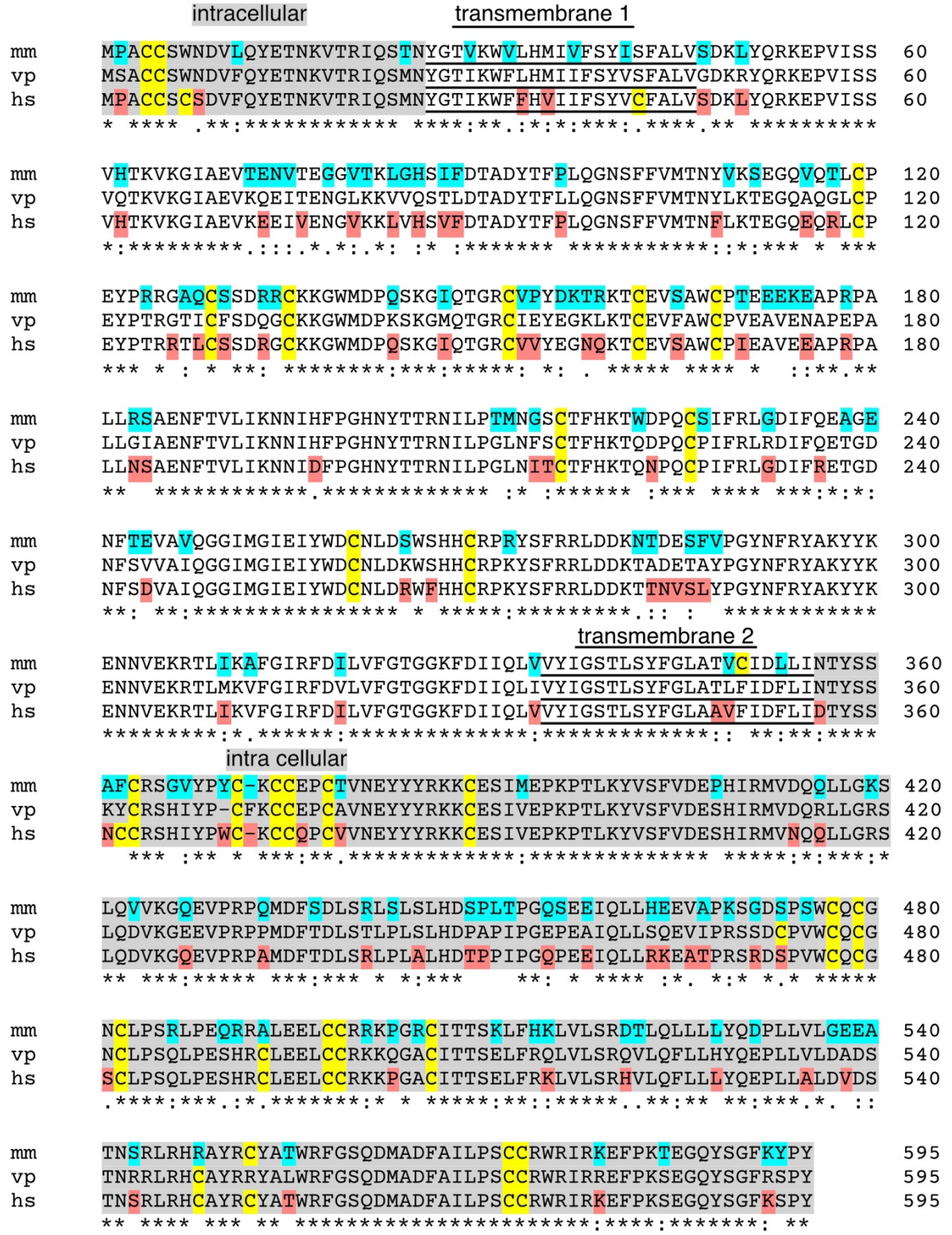

Figure 5.2 P2X7 orthologs of vicuna pacos, human and mouse. Sequences of vicugna pacos (vp, XP_006204925.1), homo sapiens (hs, NP_002553.3) and mus musculus (mm, NP_035157.2) were aligned using ClustalO. The intracellular domains are shaded gray. The two transmembrane regions are underlined. Amino acids differing between vpP2X7 and hP2X7 are highlighted in red, differences between vpP2X7 and mP2X7 are highlighted in cyan.

Elucidation of the conformational changes induced by binding of inhibitory or enhancing nanobodies might facilitate the development of small molecule antagonists or agonists by *in-silico* screening (Oken et al. 2022). The three-dimensional structure of the panda P2X7 was determined by X-ray crystallography (Karasawa et al. 2017), that of rat full length P2X7 ion channel was determined by cryo EM (McCarthy et al. 2019). Analyzing complexes of nanobodies and P2X7 by crystallography or cryo-EM will pin-point the amino acid residues involved in nanobody binding.
The results from this work and the previous study by Danquah *et al.* indicate that the epitope recognized by 1c81 and many other nanobodies may represent an immuno-dominant epitope. To obtain nanobodies against other epitopes of P2X7, phage display could be performed on other immune libraries under conditions that block this epitope. Moreover, immunization of WT or P2X7-deficient LaMice will likely yield nanobodies against other epitopes of P2X7

5.3 Mouse and human P2X5-specific antibodies from rats

Because most Europeans and Asians carry two alleles of the rs891746 SNP that abrogates correct splicing of exon 10, it is likely that these humans are functional knockouts for P2X5 (Kotnis et al. 2010). Analysis of the Ensemble database and the 1.000 human genome project confirmed that the high frequency of this SNP in the European and Asian, but not in the African population (**Figure 4.3.1 A**). Similarly, Vindija and the Altai Neanderthals, as well as chimpanzees, bonobos, and all other great apes carry functional *P2rx5* alleles (**Figure 4.3.1 E**). In mice, P2X5 was shown to be a highly expressed cell surface marker of adipocytes from brown adipose tissue (Ussar et al. 2014). It remains to be determined whether this holds also for humans that carry the ancestral, functional *P2RX5* allele.

In this work, the open reading frames for mouse and ancestral human P2X5 were designed *in silico* and cloned into a eucaryotic expression vector. Genetic immunization of rats with mP2X5 and hP2X5 yielded immune sera that specifically stained P2X5 expressed on the surface of transfected CHO cells. In addition, the antisera stained mP2X5 expressed endogenously by *in vitro* differentiated mouse

adipocytes. This not only confirmed the functionality of the antibodies, but also conclusively demonstrated the presence of P2X5 protein on the surface of mice brown adipocytes (Ussar et al. 2014). Spleen cells of the gene gun-immunized rat 21.18 were immortalized by fusion to SP2/0 myeloma cells. Screening of the resulting hybridoma supernatants for antibodies binding either mouse or human P2X5 identified one clone (R21.18A34) that specifically recognized hP2X5.

Sequencing of the VH and VL coding regions of mAb R21.18A34 will allow cloning of and expression of a recombinant antibody. Further experiments will be necessary to determine whether this mAb influences the ion channel function of P2X5 and whether it binds to endogenously expressed hP2X5. Individuals with direct Sub-Saharan ancestry are likely to carry a homozygous or heterozygous functional *P2RX5* allele. By first genotyping for the functional receptor and then staining these individuals' lymphocytes or adipocytes, cell subpopulations that endogenously express the P2X5 receptor could be identified.

As antibodies in the immune sera of all three rats were able to detect endogenous mouse P2X5 (compare **Figure 4.3.5**), additional hybridoma campaigns could be performed to recover mAbs binding the mouse ortholog.

5.4 Double deficiency of P2X4 and P2X7 rescues brown adipose tissue from pharmacologically induced inflammation

It has been shown that inactivity of BAT caused by thermoneutrality and/or high caloric intake leads to tissue remodeling (BAT involution) accompanied by macrophage infiltration and inflammation (Kotzbeck et al. 2018). In turn, this leads to degeneration of BAT tissue and reduction of energy expenditure capacity in mice as well as humans (Fischer et al. 2018; Fischer et al. 2020). Reversing these morphological changes and retaining the effects of active BAT would be beneficial for whole body metabolism and might protect against diet-induced obesity (Nedergaard et al. 2007; Becher et al. 2021; Chen et al. 2020).

The Heeren lab at the UKE has established a mouse model of futile thermogenesis that mimics the inflammation of BAT observed in thermogenin (uncoupling protein 1,

UCP-1)-deficient mice (Bond et al. 2018; Kazak et al. 2017). Injection of the β3-adrenergic agonist CL316,243 stimulates BAT and causes the liberation of fatty acids. In parallel, treatment with Etomoxir, an inhibitor of CPT1, which is involved in the import of fatty acids into mitochondria, dampens β-oxidation. The combination of the two substances leads to the release of free fatty acids (FFA), which cannot be properly handled and are therefore enriched in the cytosol (**Figure 5.3**).

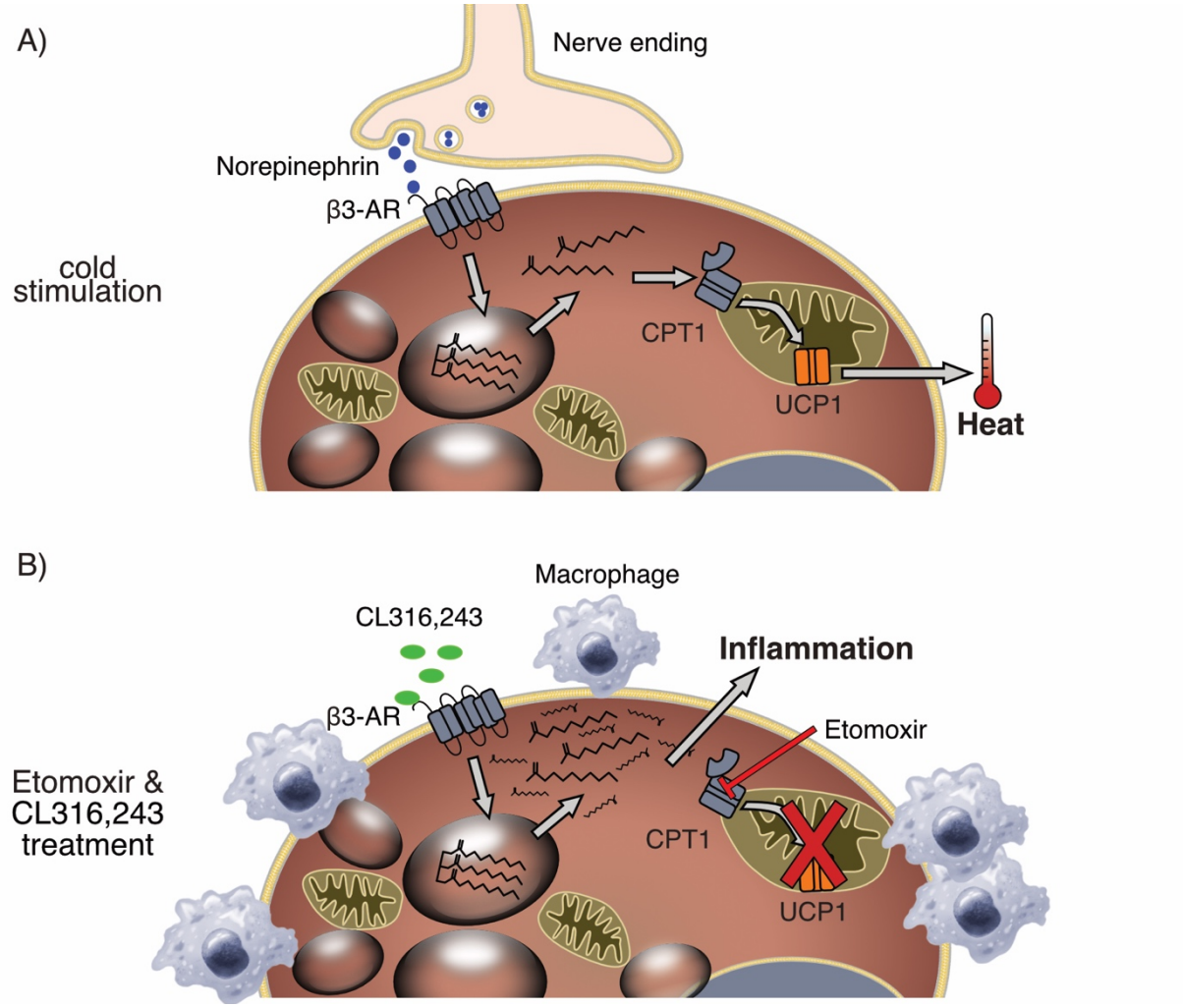

Figure 5.3 Graphical abstract of the effect of Eto/CL treatment on brown adipocytes. A) Under cold stress, BAT thermogenesis is initiated by sympathetic nerve signaling. Norepinephrine is released by nerve endings and activates β3-AR resulting in lipolysis of FFAs from lipid droplets. FFAs modified by CPT1 are shuttled into mitochondria for beta-oxidation. Release of stored protons from the inner mitochondrial membrane by thermogenin (UCP1) generates heat. B) CL316,243 agonizes β3-AR signaling, causing sympathetic nerve activation without a cold stimulus. Liberated FFAs accumulate in the cytosol as Etomoxir blocks beta-oxidation resulting in massive inflammation of BAT due to futile thermogenesis and macrophage infiltration.

As shown in **Section 4.4.2,** this treatment results in BAT inflammation, characterized by increased MAC2 staining and crown formation. As macrophages are attracted to sites of inflammation by DAMP signals such as ATP that can be released e.g. by Pannexin 1 channels (Chekeni et al. 2010), it was hypothesized that the deficiency of P2X4 and/or P2X7 might have an effect on macrophage infiltration into the inflamed BAT tissue. P2X7 deficient mice did not show any alteration in thermogenic potential and inflammation in BAT (Tian et al. 2020). This might be related to the observation that P2X4 and the P2X7 ion channel can have mutually compensatory effects (Weinhold et al. 2010).

P2rx4 and *P2rx7* are direct neighbors on chromosome 5, separated by only ~20 kilo base pairs. According to Bryant *et al*., 1 centimorgan (cM) corresponds to a genetic distance of approximately 2 million bases (Bryant et al. 2018). One cM distance represents the 1% probability of two loci being separated by homologous recombination during meiosis (Silver 1995). This means there is a 90% chance that flanking regions of 1 cM are still of donor origin even after 10 generations of backcrossing (Er-Lukowiak et al. 2020). Thus, it is practically impossible to generate a *P2rx4*$^{-/-}$/*P2rx7*$^{-/-}$ double knockout by backcrossing.

To overcome this obstacle, P2X7-inhibiting Nbs were used in this thesis to generate a functional P2X4/P2X7 double-deficient mouse model by systemically blocking P2X7 in *P2rx4*$^{-/-}$ mice. This model was used to evaluate the effect of single- and double-P2X4/P2X7 deficiency in Eto/CL-induced BAT inflammation. The results show that neither of the single deficiencies (WT mice that received the P2X7 inhibitor 13A7-dim-αAlb or *P2rx4*-/- mice) reduced BAT inflammation as revealed by MAC2 staining**.** In contrast, *P2rx4*-/- mice treated with 13A7-dim-αAlb, i.e. mice with a combined deficiency of P2X4 and P2X7 showed a markedly reduction MAC2 staining in histological sections (see **Figure 4.4.3**)**.** Western blot analysis confirmed a reduced MAC2 expression, as well as maintained expression of UCP-1 by double-deficient mice, suggesting that deficiency in both P2X4 and P2X7 prevents BAT involution and preserves a higher thermogenic capacity. Cells recovered in the vascular stromal fraction of BAT tissues from Eto/CL-treated double-deficient mice also showed increased overall cell viability and a lower total number of monocytes as compared to

Eto/CL-treated WT or single deficient mice (see **Figure 4.4.4**), consistent with a significant reduction of inflammation in these mice.

Together, these findings demonstrate a link between the signaling of P2X7 and P2X4 in this model of brown adipose tissue inflammation. P2X4 and P2X7 therefore represent promising targets for novel therapeutic strategies to prevent inflammatory BAT remodeling.

6 Abstract

Mono- and polyclonal antibodies play central roles in diagnostics and therapy. In recent years, nanobodies - the small antigen binding fragment of camelid hcAbs - have proven to be promising tools for scientific and clinical applications. The Nolte Lab has previously developed nanobody and antibody tools that target players of purinergic signaling such as P2X4 (Bergmann et al. 2019), P2X7 (Danquah et al. 2016), and the ecto-ADP-ribosyltransferase ARTC2 (Koch-Nolte et al. 2007).

In this thesis, further tools were developed for investigations of purinergic signaling. Firstly, the llama IgH-transgenic mouse model (LaMice) was harnessed to generate nanobodies specific for mIgG2c that can be used as a secondary reagent in further studies of purinergic signaling. These experiments underscore the capacity of LaMice to respond to protein immunization. Secondly, new nanobodies were isolated from llamas genetically immunized with P2X7, using an epitope blocking strategy to identify binders against new epitopes. The epitopes recognized by the selected nanobodies were compared to those of previously characterized nanobodies by cross-blockade. Thirdly, to generate reagents for the study of the P2X5 ion channel, three rats were genetically immunized with expression constructs coding for mouse and human P2X5. Polyclonal antisera were obtained that recognize endogenous P2X5 on the surface of *in vitro*-differentiated mouse brown adipocytes, as well as a monoclonal antibody that recognizes human P2X5 expressed on the surface of transfected cells. Finally, a P2X4/P2X7 double-deficient mouse model was established by injecting the mP2X7 antagonizing nanobody 13A7-dim-αAlb into *P2rx4*$^{-/-}$ mice. This model was used to study the roles of P2X4 and P2X7 in a pharmacologically-induced inflammation and involution of brown adipose tissue. The results show that the combined inactivation of P2X4 and P2X7 was necessary and sufficient to rescue BAT from drug-induced macrophage infiltration and inflammation, suggesting that P2X4 and P2X7 may represent promising new targets for novel therapeutic strategies to prevent inflammatory BAT remodeling.

7 Zusammenfassung

Monoklonale und polyklonale Antikörper spielen eine zentrale Rolle in der Diagnostik und Therapie. In den letzten Jahren haben sich Nanobodies, die antigenbindende variable Domäne von Kameliden-Schwerekettenantikörpern, als vielversprechendes Werkzeug für wissenschaftliche und klinische Anwendungen erwiesen. Im Labor der AG Nolte wurden Antikörper und Nanobodies entwickelt, die auf Akteure der purinergen Signalübertragung abzielen, wie P2X4 (Bergmann et al. 2019), P2X7 (Danquah et al. 2016), oder die Ekto-ADP-Ribosyltransferase ARTC2 (Koch-Nolte et al. 2007).

In dieser Arbeit wurden weitere Instrumente entwickelt, die die Untersuchung der purinergen Signalübertragung ermöglichen. Zunächst wurden llama-IgH-transgene Mäuse (LaMice) verwendet, um Nanobodies gegen Maus IgG2c zu erzeugen, die als Sekundärreagenzien für weitere Untersuchungen der purinergen Signaltransduktion eingesetzt werden können. Gleichzeitig bestätigen diese Ergebnisse die Fähigkeit von LaMice, mit einer Antikörperantwort auf Protein-Immunisierungen zu reagieren. Zweitens wurden neue Nanobodies aus einem mit P2X7 immunisierten llama isoliert mit einer Epitop-Blockade Strategie, um Binder gegen neue Epitope zu selektionieren. Durch Epitopkartierungen wurden die von den neuen Nanobodies erkannten Epitope mit denen bereits charakterisierter Nanobodies verglichen. Drittens wurden drei Ratten mit Expressionskonstrukten für Maus P2X5 und funktionstüchtigem human P2X5 immunisiert. Aus diesen Tieren wurden polyklonale Antikörper gewonnen, die endogen auf Maus Adipozyten exprimiertes P2X5 erkennen, sowie ein monoklonaler Antikörper, der human P2X5 spezifisch auf der Oberfläche transfizierter Zellen erkennt. Schließlich wurde durch Behandlung von *P2rx4*$^{-/-}$ Mäusen mit einem P2X7-antagonisierenden Nanobody ein funktionelles Modell mit P2X4/P2X7-Doppeldefekt etabliert. In einem Modell der pharmakologisch-induzierten Entzündung des braunen Fettgewebes war die kombinierte Inaktivierung beider Kanäle notwendig und ausreichend, um das braune Fettgewebe vor der Chemikalien-induzierten Entzündung zu schützen. P2X4 und P2X7 stellen daher vielversprechende Ziele für neue Therapieansätze zur Verhinderung des entzündlichen Umbaus von braunem Fettgewebe dar.

8 Abbreviations

%	Percent
18S	18s ribosomal RNA
Ag	Antigen
AMP	Adenosine monophosphate
ADP	Adenosine diphosphate
ATP	Adenosine triphosphate
B6	C57BL/6
BCR	B-cell receptor
BSA	Bovine serum albumin
Ca^{2+}	Calcium ions
cDNA	complementary deoxyribonucleic acid
CMV	Cytomegalovirus
DAPI	4',6-diamidino-2-phenylindole
ddH20	Double distilled purified water
DMEM	Dulbecco's modified eagle's medium
DNA	Deoxyribonucleic acid
dNTPs	Deoxyribonucleotide triphosphate
ELISA	Enzyme-linked immunosorbent assay
FACS	Fluorescence-activated cell sorting
FSC	Forward scatter
GFP	Green fluorescent protein
hcAb	Heavy chain antibody
hIgG	human IgG Fc
HRP	Horseradish peroxidase
IC	Isotype control
K^{+}	Potassium ions
LaMice	Lama IgH-transgenic mice
mAb	Monoclonal antibody
mIgG2a	mouse IgG2a Fc
mIgG2c	mouse IgG2c Fc

MFI	Median fluorescence intensity
Mg2+	Magnesium ions
MHC	Major histocompatibility complex
mM	Millimoles/liter
mRNA	Messenger RNA
Na+	Sodium ions
Nb	Nanobody
NK	Natural killer cells
P1Rs	Purinergic P1 receptors
P2Rs	Purinergic P2 receptors
P2rx4	P2X4 gene (mouse)
P2RX5	P2X5 gene (human)
P2rx7	P2X7 gene (mouse)
P2RX7	P2X7 gene (human)
P2RX7ko	P2rx7-defficient mice
P2X4	P2X4 receptor
P2X5	P2X5 receptor
P2X7	P2X7 receptor
pAb	Polyclonal antibody
PBS	Phosphate-buffered saline
PD	Pharmacodynamics
PE	Phycoerythrin
PFA	Paraformaldehyde
PK	Pharmacokinetics
rbIgG	rabbit IgG Fc
RNA	Ribonucleic acid
RPMI	Roswell park memorial institute medium
RT	Room temperature
SNP	Single nucleotide polymorphism
SSC	Side scatter
TMB	Tetramethylbenzidine
VHH	Variable domain of the heavy chain antibody

WT	Wild type
µg	Microgram
µL	Microliter
µM	Micromoles/liter

9 Supplementary material

Supplementary Table 9.1 Ligation and production efficiencies (visible SDS Page band) of amplified libraries from LaMice immunized with l+10-mIgA and MU1067-mIgG2c hcAbs.

animal	TE	organ	IgM/ IgG	legible VHH Insert (including s+16 religation)	production efficiency
24	TE01	Spleen	IgM	0/12	0
24	TE01	Spleen	IgG	9/12	9/12
24	TE01	Lymph node	IgM	4/12	1
24	TE01	Lymph node	IgG	8/12	3/12
26	TE01	Spleen	IgM	9/12	8/12
26	TE01	Spleen	IgG	9/12	9/12
26	TE01	Lymph node	IgM	4/12	6/12
26	TE01	Lymph node	IgG	11/12	11/12
28	TE02	Spleen	IgM	8/12	9/12
28	TE02	Spleen	IgG	9/12	8/12
28	TE02	Lymph node	IgM	11/12	12/12
28	TE02	Lymph node	IgG	6/12	8/12
29	TE02	Spleen	IgM	9/12	9/12
29	TE02	Spleen	IgG	8/12	8/12
29	TE02	Lymph node	IgM	8/12	11/12
29	TE02	Lymph node	IgG	8/12	10/12
31	TE03	Spleen	IgM	7/12	9/12
31	TE03	Spleen	IgG	6/12	6/12
31	TE03	Lymph node	IgM	11/12	11/12
31	TE03	Lymph node	IgG	11/12	11/12
32	TE03	Spleen	IgM	10/12	12/12
32	TE03	Spleen	IgG	11/12	12/12
32	TE03	Lymph node	IgM	12/12	0/12
32	TE03	Lymph node	IgG	11/12	0/12

Supplementary Figure 9.1 Isolated LaMice nanobodies targeting the mouse IgG2c Fc or MU1067. Amino acid sequences of α-mIgG2c Fc- and MU1067-specific nanobodies isolated from an immune library of LaMouse 31. Amino acids belonging to the CDRs are highlighted as follows: CDR1 (red), CDR2 (green) and CDR3 (blue). Cysteines are indicated with yellow background. Somatic hypermutations, differing amino acids from the most closely related germline QREL sequence, are indicated with a cyan background.

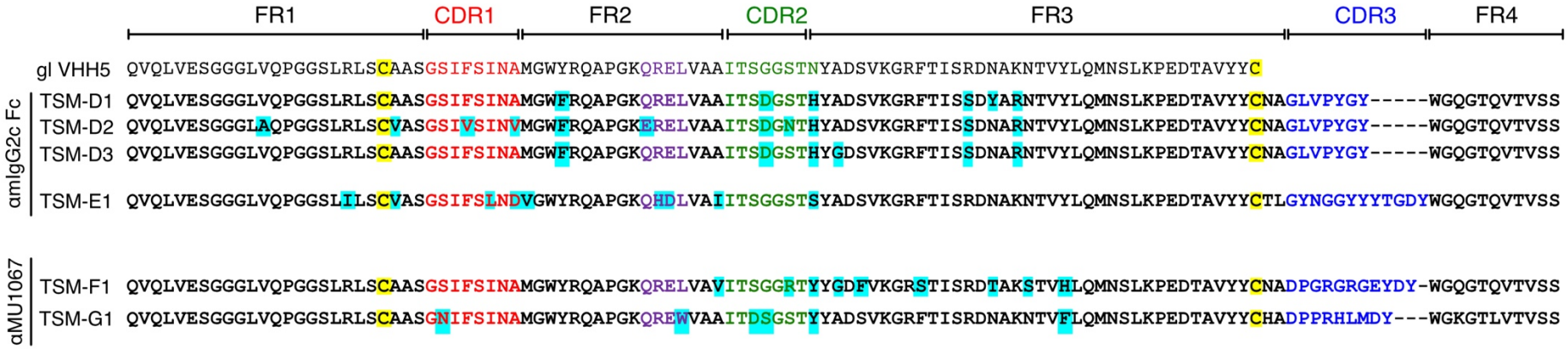

Supplementary Figure 9.2 VHH sequences from the first two rows of 96-well plasmid preparations after ligation of PCR-amplified libraries from LaMice immunized with I+10-mIgA and MU1067-mIgG2c. Amino acids belonging to the CDRs are highlighted as follows: CDR1 (red), CDR2 (green) and CDR3 (blue). Cysteines are indicated with yellow background. Somatic hypermutations corresponding to differing amino acids from the most closely related germline V element sequence (indicated at the top in lighter font) are color coded with a cyan background.

LaMouse TE01-24

IgM repertoire: 4/24 legible sequences, 1xGLEW, 3x religation

```
Germline VH     EVQLVESGGGLVQPGGSLRLSCAASGFTFDDYAMSWVRQAPGKGLEWVSAISWNGGSTYYAESMKGRFTISRDNAKNTLYLQMNSLKSEDTAVYYCAK
24-LN-IgM-B1    QVQLVESGGGLVQPGGSLRLSCAASGFTFDDYAMSWVRQAPGKGLEWVSAISWNGGSTYYAESMKGRFTISRDNAKNTLYLQMNSLKSEDTAVYYCAKGTVVAGTQYDY---------WGQGTQVTVSS

24-LN-IgM-B4    s+16dim religation
24-LN-IgM-B3    s+16dim religation
24-LN-IgM-B6    s+16dim religation
```

IgG repertoire: 18/24 legible sequences, 15xEREF, 2xGLEW 1x religation

```
Germline VHH6   EVQLVESGGGLVQAGGSLRLSCAASGRTFSSYAMGWFRQAPGKEREFVAAISWSGGSTYYADSVKGRFTISRDNAKNTVYLQMNSLKPEDTAVYYCAK
24-Sp-IgG-A7    QVQLVESGGGLVQAGGSLRLSCVGSGRTFSRSGVAWFRQAPGKEREFVAAISWSGGSTYYADPVKGRFTISRDNAKNTVYLQMNSLQPDDTADYYCAAEERKWFGLEVLITTPGEYDYWGQGTQVTVSS
24-Sp-IgG-A8    QVQLVESGGGLVQAGGSLRLSCVGSGRTFSRSGVAWFRQAPGKEREFVAAITWSGDRINYADSVKGRFTISRDNAKNTVYLQMNSLQPDDTADYYCAAEERKWFGLEVLITTPGEYDYWGQGTQVTVSS
24-Sp-IgG-A9    QVQLVESGGGLVQAGGSLRLSCVGSGRTFSRSGVAWFRQAPGKEREFVAAITWSGDRINYADSEKGRFTISRDNAKNTVYLQMNSLQPDDTADYYCASEERKWFGLEVLITTPGEYDYWGQGTQVTVSS
24-Sp-IgG-B10   QVQLVESGGGLVQAGGSLRLSCVGSGRTFSRSGVAWFRQAPGKEREFVAAITWSGDRINYADSVKGRFTISRDNAKNTVYLQMNSLQPEDTADYYCAAEERKWFGLEVLITTPGEYDYWGQGTQVTVSS
24-Sp-IgG-B11   QVQLVESGGGLVQAGGSLRLSCAGSGRTFSSSVVSWFRQAPGKEREFVAAITWSGDRVNYADSVKGRFTISRDNAKNTVYLLMHSLQFEDTAVYYCAAEERKWFGLEVLLNTPGEYDYWGQGTQVTVSS
24-Sp-IgG-B12   QVQLVESGGGLVQAGGSLRLSCVGSGRTFSRSGVAWFRQAPGKEREFVAAITWSGDRINYADSVKGRFTISRDNAKNTVYLQMNSLQPDDTADYYCAADERKWFGLEVLITTPGEYDYWGQGTQVTVSS
24-LN-IgG-A12   QVQLVESGGGLVQTGDSLRLSCAASGRTFSRNAMAWFRQAPEKKREFVAGVTWNGDNANYADSVKGRFTISRDNAKNTVYLQMNSLKPEDTAVYYCAAEGVIGSYGMDY---------WGKGTLVTVSS
24-LN-IgG-A10   QVQLVESGGGLVQAGGSLRLSCAASGRTFSSYAMGWFRQAPGKEREFVA-----GGSTYYADSVKGRFTISRDNAKNTVYLQMNSLKPEDTAVYYCAAEGVAGSYGMDY---------WGKGTLVTVSS
24-LN-IgG-A7    QVQLVESGGGLVQAGGSLRLSCAASGRTFSSYAMGWFRQAPGKEREFVA-----GGSTYYADSVKGRFTISRDNAKNTVYLQMNSLKPEDTAVYYCAAEGVAGSYGMDY---------WGKGTLVTVSS
24-LN-IgG-A8    QVQLVESGGGLVQAGGSLRLSCAASGRTFSSYAMGWFRQAPGKEREFVA-----GGSTYYADSVKGRFTISRDNAKNTVYLQMNSLKPEDTAVYYCAAEGVAGSYGMDY---------WGKGTLVTVSS
24-LN-IgG-A9    QVQLVESGGGLVQAGGSLRLSCAASGRTFSSYAMGWFRQAPGKEREFVA-----GGSTYYADSVKGRFTISRDNAKNTVYLQMNSLKPEDTAVYYCAAEGVAGSYGMDY---------WGKGTLVTVSS
24-LN-IgG-B11   QVQLVESGGGLVQAGGSLRLSCAASGRTFSSYAMGWFRQAPGKEREFVA-----GGSTYYADSVKGRFTISRDNAKNTVYLQMNSLKPEDTAVYYCAAEGVAGSYGMDY---------WGKGTLVTVSS
24-LN-IgG-B8    QVQLVESGGGLVQAGGSLRLSCAASGRTFSSYAMGWFRQAPGKEREFVA-----GGSTYYADSVKGRFTISRDNAKNTVYLQMNSLKPEDTAVYYCAAEGVAGSYGMDY---------WGKGTLVTVSS
24-LN-IgG-B9    QVQLVESGGGLVQAGGSLRLSCAASGRTFSSYAMGWFRQAPGKEREFVA-----GGSTYYADSVKGRFTISRDNAKNTVYLQMNSLKPEDTAVYYCAAEGVAGSYGMDY---------WGKGTLVTVSS
24-LN-IgG-B10   QVQLVESGGGLVQAGGSLRLSCAASGRTFSSYAMGWFRQAPGKEREFVAAISWSGGSTYYADSVKGRFTISRDNAKNTVYLQMNSLKPEDTAVYYCAADQRL----------------WGKGTLVTVSS

Germline VH    EVQLVESGGGLVQPGGSLRLSCAASGFTFDDYAMSWVRQAPGKGLEWVSAISWNGGSTYYAESMKGRFTISRDNAKNTLYLQMNSLKSEDTAVYYCAK
24-Sp-IgG-A12   QVQLVESGGGLVQPGGSLRLSCAASGFTFEDYAMSWVRQAPGKGLEWVSAISWNGGNTYYAESMKGRFIISRDNAKNTLYLQMNSLKSEDTAVYYCTKGRGRSWNRIRPDYGS-----WGQGTQVTVSS
24-Sp-IgG-A11   QVQLVESGGGLVQPGGSLRLSCAASGFTFEDYAMSWVRQAPGKGLEWVSAISWNGGNTYYAESMKGRFIISRDNAKNTLYLQMNSLKSEDTAVYYCSKGRGRSWNRIRPDYGS-----WGQGTQVTVSS

24-Sp-IgG-B9    s+16dim religation
```

LaMouse TE01-26

IgM repertoir3: 13/24 legible sequences, 7xEREF, 5xGLEW, 1x religation

```
Germline VHH6    EVQLVESGGGLVQAGGSLRLSCAASGRTFSSYAMGWFRQAPGKEREFVAAISWSGGSTYYADSVKGRFTISRDNAKNTVYLQMNSLKPEDTAVYYCAK
26-Sp-IgM-B3     QVQLVESGGGLVQAGGSLRLSCAASGRTFSSYAMGWFRQAPGKEREFVAAISWSGGSTYYADSVKGRFTISRDNAKNTVYLQMNSLKSEDTAVYYCAKDRLRTVVAGYFGS-------WGQGTQVTVSS
26-LN-IgM-A6     QVQLVESGGGLVQAGGSLRLSCAASGRTFSSYAMAWFRQAPGKEREFVAAISWSGGSTYYADSVKGRFTISRDNAKNTVYLQMNSLKPEDTAVYYCAAELGGVVAATLYDY-------WGQGTQVTVSS
26-Sp-IgM-A1     QVQLVESGGGLVQAGGSLRLSCAASGRTFSSYAMGWFRQAPGKEREFVAAISWSGGSTYYADSVKGRFTISRDNAKNTVYLQMNSLKPEDTAVYYCAAPSGSSWEGEYDY--------WGQGTQVTVSS
26-LN-IgM-B1     QVQLVESGGGLVQAGGSLRLSCAASGRTFSSYAMGWFRQAPGKEREFVAAISWSGGSTYYADSVKGRFTISRDNAKNTVYLQMNSLKPEDTAVYYCAAGSSSWSADFGS---------WGQGTQVTVSS
26-Sp-IgM-A5     QVQLVESGGGLVQAGGSLRLSCAASGRTFSSYAMGWFRQAPGKEREFVAAISWSGGSTYYAESMKGRFTISRDNAKNTVYLQMNSLKPEDTAVYYCAADPVGSWVEYDY---------WGQGTQVTVSS
26-Sp-IgM-A4     QVQLVESGGGLVQAGGSLRLSCAASGRTFSSYAMGWFRQAPGKEREFVAAISWSGGSTYYADSVKGRFTISRDNAKNTVYLQMNSLKPEDTAVYYCAADRGVTGEYDY----------WGQGTQVTVSS
26-Sp-IgM-A6     QVQLVESGGGLVQAGGSLRLSCAASGRTFSSYAMGWFRQAPGKEREFVAAISWNGGSTYYAESMKGRFTISRDNAKNTLYLQMNSLKSEDTAVYYCAKGGRREYDY-----------WGQGTQVTVSS

Germline VH     EVQLVESGGGLVQPGGSLRLSCAASGFTFDDYAMSWVRQAPGKGLEWVSAISWNGGSTYYAESMKGRFTISRDNAKNTLYLQMNSLKSEDTAVYYCAK
26-LN-IgM-A3     QVQLVESGGGLVQPGGSLRLSCAASGFTFDDYSMSWVRQAPGKGLEWVSAISWNGGSTYYAESMKGRFTISRDNAKNTLYLQMNSLKSEDTAVYYCAKDKNGSSWYVYDY--------WGQGTQVTVSS
26-Sp-IgM-B6     QVQLVESGGGLVQPGGSLRLSCAASGFTFDDHAMSWVRQAPGKGLEWIATIHWNGVTTYYGESMKGRVTISRDNAKNTLYLQMNSLKSEDTAVYYCAKNRGSNWFEGFDY--------WGQGTQVTVSS
26-Sp-IgM-B4     QVQLVESGGGLVQPGGSLRLSCAASGFTFDDYAMSWVRQAPGKGLEWVSAISWNGGSTYYAESMKGRFTISRDNAKNTLYLQMNSLKSEDTAVYYCAKGYSGSYYYLDY---------WGQGTQVTVSS
26-LN-IgM-A5     QVQLVESGGGLVQPGGSLRLSCAASGFTFDDYAMSWVRQAPGKGLEWVSAISWNGGSTYYAESMKGRFTISRDNAKNTLYLQMNSLKSEDTAVYYCARSSWSDEYDY----------WGQGTQVTVSS
26-Sp-IgM-A2     QVQLVESGGGLVQPGGSLRLSCAASGFTFDDYAMSWVRQAPGKGLEWVSAISWNGGSTYYAESMKGRFTISRDNAKNTLYLQMNSLKSEDTAVYYCAKYSGSYYYDY----------WGQGTQVTVSS

26-Sp-IgM-B2     s+16dim religation
```

IgG repertoire: 20/24 legible sequences, 6xEREF, 10xGLEW, 3x religation

```
Germline VHH6    EVQLVESGGGLVQAGGSLRLSCAASGRTFSSYAMGWFRQAPGKEREFVAAISWSGGSTYYADSVKGRFTISRDNAKNTVYLQMNSLKPEDTAVYYCAK
26-LN-IgG-A11    QVQLVESGGGLVQAGGSLRLSCAASGRTFSSYAMGWFRQAPGKEREFVAAISWSGGSTYYADSVKGRFTISRDNAKNTVYLQMNSLKPEDTAVYYCAAEDVHTIVVVTTKDEYDY---WGQGTQVTVSS
26-Sp-IgG-B12    QVQLVESGGGLVQAGDSLRLSCAASGGNFSNYILDWFRQAPGKEREFVATIRWNSGSTNFADSVKGRFTISRDNARNTAYLQMNSLKPADTAVYYCAAELPGRGEYDY----------WGQGTQVTVSS
26-Sp-IgG-A10    QVQLVESGGGLVQAGDSLRLSCAASGGNFSNYILDWFRQAPGKEREFVATIRWNSGSTNFADSVKGRFTISRDNARNTAYLQMNSLKPADTAVYYCAAELPGRGEYDY----------WGQGTQVTVSS
26-LN-IgG-A12    QVQLVESGGGLVQAGGSLRLSCAASGRTFSSYAMGWFRQAPGKEREFVAAISWSGGSTYYADSVKGRFTISRDNAKNTVYLQMNSLKPEDTAVYYCAEYGSFEYDY------------WGQGTQVTVSS
26-LN-IgG-B7     QVQLVESGGGLVQAGGSLRLSCAASGRTFSSYAMGWFRQAPGKEREFVAAISWSGGSTYYADSVKGRFTISRDNAKNTVYLQMNSLKPEDTAVYYCAEYGSFEYDY------------WGQGTQVTVSS
26-LN-IgG-A7     QVQLVESGGGLVQAGGSLRLSCAASGRTFSSYAMGWFRQAPGKEREFVAAISWSGGSTYYADSVKGRFTISRDNAKNTVYLQMNSLKPEDTAVYYCAADRDDY---------------WGQGTQVTVSS

Germline VH     EVQLVESGGGLVQPGGSLRLSCAASGFTFDDYAMSWVRQAPGKGLEWVSAISWNGGSTYYAESMKGRFTISRDNAKNTLYLQMNSLKSEDTAVYYCAK
26-Sp-IgG-A11    QVQLVESGGGLVQPGGSLRLSCAASGFTFDDHAMSWVRQAPGKGLEWVSTISWKDNITYYGESMKGRVTISRDNAKNTLYLQMHSLKSEDTAVYYCAVDSGDREHDY-----------WGQGTQVTVSS
26-Sp-IgG-A12    QVQLVESGGGLVQPGGSLRLSCAASGFTFDDYGMSWVRQAPGKGLEWVSTISWKDNITYYAESMKGRFTISRDNAKNTLYLQMHSLKSEDTAVYYCAVDSGDREHDY-----------WGQGTQVTVSS
26-Sp-IgG-A9     QVQLVESGGGLVQPGGSLRLSCAASGFTFDDHAMSWVRQAPGKGLEWVSTISWKDNITYYGESMKGRVTISRDNAKNTLYLQMHSLKSEDTAVYYCAVDSGDREHDY-----------WGQGTQVTVSS
26-Sp-IgG-B10    QVQLVESGGGLVQPGGSLRLSCAASGFTFDDHAMSWVRQAPGKGLEWVSTISWKDNITYYGESMKGRVTISRDNAKNTLYLQMHSLKSEDTAVYYCAVDSGDREHDY-----------WGQGTQVTVSS
26-Sp-IgG-B7     QVQLVESGGGLVQPGGSLRLSCAASGFTFDDHAMSWVRQAPGKGLEWVSTISWKDNITYYGESMKGRVTISRDNAKNTLYLQMHSLKSEDTAVYYCAVDSGDREHDY-----------WGQGTQVTVSS
26-Sp-IgG-B8     QVQLVESGGGLVQPGGSLRLSCAASGFTFDDHAMSWVRQAPGKGLEWVSTISWKDNITYYGESMKGRVTISRDNAKNTLYLQMHSLKSEDTAVYYCAVDSGDREHDY-----------WGQGTQVTVSS
26-LN-IgG-B10    QVQLVESGGGLVQPGGSLRLSCAASGFTFDDYAMSWVRQAPGKGLEWVSTISWKDNITYYAESMKGRFTISRDNAKNTLYLQMHSLKSEDTAVYYCAKDSGDREHDY-----------WGQGTQVTVSS
26-LN-IgG-B11    QVQLVESGGGLVQPGGSLRLSCAASGFTFDDYAMSWVRQAPGKGLEWVSTISWKDNITYYAESMKGRFTISRDNAKNTLYLQMHSLKSEDTAVYYCAVDSGDREHDY-----------WGQGTQVTVSS
26-LN-IgG-B8     QVQLVESGGGLVQPGGSLRLSCAASGFTFDDYAMSWVRQAPGKGLEWVSTISWKDNITYYAESMKGRFTISRDNAKNTLYLQMHSLKSEDTAVYYCAVDSGDREHDY-----------WGQGTQVTVSS
26-LN-IgG-B9     QVQLVESGGGLVQPGGSLRLSCAASGFTFDDYAMSWVRQAPGKGLEWVSTISWKDNITYYAESMKGRFTISRDNAKNTLYLQMHSLKSEDTAVYYCAVDSGDREHDY-----------WGQGTQVTVSS

26-LN-IgG-A8     s+16dim religation
26-LN-IgG-A9     s+16dim religation
26-LN-IgG-A10    s+16dim religation
26-Sp-IgG-A7     s+16dim religation
```

LaMouse TE02-28

IgM repertoire: 19/24 legible sequences, 3xEREF, 12, QREL, 1xGLEW, 3x religation

```
Germline VHH6   EVQLVESGGGLVQAGGSLRLSCAASGRTFSSYAMGWFRQAPGKEREFVAAISWSGGSTYYADSVKGRFTISRDNAKNTVYLQMNSLKPEDTAVYYCAK
28-LN-IgM-B2    QVQLVESGGGLVQAGGSLRLSCAASGRTFSSYAMGWFRQAPGKEREFVAAISWSGGSTYYADSVKGRFTISRDNAKNTVYLQMNSLKPEDTAVYYCNAEYGSRGYGMDY-------WGKGTQVTVSS
28-Sp-IgM-B8    QVQLVESGGGLVQAGGSLRLSCAASGRTFSSYAMGWFRQAPGKEREFVAAISWSGGSTYYADSVKGRFTISRDNAKNTVYLQMNSLKPEDTAVYYCNAGSLRQGY-----------WGQGTQVTVSS
28-LN-IgM-B1    QVQLVESGGGLVQPGGSLRLSCAASGRTFSSYAMGWFRQAPGKEREFVAAISWSGGSTYYADSVKGRFTISRDNAKNTMYLQMNSLRPEDTAVYYCNADYSDYLL-----------WGKGTLVTVSS

Germline VHH5   EVQLVESGGGLVQPGGSLRLSCAASGSIFSINAMGWYRQAPGKQRELVAAIT-SGGSTNYADSVKGRFTISRDNAKNTVYLQMNSLKPEDTAVYYCNA
28-LN-IgM-B5    QVQLVESGGGLVQPGGSLRLSCAASGSIFSINAMGWYRQAPGKQRELVAAIT-SGGSTNYADSVKGRFTISRDNAKNTVYLQMNSLKPEDTAVYYCNLYGSSWTPYYGMDY-----WGKGTLVTVSS
28-LN-IgM-A2    QVQLVESGGGLVQPGGSLRLSCAASGSIFSINAMGWYRQAPGKQRELVAAIT-SGGSTNYADSVKGRFTISRDNAKNTVYLQMNSLKPEDTAVYYCNASPEGGSYYYEYDY-----WGQGTQVTVSS
28-Sp-IgM-B1    QVQLVESGGGLVQPGGSLRLSCAASGSIFSINAMGWYRQAPGKQRELVAAIT-SGGSTNYADSVKGRFTISRDNAKNTVYLQMNSLKPEDTAVYYCNAELVAAYSYEYDY------WGQGTQVTVSS
28-LN-IgM-A1    QVQLVESGGGLVQPGGSLRLSCAASGSIFSINAMGWYRQAPGKQRELVAAIT-SGGSTNYADSVKGRFTISRDNAKNTVYLQMNSLKFEDTAVYYCHVESKWPDGYSYDY------WGQGTQVTVSS
28-Sp-IgM-A2    QVQLVESGGGLVQPGGSLRLSCAASGSIFSINAMGWYRQAPGKQRELVAAIT-SGGSTNYADSVKGRFTISRDNAKNTLYLQMNSLKPEDTAVYYCNVSRRSSWYGMDY-------WGKGTLVTVSS
28-Sp-IgM-A4    QVQLVESGGGLVQPGGSLRLSCAASGSIFSINAMGWYRQAPGKQRELVAAIT-SGGSTNYADSVKGRFTISRDNAKNTVYLQMNSLKPEDTAVYYCNVSRRSSWYGMDY-------WGKGTLVTVSS
28-Sp-IgM-B6    QVQLVESGGGLVQSGGSLRLSCAASKSIFSINAMGWYRQAPGKQRELVAAIT-SGGSTNYADSVKGRFTISRDNAKNTVYLQMNSLKPEDTAIYYCNADIIVVVKYDY--------WGQGTQVTVSS
28-LN-IgM-A3    QVQLVESGGGLVQPGGSLRLSCAASGSIFSINAMGWYRQAPGKQRELVAAIT-SGGSTNYADSVKGRFTISRDNAKNTVYLQMNSLKPEDTAVYYCNADRATILMDY---------WGKGTLVTVSS
28-LN-IgM-A6    QVQLVESGGGLVQPGGSLRLSCAASGSIFSINAMGWYRQAPGKQRELVAAIT-SGGSTNYADSVKGRFTISRDNAKNTVYLQMNSLKSEDTAVYYCAKGGSRDEYDY---------WGQGTQVTVSS
28-LN-IgM-B3    QVQLVESGGGLVQPGGSLRLSCAASGSIFSINAMGWYRQAPGKQRELVAAIT-SGGSTNYADSVKGRFTISRDNAKNTVYLQMNSLKPEDTAVYYCNAEGSSWFGS----------WGQGTQVTVSS
28-LN-IgM-B6    QVQLVESGGGLVQPGGSLRLSCAASGSIFSINAMGWYRQAPGKQRELVAAIT-SGGSTNYADSVKGRFTISRDNAKNTVYLQMNSLKPEDTAVYYCNADEYDY------------WGQGTQVTVSS

Germline VH    EVQLVESGGGLVQPGGSLRLSCAASGFTFDDYAMSWVRQAPGKGLEWVSAISWNGGSTYYAESMKGRFTISRDNAKNTLYLQMNSLKSEDTAVYYCAK
28-Sp-IgM-B2    QVQLVESGGGLVQPGGSLRLSCAASGFTFDDYAMSWVRQAPGKGLEWVSAISWNGGSTYYAESMKGRFTISRDNAKNTVYLQMNSLKPEDTAVYYCNADVVAGWGYDY--------WGQGTQVTVSS

28-LN-IgM-A4    s+16dim religation
28-LN-IgM-B4    s+16dim religation
28-Sp-IgM-A6    s+16dim religation
28-Sp-IgM-B5    s+16dim religation
```

IgG repertoire: 15/24 legible sequences, 5xEREF, 5xQREL, 2x GLEA, 3x religation

```
Germline VHH6   EVQLVESGGGLVQAGGSLRLSCAASGRTFSSYAMGWFRQAPGKEREFVAAISWSGGSTYYADSVKGRFTISRDNAKNTVYLQMNSLKPEDTAVYYCAK
28-LN-IgG-A10   QVQLVESGGGLVQAGGSLRLSCAGSGRTFSSYTMGWFRQAPGKEREGVAAITWSGGSTYYADSVKGRFTISRDNDEKTVYLQMNSLKPEDTAVYYCNADLAGTLYDY---------WGQGTQVTVSS
28-Sp-IgG-A12   QVQLVESGGGLVQAGGSLRLSCAASGRTFSSYAMGWFRQAPGKEREFVAAISWSGGSTYYADSVKGRFTISRDNAKNTVYLQMNSLKPEDTAVYYCAEYGSFEYDY---------WGQGTQVTVSS
28-Sp-IgG-B11   QVQLVESGGGLVQAGGSLRLSCAASGRTFSSYAMGWFRQAPGKEREFVAAISWSGGSTYYADSVKGRFTISRDNAKNTVYLQMNSLKPEDTAVYYCAEYGSFEYDY---------WGQGTQVTVSS
28-LN-IgG-A9    QVQLVESGGGLVQAGGSLRLSCAASGRTFSSYAMGWFRQAPGKEREFVAAISWSGGSTYYADSVKGRFTISRDNAKNTVYLQMNSLKPEDTAVYYCAEYGSFEYDY---------WGQGTQVTVSS
28-LN-IgG-A11   QVQLVESGGGLVQAGGSLRLSCAASGRTFSSYAMGWFRQAPGKEREFVAAISWSGGSTYYADSVKGRFTISRDNAKNTVYLQMNSLKPEDTAVYYCAEYGSFEYDY---------WGQGTQVTVSS

Germline VHH5   EVQLVESGGGLVQPGGSLRLSCAASGSIFSINAMGWYRQAPGKQRELVAAIT-SGGSTNYADSVKGRFTISRDNAKNTVYLQMNSLKPEDTAVYYCNA
28-Sp-IgG-A11   QVQLVESGGGLVQAGGSLRLSCAASGRTFSSYAMDWFRQAPGKERELVAAIT-SGGITNYADSVKGRFTISRDSVKNTVYLQMNSLEPEDTAVYYCNADGTVVAGIDYGMDY----WGKGTLVTVSS
28-Sp-IgG-A9    QVQLVESGGGLVQPGGSLRLSCAASGSIFSINAMAWYRQAPGKQRELVAAIT-FGGNTDYADSVKGRFTISRDSAKNTVYLQMNSLKPEDTAVYYCNVYGDYDGHSYGMDY-----WGKGTLVTVSS
28-Sp-IgG-A10   QVQLVESGGGLVQPGGSLRLSCAASGSIFSVNAMGWYRQAPGKQRELVAAIT-SGGSINYADSVKGRFTISRDNAKNTVYLQMNSLKPEDTAVYYCNVYGDYDGHSYGMDY-----WGKGTLVTVSS
28-LN-IgG-B8    QVQLVESGGGLVQPGGSLRLSCAASGSILSINAMGWERQAPGNQRELVAAIT-SGGRTTYADSVKGRFTISRDNAKNTVYLQMNSLKPEDTAVYYCYAVMTGEARLLRMDY-----WGKGTLVTVSS
28-LN-IgG-B11   QVQLVESGGGLVQSGGSLRLSCAASGGIFSFRGMGWYRQAPGKQRELVAALT-RGGNTNYADSVKGRFTVSRDNAKSTVYLQMNSLKPEDTAVYSCNARSKWYGDY---------WGQGTQVTVSS

Germline VHH3   EVQLVESGGGLVQPGGSLRLSCAASGRTFSSYAMGWFRQAPGKGLEAVAAISWIGGSTYYADSVKGRFTISRDNSKNTLYLQMNSLRAEDTAVYYCAK
28-LN-IgG-B12   QVQLVESGGGQVQPGGSLRLSCAASGRTFSSYAMGWFRQAPGKGLEAVAAISWIGGSTKYADSVKGRFTISRDNSKNTLYLQMNSLRAEDTAVYYCAADPLSYGSNWPSDFGS---WGQGTQVTVSS
28-Sp-IgG-B8    QVQLVESGGGLVQPGGSLRLSCAASGRTFSSYAMGWFRQAPGKGLEAVAAISWIGGSTYYADSVKGRFTISRDNSKNTLYLQMNSLRAEDTAVYYCAAGAYSDYDY----------WGQGTQVTVSS

28-Sp-IgG-A7    s+16dim religation
28-Sp-IgG-B7    s+16dim religation
28-Sp-IgG-B12   s+16dim religation
```

LaMouse TE02-29

IgM repertoire: 17/24 legible sequences, 1xEREF, 13xQREL, 3x religation

```
Germline VHH6   EVQLVESGGGLVQAGGSLRLSCAASGRTFSSYAMGWFRQAPGKEREFVAAISWSGGSTYYADSVKGRFTISRDNAKNTVYLQMNSLKPEDTAVYYCAK
29-LN-IgM-B6    QVQLVESGGGLVQAGGSLRLSCAASGRTFSSYAMGWFRQAPGKEREFVAAISWSGGSTHYADSVKGRFTISRDNAKNTVYLQMNSLKPEDTAVYYCNADYYGMDY----------WGKGTLVTVSS

Germline VHH5   EVQLVESGGGLVQPGGSLRLSCAASGSIFSINAMGWYRQAPGKQRELVAAIT-SGGSTNYADSVKGRFTISRDNAKNTVYLQMNSLKPEDTAVYYCNA
29-Sp-IgM-B5    QVQLVESGGGLVQPGGSLRLSCAASGSIFSINAMGWYRQAPGKQRELVAAIT-SGGSTNYADSVKGRFTISRDNAKNTVYLQMNSLKPEDTAVYYCNAEVVPGEDYHGMYY-----WGKGTLVTVSS
29-Sp-IgM-B6    QVQLVESGGGSVQPGESLRLSCAVSGSIFSINAMGWYRQVPGKQRELVAAIT-SGGSTNYADSVKGRFTISRDNAKNTVYLQMNSLKPEDTAVYYCNAEIVPGEDYFGMDY-----WGKGTQVTVSS
29-Sp-IgM-A3    QVQLVESGGGLVQPGGSLRLSCAASGSIFSINAMGWYRQAPGKQRELVAAIT-SGGSTNYAASVKGRFTISRDNAKNTVSLQMNSLKPEDTAVYYCSAEIVIHEDYFDMDY-----WGKGTLVTVSS
29-Sp-IgM-A4    QVQLVESGGGVVQPGGSLRLSCAASGSIFSINAMGWYRQAPKKQRELVAAIT-SGGSTNYADSVKGRFTISRDNAKNTVYLQMNSLKPEDTAVYYCNADITVAVDYYGMDY-----WGKGTLVTVSS
29-LN-IgM-A1    QVQLVESGGGLVQPGGSLRLSCAASGSIFSINAMGWYRQAPGKQRELVAAIT-SGGSTNYADSVKGRFTISRDNAKNTVYLQMNSLKPEDTAVYYCNAGPATTVQGYGMDY-----WGKGTLVTVSS
29-LN-IgM-B5    QVQLVESGGGLVQPGGSLRLSCAASGSIFSINAMGWYRQAPGKQRELVAAIT-SGGSTNYADSVKGRFTISRDNAKNTVYLQMNSLKPEDTAAYYCNAEVVVDPDYYGMDY-----WGKGTLVTVSS
29-LN-IgM-A4    QVQLVESGGNLVQPGGSLRLSCAASGSIFSINAMGWYRQAPGKQRELVAAIT-SGGSTNYADSVKGRFTISRDNAKNTVYLQMNSLKPEDTAVYYCNGRVVAGTNYYGMDY-----WGKGTLVTVSS
29-LN-IgM-B3    QVQLVESGGGSVQPGGSLRLSCAASGTIFSINVMGWYRQAPGKQRDLVAFLT-SDGRAIYADSVKGRFTISRDNAKNTVYLQMNSLKPEDTAVYCCNIESRWPDGYSYDY-----WGQGTQVTVSS
29-LN-IgM-A6    QVQLVESGGGLVQPGGSLRLSCAASGSIFSINAMGWYRQAPGKQRELVAAIT-SGGSTNYADSVKGRFTISRDNAKNTVYLQMNSLKPEDTAVYYCNADIRVDYGMDY-------WGKGTLVTVSS
29-Sp-IgM-A5    QVQLVESGGGLVQPGGSLRLSCAASGSIFSINAMGWYRQAPGKQRELVAAIT-SGGSTNYADSVKGRFTISRDNAKNTVYLQMNSLKPEDTAVYYCNAEEVVAGAGDY-------WGQGTQVTVSS
29-Sp-IgM-B2    QVQLVESGGGLVQPGGSLRLSCAASGSIFSINAMGWYRQAPGKQRELVAAIT-SGGSTNYADSVKGRFTISRDNAKNTVYLQMNSLKPEDTAVYDCNADHLGALHDY---------WGQGTQVTVSS
29-Sp-IgM-B1    QVQLVESGGGLVQPGGSLRLSCAASGSIFSINAMGWYRQAPGKQRELVAAIT-SGGSTNYADSVKGRFTISRDNAKNTVYLQMNSLKPEDTAVYYCNAEGSRR----------------GTQVTVSS
29-LN-IgM-B4    QVQLVESGGGLVQPGGSLRLSCAASGSIFSINAMGWYRQAPGKQRELVAAIT-SGGSTNYADSVKGRFTISRDNAKNTVYLQMNSLKPEDTAVYYCNAAY----------------WGQGTQVTVSS

29-LN-IgM-A5    s+16dim religation
29-Sp-IgM-A2    s+16dim religation
29-Sp-IgM-B3    s+16dim religation
```

IgG repertoire: 15/24 legible sequences, 5xEREF, 6xQREL, 1xGLEW, 3x religation

```
Germline VHH6   EVQLVESGGGLVQAGGSLRLSCAASGRTFSSYAMGWFRQAPGKEREFVAAISWSGGSTYYADSVKGRFTISRDNAKNTVYLQMNSLKPEDTAVYYCAK
29-Sp-IgG-A7    QVQLVESGGGLVQAGGSLRLSCAASGRTFSSYAMGWFRQAPGKEREFVPAISWSGGSTYYADSVKGRFTISRDNAKNTVYLQMNSLKPEDTAVYYCAADRGSSWYDYGMDY-----WGKGTLVTVSS
29-LN-IgG-B7    QVQLVESGGGLVQAGGSLRLSCAASGRTFSTYAMGWFRQAPGKEREFVAAISSSGGGYKHYTDSVKGRFTISRDNAKNTVYLQMNSLKPEDTAVYYCNADEVTGGVFGS--------WGQGTQVTVSS
29-LN-IgG-A9    QVQLVESGGGLVQAGGSLRLSCAASGRTFSSYAMGWFRQAPGKEREFVAAISWSGGSTYYADSVKGRFTISRDNAKNTVYLQMNSLKPEDTAVYYCAEYGSFEYDY----------WGQGTQVTVSS
29-Sp-IgG-B8    QVQLVESGGGLVQAGGSLRLSCAASGRTFSSYAMGWFRQAPGKEREFVAAISWSGGSTYYADSVKGRFTISRDNAKNTVYLQMNSLKPEDTAVYYCAEYGSFEYDY----------WGQGTQVTVSS
29-Sp-IgG-B11   QVQLVESGGGLVQAGGSLRLSCAASGRTFSSYAMGWFRQAPGKEREFVAAISWSGGSTYYADSVKGRFTISRDNAKNTVYLQMNSLKPEDTAVYYCAEYGSFEYDY----------WGQGTQVTVSS

Germline VHH5   EVQLVESGGGLVQPGGSLRLSCAASGSIFSINAMGWYRQAPGKQRELVAAIT-SGGSTNYADSVKGRFTISRDNAKNTVYLQMNSLKPEDTAVYYCNA
29-Sp-IgG-A8    QVQLVESGGGLVQPGGSLRLSCAASGSIFSINAMGWYRQAPGKQRELVAAIT-SGGSTNYADSVKGRFTISRDNAKNTVYLQMNSLKPEDTAVYYCNADQDVRVVAGTDYYGMDY-WGKGTLVTVSS
29-Sp-IgG-B9    QVQLVESGGGLVQPGGSLRLSCAASGSIFSINAMGWYRQAPGKQRELVAAIT-SGGSTNYADSVKGRFTISRDNAKNTVYLQMNSLKPEDTAVYYCNADQDVRVVAGTDYYGMDY-WGKGTLVTVSS
29-Sp-IgG-B10   QVQLVESGGGLVQPGGSLRLSCAASGSIFSINAMGWYRQAPGKQRELVAAIT-SGGSTNYADSVKGRFTISRDNAKNTVYLQMNSLKPEDTAVYYCNADQDVRVVAGTDYYGMDY-WGKGTLVTVSS
29-LN-IgG-A10   QVQLVESGGGLVQPGGSLRLSCAASGSIFSIDAMGWYRQAPGKQRELVAVIT-SAGSTNYAASVKGRFTISRDNAKNTVYLQMNSLKPEDTAVYYCNAEIIPGEDYFAMDY-----WGKGTLVTVSS
29-LN-IgG-B10   QVQLVESGGGLVQPGGSLRLSCAASGSIFSAIAMGWYRQAPGKQRELVAAISWSGGITKYADSVKGRFTVSRDNAKNTVDLQMNSLKPEDTAVYYCAAEGVPGSYAMDY-------WGIGTLVTVSS
29-Sp-IgG-A9    QVQLVESGGGLVQPGGSLRLSCAASGSIFSINAMGWYRQAPGKQRELVAAIT-SGGSTNYADSVKGRFTISRDNAKNTVYLQMNSLKPEDTAVYYCKVVAGIGDY----------WGQGTQVTVSS

Germline VH    EVQLVESGGGLVQPGGSLRLSCAASGFTFDDYAMSWVRQAPGKGLEWVSAISWNGGSTYYAESMKGRFTISRDNAKNTLYLQMNSLKSEDTAVYYCAK
29-LN-IgG-A11   QVQLVESGGGLVQPGGSLRLSCAASGFTFDDYAMSWVRQAPGKGLEWVSAISWNGDITYYAESMKGRFTISRDNAKNTLYLQMNSLTSEDTAVYYCAKGTRELYYRVPYAYDY---WGQGTPVTVSS

29-LN-IgG-A7    s+16dim religation
29-LN-IgG-A8    s+16dim religation
29-Sp-IgG-B12   s+16dim religation
```

LaMouse TE03-31

IgM repertoire: 19/24 legible sequences, 3xEREF, 12xQREL, 1x GLEA, 3x religation

```
Germline VHH6   EVQLVESGGGLVQAGGSLRLSCAASGRTFSSYAMGWFRQAPGKEREFVAAISWSGGSTYYADSVKGRFTISRDNAKNTVYLQMNSLKPEDTAVYYCAK
31 SP-IgM-B5    QVQLVESGGGLVQPGESLRLSCAASGSTFSSYAMGWFRQAPGKEREFVAAISWSGGSTYYADSVKGRFTISRDNAKNTVYLQMNSLKPEDTAVYYCNACLTIATMGEYDY-----WGQGTQVTVSS
31 LN-IgM-B2     QVQLVESGGGLVQPGGSLRLSCVASGSIFSINAMGWYRQAPGKEREFVAAISWSGGSTYYADSVKGRFTISRDNAKNTVYLQMNSLKPEDTAVYYCNAPYGSSWHDY--------WGQGTQVTVSS
31 LN-IgM-B6     QVQLVESGGGLVQAGGSLRLSCAASGRTFSSYAMGWFRQAPGKEREFVAAISWSGGSTYYADSVKGRFTISRDNAKNTVYLQMNSLKPEDTAVYYPYGSSWYDGMDY--------WGKGTLVTVSS

Germline VHH5   EVQLVESGGGLVQPGGSLRLSCAASGSIFSINAMGWYRQAPGKQRELVAAIT-SGGSTNYADSVKGRFTISRDNAKNTVYLQMNSLKPEDTAVYYCNA
31 SP-IgM-B1    QVQLVESGGGLVQPGGSLRLSCAASGSIFSINAMGWYRQAPGKQRELVAAIT-SGGSTNYADSVKGRFTISRDNAKNTVYLQMNSLKPEDTAVYYCNAESLSGSSWYRVGS----WGQGTQVTVSS
31 SP-IgM-A4    QVQLVESGGGLVQPGGSLRLSCAASGSIFSINAMGWYRQAPGKQRELVATIT-SGGSTNYADSVKGRFTISRDNAKNTVYLQMNSLKPEDTAVYYCNAESLSGSSWYRFGS----WGQGTQVTVSS
31 LN-IgM-A5     QVQLVESGGGLVQPGGSLRLSCVASGSIFSINAMGWYRQAPGKQRELVATMT-NGGTTNYADSVKGRFTISRDNAKNTVYLQMNSLKPEDTAVYYCNAEGLSGSTWYRFGS----WGQGTQVTVSS
31 LN-IgM-B3     QVQLVESGGGLVQPGGSLRLSCAASGNIFSINAMGWYRQAPGKQRELVATIS-SGGSTNYADSVKGRFTISRDNAKNTVFLQMNSLKPEDTAVYYCNAESLSASSWYRFGS----WGQGTQVTVSS
31 SP-IgM-B6     QVQLVESGGGLVQPGGSLRLSCAASGSIFSINAMGWYRQVSGKQRELVATIT-SGGSTNYADSVKGRFTISRDNAKNTVYLQMNSLKPEDTAVYYCNAESLSGSSWYRVGS----WGPGTQVTVSS
31 LN-IgM-B4     QVQLVESGGGLVQPGGSLRLSCAASGSIFSINAMGWYRQAPGKQRELVAAIT-SGGSTNYADSVKGRFTISRDNAKNTVYLQMNSLKPEDTAVYYCNAVTIATMDEYDY------WGQGTQVTVSS
31 LN-IgM-B1     QVQLVESGGGLVQPGGSLRLSCAASGSIFSINAMGWYRQAPGKQRELVAAIT-SGGSTNYADSVKGRFTISRDNAKNTVYLQMNSLKPEDTAVYYCNAEGSWYRDEYDY------WGQGTQVTVSS
31 SP-IgM-B4     QVQLVESGGGLVQPGGSLRLSCAASGSIFSINAMGWYRQAPGKQRELVAAIT-SGGSTNYADSVKGRFTISRDNAKNTVYLQMNSLKPEDTAVYYCNAVVVVLYEYDY-------WGQGTQVTVSS
31 LN-IgM-A1     QVQLVESGGGLVQPGGSLRLSCAASGSIFSINAMGWYRQAPGKQRELVAAIT-SGGSTNYADSVKGRFTISRDNAKNTVYLQMNSLKPEDTAVYYFGVVTTDGMDY---------WGKGTLVTVSS
31 SP-IgM-A1     QVQLVESGGGLVQPGGSLRLSCAASGTIFSINAMGWYRQAPGKQRELVASIT-SGGSTNYADSVKGRFTISRDNAKNTVYLQMNSLKPEDTAVYYCNALVAGHDY----------WGQGTQVTVSS
31 LN-IgM-A3     QVQLVESGGGLVQPGGSLRLSCAASGSIFSINAMGWYRQAPGKQRELVAAIT-SGGSTNYADSVKGRFTISRDNAKNTVYLQMNSLKPEDTAVYYCNAKLALYDY----------WGQGTQVTVSS
31 LN-IgM-A6     QVQLVESGGGLVQPGGSLRLSCAASGSIFSINAMGWYRQAPGKQRELVAAIT-SGGSTNYADSVKGRFTISRDNAKNTVYLQMNSLKPEDTAVYYCNADGGR------------WGQETRVTVSS

Germline VHH3   EVQLVESGGGLVQPGGSLRLSCAASGRTFSSYAMGWFRQAPGKGLEAVAAISWIGGSTYYADSVKGRFTISRDNSKNTLYLQMNSLRAEDTAVYYCAK
31 LN-IgM-B5    QVQLVESGGGLVQPGGSLRLSCAASGRTFSSYAMGWFRQAPGKGLEAVAAISWIGGSTYYADSVKGRFTISRDNSKNTLYLQMNSLRAEDTAVYYCAAEVVAGTNYGMDY-----WGKGTLVTVSS

31-LN-IgM-A2   s+16dim religation
31-SP-IgM-A3   s+16dim religation
31-SP-IgM-A6   s+16dim religation
```

IgG repertoire: 17/24 legible sequences, 1xEREF, 11xQREL, 2x GLEW, 3x religation

```
Germline VHH6   EVQLVESGGGLVQAGGSLRLSCAASGRTFSSYAMGWFRQAPGKEREFVAAISWSGGSTYYADSVKGRFTISRDNAKNTVYLQMNSLKPEDTAVYYCAK
31 LN-IgG-A11   QVQLVESGGGLVQAGGSLRLSCAASGRTFSNYAMGWFRQAPGKERELVAAIS-SGGSFYSADSMKGRFTISRDNAKNTVYLQMNSLKPEDTAVYYCAAEGVAGSYGMDY------WGKGTQVTVSS

Germline VHH5   EVQLVESGGGLVQPGGSLRLSCAASGSIFSINAMGWYRQAPGKQRELVAAIT-SGGSTNYADSVKGRFTISRDNAKNTVYLQMNSLKPEDTAVYYCNA
31 SP-IgG-A7    QVQLVESGGGLVQPGGSLRLSCAASGSIFSINAMGWYRQAPGKQRELVATIS-SGGTTNYGDSVKGRFTISRDNAKNTMYLQMNSLKPEDTAVYYCNAESLSGSSWYRVGS----WGQGTQVTVSS
31 SP-IgG-B12   QVQLVESGGGLVQPGGSLRLSCAASGSIFSINAMGWYRQAPGKQRELVATIS-SGGTTNYGDSVKGRFTISRDNAKNTVYLQMNSLKPEDTAVYYCNAESLSGSSWYRVGS----WGQGTQVTVSS
31 LN-IgG-A7     QVQLVESGGGLVQPGGSLRLSCAASGNIFSVNAMGWYRQVSGKQRELVATIT-SGGNTNYADSVKGRFTISRDNAKNTVYLQMNSLKPEDTAVYYCNAESLSASSWYRFGS----WGQGTQVTVSS
31 LN-IgG-B7     QVQLVESGGGLVQPGGSLRLSCAASGSIVSSNAMVWYRQAPGKQRELVAAIS-SGGSPYSADSMKGRFTISRDNAKNTVYLQMNSLKPEDTAVYYCAAEGVAGSYGMDY------WGKGTLVTVSS
31 LN-IgG-B11   QVQLVESGGGLVQPGGSLRLSCAASGSILSIKAMGWYRQAPGKRRELVAAIT-SGGSTNYADSMKGRFTISRDNAKNTVYLQMNSLKPEDTAVYYCAAEGVAGSYGMDY------WGKGTLVTVSS
31 LN-IgG-B9    QVQLVESGGGLVQPGGSLRLSCAASGSIFSINAMGWYRQAPGKQRELVAVIT-SGGRTYYADSVKGRFTISRDSAKSTVYLQMNSLKPEDTAVYYCNADPGWGRGEYDY------WGQGTQVTVSS
31 LN-IgG-B8    QVQLVESGGGLVQPGGSLRLSCAASGSIFRINAMVWYRQAPGKQRELVADIS-SGGSTNYADSVKGRFTISRDNAKNTVYLQMNSLKPEDTAVYYCIPDGSREGFDY--------WGQGTRVTVSS
31 LN-IgG-B12   QVQLVESGGGLVQPGGSLRLSCAASGSIFRINAMVWYRQAPGKQRELVADIS-SGGSTNYADSVKGRFTISRDNAKNTVYLQMNSLKPEDTAVYYCIPDGSREGFDY--------WGQGTRVTVSS
31 SP-IgG-B11   QVQLVESGGGLVQPGGSLRLSCAASGSIFSINAMGWYRQAPGKQRELVAAIT-SGGSTNYADSVKGRFTISRDNAKNTVYLQMNSLKPEDTAVYYCKVVAGTGDY----------WGQGTQVTVSS
31 LN-IgG-A9    QVQLVESGGGLVQPGGSLILSCVASGSIFSLNDVGWYRQAPGKQHDLVAIIT-SGGSTNYADSVKGRFTISSDNARYTVYLQMNSLKPEDTAVYYCNAGLVPYGY----------WGQGTQVTVSS
31 LN-IgG-A10   QVQLVESGGGLVQPGGSLRLSCAASGSIFSINAMGWFRQAPGKQRELVAAIT-SDGSTHYADSVKGRFTISSDYARNTVYLQMNSLKPEDTAVYYCNAGLVPYGY----------WGQGTQVTVSS

Germline VH    EVQLVESGGGLVQPGGSLRLSCAASGFTFDDYAMSWVRQAPGKGLEWVSAISWNGGSTYYAESMKGRFTISRDNAKNTLYLQMNSLKSEDTAVYYCAK
31 SP-IgG-B7    QVQLVESGGGLVQPGGSLRLSCAASGFTFDDYAMSWVRQAPGKGLEWVSAISWNGGSTHYADSVKGRFTISSDNARNTVYLQMNSLKPEDTAVYYCNAESLSASSWYRFGS----WGQGTQVTVSS
31 SP-IgG-A8    QVQLVESGGGLVQPGGSLRLSCAASGFTFDDYAMSWVRQAPGKGLEWVSAISWNGGSTYYAESMKGRFTISRDNAKNTLYLQMNSLKSEDTAVYYCATTVVAGPDY---------WGQGTQVTVSS

31-LN-IgG-A8   s+16dim religation
31-LN-IgG-B10  s+16dim religation
31-SP-IgG-B10  s+16dim religation
```

LaMouse TE03-32

IgM repertoire: 22/24 legible sequences, 22xQREL, 0x religation

```
Germline VHH5   EVQLVESGGGLVQPGGSLRLSCAASGSIFSINAMGWYRQAPGKQRELVAAIT-SGGSTNYADSVKGRFTISRDNAKNTVYLQMNSLKPEDTAVYYCNA
32 LN-IgM-B2    QVQLVESGGGLVQPGGSLRLSCAAGSIFSINAMGWYRQAPGKQRELVAAIT-SGGSTNYADSVKGRFTISRDNAKNTVYLQMNSLKPEDTAVYYCNAERAYGSSWYDGMDY----WGKGTLVTVSS
32 LN-IgM-B1    QVQLVESGGGLVQPGGSLRLSCAAGSIFSINAMGWYRQAPGKQRELVAAIT-SGGSTNYADSVKGRFTISRDNAKNTVYLQMNSLKPEDTAVYYCNAGAVVAGRYDY-----WGQGTQVTVSS
32 LN-IgM-A3    QVQLVESGGGLVQPGGSLRLSCAAGSIFSINAMGWYRQAPGKQRELVAAIT-SGGSTNYADSVKGRFTISRDNAKNTVYLQMNSLKPEDTAVYYCNAYTGDYGMDY----------WGKGTLVTVSS
32 LN-IgM-B4    QVQLVESGGGLVQPGGSLRLSCAAGSIFSINAMGWYRQAPGKQRELVAAIT-SGGSTNYADSVKGRFTISRDNAKNTVYLQMNSLKPEDTAVYYCNADSSWYVLDA----------WGQGTLVTVSS
32 SP-IgM-A1    QVQLVESGGGLVQAGGSLRLSCAASGRTFSSYAMGWFRQAPGKEREFVAAISWSGGSTYYADSVKGRFTISRDNAKNTVYLQMNSLKPEDTAVYYCAEYGSPEYDY----------WGQGTQVTVSS
32 SP-IgM-A3    QVQLVESGGGLVQPGGSLRLSCAAGSIFSINAMGWYRQAPGKQRELVAAIT-SGGSTNYADSVKGRFTISRDNAKNTVYLQMNSLKPEDTAVYYCNAYIVVVTY----------WGQGTQVTVSS
32 SP-IgM-A4    QVQLVESGGGLVQPGGSLRLSCAAGSIFSINAMGWYRQAPGKQRELVAAIT-SGGSTNYADSVKGRFTISRDNAKNTVYLQMNSLKPEDTAVYYCNAYIVLVTY----------WGQGTQVTVSS
32 SP-IgM-A5    QVQLVESGGGLVQPGGSLRLSCAAGSIFSINAMGWYRQAPGKQRELVAAIT-SGGSTNYADSVKGRFTISRDNAKNTVYLQMNSLKPEDTAVYYCNAYIVVVTY----------WGQGTQVTVSS
32 SP-IgM-A6    QVQLVESGGGLVQPGGSLRLSCAAGSIFSINAMGWYRQAPGKQRELVAAIT-SGGSTNYADSVKGRFTISRDNAKNTVYLQMNSLKPEDTAVYYCNAYIVVVTY----------WGQGTQVTVSS
32 SP-IgM-B1    QVQLVESGGGLVQPGGSLRLSCAAGSIFSINAMGWYRQAPGKQRELVAAIT-SGGSTNYADSVKGRFTISRDNAKNTVYLQMNSLKPEDTAVYYCNAYIVVVTY----------WGQGTQVTVSS
32 SP-IgM-B3    QVQLVESGGGLVQPGGSLRLSCAAGSIFSINAMGWYRQAPGKQRELVAAIT-SGGSTNYADSVKGRFTISRDNAKNTVYLQMNSLKPEDTAVYYCNAYIVVVTY----------WGQGTQVTVSS
32 SP-IgM-B4    QVQLVESGGGLVQPGGSLRLSCAAGSIFSINAMGWYRQAPGKQRELVAAIT-SGGSTNYADSVKGRFTISRDNAKNTVYLQMNSLKPEDTAVYYCNAYIVVVTY----------WGQGTQVTVSS
32 SP-IgM-B5    QVQLVESGGGLVQPGGSLRLSCAAGSIFSINAMGWYRQAPGKQRELVAAIT-SGGSTNYADSVKGRFTISRDNAKNTVYLQMNSLKPEDTAVYYCNAYIVVVTY----------WGQGTQVTVSS
32 SP-IgM-B6    QVQLVESGGGLVQPGGSLRLSCAAGSIFSINAMGWYRQAPGKQRELVAAIT-SGGSTNYADSVKGRFTISRDNAKNTVYLQMNSLKPEDTAVYYCNAYIVVVTY----------WGQGTQVTVSS
32 LN-IgM-A1    QVQLVESGGGLVQPGGSLRLSCAAGSIFSINAMGWYRQAPGKQRELVAAIT-SGGSTNYADSVKGRFTISRDNAKNTVYLQMNSLKPEDTAVYYCNAYIVVVTY----------WGQGTQVTVSS
32 LN-IgM-A2    QVQLVESGGGLVQPGGSLRLSCAAGSIFSINAMGWYRQAPGKQRELVAAIT-SGGSTNYADSVKGRFTISRDNAKNTVYLQMNSLKPEDTAVYYCNAYIVVVTY----------WGQGTQVTVSS
32 LN-IgM-A5    QVQLVESGGGLVQPGGSLRLSCAAGSIFSINAMGWYRQAPGKQRELVAAIT-SGGSTNYADSVKGRFTISRDNAKNTVYLQMNSLKPEDTAVYYCNAYIVVVTY----------WGQGTQVTVSS
32 LN-IgM-A6    QVQLVESGGGLVQPGGSLRLSCAAGSIFSINAMGWYRQAPGKQRELVAAIT-SGGSTNYADSVKGRFTISRDNAKNTVYLQMNSLKPEDTAVYYCNAYIVVVTY----------WGQGTQVTVSS
32 LN-IgM-B3    QVQLVESGGGLVQPGGSLRLSCAAGSIFSINAMGWYRQAPGKQRELVAAIT-SGGSTNYADSVKGRFTISRDNAKNTVYLQMNSLKPEDTAVYYCNAYIVVVTY----------WGQGTQVTVSS
32 LN-IgM-B5    QVQLVESGGGLVQPGGSLRLSCAAGSIFSINAMGWYRQAPGKQRELVAAIT-SGGSTNYADSVKGRFTISRDNAKNTVYLQMNSLKPEDTAVYYCNAYIVVVTY----------WGQGTQVTVSS
32 LN-IgM-B6    QVQLVESGGGLVQPGGSLRLSCAAGSIFSINAMGWYRQAPGKQRELVAAIT-SGGSTNYADSVKGRFTISRDNAKNTVYLQMNSLKPEDTAVYYCNAYIVVVTY----------WGQGTQVTVSS
32 LN-IgM-A4    QVQLVESGGGLVQAGGSLRLSCAAGRTFSSYAMGWYRQAPGKQRELVAAIT-SGGSTNYADSVKGRFTISRDNAKNTVYLQMNSLKPEDTAVYYCNAAY----------WGQGTQVTVSL
```

LaMouse TE03-32

IgG repertoire: 22/24 legible sequences, 11xEREF, 6xQREL, 4xGLEW, 1x religation

```
Germline VHH6   EVQLVESGGGLVQAGGSLRLSCAASGRTFSSYAMGWFRQAPGKEREFVAAISWSGGSTYYADSVKGRFTISRDNAKNTVYLQMNSLKPEDTAVYYCAK
32 SP-IgG-A12   QVQLVESGGGLVQAGGSLRLSCAASGRTFSSYAMGWFRQAPGKEREFVVAISWSGGSTYYADSVKGRFTISRDNAKNTVYLQMNSLKPEDTAVYYCAAGSSWYGTYEFDY------WGQGTQVTVSS
32 LN-IgG-B8     QVQLVESGGGLVQAGGSLRLSCAASGRTFSSYAMGWFRQAPGKEREFVVAISWSGGSTYYADSVKGRFTISRDNAKNTVYLQMNSLKPEDTAVYYCAAGSSWYGTYEFDY------WGQGTQVTVSS
32 LN-IgG-A10    QVQLVESGGGLVQTGDSLRLSCAASGRTFSRNAMAWFRQAPEKKREFVAGVTWNGDNANYADSVKGRFTISRDNAKNTVYLQMNSLKPEDTAVYYCAAEGVIGSYGMDY-------WGKGTLVTVSS
32 LN-IgG-A12    QVQLVESGGGLVQAGGSLRLSCAASGRTFSSYAMGWFRQAPGKEREFVAAISWSGGSTYYADSVKGRFTISRDNAKNTVYLQMNSLKPEDTAVYYCAAEGVAGSYGMDY-------WGKGTLVTVSS
32 LN-IgG-A7     QVQLVESGGGLVQAGGSLRLSCAASGRTFSSYAMGWFRQAPGKEREFVA-----GGSTYYADSVKGRFTISRDNAKNTVYLQMNSLKPEDTAVYYCAAEGVAGSYGMDY-------WGKGTLVTVSS
32 LN-IgG-A8     QVQLVESGGGLVQAGGSLRLSCAASGRTFSSYAMGWFRQAPGKEREFVA-----GGSTYYADSVKGRFTISRDNAKNTVYLQMNSLKPEDTAVYYCAAEGVAGSYGMDY-------WGKGTLVTVSS
32 LN-IgG-A11    QVQLVESGGGLVQAGGSLRVSCAASGRTFSSYAMGWFRQAPGKEREFVA-----GGSTYYADSVKGRFTISRDNAKNTVYLQMNSLKPEDTAVYYCAAEGVAGSYGMDY-------WGKGTLVTVSS
32 LN-IgG-B9     QVQLVESGGGLVQAGGSLRLSCAASGRTFSSYAMGWFRQAPGKEREFVA-----GGSTYYADSVKGRFTISRDNAKNTVYLQMNSLKPEDTAVYYCAAEGVAGSYGMDY-------WGKGTLVTVSS
32 LN-IgG-B11    QVQLVESGGGLVQAGGSLRLSCAASGRTFSSYAMGWFRQAPGKEREFVA-----GGSTYYADSVKGRFTISRDNAKNTVYLQMNSLKPEDTAVYYCAAEGVAGSYGMDY-------WGKGTLVTVSS
32 LN-IgG-B12    QVQLVESGGGLVQAGGSLRLSCAASGRTFSSYAMGWFRQAPGKEREFVA-----GGSTYYADSVKGRFTISRDNAKNTVYLQMNSLKPEDTAVYYCAAEGVAGSYGMDY-------WGKGTLVTVSS
32 SP-IgG-B10    QVQLVESGGGLVQAGGSLRLSCAASGRTFSSYAMGWFRQAPGKEREFVAAISWSGGSTYYADSVKGRFTISRDNAKNTVYLQMNSLKPEDTAVYYCAEYGSFEYDY----------WGQGTQVTVSS

Germline VHH5   EVQLVESGGGLVQPGGSLRLSCAASGSIFSINAMGWYRQAPGKQRELVAAIT-SGGSTNYADSVKGRFTISRDNAKNTVYLQMNSLKPEDTAVYYCNA
32 LN-IgG-B7    QVQLVESGGGLVQPGGSLRLSCAVSGSVFSVTAMGWYRQAPGKQRELVAAVS-SGGTTNYTGSVKGRFTISRDNAKNTVYLDMNSLKPEDTAVYYCYAKYPIIAGARGYDY-----WGQGTQVTVSS
32 SP-IgG-A11    QVQLVESGGGLVQPGGSLRLSCAASGSIFSINAMGWYRQAPGKQRELVAAIT-SGGSTNYADSVKGRFTISRDNAKNTVYLQMNSLKPEDTAVYYCAAEGVAGSYGMDY-------WGKGTLVTVSS
32 SP-IgG-B8    QVQLVESGGGLVQAGGSLRLSCAASGSIFSINAMGWYRQAPGKQRELVAAIT-SGGSTNYADSVKGRFTISRDNAKNTVYLQMNSLKPEDTAVYYCAAEGVAGSYGMDY-------WGKGTLVTVSS
32 SP-IgG-A10    QVQLVESGGGLVQPGGSLRLSCAASGSIFSINAMGWYRQAPGKQRELVAAIT-SGGSTNYADSVKGRFTISRDTAKNTVYLQMNSLKPEDTAVYYCTESYSYEYAY----------WGQGTQVTVSS
32 SP-IgG-B7    QVQLVESGGGLVQPGGSLRLSCAASGSIFSINVMGWYRQAPGKQRELVAAIT-SGGSTNYADSVKGRFTISRDNAKNTVYLQMNSLKPEDTAVYYCNAYIVVVTY-----------WGQGTQVTVSS
32 SP-IgG-B11   QVQLVESGGGLVQPGGSLRLSCAASGSIFSINAMGWYRQAPGKQRELVAAIT-SGGSTNYADSVKGRFTISRDNAKNTVYLQMNSLKPEDTAVYYCNAYIVVVTY-----------WGQGTQVTVSS

Germline VH    EVQLVESGGGLVQPGGSLRLSCAASGFTFDDYAMSWVRQAPGKGLEWVSAISWNGGSTYYAESMKGRFTISRDNAKNTLYLQMNSLKSEDTAVYYCAK
32 SP-IgG-A7    QVQLVESGGGLVQPGGSLRLSCAASGFTFDDYAMSWVRQAPGKGLEWVSAISWNGGSTYYAESMKGRFTISRDNAKNTLYLQMNSLKSEDTAVYYCAKGLSPDGMDY---------WGKGTLVTVSS
32 SP-IgG-A8    QVQLVESGGGLVQPGGSLRLSCAASGFTFDDYAMSWVRQAPGKGLEWVSAISWNGGSTYYAESMKGRFTISRDNAKNTLYLQMNSLKSEDTAVYYCAKGLSPDGMDY---------WGKGTLVTVSS
32 SP-IgG-A9    QVQLVESGGGLVQPGGSLRLSCAASGFTFDDYAMSWVRQAPGKGLEWVSAISWNGGSTYYAESMKGRFTISRDNAKNTLYLQMNSLKSEDTAVYYCAKGLSPDGMDY---------WGKGTLVTVSS
32 SP-IgG-B12   QVQLVESGGGLVQPGGSLRLSCAASGFTFDDYAMSWVRQAPGKGLEWVSAISWNGGSTYYAESMKGRFTISRDNAKNTLYLQMNSLKSEDTAVYYCAKGLSPDGMEQ---------WGKGTLPPPPP

32-LN-IgG-A9   s+16dim religation
```

s+16dim religation

```
Germline VHH4   QVQLVESVGGLVQDGGSLRLSCAASGRTFSRSAMRWFRQAPGKEREWVSCISSSDGSTNYADSVKARFTISRDNAKNTLYLQMNSLKPEDTAVYYCAA
s+16dim         QVQLQESGGGLVQPGGALRLSCAASGLTLADTATGWFRQAPGKEREWVACISRRKAGTFYADSLKDRFTISRDDSVNTVYLQIISLKPDDTANYVCVQIPFCNEFMRGDLDRAIL--GQGTQVTVAS
```

Supplementary Figure 9.3 Isolated VHH sequences from two rounds panning on mouse or human P2X7. Amino acids belonging to the CDRs are highlighted as follows: CDR1 (red), CDR2 (green) and CDR3 (blue). Cysteines are indicated with yellow background. Somatic hypermutations corresponding to differing amino acids from the most closely related germline V element sequence (indicated at the top in lighter font) are color coded with a cyan background.

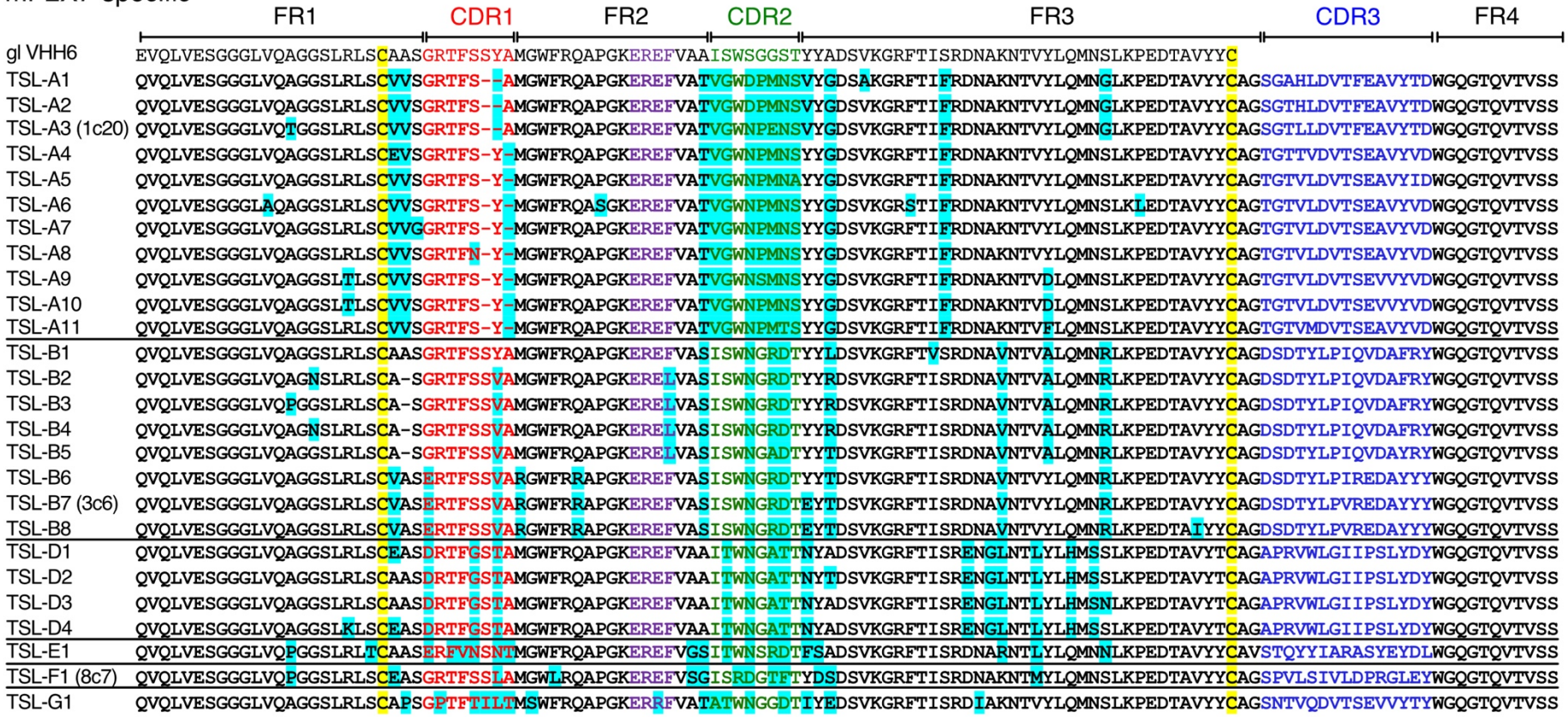

mP2X7 & hP2X7-cross reactive

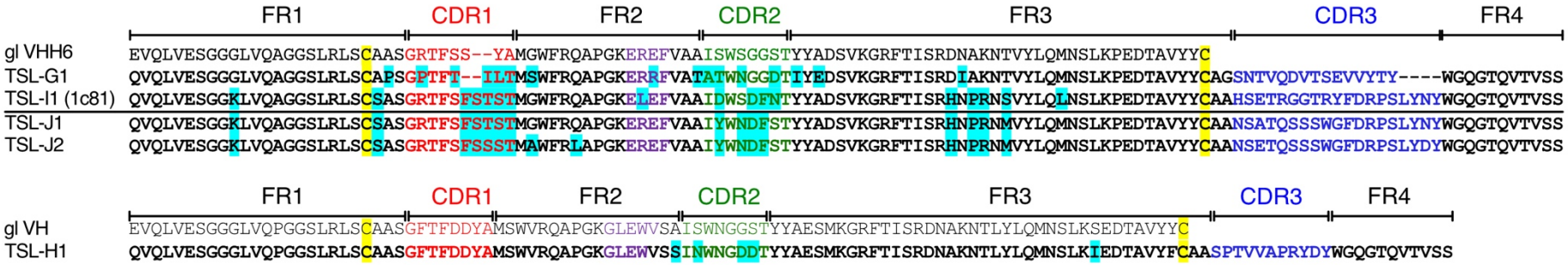

hP2X7-specific

unspecific

10 References

Adriouch S, Dox C, Welge V, Seman M, Koch-Nolte F, Haag F (2002) Cutting edge: a natural P451L mutation in the cytoplasmic domain impairs the function of the mouse P2X7 receptor. J Immunol 169 (8):4108-4112. doi:10.4049/jimmunol.169.8.4108

Allard B, Longhi MS, Robson SC, Stagg J (2017) The ectonucleotidases CD39 and CD73: Novel checkpoint inhibitor targets. Immunol Rev 276 (1):121-144. doi:10.1111/imr.12528

Becher T, Palanisamy S, Kramer DJ, Eljalby M, Marx SJ, Wibmer AG, Butler SD, Jiang CS, Vaughan R, Schoder H, Mark A, Cohen P (2021) Brown adipose tissue is associated with cardiometabolic health. Nat Med 27 (1):58-65. doi:10.1038/s41591-020-1126-7

Behar G, Siberil S, Groulet A, Chames P, Pugniere M, Boix C, Sautes-Fridman C, Teillaud JL, Baty D (2008) Isolation and characterization of anti-FcgammaRIII (CD16) llama single-domain antibodies that activate natural killer cells. Protein Eng Des Sel 21 (1):1-10. doi:10.1093/protein/gzm064

Bergmann P, Garcia de Paco E, Rissiek B, Menzel S, Dubberke G, Hua J, Rassendren F, Ulmann L, Koch-Nolte F (2019) Generation and Characterization of Specific Monoclonal Antibodies and Nanobodies Directed Against the ATP-Gated Channel P2X4. Front Cell Neurosci 13:498. doi:10.3389/fncel.2019.00498

Bo X, Jiang LH, Wilson HL, Kim M, Burnstock G, Surprenant A, North RA (2003) Pharmacological and biophysical properties of the human P2X5 receptor. Mol Pharmacol 63 (6):1407-1416. doi:10.1124/mol.63.6.1407

Bolotin DA, Poslavsky S, Mitrophanov I, Shugay M, Mamedov IZ, Putintseva EV, Chudakov DM (2015) MiXCR: software for comprehensive adaptive immunity profiling. Nat Methods 12 (5):380-381. doi:10.1038/nmeth.3364

Bond LM, Burhans MS, Ntambi JM (2018) Uncoupling protein-1 deficiency promotes brown adipose tissue inflammation and ER stress. PLoS One 13 (11):e0205726. doi:10.1371/journal.pone.0205726

Bork P, Holm L, Sander C (1994) The immunoglobulin fold. Structural classification, sequence patterns and common core. J Mol Biol 242 (4):309-320. doi:10.1006/jmbi.1994.1582

Broz P, Dixit VM (2016) Inflammasomes: mechanism of assembly, regulation and signalling. Nat Rev Immunol 16 (7):407-420. doi:10.1038/nri.2016.58

Bryant C, Ferris M, De Villena F, Damaj M, Kumar V, Mulligan M, Gerlai R (2018) Molecular-genetic and statistical techniques for behavioral and neural research.

Buell G, Chessell IP, Michel AD, Collo G, Salazzo M, Herren S, Gretener D, Grahames C, Kaur R, Kosco-Vilbois MH, Humphrey PP (1998) Blockade of human P2X7 receptor function with a monoclonal antibody. Blood 92 (10):3521-3528

Burnstock G (2006) Pathophysiology and therapeutic potential of purinergic signaling. Pharmacol Rev 58 (1):58-86. doi:10.1124/pr.58.1.5

Cannon B, Nedergaard J (2004) Brown adipose tissue: function and physiological significance. Physiol Rev 84 (1):277-359. doi:10.1152/physrev.00015.2003

Chanier T, Chames P (2019) Nanobody Engineering: Toward Next Generation Immunotherapies and Immunoimaging of Cancer. Antibodies (Basel) 8 (1). doi:10.3390/antib8010013

Chekeni FB, Elliott MR, Sandilos JK, Walk SF, Kinchen JM, Lazarowski ER, Armstrong AJ, Penuela S, Laird DW, Salvesen GS, Isakson BE, Bayliss DA, Ravichandran KS (2010) Pannexin 1 channels mediate 'find-me' signal release and membrane permeability during apoptosis. Nature 467 (7317):863-867. doi:10.1038/nature09413

Chen J, Trounstine M, Alt FW, Young F, Kurahara C, Loring JF, Huszar D (1993) Immunoglobulin gene rearrangement in B cell deficient mice generated by targeted deletion of the JH locus. Int Immunol 5 (6):647-656. doi:10.1093/intimm/5.6.647

Chen KY, Brychta RJ, Abdul Sater Z, Cassimatis TM, Cero C, Fletcher LA, Israni NS, Johnson JW, Lea HJ, Linderman JD, O'Mara AE, Zhu KY, Cypess AM (2020) Opportunities and challenges in the therapeutic activation of human energy expenditure and thermogenesis to manage obesity. J Biol Chem 295 (7):1926-1942. doi:10.1074/jbc.REV119.007363

Chin SE, Ferraro F, Groves M, Liang M, Vaughan TJ, Dobson CL (2015) Isolation of high-affinity, neutralizing anti-idiotype antibodies by phage and ribosome display for application in

immunogenicity and pharmacokinetic analyses. J Immunol Methods 416:49-58. doi:10.1016/j.jim.2014.10.013

Chinestra P, Lajoie-Mazenc I, Faye JC, Favre G (2012) Use of phage display for the identification of molecular sensors specific for activated Rho. Methods Mol Biol 827:283-303. doi:10.1007/978-1-61779-442-1_19

Chothia C, Gelfand I, Kister A (1998) Structural determinants in the sequences of immunoglobulin variable domain. J Mol Biol 278 (2):457-479. doi:10.1006/jmbi.1998.1653

Clarke L, Zheng-Bradley X, Smith R, Kulesha E, Xiao C, Toneva I, Vaughan B, Preuss D, Leinonen R, Shumway M, Sherry S, Flicek P, Genomes Project C (2012) The 1000 Genomes Project: data management and community access. Nat Methods 9 (5):459-462. doi:10.1038/nmeth.1974

Colgan SP, Eltzschig HK, Eckle T, Thompson LF (2006) Physiological roles for ecto-5'-nucleotidase (CD73). Purinergic Signal 2 (2):351-360. doi:10.1007/s11302-005-5302-5

Cox JA, Barmina O, Voigt MM (2001) Gene structure, chromosomal localization, cDNA cloning and expression of the mouse ATP-gated ionotropic receptor P2X5 subunit. Gene 270 (1-2):145-152. doi:10.1016/s0378-1119(01)00484-x

Cristalli G, Costanzi S, Lambertucci C, Lupidi G, Vittori S, Volpini R, Camaioni E (2001) Adenosine deaminase: functional implications and different classes of inhibitors. Med Res Rev 21 (2):105-128. doi:10.1002/1098-1128(200103)21:2<105::aid-med1002>3.0.co;2-u

Crivianu-Gaita V, Thompson M (2016) Aptamers, antibody scFv, and antibody Fab' fragments: An overview and comparison of three of the most versatile biosensor biorecognition elements. Biosens Bioelectron 85:32-45. doi:10.1016/j.bios.2016.04.091

Danquah W (2012) Selection and characterization of llama-derived anti-P2X7 single domain antibodies. Staats-und Universitätsbibliothek Hamburg Carl von Ossietzky,

Danquah W, Meyer-Schwesinger C, Rissiek B, Pinto C, Serracant-Prat A, Amadi M, Iacenda D, Knop JH, Hammel A, Bergmann P, Schwarz N, Assuncao J, Rotthier W, Haag F, Tolosa E, Bannas P, Boue-Grabot E, Magnus T, Laeremans T, Stortelers C, Koch-Nolte F (2016) Nanobodies that block gating of the P2X7 ion channel ameliorate inflammation. Sci Transl Med 8 (366):366ra162. doi:10.1126/scitranslmed.aaf8463

de Jong JMA, Sun W, Pires ND, Frontini A, Balaz M, Jespersen NZ, Feizi A, Petrovic K, Fischer AW, Bokhari MH, Niemi T, Nuutila P, Cinti S, Nielsen S, Scheele C, Virtanen K, Cannon B, Nedergaard J, Wolfrum C, Petrovic N (2019) Human brown adipose tissue is phenocopied by classical brown adipose tissue in physiologically humanized mice. Nat Metab 1 (8):830-843. doi:10.1038/s42255-019-0101-4

De Silva NS, Klein U (2015) Dynamics of B cells in germinal centres. Nat Rev Immunol 15 (3):137-148. doi:10.1038/nri3804

Derer S, Kellner C, Berger S, Valerius T, Peipp M (2012) Fc engineering: design, expression, and functional characterization of antibody variants with improved effector function. Methods Mol Biol 907:519-536. doi:10.1007/978-1-61779-974-7_30

Di Virgilio F, Chiozzi P, Ferrari D, Falzoni S, Sanz JM, Morelli A, Torboli M, Bolognesi G, Baricordi OR (2001) Nucleotide receptors: an emerging family of regulatory molecules in blood cells. Blood 97 (3):587-600. doi:10.1182/blood.v97.3.587

Di Virgilio F, Sarti AC, Coutinho-Silva R (2020) Purinergic signaling, DAMPs, and inflammation. Am J Physiol Cell Physiol 318 (5):C832-C835. doi:10.1152/ajpcell.00053.2020

Di Virgilio F, Schmalzing G, Markwardt F (2018) The Elusive P2X7 Macropore. Trends Cell Biol 28 (5):392-404. doi:10.1016/j.tcb.2018.01.005

Duckwitz W, Hausmann R, Aschrafi A, Schmalzing G (2006) P2X5 subunit assembly requires scaffolding by the second transmembrane domain and a conserved aspartate. J Biol Chem 281 (51):39561-39572. doi:10.1074/jbc.M606113200

Eden T (2018) Herstellung und Charakterisierung von Lama Schwere-Ketten-Antikörper produzierenden transgenen Mäusen. Doctoral thesis, Universität Hamburg,

Eden T, Menzel S, Wesolowski J, Bergmann P, Nissen M, Dubberke G, Seyfried F, Albrecht B, Haag F, Koch-Nolte F (2017) A cDNA Immunization Strategy to Generate Nanobodies against Membrane Proteins in Native Conformation. Front Immunol 8:1989. doi:10.3389/fimmu.2017.01989

Eichhoff AM, Borner K, Albrecht B, Schafer W, Baum N, Haag F, Korbelin J, Trepel M, Braren I, Grimm D, Adriouch S, Koch-Nolte F (2019) Nanobody-Enhanced Targeting of AAV Gene Therapy Vectors. Mol Ther Methods Clin Dev 15:211-220. doi:10.1016/j.omtm.2019.09.003

Er-Lukowiak M, Duan Y, Rassendren F, Ulmann L, Nicke A, Ufer F, Friese MA, Koch-Nolte F, Magnus T, Rissiek B (2020) A P2rx7 Passenger Mutation Affects the Vitality and Function of T cells in Congenic Mice. iScience 23 (12):101870. doi:10.1016/j.isci.2020.101870

Evavold CL, Ruan J, Tan Y, Xia S, Wu H, Kagan JC (2018) The Pore-Forming Protein Gasdermin D Regulates Interleukin-1 Secretion from Living Macrophages. Immunity 48 (1):35-44 e36. doi:10.1016/j.immuni.2017.11.013

Falconer DJ, Barb AW (2018) Mouse IgG2c Fc loop residues promote greater receptor-binding affinity than mouse IgG2b or human IgG1. PLoS One 13 (2):e0192123. doi:10.1371/journal.pone.0192123

Fischer AW, Cannon B, Nedergaard J (2018) Optimal housing temperatures for mice to mimic the thermal environment of humans: An experimental study. Mol Metab 7:161-170. doi:10.1016/j.molmet.2017.10.009

Fischer AW, de Jong JMA, Sass F, Schlein C, Heeren J, Petrovic N (2020) Thermoneutrality-Induced Macrophage Accumulation in Brown Adipose Tissue Does Not Impair the Tissue's Competence for Cold-Induced Thermogenic Recruitment. Front Endocrinol (Lausanne) 11:568682. doi:10.3389/fendo.2020.568682

Fischer AW, Jaeckstein MY, Gottschling K, Heine M, Sass F, Mangels N, Schlein C, Worthmann A, Bruns OT, Yuan Y, Zhu H, Chen O, Ittrich H, Nilsson SK, Stefanicka P, Ukropec J, Balaz M, Dong H, Sun W, Reimer R, Scheja L, Heeren J (2021) Lysosomal lipoprotein processing in endothelial cells stimulates adipose tissue thermogenic adaptation. Cell Metab 33 (3):547-564 e547. doi:10.1016/j.cmet.2020.12.001

Fischer AW, Schlein C, Cannon B, Heeren J, Nedergaard J (2019) Intact innervation is essential for diet-induced recruitment of brown adipose tissue. Am J Physiol Endocrinol Metab 316 (3):E487-E503. doi:10.1152/ajpendo.00443.2018

Frayn KN, Karpe F, Fielding BA, Macdonald IA, Coppack SW (2003) Integrative physiology of human adipose tissue. Int J Obes Relat Metab Disord 27 (8):875-888. doi:10.1038/sj.ijo.0802326

Garcia RA, Roemmich JN, Claycombe KJ (2016) Evaluation of markers of beige adipocytes in white adipose tissue of the mouse. Nutr Metab (Lond) 13:24. doi:10.1186/s12986-016-0081-2

Geiger M, Stubenrauch KG, Sam J, Richter WF, Jordan G, Eckmann J, Hage C, Nicolini V, Freimoser-Grundschober A, Ritter M, Lauer ME, Stahlberg H, Ringler P, Patel J, Sullivan E, Grau-Richards S, Endres S, Kobold S, Umana P, Brunker P, Klein C (2020) Protease-activation using anti-idiotypic masks enables tumor specificity of a folate receptor 1-T cell bispecific antibody. Nat Commun 11 (1):3196. doi:10.1038/s41467-020-16838-w

Ghiringhelli F, Apetoh L, Tesniere A, Aymeric L, Ma Y, Ortiz C, Vermaelen K, Panaretakis T, Mignot G, Ullrich E, Perfettini JL, Schlemmer F, Tasdemir E, Uhl M, Genin P, Civas A, Ryffel B, Kanellopoulos J, Tschopp J, Andre F, Lidereau R, McLaughlin NM, Haynes NM, Smyth MJ, Kroemer G, Zitvogel L (2009) Activation of the NLRP3 inflammasome in dendritic cells induces IL-1beta-dependent adaptive immunity against tumors. Nat Med 15 (10):1170-1178. doi:10.1038/nm.2028

Hambach J, Fumey W, Stähler T, Gebhardt AJ, Adam G, Weisel K, Koch-Nolte F, Bannas P (2022) Half-Life Extended Nanobody-Based CD38-Specific Bispecific Killercell Engagers Induce Killing of Multiple Myeloma Cells. Front Immunol 13:838406. doi:10.3389/fimmu.2022.838406

Hamers-Casterman C, Atarhouch T, Muyldermans S, Robinson G, Hamers C, Songa EB, Bendahman N, Hamers R (1993) Naturally occurring antibodies devoid of light chains. Nature 363 (6428):446-448. doi:10.1038/363446a0

Hasko G, Cronstein BN (2004) Adenosine: an endogenous regulator of innate immunity. Trends Immunol 25 (1):33-39. doi:10.1016/j.it.2003.11.003

Henderson NC, Sethi T (2009) The regulation of inflammation by galectin-3. Immunol Rev 230 (1):160-171. doi:10.1111/j.1600-065X.2009.00794.x

Hoefman S, Ottevaere I, Baumeister J, Sargentini-Maier M (2015) Pre-Clinical Intravenous Serum Pharmacokinetics of Albumin Binding and Non-Half-Life Extended Nanobodies®. Antibodies 4 (3):141-156. doi:10.3390/antib4030141

Hongo JS, Laramee GR, Urfer R, Shelton DL, Restivo T, Sadick M, Galloway A, Chu H, Winslow JW (2000) Antibody binding regions on human nerve growth factor identified by homolog- and alanine-scanning mutagenesis. Hybridoma 19 (3):215-227. doi:10.1089/02724570050109611

Huang JX, Bishop-Hurley SL, Cooper MA (2012) Development of anti-infectives using phage display: biological agents against bacteria, viruses, and parasites. Antimicrob Agents Chemother 56 (9):4569-4582. doi:10.1128/AAC.00567-12

Huo J, Le Bas A, Ruza RR, Duyvesteyn HME, Mikolajek H, Malinauskas T, Tan TK, Rijal P, Dumoux M, Ward PN, Ren J, Zhou D, Harrison PJ, Weckener M, Clare DK, Vogirala VK, Radecke J, Moynie L, Zhao Y, Gilbert-Jaramillo J, Knight ML, Tree JA, Buttigieg KR, Coombes N, Elmore MJ, Carroll MW, Carrique L, Shah PNM, James W, Townsend AR, Stuart DI, Owens RJ, Naismith JH (2020) Neutralizing nanobodies bind SARS-CoV-2 spike RBD and block interaction with ACE2. Nat Struct Mol Biol 27 (9):846-854. doi:10.1038/s41594-020-0469-6

Hwang JR, Byeon Y, Kim D, Park SG (2020) Recent insights of T cell receptor-mediated signaling pathways for T cell activation and development. Exp Mol Med 52 (5):750-761. doi:10.1038/s12276-020-0435-8

Illes P, Muller CE, Jacobson KA, Grutter T, Nicke A, Fountain SJ, Kennedy C, Schmalzing G, Jarvis MF, Stojilkovic SS, King BF, Di Virgilio F (2021) Update of P2X receptor properties and their pharmacology: IUPHAR Review 30. Br J Pharmacol 178 (3):489-514. doi:10.1111/bph.15299

Jäckstein MY (2022) Intercellular crosstalk in adipose tissues shapes thermogenic function and adaptation. Doctoral thesis, Universität Hamburg,

Janeway CA (1989) Approaching the asymptote? Evolution and revolution in immunology. Cold Spring Harb Symp Quant Biol 54 Pt 1:1-13. doi:10.1101/sqb.1989.054.01.003

Janeway CA, Travers P, Walport M (2001a) B-cell activation by armed helper T cells. In: Science NYG (ed) Immunobiology: The Immune System in Health and Disease. 5th edition edn.,

Janeway CA, Travers P, Walport M, Shlomchik MJ (2001b) Immunobiology: The Immune System in Health and Disease, 5th ediition. Garland Science

Janssens R, Dekker S, Hendriks RW, Panayotou G, van Remoortere A, San JK, Grosveld F, Drabek D (2006) Generation of heavy-chain-only antibodies in mice. Proc Natl Acad Sci U S A 103 (41):15130-15135. doi:10.1073/pnas.0601108103

Jumper J, Evans R, Pritzel A, Green T, Figurnov M, Ronneberger O, Tunyasuvunakool K, Bates R, Zidek A, Potapenko A, Bridgland A, Meyer C, Kohl SAA, Ballard AJ, Cowie A, Romera-Paredes B, Nikolov S, Jain R, Adler J, Back T, Petersen S, Reiman D, Clancy E, Zielinski M, Steinegger M, Pacholska M, Berghammer T, Bodenstein S, Silver D, Vinyals O, Senior AW, Kavukcuoglu K, Kohli P, Hassabis D (2021) Highly accurate protein structure prediction with AlphaFold. Nature 596 (7873):583-589. doi:10.1038/s41586-021-03819-2

Kambayashi T, Laufer TM (2014) Atypical MHC class II-expressing antigen-presenting cells: can anything replace a dendritic cell? Nature Reviews Immunology 14 (11):719-730. doi:10.1038/nri3754

Karasawa A, Michalski K, Mikhelzon P, Kawate T (2017) The P2X7 receptor forms a dye-permeable pore independent of its intracellular domain but dependent on membrane lipid composition. Elife 6. doi:10.7554/eLife.31186

Kawate T, Michel JC, Birdsong WT, Gouaux E (2009) Crystal structure of the ATP-gated P2X(4) ion channel in the closed state. Nature 460 (7255):592-598. doi:10.1038/nature08198

Kazak L, Chouchani ET, Stavrovskaya IG, Lu GZ, Jedrychowski MP, Egan DF, Kumari M, Kong X, Erickson BK, Szpyt J, Rosen ED, Murphy MP, Kristal BS, Gygi SP, Spiegelman BM (2017) UCP1 deficiency causes brown fat respiratory chain depletion and sensitizes mitochondria to calcium overload-induced dysfunction. Proc Natl Acad Sci U S A 114 (30):7981-7986. doi:10.1073/pnas.1705406114

Khakh BS, North RA (2006) P2X receptors as cell-surface ATP sensors in health and disease. Nature 442 (7102):527-532. doi:10.1038/nature04886

King BF (2022) Rehabilitation of the P2X5 receptor: a re-evaluation of structure and function. Purinergic Signal. doi:10.1007/s11302-022-09903-0

Klaver D, Thurnher M (2021) Control of Macrophage Inflammation by P2Y Purinergic Receptors. Cells 10 (5). doi:10.3390/cells10051098

Koch-Nolte F, Duffy T, Nissen M, Kahl S, Killeen N, Ablamunits V, Haag F, Leiter EH (1999) A new monoclonal antibody detects a developmentally regulated mouse ecto-ADP-ribosyltransferase on T cells: subset distribution, inbred strain variation, and modulation upon T cell activation. J Immunol 163 (11):6014-6022

Koch-Nolte F, Reyelt J, Schossow B, Schwarz N, Scheuplein F, Rothenburg S, Haag F, Alzogaray V, Cauerhff A, Goldbaum FA (2007) Single domain antibodies from llama effectively and

specifically block T cell ecto-ADP-ribosyltransferase ART2.2 in vivo. FASEB J 21 (13):3490-3498. doi:10.1096/fj.07-8661com

Kohler G, Milstein C (1975) Continuous cultures of fused cells secreting antibody of predefined specificity. Nature 256 (5517):495-497. doi:10.1038/256495a0

Kosteli A, Sugaru E, Haemmerle G, Martin JF, Lei J, Zechner R, Ferrante AW, Jr. (2010) Weight loss and lipolysis promote a dynamic immune response in murine adipose tissue. J Clin Invest 120 (10):3466-3479. doi:10.1172/JCI42845

Kotnis S, Bingham B, Vasilyev DV, Miller SW, Bai Y, Yeola S, Chanda PK, Bowlby MR, Kaftan EJ, Samad TA, Whiteside GT (2010) Genetic and functional analysis of human P2X5 reveals a distinct pattern of exon 10 polymorphism with predominant expression of the nonfunctional receptor isoform. Mol Pharmacol 77 (6):953-960. doi:10.1124/mol.110.063636

Kotzbeck P, Giordano A, Mondini E, Murano I, Severi I, Venema W, Cecchini MP, Kershaw EE, Barbatelli G, Haemmerle G, Zechner R, Cinti S (2018) Brown adipose tissue whitening leads to brown adipocyte death and adipose tissue inflammation. J Lipid Res 59 (5):784-794. doi:10.1194/jlr.M079665

Kristensen P, Winter G (1998) Proteolytic selection for protein folding using filamentous bacteriophages. Fold Des 3 (5):321-328. doi:10.1016/S1359-0278(98)00044-3

Lakbub JC, Shipman JT, Desaire H (2018) Recent mass spectrometry-based techniques and considerations for disulfide bond characterization in proteins. Anal Bioanal Chem 410 (10):2467-2484. doi:10.1007/s00216-017-0772-1

Lê KT, Paquet M, Nouel D, Babinski K, Séguéla P (1997) Primary structure and expression of a naturally truncated human P2X ATP receptor subunit from brain and immune system. FEBS Lett 418 (1-2):195-199. doi:10.1016/s0014-5793(97)01380-x

Lewis C, Neidhart S, Holy C, North RA, Buell G, Surprenant A (1995) Coexpression of P2X2 and P2X3 receptor subunits can account for ATP-gated currents in sensory neurons. Nature 377 (6548):432-435. doi:10.1038/377432a0

Lim SY, Chan CE, Lisowska MM, Hanson BJ, MacAry PA (2015) The Molecular Engineering of an Anti-Idiotypic Antibody for Pharmacokinetic Analysis of a Fully Human Anti-Infective. PLoS One 10 (12):e0145381. doi:10.1371/journal.pone.0145381

Liu X, Zhang Z, Ruan J, Pan Y, Magupalli VG, Wu H, Lieberman J (2016) Inflammasome-activated gasdermin D causes pyroptosis by forming membrane pores. Nature 535 (7610):153-158. doi:10.1038/nature18629

Lowell BB, Flier JS (1997) Brown adipose tissue, beta 3-adrenergic receptors, and obesity. Annu Rev Med 48:307-316. doi:10.1146/annurev.med.48.1.307

Lumeng CN, DelProposto JB, Westcott DJ, Saltiel AR (2008) Phenotypic switching of adipose tissue macrophages with obesity is generated by spatiotemporal differences in macrophage subtypes. Diabetes 57 (12):3239-3246. doi:10.2337/db08-0872

Magaki S, Hojat SA, Wei B, So A, Yong WH (2019) An Introduction to the Performance of Immunohistochemistry. Methods Mol Biol 1897:289-298. doi:10.1007/978-1-4939-8935-5_25

Mann AM, Schäfer W, Adriouch S, Börner K, Grimm D, Braren I, Koch-Nolte F (2022) Enhanced Transduction of P2X7-Expressing Cells with Recombinant rAAV Vectors. In: Nicke A (ed) The P2X7 Receptor: Methods and Protocols. Springer US, New York, NY, pp 129-144. doi:10.1007/978-1-0716-2384-8_7

McCarthy AE, Yoshioka C, Mansoor SE (2019) Full-Length P2X(7) Structures Reveal How Palmitoylation Prevents Channel Desensitization. Cell 179 (3):659-670 e613. doi:10.1016/j.cell.2019.09.017

Meyer M, Kircher M, Gansauge MT, Li H, Racimo F, Mallick S, Schraiber JG, Jay F, Prüfer K, de Filippo C, Sudmant PH, Alkan C, Fu Q, Do R, Rohland N, Tandon A, Siebauer M, Green RE, Bryc K, Briggs AW, Stenzel U, Dabney J, Shendure J, Kitzman J, Hammer MF, Shunkov MV, Derevianko AP, Patterson N, Andrés AM, Eichler EE, Slatkin M, Reich D, Kelso J, Pääbo S (2012) A high-coverage genome sequence from an archaic Denisovan individual. Science 338 (6104):222-226. doi:10.1126/science.1224344

Mielke D, Bandawe G, Pollara J, Abrahams MR, Nyanhete T, Moore PL, Thebus R, Yates NL, Kappes JC, Ochsenbauer C, Garrett N, Abdool Karim S, Tomaras GD, Montefiori D, Morris L, Ferrari G, Williamson C (2019) Antibody-Dependent Cellular Cytotoxicity (ADCC)-Mediating Antibodies Constrain Neutralizing Antibody Escape Pathway. Front Immunol 10:2875. doi:10.3389/fimmu.2019.02875

Moonen MPB, Nascimento EBM, van Marken Lichtenbelt WD (2019) Human brown adipose tissue: Underestimated target in metabolic disease? Biochim Biophys Acta Mol Cell Biol Lipids 1864 (1):104-112. doi:10.1016/j.bbalip.2018.05.012

Morgado MG, Cam P, Gris-Liebe C, Cazenave PA, Jouvin-Marche E (1989) Further evidence that BALB/c and C57BL/6 gamma 2a genes originate from two distinct isotypes. EMBO J 8 (11):3245-3251. doi:10.1002/j.1460-2075.1989.tb08484.x

Muyldermans S (2013) Nanobodies: Natural Single-Domain Antibodies. Annual Review of Biochemistry 82 (1):775-797. doi:10.1146/annurev-biochem-063011-092449

Nedergaard J, Bengtsson T, Cannon B (2007) Unexpected evidence for active brown adipose tissue in adult humans. Am J Physiol Endocrinol Metab 293 (2):E444-452. doi:10.1152/ajpendo.00691.2006

Nemazee D (2017) Mechanisms of central tolerance for B cells. Nature Reviews Immunology 17 (5):281-294. doi:10.1038/nri.2017.19

North RA (2002) Molecular physiology of P2X receptors. Physiol Rev 82 (4):1013-1067. doi:10.1152/physrev.00015.2002

North RA, Surprenant A (2000) Pharmacology of Cloned P2X Receptors. Annual Review of Pharmacology and Toxicology 40 (1):563-580. doi:10.1146/annurev.pharmtox.40.1.563

Oken AC, Krishnamurthy I, Savage JC, Lisi NE, Godsey MH, Mansoor SE (2022) Molecular Pharmacology of P2X Receptors: Exploring Druggable Domains Revealed by Structural Biology. Front Pharmacol 13:925880. doi:10.3389/fphar.2022.925880

Ouellet V, Labbe SM, Blondin DP, Phoenix S, Guerin B, Haman F, Turcotte EE, Richard D, Carpentier AC (2012) Brown adipose tissue oxidative metabolism contributes to energy expenditure during acute cold exposure in humans. J Clin Invest 122 (2):545-552. doi:10.1172/JCI60433

Pantelic N (2018) Selection and characterization of AAV-specific nanobodies. Masterthesis, Hochschule Bremen.,

Pelleymounter MA, Cullen MJ, Baker MB, Hecht R, Winters D, Boone T, Collins F (1995) Effects of the obese gene product on body weight regulation in ob/ob mice. Science 269 (5223):540-543. doi:10.1126/science.7624776

Pinaud E, Khamlichi AA, Le Morvan C, Drouet M, Nalesso V, Le Bert M, Cogne M (2001) Localization of the 3' IgH locus elements that effect long-distance regulation of class switch recombination. Immunity 15 (2):187-199. doi:10.1016/s1074-7613(01)00181-9

Pinto-Espinoza C, Guillou C, Rissiek B, Wilmes M, Javidi E, Schwarz N, Junge M, Haag F, Liaukouskaya N, Wanner N, Nicke A, Stortelers C, Tan YV, Adriouch S, Magnus T, Koch-Nolte F (2022) Effective targeting of microglial P2X7 following intracerebroventricular delivery of nanobodies and nanobody-encoding AAVs. Front Pharmacol 13:1029236. doi:10.3389/fphar.2022.1029236

Prufer K, Racimo F, Patterson N, Jay F, Sankararaman S, Sawyer S, Heinze A, Renaud G, Sudmant PH, de Filippo C, Li H, Mallick S, Dannemann M, Fu Q, Kircher M, Kuhlwilm M, Lachmann M, Meyer M, Ongyerth M, Siebauer M, Theunert C, Tandon A, Moorjani P, Pickrell J, Mullikin JC, Vohr SH, Green RE, Hellmann I, Johnson PL, Blanche H, Cann H, Kitzman JO, Shendure J, Eichler EE, Lein ES, Bakken TE, Golovanova LV, Doronichev VB, Shunkov MV, Derevianko AP, Viola B, Slatkin M, Reich D, Kelso J, Paabo S (2014) The complete genome sequence of a Neanderthal from the Altai Mountains. Nature 505 (7481):43-49. doi:10.1038/nature12886

Qureshi OS, Paramasivam A, Yu JC, Murrell-Lagnado RD (2007) Regulation of P2X4 receptors by lysosomal targeting, glycan protection and exocytosis. J Cell Sci 120 (Pt 21):3838-3849. doi:10.1242/jcs.010348

Razzoli M, Frontini A, Gurney A, Mondini E, Cubuk C, Katz LS, Cero C, Bolan PJ, Dopazo J, Vidal-Puig A, Cinti S, Bartolomucci A (2016) Stress-induced activation of brown adipose tissue prevents obesity in conditions of low adaptive thermogenesis. Mol Metab 5 (1):19-33. doi:10.1016/j.molmet.2015.10.005

Richardson MF, Munyard K, Croft LJ, Allnutt TR, Jackling F, Alshanbari F, Jevit M, Wright GA, Cransberg R, Tibary A, Perelman P, Appleton B, Raudsepp T (2019) Chromosome-Level Alpaca Reference Genome VicPac3.1 Improves Genomic Insight Into the Biology of New World Camelids. Front Genet 10:586. doi:10.3389/fgene.2019.00586

Roberts-Toler C, O'Neill BT, Cypess AM (2015) Diet-induced obesity causes insulin resistance in mouse brown adipose tissue. Obesity (Silver Spring) 23 (9):1765-1770. doi:10.1002/oby.21134

Roth DB (2014) V(D)J Recombination: Mechanism, Errors, and Fidelity. Microbiol Spectr 2 (6). doi:10.1128/microbiolspec.MDNA3-0041-2014

Saito M, Okamatsu-Ogura Y, Matsushita M, Watanabe K, Yoneshiro T, Nio-Kobayashi J, Iwanaga T, Miyagawa M, Kameya T, Nakada K, Kawai Y, Tsujisaki M (2009) High incidence of metabolically active brown adipose tissue in healthy adult humans: effects of cold exposure and adiposity. Diabetes 58 (7):1526-1531. doi:10.2337/db09-0530

Schneider M, Prudic K, Pippel A, Klapperstuck M, Braam U, Muller CE, Schmalzing G, Markwardt F (2017) Interaction of Purinergic P2X4 and P2X7 Receptor Subunits. Front Pharmacol 8:860. doi:10.3389/fphar.2017.00860

Schroeder HW, Jr., Cavacini L (2010) Structure and function of immunoglobulins. J Allergy Clin Immunol 125 (2 Suppl 2):S41-52. doi:10.1016/j.jaci.2009.09.046

Schulz H (1991) Beta oxidation of fatty acids. Biochim Biophys Acta 1081 (2):109-120. doi:10.1016/0005-2760(91)90015-a

Silver LM (1995) Mouse genetics: concepts and applications. Oxford University Press,

Smith GP (1985) Filamentous fusion phage: novel expression vectors that display cloned antigens on the virion surface. Science 228 (4705):1315-1317. doi:10.1126/science.4001944

Stähler T, Danquah W, Demeules M, Gondé H, Hardet R, Haag F, Adriouch S, Koch-Nolte F, Menzel S (2022) Development of Antibody and Nanobody Tools for P2X7. Methods Mol Biol 2510:99-127. doi:10.1007/978-1-0716-2384-8_6

Sun LF, Liu Y, Wang J, Huang LD, Yang Y, Cheng XY, Fan YZ, Zhu MX, Liang H, Tian Y, Wang HS, Guo CR, Yu Y (2019) Altered allostery of the left flipper domain underlies the weak ATP response of rat P2X5 receptors. J Biol Chem 294 (51):19589-19603. doi:10.1074/jbc.RA119.009959

Sun Y, Liu Z, Ren L, Wei Z, Wang P, Li N, Zhao Y (2012) Immunoglobulin genes and diversity: what we have learned from domestic animals. Journal of Animal Science and Biotechnology 3 (1):18. doi:10.1186/2049-1891-3-18

Surprenant A (1996) Functional properties of native and cloned P2X receptors. Ciba Found Symp 198:208-219; discussion 219-222. doi:10.1002/9780470514900.ch12

Tian T, Heine M, Evangelakos I, Jaeckstein MY, Schaltenberg N, Stahler T, Koch-Nolte F, Kumari M, Heeren J (2020) The P2X7 ion channel is dispensable for energy and metabolic homeostasis of white and brown adipose tissues. Purinergic Signal. doi:10.1007/s11302-020-09738-7

Trayhurn P, Beattie JH (2001) Physiological role of adipose tissue: white adipose tissue as an endocrine and secretory organ. Proc Nutr Soc 60 (3):329-339. doi:10.1079/pns200194

Ussar S, Lee KY, Dankel SN, Boucher J, Haering MF, Kleinridders A, Thomou T, Xue R, Macotela Y, Cypess AM, Tseng YH, Mellgren G, Kahn CR (2014) ASC-1, PAT2, and P2RX5 are cell surface markers for white, beige, and brown adipocytes. Sci Transl Med 6 (247):247ra103. doi:10.1126/scitranslmed.3008490

Varadi M, Anyango S, Deshpande M, Nair S, Natassia C, Yordanova G, Yuan D, Stroe O, Wood G, Laydon A, Zidek A, Green T, Tunyasuvunakool K, Petersen S, Jumper J, Clancy E, Green R, Vora A, Lutfi M, Figurnov M, Cowie A, Hobbs N, Kohli P, Kleywegt G, Birney E, Hassabis D, Velankar S (2022) AlphaFold Protein Structure Database: massively expanding the structural coverage of protein-sequence space with high-accuracy models. Nucleic Acids Res 50 (D1):D439-D444. doi:10.1093/nar/gkab1061

Viant C, Escolano A, Chen ST, Nussenzweig MC (2021) Sequencing, cloning, and antigen binding analysis of monoclonal antibodies isolated from single mouse B cells. STAR Protoc 2 (2):100389. doi:10.1016/j.xpro.2021.100389

Vu KB, Ghahroudi MA, Wyns L, Muyldermans S (1997) Comparison of llama VH sequences from conventional and heavy chain antibodies. Mol Immunol 34 (16-17):1121-1131. doi:10.1016/s0161-5890(97)00146-6

Wang N, Smith WF, Miller BR, Aivazian D, Lugovskoy AA, Reff ME, Glaser SM, Croner LJ, Demarest SJ (2009) Conserved amino acid networks involved in antibody variable domain interactions. Proteins 76 (1):99-114. doi:10.1002/prot.22319

Weinhold K, Krause-Buchholz U, Rodel G, Kasper M, Barth K (2010) Interaction and interrelation of P2X7 and P2X4 receptor complexes in mouse lung epithelial cells. Cell Mol Life Sci 67 (15):2631-2642. doi:10.1007/s00018-010-0355-1

Wesolowski J (2011) Klonierung des Lama glama Schwereketten-Antikörper Genlokus und Herstellung von Konstrukten für Lama Antikörper produzierende transgene Mäuse. Doctoral thesis

, Universität Hamburg,

Winters A, McFadden K, Bergen J, Landas J, Berry KA, Gonzalez A, Salimi-Moosavi H, Murawsky CM, Tagari P, King CT (2019) Rapid single B cell antibody discovery using nanopens and structured light. MAbs 11 (6):1025-1035. doi:10.1080/19420862.2019.1624126

Winzer R, Serracant-Prat A, Brock VJ, Pinto-Espinoza C, Rissiek B, Amadi M, Eich N, Rissiek A, Schneider E, Magnus T, Guse AH, Diercks BP, Koch-Nolte F, Tolosa E (2022) P2X7 is expressed on human innate-like T lymphocytes and mediates susceptibility to ATP-induced cell death. Eur J Immunol 52 (11):1805-1818. doi:10.1002/eji.202249932

Xu J, Chai H, Ehinger K, Egan TM, Srinivasan R, Frick M, Khakh BS (2014) Imaging P2X4 receptor subcellular distribution, trafficking, and regulation using P2X4-pHluorin. J Gen Physiol 144 (1):81-104. doi:10.1085/jgp.201411169

Yaron JR, Gangaraju S, Rao MY, Kong X, Zhang L, Su F, Tian Y, Glenn HL, Meldrum DR (2015) K(+) regulates Ca(2+) to drive inflammasome signaling: dynamic visualization of ion flux in live cells. Cell Death Dis 6 (10):e1954. doi:10.1038/cddis.2015.277

Young MT, Pelegrin P, Surprenant A (2006) Identification of Thr283 as a key determinant of P2X7 receptor function. Br J Pharmacol 149 (3):261-268. doi:10.1038/sj.bjp.0706880

Zhang X, Mosser DM (2008) Macrophage activation by endogenous danger signals. J Pathol 214 (2):161-178. doi:10.1002/path.2284

Zhang Z, Goldschmidt T, Salter H (2012) Possible allelic structure of IgG2a and IgG2c in mice. Molecular Immunology 50 (3):169-171. doi:doi.org/10.1016/j.molimm.2011.11.006

Zimmermann H (2000) Extracellular metabolism of ATP and other nucleotides. Naunyn Schmiedebergs Arch Pharmacol 362 (4-5):299-309. doi:10.1007/s002100000309

Zuo E, Cai YJ, Li K, Wei Y, Wang BA, Sun Y, Liu Z, Liu J, Hu X, Wei W, Huo X, Shi L, Tang C, Liang D, Wang Y, Nie YH, Zhang CC, Yao X, Wang X, Zhou C, Ying W, Wang Q, Chen RC, Shen Q, Xu GL, Li J, Sun Q, Xiong ZQ, Yang H (2017) One-step generation of complete gene knockout mice and monkeys by CRISPR/Cas9-mediated gene editing with multiple sgRNAs. Cell Res 27 (7):933-945. doi:10.1038/cr.2017.81

11 Acknowledgements

First, I would like to thank my supervisor Prof. Dr. Friedrich Koch-Nolte for granting me the opportunity to work on this wonderful topic, and for his continuous guidance and support.
In addition, acknowledgements go to Prof. Dr. rer. nat. Jörg Heeren and Prof. Dr. med. Peter Bannas for the examination of my doctoral thesis and defense.
My sincere thanks go to all the present and former colleagues of the Institute of Immunology. Looking back on the last few years, there has not been one single day I disliked going to work, even when experiments did not check out as planned. The lovely atmosphere, friendly and helpful colleagues as well as innumerable coffee breaks made my day, every day.
Special thanks go to former Post-Docs Dr. Thomas Eden and Dr. Stephan Menzel who guided me through the first two years of my PhD with overwhelming patience and endurance in giving advice. My heartfelt thanks to my colleague and dear friend Waldemar Schäfer, whom I got to know while working towards my Bachelor's degree and we are still sticking together now. Let's see where we head next together.
Thank you, too, to the numerous other colleagues for their support during working hours, for making lunch breaks fun and for severe distraction after work. In addition, I want to thank all the lab technician students who contributed to the success of this thesis. Fabienne Seyfried, Gudrun Dubbercke, Josephine Gebhardt and Natalie Tode, the good souls of the lab, always had valuable advice and supplied help for almost all applied experiments. Thanks also go to Dr. Michelle Yvonne Jäckstein for the close collaboration, insights into fat tissue metabolism and the possibilities for applying nanobodies in research fields I would have missed without her.
I deeply appreciate the time invested by various colleagues in this work; the critical reading as well as the corrections they supplied.
My family I thank for their constant belief in my success and their ongoing support.
Finally, I thank my wife Ann-Kathrin for her continuous support during the last decade and her encouragement to finish my thesis. Thank you for always having an open ear, even when I complained about experiments that failed. Thank you for each and every smile you awakened in me while I was writing this thesis.

12 Curriculum vitae

Lebenslauf entfällt aus datenschutzrechtlichen Gründen.

13 Eidesstattliche Versicherung

Ich versichere ausdrücklich, dass ich die Arbeit selbständig und ohne fremde Hilfe verfasst, andere als die von mir angegebenen Quellen und Hilfsmittel nicht benutzt und die aus den benutzten Werken wörtlich oder inhaltlich entnommenen Stellen einzeln nach Ausgabe (Auflage und Jahr des Erscheinens), Band und Seite des benutzten Werkes kenntlich gemacht habe.
Ferner versichere ich, dass ich die Dissertation bisher nicht einem Fachvertreter an einer anderen Hochschule zur Überprüfung vorgelegt oder mich anderweitig um Zulassung zur Promotion beworben habe.
Ich erkläre mich einverstanden, dass meine Dissertation vom Dekanat der Medizinischen Fakultät mit einer gängigen Software zur Erkennung von Plagiaten überprüft werden kann.

Ich danke den folgenden Mitarbeitern am Institut für Immunologie (IfI) und am Institut für Biochemie und Molekulare Zellbiologie (IBMZ) für die Bereitstellung folgender Materialien und Ergebnisse:
Dr. Welbeck Danquah und Prof. Dr. Friedrich Nolte (IfI) für klonierte Phagen-Display-Bibliotheken und P2X7-spezifische Nanobodies (Abschnitt 4.2, Abb. 4.2.1 & Abschnitt 4.4, Abb. 4.4.1),
Dr. Michelle Yvonne Jäckstein und Prof. Dr. Jörg Heeren (IZMB) für die Ergebnisse mit in vitro differenzierten braunen Adipozyten und dem Maus Model zur Entzündung des braunen Fettgewebes (Abschnitt 4.3, Abb. 4.3.5; Abschnitt 4.4, Abb. 4.4.2 & 4.4.3.).

Unterschrift: .....